DOKUZ EYLÜL UNIVERSITY

GRADUATE SCHOOL OF NATURAL AND APPLIED SCIENCES

PHOTOCATALYTIC OXIDATION OF POLLUTANTS

by

Gülek ÖNER

April, 2015

İZMİR

PHOTOCATALYTIC OXIDATION OF POLLUTANTS

A Thesis Submitted to the
Graduate School of Natural and Applied Sciences of Dokuz Eylül University
In Partial Fulfillment of the Requirements for the Degree of Doctor of Philosophy in Environmental Engineering, Environmental Science Program

by

Gülek ÖNER

April, 2015
İZMİR

Ph. D. THESIS EXAMINATION RESULT FORM

We have read the thesis entitled **"PHOTOCATALYTIC OXIDATION OF POLLUTANTS"** completed by **GÜLEK ÖNER** under supervision of **PROF. DR. AYŞEGÜL PALA** and we certify that in our opinion it is fully adequate, in scope and in quality, as a thesis for the degree of Doctor of Philosophy.

.....

Prof. Dr. Ayşegül PALA

Supervisor

.....

Prof. Dr. Delia SPONZA

Thesis Committee Member

.....

Prof. Dr. Erdal ÇELİK

Thesis Committee Member

.....

Prof. Dr. Şule AYTAŞ

Examining Committee Member

.....

Doç. Dr. Gökhan Akınal

Examining Committee Member

Prof.Dr. Ayşe OKUR

Director

Graduate School of Natural and Applied Sciences

ACKNOWLEDGMENTS

I would like to express my special thanks to my advisor Professor Dr. Ayşegül PALA, for her priceless support, continuous supervision, considerable effort and significant concern to carry out this study. It has been a great honor and privilege to work with her.

I would like to also thank Prof. Dr. Erdal ÇELİK for supervising this study, with his guidance and valuable supports in the metallurgical and material step of this project and extend my appreciation to the crew of EMUM.

I am thankful to Research Assist. Prof. Dr. Mustafa EROL for his advices and comments. I am also appreciated to Fatma BAKAL for her helps in metallurgical and material part of the thesis and Güneş KURŞUN for his helps in various steps of the thesis.

My greatest gratitude goes to Ruti POLİTİ for her various helps and supports for every step of this thesis.

This work is supported by TÜBİTAK (The Scientific and Technological Research Council of Turkey) 1001 - The Support Program for Scientific and Technological Research Project. The number of the project is 112Y162 (Transformation of industrial organic pollutants to clean compounds using new generation photocatalytic materials). In addition, Dokuz Eylül University Department of Scientific Research Project (BAP) provided support. The number of the project was 2010.KB.FEN.0302010111.

Finally, I want to thank specially to my family for their moral support, motivation and encouragement.

Gülek ÖNER

PHOTOCATALYTIC OXIDATION OF POLLUTANTS

ABSTRACT

The major objectives of this thesis are to produce thin films (potassium lanthanum titanium oxide - KLTO) via sol-gel and spin coating method and to observe the photocatalytic degradation efficiencies of the persistent compounds in wastewater under the influence of pH and light intensity. The production of advanced nanomaterials and coatings are improving day by day. Thin film photocatalysts are generated since they are more environmentalist than the particulate catalysts which are difficult to separate from water. In order to generate thin film structure; material characterization, phase analyses, elemental analyses, microstructure and film characterization were performed to evaluate structural and morphological characterization processes of the photocatalysts (KLTO). Phenol (organic matter), methylene blue (azo dye) and cyanide (inorganic matter) photocatalytic performance experiments with different pH, initial concentration, reaction time and light intensity levels were carried out in a solar box ATLAS SUNTEST CPS+ which is simulating natural solar radiation. As a result of the studies, 13 different thin films were examined and the most effective thin film photocatalysts were determined as 0.5 Sm doped potassium lanthanum titanium oxide.In this respect, three main parts were composed. First, pH and light intensity are selected as variables and their effects on degradation are investigated. 75.3% of degradation of phenol was achieved at pH of 7 and 750 W/m square of light intensity. 97% of methylene blue was degraded after three hours of radiation. And, cyanide was degraded 80.2% under alkali condition. As a second step, the kinetic of methylene blue degradation was investigated and it is fitted to a first order reaction law. Finally, ANOVA test was performed for methylene blue and according to the findings; pH and light intensity were found as the significant factors for degradation of methylene blue.

Keywords: Sol-gel technique, spin coating, photocatalytic oxidation, potassium lanthanum titanium oxide, phenol, methylene blue, cyanide.

KİRLETİCİLERİN FOTOKATALİTİK OKSİDASYONLA ARITIMI

ÖZ

Bu tezin en önemli amaçları ince filmlerin (potasyum lantanyum titanyum oksit - KLTO) sol-jel ve döndürmeli kaplama yöntemi ile üretilmesi ve suyun içinde zor parçalanan bileşiklerin fotokatalik parçalanma verimlerinin farklı pH ve ışık şiddeti etkilerinin incelenmesidir. Nano malzemelerin ve kaplamaların üretimleri gün geçtikçe ilerlemektedir. Bu nedenle partikül halindeki fotokatalizörlere göre daha çevreci olan ince film fotokatalizörler üretilerek partikül haldeki katalizörlerin sudan ayırma işlemi gibi ekstra bir işlem gerektirmeden arıtım sağlanacaktır. İnce film üretiminde filmin yapısına etki eden yapısal ve morfolojik karakterizasyon işlemleri, malzeme karakterizasyonu, faz analizi, elementel analiz, mikroyapı analizi ve film karakterizasyonu yapılmıştır. Fenol (organik madde), azo boyar madde olan metilen mavisi) ve siyanür (inorganik madde) gibi kirleticiler kullanılarak fotokatalitik oksidasyon farklı pH, başlangıç konsantrasyonu, reaksiyon süresi ve ışık şiddeti değişken değerleri ile incelenerek güneş simülatörü (ATLAS SUNTEST CPS+) yardımıyla performans testleri yapılmıştır. 13 faklı fotokatalizör ile yapılan deneyler sonucunda en verimlisi 0.5 Sm doplu potasyum lantanyum titanyum oksit olarak bulunmuştur. Bu çerçevede 3 ana kısım oluşturulmuştur. İlk olarak pH ve ışık şiddeti araştırılacak değişken olarak seçilmiş ve arıtmaya etkileri araştırılmıştır. Fenol örnekleri ile yapılan testlerde %75,3 parçalanma verimine pH 7 ve 750 W/m kare ışık şiddetinde ulaşılmıştır. Metilen mavisi deneyi sonucu %97 arıtım 3 saat sonunda gerçekleşmiştir. Ayrıca alkali koşulda siyanür ile yapılan deneyler sonucunda %80,2 arıtım sağlanmıştır. Diğer yandan metilen mavisinin reaksiyon kinetikleri incelenmiş ve birinci derece reaksiyon kinetiğine uyduğu görülmüştür. Son olarak metilen mavisi için ANOVA testi yapılarak pH ve ışık şiddetinin arıtımda kendi başlarına etkili olduğu görülmüştür.

Anahtar Kelimeler: Sol - jel tekniği, döndürme kaplama, fotokatalitik oksidasyon, potasyum lantanyum titanyum oksit, fenol, metilen mavisi, siyanür.

CONTENTS

Page

LIST OF FIGURES

Page

LIST OF TABLES

CHAPTER ONE
INTRODUCTION

Over the past decades, environmental issues have become more significant because of the consumption of natural sources due to the increase of the population and technological improvements. The water pollution problem becomes important and environmental regulations are established more strictly. That is why; the increase of the environmental consciousness and awareness gained worldwide importance. An important part of pollutants of surface water and underground water is come from uncontrolled industrial wastewaters discharge.

Phenol and its derives are very toxic and these contaminants are released into water bodies from many industrial plants, including oil refineries, petrochemical industry, coking, synthetic rubber, plastics, pulp and paper, pharmaceutical, pesticide industries and by several other chemical plant (Babuponnusami et al., 2012 and Bayramoğlu et al, 2009). On the other hand, cyanide is also produced from various industrial effluents which include metal cleaning, plating, electroplating, metal processing, automobile parts manufacture, steel tempering, mining, photography, pharmaceuticals, coal coking, ore leaching, plastics etc (Aazam, 2013). Another example of the pollutant is dye pollutants. Large amounts of dyes are discharged by different industries, including textile, cosmetic, leather, paper, pharmaceutical and nutrition industries (Zhang, 2012). The examples of the pollutants and their related industries can be multiplied. Even the trace concentrations of the pollutants in the effluent cause many environmental problems.

Different treatment methods, including mechanical, biological, physical and chemical are usually in used for industrial wastewater treatment process. But these conventional treatment methods are insufficient or very expensive to purify the wastewaters (Yao & Wang, 2010). Chemical coagulation, flocculation and sedimentation are conventional methods to remove toxic and persistent matters, but their efficiencies are very low. For example, for cyanide treatment, the treatment methods except oxidation give high concentrated product in which toxic cyanides

still exist (Osathaphan et al., 2008). Especially, certain forms of cyanide for example hydrogen cyanide (HCN) are very toxic. That is why, acceptable limits of cyanide in water are very low (Dzombak et al., 2005).

Photocatalytic oxidation process is found sustainable and economical to remove different pollutants by oxidizing organics, aromatics and inorganics. Photodegradation is a method for the treatment of toxic and bioresistant pollutants (D'Oliveria et al., 1990; Kochany, 1993). The principal of the photodegradation process is hydroxyl radical ($OH^{\bullet}$) formation. High removal rates of organic pollutant can be obtained by using this method. In order to degrade the pollutants, other different methods have a remaining residue called sludge. It is an important advantage of the sol-gel method which is a nanotechnologic method is the prevention of the system from the additional waste.

The importance of the photocatalysts in treatment process emerged in 1969, by a Japan researcher called Fujishima. Honda and Fujishima had realized a prototype about fine powders which are doped with metal and/or metal oxide particles and these particles were used as a photocatalyst in chemical reactions. These fine powders had a semiconductor characteristic. TiO_2 utilization in the photocatalytic reactions were discovered by them. According to this finding, many researches have been observed to improve the photocatalytic systems (Kodama & Suzuki, 2007).

Photocatalytic process starts with the absorption of light by the presence of the semiconductor structure. Semiconductors are created an energy gap and this energy gap constitutes valance and conductivity band. If the exposure of the photocatalyst to photon energy is greater than its own energy gap, it gives its energy to an electron which is in the valance band and electron is reached to the conductivity band. At the end of this reaction, electron – hole pairs occur. Electron – hole pairs which are located in valance and conductivity band become power supply (Kaneko & Okura, 2002).

After the improvements of TiO_2 photocatalyst, new approaches are enhanced including perovskite type layered materials. According to the researches, these types are more active than TiO_2. Nowadays, the layered perovskite type photocatalyst $K_2Ln_2Ti_3O_{10}$ (Ln= La, Nd, Gd, Sm, Dy) (KLTO) attracted attention due to its properties and photocatalytic activity. $Ln_2Ti_3O10^{2-}$ octahedral perovskite layers and substitutional K ions constitute this structure. This structure provides hydration of toxic and persistent organic matters in aqueous solutions by the presence of UV light; thus $K_2Ln_2Ti_3O_{10}$ presents high photocatalytic activity (Takata et al., 1997). Some researches show that some ion additives enhance lanthanum - titanium structure in which K ion is located between the layers or Ti ions replaced with other dopants.

According to the literature, Yahui et al. (2006) doped B into $K_2La_2Ti_3O_{10}$ structure and examined the photocatalytic activity. In consequence of the study, B addition enhances the photocatalytic degradation effect.

Cui et al. (2006) were generated layered perovskite $K_2La_2Ti_3O_{10}$ by high temperature solid state sintering and characterized by XRD and UV-Vis DRS. Pt was loaded onto $K_2La_2Ti_3O_{10}$ as a dopants to understand the effectiveness. The best result for hydrogen evaluation was obtained by Pt/ $K_2La_2Ti_3O_{10}$.

Huang et al. (2008) produced a layered perovskite, $K_2La_2Ti_3O_{10}$ photocatalysts by using two different methods which including solid state reaction method and hydrothermal method. The photocatalysts prepared by hydrothermal technique showed better photocatalytic activity than the prepared by conventional solid state reaction method.

Yang et al. (2009) were produced $K_2La_2Ti_3O_{10}$ by sol-gel method and by doping with vanadium (V). V was enhanced the photocatalytic activity. Liu et al. (2010) were generated Ce - based $K_2La_2Ti_3O_{10}$ structure by solid state reaction and characterized by using XRD, UV-Vis DRS, TEM and XPS. The photocatalytic activity was examined by visible light region. The Ce doped $K_2La_2Ti_3O_{10}$ showed higher photocatalytic activity than $K_2La_2Ti_3O_{10}$.

It can be clearly seen that, the studies were focused on the production of $K_2Ln_2Ti_3O_{10}$ by using solid state reaction, polymerization complex method and sol-gel method. In addition $K_2Ln_2Ti_3O_{10}$ coating on Si(100) substrate cannot be found in the literature. For this reason, the aim of this thesis is to produce $K_2Ln_2Ti_3O_{10}$ (*Ln* = La) thin films on Si(100) substrate by sol-gel method.

A laboratory study was performed to examine the effectiveness of $K_2Ln_2Ti_3O_{10}$ (*Ln* = La, Nd, Gd, Sm, Dy) thin films, and the photocatalytic degradation of phenol, methylene blue and cyanide. Three types of pollutant including, organic (phenol, methylene blue as azo dye) and inorganic (cyanide) are selected to examine the photocatalytic degradation efficiency. The effect of pH and the light intensity were selected as variables. The efficiency of photocatalytic degradations was studied. Based on the approaches, major objectives of this thesis can be summarized as follows:

- ✓ Production and characterization of $K_2Ln_2Ti_3O_{10}$ (*Ln* = La, Nd, Gd, Sm, Dy) thin film photocatalysis on Si(100) substrate with using sol-gel and spin coating methods,

- ✓ Understand the influence of pH and light intensity with ATLAS SUNTEST CPS+ by using $K_2Ln_2Ti_3O_{10}$ (*Ln* = La,Nd, Gd, Sm, Dy),

- ✓ Examine the effectiveness of $K_2Ln_2Ti_3O_{10}$ (*Ln* = La, Nd, Gd, Sm, Dy) thin films with a comparison of blank (without photocatalyst),

- ✓ Observe the effect of the pollutants on SUVA, TOC and DOC degradation efficiencies,

- ✓ Investigate the reaction order kinetics,

- ✓ Examine the effectiveness of the parameters based on ANOVA statistical tests.

This thesis includes five chapters. General introduction of photocatalytic oxidation and photocatalysis, the importance of water treatment and literature reviews are introduced in Chapter One. In Chapter Two, a detailed literature review of fundamental aspects of semiconductors, sol-gel method and photocatalytic degradation mechanisms are explained. In Chapter Three, materials and methods which are used in the experimental procedures of KLTO coatings are clarified. In Chapter Four, results of the characterization and photocatalytic tests are stated and the results are discussed in details. And finally in Chapter Five, the conclusion and recommendations are summarized and future plans are investigated.

CHAPTER TWO
THEORETICAL ASPECTS OF PHOTOCATALYTIC SYSTEM

2.1 Introduction

Throughout the century, titanium dioxide and its effects on water treatment was very popular as a photocatalysis and was discussed in several studies. Firstly, the properties of semiconductors were investigated. The generation of •OH radical and their effect was discovered by Bard and co – workers. After the innovation of •OH radical effects on TiO_2, photocatalytic oxidation of organic compounds has attracted considerable attention by many scientists. Recently, photocatalytic degradation of pollutants gains importance due to its advantages and subjected to many studies (Sobczynski et al., 2003). Studies were focused on TiO_2, niobates, titanates, tantalates, ferrate and vanadate. In the past, photocatalytic materials were limited, but now the modifications have been extended by newly generated systems with using solar energy or artificial energy source (Yang et al., 2009).

Recently, the layered perovskite photocatalyst $K_2La_2Ti_3O_{10}$ has attracted attention thanks to its unique optical properties, electrical transport properties, and especially its photocatalytic activity. In addition, a lot of derivatives of $K_2La_2Ti_3O_{10}$ can be generated by doping with other elements (Yang et al., 2007).

2.2 General Information about Semiconductors and Photocatalytic System

The increased awareness of environmental concerns has speed up the need to develop new treatment methods with photocatalysis which is attracted a lot of attention in the field of pollutant degradation. The natural treatment processes including, lagoons, ponds, streams, rivers and lakes are taken action in the presence of sunlight which initiating the degradation of organic compound and convert to carbon dioxide and other mineral products. Some reagents accelerate this process. The utilization of ‘colloidal semiconductors’ to speed up the reaction were developed in 1976. From that time, laboratory researches have augmented to create artificial

medium to increase semiconductors and solar purification process (Beydoun et al., 1999). Semiconductor photocatalysts are attracting large scale research area for the treatment of pollutants. These semiconductor photocatalysis have cost-effective configuration and can make complete degradation without generation of toxic byproducts. Semiconductor photocatalysis are commercially applying as a self - cleaning coating on building and glass materials in Japan and South Korea (Krishna, Noguchi, Koopman, & Moundgil, 2006).

2.2.1 Principles of Semiconductor Theory

Materials are divided into three different types according to their electrical properties. These types are conductors, insulators and semiconductors. Insulators have large energy gap between valence and conduction bands. Semiconductors have less energy gap between valence and conduction bands. The valence band and the conduction band of the conductor are overlapping. The purpose of this study is to produce $K_2Ln_2Ti_3O_{10}$ (Ln= La, Nd, Gd, Sm, Dy) and this material is semiconductor. The most well known conductor is metals. Metals can carry the electric flow by the reason of its free electrons which can pass from one atom to the next. This opportunity provides the electric flow to travel through the length of the metal.

Semiconductors can be conducted by the external effects of conductors. Indeed, these materials are conductor but when an external effect including, heat, light, magnetic effect or electrical stress are applied, some electrons become independent and become conductor. When these external effects are removed, semiconductors return to their old type as insulator. Conductor, insulator and semiconductor energy band diagram can be shown in Figure 2.1 (Sayılkan, 2007).

It can be clearly seen in Figure 2.1 that the main difference between semiconductors and conductors is a natural overlap of the conductors between the valence band and the conduction band, while semiconductors have a noticeable gap between the two bands. So, the electrons of the conductors are able to carry a current under any condition. And insulators have a large energy gap between valence and

conduction bands (Larsen, n.d). The electron of the valence band from semiconductor photocatalyst (for e.g. TiO_2) becomes excited when it is illuminated by light. The excess energy of this excited electron promoted the electron to the conduction band of TiO_2. For this reason it creates the negative-electron (e^-) and positive-hole (h^+) pairs. This stage is called the semiconductor's ' photo-excitation ' stage. The energy difference between the valence band and the conduction band is known the 'Band Gap'. It can be seen that the conduction bands are empty. On the other hand, the valence bands are filled (Callister, 2008).

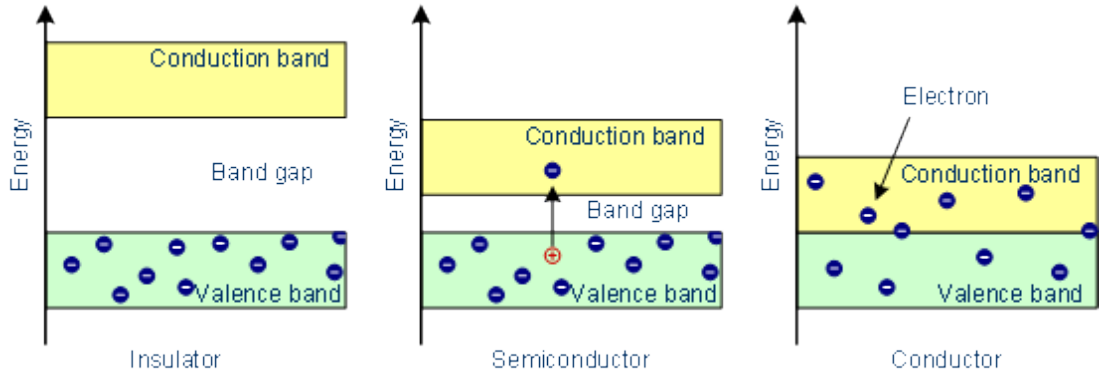

Figure 2.1 Insulator, conductor and semiconductor band energy levels (Shapley, 2012).

Electron holes increase the conductivity of the semiconductor. Firstly, hole conduction requires an electron to excite its valence band to the conduction band (Larsen, n.d). To produce electron-hole pairs, the photons excite the electrons from the valence band to the conduction band. After this process, absorption of light, reduction and oxidation mechanism occurred. In the reduction mechanism, excited electron is transferred from the conduction band to the adsorbed particle. In the oxidation mechanism, the redox potential of the donor (adsorbate) is above the valence band of the semiconductor to donate an electron to the vacant hole in the valence band. Oxygen and water are the adsorbates in the photocatalytic reactions (Banerjee et al., 2006).

Figure 2.2 demonstrates the mechanism of photocatalyst. Four processes occur after the light absorption including, electron-hole pair recombination, migration to the surface leading to oxidation and reduction of the acceptor (adsorbates).

Recombination occurs at the surface or within the bulk of the photocatalyst (Tek, 2008).

In presence of water and oxygen, a reaction series occur. This cycle continues when light is available. Positive holes are oxidized the water and photoelectrons of the conduction band are reduced oxygen. Reactive oxygen species like H_2O_2, hydroxyl radical $^{\cdot}OH$ can be produced. The reaction that is generated by the absorption of photon (hυ) is given as follow (Tek, 2008).

$$\text{Semiconductor (SC)} + h\upsilon \rightarrow \text{SC}\,(e^- + h^+) \quad (2.1)$$

The reactions which are started by the conduction band (e^-) can be given as below (Tek, 2008).

$$\text{SC}\,(e^-) + O_2 \rightarrow \text{SC} + {}^{\cdot}O_2^- \quad (2.2)$$
$$\text{SC}\,(e^-) + O_2^- + 2H^+ \rightarrow \text{SC} + H_2O_2 \quad (2.3)$$
$$\text{SC}\,(e^-) + H_2O_2 \rightarrow \text{SC} + {}^{\cdot}OH + OH^- \quad (2.4)$$
$${}^{\cdot}O_2^- + H_2O_2 \rightarrow {}^{\cdot}OH + OH^- + O_2 \quad (2.5)$$
$${}^{\cdot}O_2^- + H^+ \rightarrow {}^{\cdot}HO_2^- \quad (2.6)$$
$$\text{SC}\,(e^-) + {}^{\cdot}HO_2^- \rightarrow \text{SC} + HO_2^- \quad (2.7)$$
$$HO_2^- + H^+ \rightarrow H_2O_2 \quad (2.8)$$
$$2\,{}^{\cdot}HO_2 \rightarrow O_2 + H_2O_2 \quad (2.9)$$

The reactions which are started by the valence band (h^+) can be given as below (Tek, 2008).

$$\text{SC}\,(h^+) + H_2O_{(ads)} \rightarrow \text{SC} + {}^{\cdot}OH_{(ads)} + H^+ \quad (2.10)$$
$$\text{SC}\,(h^+) + 2H_2O_{(ads)} \rightarrow \text{SC} + 2H^+ + H_2O \quad (2.11)$$
$$\text{SC}\,(h^+) + OH^-_{(ads)} \rightarrow \text{SC} + {}^{\cdot}OH_{(ads)} \quad (2.12)$$

As a result of the highly reactive oxygen species and hydroxyl radical, the organic pollutants on the surface can be degraded. That is why; the degradation and

mineralization of the compounds can be occurred by the optically illuminated semiconductor photocatalyst (Tek, 2008).

Titanium dioxide (TiO_2), (E_g = 3.2 eV) was mostly used for the photocatalytic reaction between the various type of semiconductors. When photocatalyst TiO_2 absorbs ultraviolet (UV) radiation from sunlight or illuminated light source, it will generate pairs of electrons and holes. Today, semiconductors are usually chosen as photocatalysts, because semiconductors need to absorb equal or more energy than its energy gap.

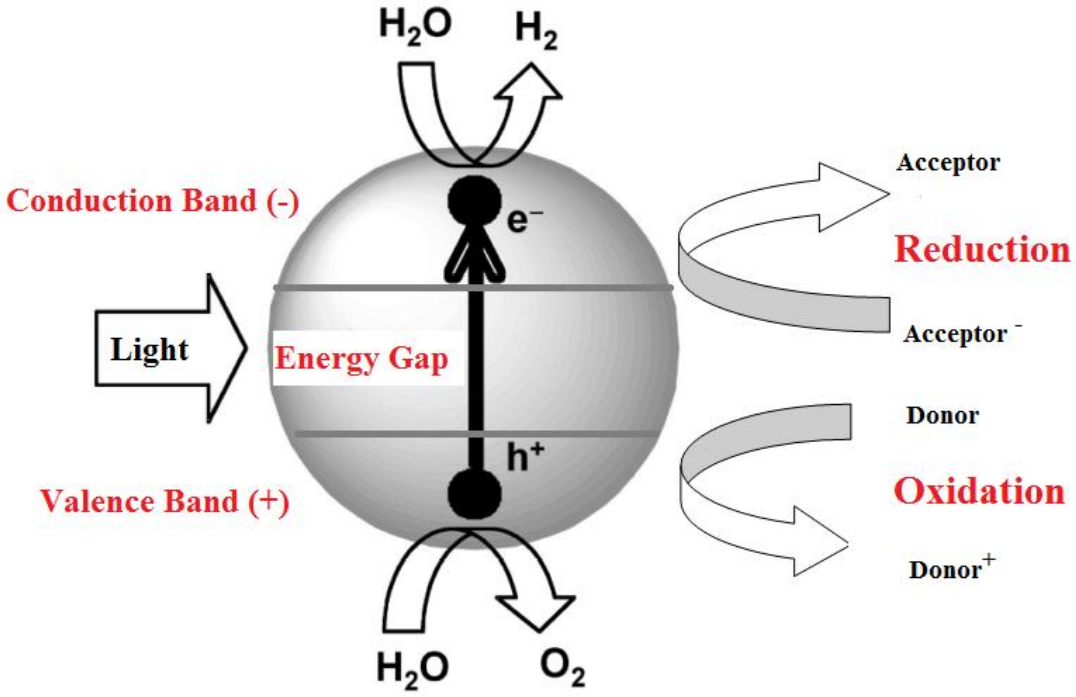

Figure 2.2 Semiconductor particle (based on Grimes Bahnemann, 2008).

Semiconductors are separated into two categories: *intrinsic* and *extrinsic* (n or p-type). Si, Ge, GaAs can be done as examples for intrinsic semiconductors which are pure enough and the impurities do not affect its electrical behavior. At absolute zero (O °K), intrinsic semiconductors are no charge carriers and therefore, material becomes as an insulator (Bakal, 2014). Figure 2.3 shows the differences between intrinsic and extrinsic semiconductors. Extrinsic semiconductors are formed by the addition of impurities into intrinsic semiconductors. This process is called as *doping*.

The impurity addition to the crystalline lattice increases the number of charge. The dense of electron or hole can be change by the impurity addition. If the electrons are the majority carriers and the gaps are the minority carriers in the semiconductor structure, these types are called n-type (donor doped - n stands for negative) semiconductor. Briefly, Semiconductors which are doped with donors are n-type. If the total opposite of this is occurred (majority carriers are gaps and minority carriers are electrons), this type is called p-type (acceptor doped - p stands for positive) semiconductor. Basically, impurity atoms that take away an electron from the semiconductors are p-type (Kaneko & Okura, 2002).

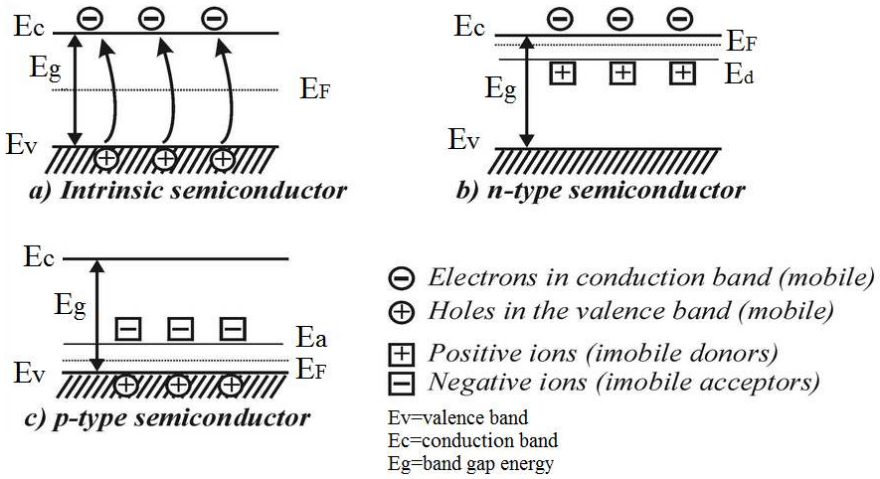

Figure 2.3 The three types of semiconductors: (a) Instrinsic semiconductors, (b) n-type semiconductors, (c) p-type semiconductors (Tiginyanu, Langa, Foell & Ursachi, 2009).

Different n-type semiconductor metal oxides including, TiO_2, ZnO, CdS, SnO_2, and WO_3 have been tested for photocatalytic oxidation of organic pollutants in water and air (Chin, 2008). Due to the high chemical stability, favorable light absorption properties, electronic structure, charge transport characteristics and the proper energy band structure, the layered perovskite photocatalyst $K_2La_2Ti_3O_{10}$ has drawn a lot of attention for its applications in water photocatalytic oxidation. The photocatalyst $K_2Ln_2Ti_3O_{10}$ (Ln= La, Nd, Gd, Sm, Dy) has one interlayer and this structure is very suitable for the improvement of the photocatalytic reactivity of water degradation. After the light absorption, the light-generated electrons move from the interlayer of

$K_2La_2Ti_3O_{10}$ to external surface and light-generated holes oxidize the water to produce O_2 in the interlayer (Yang, Qui, Chen, Feng & Yin, 2007).

Semiconductors are very effective as photocatalysts due to their light absorption properties, electronic structure, charge transport characteristics and excited-state lifetimes. Semiconductor photocatalysts are currently draw attention because of the wide range interdisciplinary research areas (Bakal, 2014).

2.2.2 Photocatalytic Degradation Mechanisms

Photocatalytic degradation process has attracted a great attention as an environmental friendly and sustainable treatment technology. A good photocatalyst is a semiconductor material which should be proactive, non toxic, and should be photocatalytically activated under light source (Tek, 2008). Due to its properties such as cheap, insoluble in water, resistant to most chemicals, titanium dioxide is the most frequently used photocatalysts (Chong et al, 2009). TiO_2, ZnO, WO_3, CdS, ZnS, $SrTiO_3$, SnO_2, WSe_2, Fe_2O_3 can be given as the examples of semiconductor solids that used as photocatalysts. High photocatalytic activity in daylight can be achieved by the photocatalyst whose band gap energy is smaller than 3eV. Studies have been reported that all kinds of organic and inorganic pollutants and heavy metals can be treated by photocatalaytic oxidation (Tek, 2008). Photocatalysis applications are not only including environmental issues but also different applications including, agricultural, medical, residential and electrical issues. Figure 2.4 shows the applications of TiO_2 photocatalysis (Nakata & Fujishima, 2012).

Wastewater can be purified by using powder form of TiO_2. But this treatment process requires an additional operation to separate the suspended powders. The coating of fine powders on glass surface is proposed to avoid this situation. The thin films adhere to the glass substrate which is usually negative charged due to the electrostatic charge of TiO_2 (Bakal, 2014). Recently, new generated perovskite layered structures attract attention because the ion exchange mechanism is very easy. The geometry of the structure provides ion exchange. Literature studies are

continuously developing. It has been reported that lanthan-titanates ($K_2Ln_2Ti_3O_{10}$ (Ln= La, Nd, Gd, Sm, Dy)) structures are photocatalytically more active than TiO_2 (Yang et al., 2009).

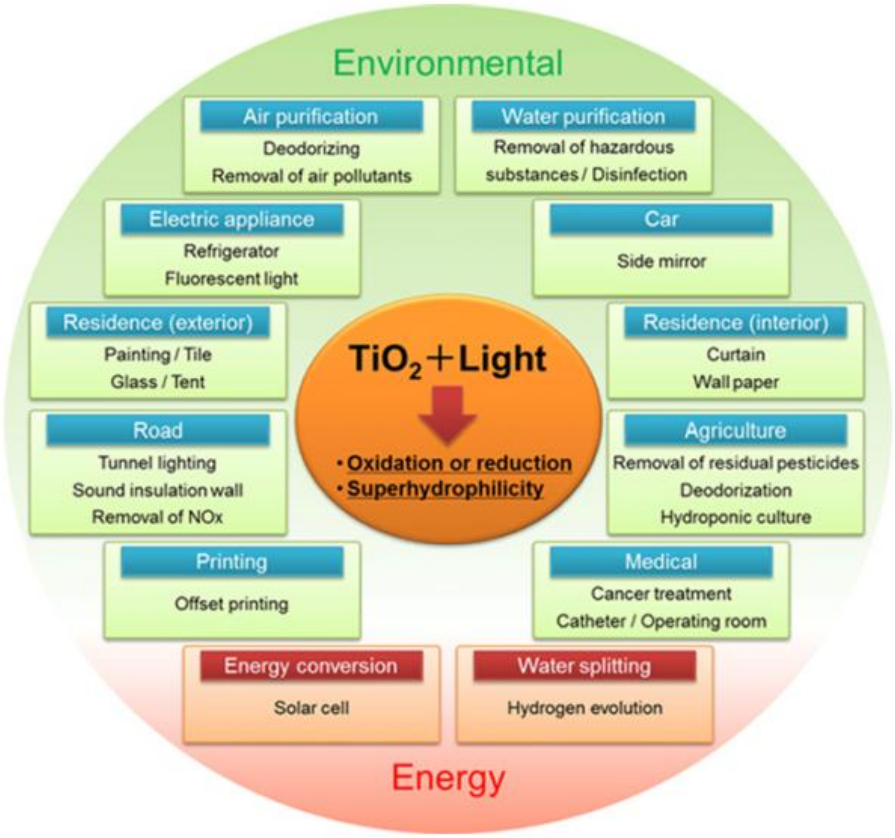

Figure 2.4 Applications of TiO_2 photocatalysis (Nakata & Fujishima, 2012).

A catalyst is not changing and also it is not being consumed during the reaction. And it does not change the speed of the reaction. Photocatalysis can be explained as "acceleration by the existence of catalyst". In other saying, the same process of catalyst occurs with the presence of the sunlight and semiconductor. The main difference between catalytic and photocatalytic systems are the activated zones (Ohtani, 2010). Photocatalysts creates strong oxidation agent to degrade the pollutants to carbon dioxide and water in the presence of photocatalyst, light and water (Politi, 2014).

Photocatalyst requires a light source to start the degradation reactions. Light has a wavelength and frequency. The energy (E=h.υ) can be estimated by the formula of the wavelength (λ=c/υ). In this formulation h is the Planck constant ($6.63x10^{-34}$ J.s) and c is the velocity of light ($3x10^{8}$ m/s), υ is the frequency (1/s) and λ is the wavelength (nm). If the frequency is increased, the wavelength will be decreased and the energy will be raised. That is why electromagnetic spectrum has an importance on photocatalyic reactions. The photocatalytic activity is directly affected by the energy (h.υ) of the ray because different wavelengths have different energy level (Nimetoğlu, 2011).

The main parameters of the photocatalytic system are water, semiconductor particles or coatings and light source for illumination. Photocatalytic process is initiated by the absorption of light with the aid of semiconductor nanoparticles. A reaction series are occurring when photocatalyst absorbs the energy from sun and as a result of the reactions, organic compounds in surface is converted to H_2O and CO_2 (Kaneko & Okura, 2002).

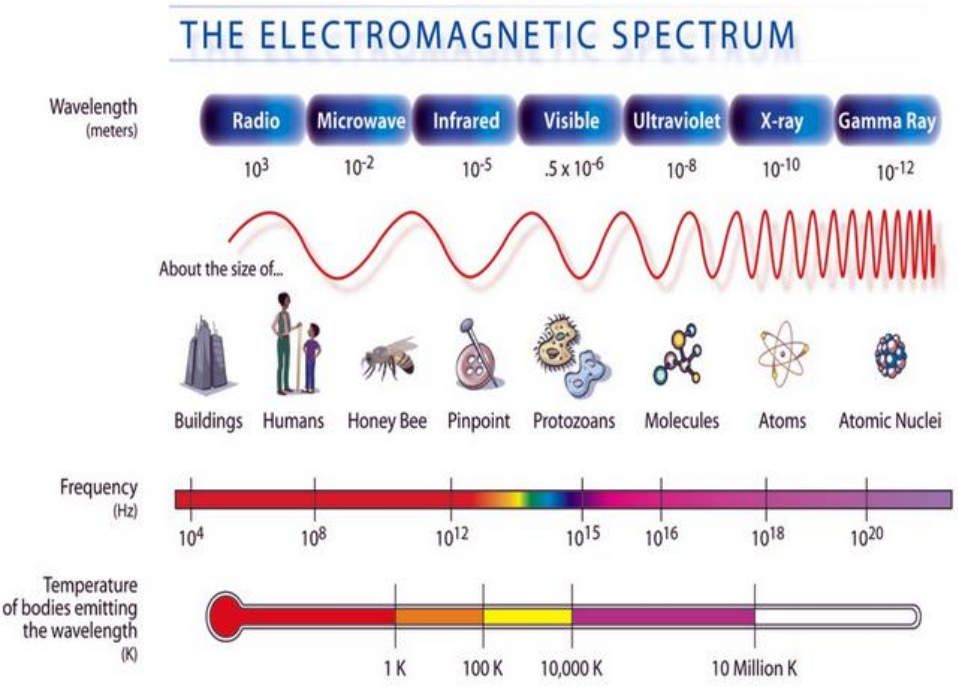

Figure 2.5 Electromagnetic spectrum (Chambers, n.d).

Sun radiation emits different wavelengths and frequencies. *Electromagnetic Spectrum* is the range of all possible frequencies of electromagnetic radiation. Figure 2.5 shows the electromagnetic spectrum which is divided into Gamma rays, X-rays, Ultraviolet Radiation, Visible light, infrared radiation, microwaves and Radio waves, respectively. Table 2.1 demonstrates the wavelengths and the frequencies of visible light (Sowa et al., 2012). Active photocatalytic nanoparticles like TiO_2 and ZnO have wide band gap. These semiconductors can absorb UV light at smaller wavelengths (smaller than ~388 nm). The goal of this thesis is to use the visible content of sunlight to extend the photocatalytic activity. This thesis is focused on the solar energy simulated light and the ability of $K_2Ln_2Ti_3O_{10}$ (Ln= La, Nd, Gd, Sm, Dy) to destroy phenol, methylene blue and cyanides. Photocatalytic degradations of phenol, methylene blue and cyanide were performed in a solar box ATLAS Suntest CPS+ simulating natural radiation and equipped with a Xenon lamp.

Table 2.1 Visible color bands (Sowa et al., 2012)

Visible color bands	**Wavelengths (nm)**
Red	780-625
Orange	625-590
Yellow	590-565
Green	565-500
Blue	500-435
Violet	435-380

The most important advantage of the layered components is the photocatalytic activity and the changeability of the cations into the intermediate layer. Some layered components are more effective than bulk catalysts. Looking at the photocatalytic studies in the literature, some perovskite layered oxides are mostly used especially for the formation of hydrogen and oxygen. These oxides demonstrate interlamellar activity and are divided two main classes: i) Dion - Jacobson Series (DJ Series), (the general formula $AM_{n-1}B_nO_{3m+1}$, (e.g. $KCa_2Nb_3O_{10}$)) and ii) the Ruddlesden – Popper

series (RP series) (general formula $A_2M_{n-1}B_nO_{3n+1}$ (e.g. $Na_2Gd_2Ti_3O_{10}$ and $K_2La_2Ti_3O_{10}$)) (Kaneko & Okura, 2002).

2.3 Principles of Semiconductor Photocatalyst $K_2Ln_2Ti_3O_{10}$

In 1960s, photochemical power of TiO_2 attracted attention. Considering the historical development of photocatalytic, Fujishima and Honda discovered photocatalytic splitting by using TiO_2 electrodes in 1972. In 1980s several studies and new inventions were developed about photocatalyst and its applications. In 1990s TiO_2 coatings were used as a self-cleaning surface. As a results of these developments, scientists were introduced the photocatalytic efficiencies of semiconductors into several research area (Tek, 2008). The latest innovation about photocatalytst is about layered structures which have displayed high photo-catalysis activity in water treatment applications. The activity of the layered photocatalyst is reported very high. The first layered photocatalyst was reported by Kudo and his coworkers. Kudo and coworkers reached that $K_4Nb_6O_{17}$ photocatalyst was effective for water decomposition reactions and to generate hydrogen and oxygen after being loaded with Ni (Cui et al., 2006).

It has been reported that $K_2La_2Ti_3O_{10}$ which is one of the layered perovskite type compounds with octahedral perovskite-layer ($La_2Ti_3O_{10}^{2-}$) is more photoactive than TiO_2 because K ions are located between the perovskite layers and perovskite layered structure can easily provided ion exchange due to the geometry (Yang et al., 2009). Takata and coworkers figured out that $K_2La_2Ti_3O_{10}$ presented a remarkable catalytic activity for water splitting under UV light irradiation after loading with nickel (Cui et al., 2006). This new generated layered compound has attracted attention and the researches are increasingly generating with a big interest (Yang et al., 2009).

2.3.1 Crystalline Structure of $K_2Ln_2Ti_3O_{10}$ (Ln= La, Nd, Gd, Sm, Dy)

$K_2Ln_2Ti_3O_{10}$ (Ln= La, Nd, Gd, Sm, Dy) is an n type of layered perovskite compound and can be shown in Figure 2.6. The $K_2La_2Ti_3O_{10}$ is consisting of

negatively charge lanthanum titanate perovskite layer and interlayer K^+ ions. $La_2Ti_3O_{10}$ which is the adjacent triple perovskite layers, are stacked with a displacement by 1/2 along the (001) direction. A lanthanum ion occupies in the center of the perovskite lattice. X-ray diffraction data shows that the cell parameters of $K_2La_2Ti_3O_{10}$ are found as a=b=0.387 nm, c=2.98 nm, face distance (001) =1.49 nm, and the thickness of the $La_2Ti_3O_{10}^{2-}$ is 1.19 nm. The interlayers are bonded by static force. According to the weak combination between inter layers, $K_2La_2Ti_3O_{10}$ is ready to intercalate exchange and expand in the field of the interlayer (Huang et al, 2010).

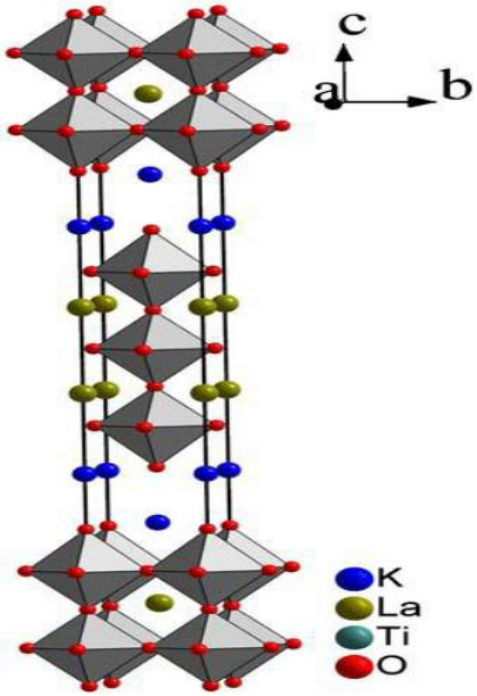

Figure 2.6 $K_2La_2Ti_3O_{10}$ crystalline structure (Huang et al, 2010).

The band gap of $K_2La_2Ti_3O_{10}$ is shown in Figure 2.7. The zone of the valance band between -5 and 0 eV is consisted of 2p orbitals. The conduction band from 2–7 eV composes of Ti_3 d and La_5 d orbitals. The value of the band gap is approximately 2.0 eV and it is much smaller than the experimental optical band gap (3.69 eV) (Huang et al, 2010).

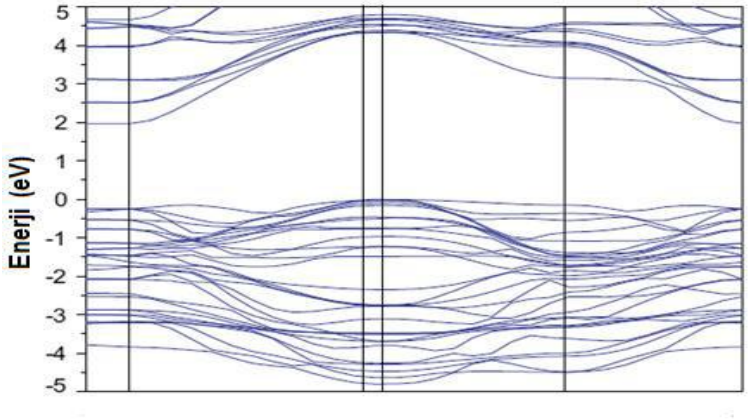

Figure 2.7 $K_2La_2Ti_3O_{10}$ energy band gap (Huang et al, 2010).

2.3.2 Photocatalytic Mechanisms of $K_2Ln_2Ti_3O_{10}$ (Ln= La, Nd, Gd, Sm, Dy)

Layered perovskite oxides draw photocatalytically attention due to the structure which is consist of two dimensional perovskite slabs interleaved with cations and this structure increase the lifetime of the electrons and holes, so the efficiency of the semiconductor photocatalyst is increasing (Bakal, 2014). Some oxide semiconductors have sufficient band gap energy to initiate photocatalytic reactions. The semiconductor property of the perovskite $K_2Ln_2Ti_3O_{10}$ comes from TiO_2. In other words, the perovskite slabs are made up by metals including, Ti, Nb, or Ta. According to the band theory, valance band is an energy level with full of the stimulated electrons via an external effect, and conduction band is the empty energy level until the electrons will be stimulated (Cui et al., 2006). According to these reasons, the layered perovskite oxides, $K_2Ln_2Ti_3O_{10}$, is an interesting and attractive photocatalyst to degrade the pollutants into aqueous solutions.

2.3.3 Parameters Affecting Photocatalyst Efficiency

Degradation of the pollutants takes place on the surface of the photocatalyst. It has been reported that some parameters are affecting the degradation efficiency. Light intensity, pH of the solution, initial concentration of the pollutants, type of catalyst, photocatalyst, presence of ions and surface properties of semiconductors can be cited (Subramanianet al., 2000). According to the literature reviews, pH and light intensity are selected as variables and their effects are investigated by changing the values.

2.3.3.1 Light Intensity

Photocatalytic degradation rate depends on light intensity (Curco et al., 2002). The degradation mechanism is started with the absorption of light by the photocatalyst. The photon energy of the incident light must be greater than the band gap energy of the semiconductor. That is why, as mentioned before, activation wavelength is an important parameter for the photocatalytic degradation reactions. The photocatalysts which are used must have wide band gap to be activated in UV light. Electromagnetic radiation of sun contains 7% of UV which strikes the atmosphere and it decreases during the penetration of the atmosphere (Tek, 2008). According to the literature, photocatalytic degradation is increasing with the increase of the light intensity (Qamar et al., 2002).

2.3.3.2 pH

The pH effect depends on the kind of semiconductor and pollutant. The increase or decrease of pH levels changes the degradation rate. pH controls the surface charge of the photocatalyst. Lower and higher pH values have different effect for degradation mechanism. At lower values, the degradation of pollutants is faster. On the other hand, at higher pH values above 9, degradation rate is also enhanced because of the increase of OH^- anions on the photocatalyst surface (Theurich et al., 1996; Subramanian et al., 2000; Tek, 2008).

2.3.3.3 Particle Size and Concentration of Photocatalyst

The particle size of photocatalyst is an important parameter on photocatalytic activity. If the size of the photocatalys is decreased, surface-volume ratio will be increased and the photocatalytic activity will be increased. That is why; nanosized semiconductors have superior photocatalytic activity than normal sized semiconductors (Tek, 2008). The optimum photocatalyst concentration must be determined to avoid excess catalyst and to obtain optimum phase (Bakal, 2014).

2.3.3.4 Surface Properties of Semiconductor

The surface properties of semiconductor photocatalyst affect the photocatalytic degradation mechanism. The surface morphology and structure of sol-gel thin films and heat treatment process can modify structure leading to an increased photocatalytic activity (Yu et al., 2000). For these reasons, material characterization processes was precisely performed.

2.4 The Synthesis Methods of Photocatalysts: Sol–Gel Thin Film Coating

The sol-gel method is an effective method to produce various functional materials in which particle size, porosity, thin layer thickness and structures can be controlled and successful applications have been achieved. The development of materials by using sol-gel technology has attracted attention owing to the nanostrucured materials which the attention of modern scientists is focused (Dimitriev et al., 2008). The sol-gel method is a process to generate colloidal nanoparticles from liquid phase. Sols and gels are two forms of matter that exist naturally (Pierre, 1998).

Sol-gel technology has a wide application area to produce ceramics, glass and composite materials. The sol-gel process includes the evolution of inorganic materials including metal oxide solutions, metal powders, nitrates, hydroxides and oxides through the formation of a colloidal suspension (sol) and gelation of the sol in a continuous liquid phase (gel). Sol is the suspension of the colloidal solid particles at liquid phase. The dispersion forces of these particles are greater than the gravity. Colloids are smaller than 500 nm and cannot be seen in normal optical microscope. Gel is a composition from the precipitation of the colloidal particles and it is a phase between solid and liquid. The precursors for synthesizing these colloids generally formed of a metal or metalloid element (Suneel, n.d).

If inorganic sols and gels can be obtained by various methods, they are often directly synthesized from chemical reactants dissolved in a liquid medium. The chemical reactants which contain the cation M (metal) present in the final inorganic sol or gel is called the *chemical precursor*. Its chemical transformations are complex

and involve a competition at the molecular level between the reaction responsible for the formation of open structures and the one leading to dense solid. Those same reactions are responsible for the controlled dispersion of dense colloidal particles in a sol or their agglomeration into a gel (Pierre, 1998). The steps of sol-gel method can be explained as follows:

Alkoxide Hydrolysis and Condensation Reaction: Metal alkoxides are the precursors for the formation of the sol. The general formula of the metal alkoxides is $M(OR)_n$ in which M is the metal compound which will be covered and R is the alkyl group. The affected factors of the hydrolysis rate are the amount of water, catalyst, solvent concentration and temperature (Evcin, n.d). Hydrolysis can be expressed by deprotonation of M cation. After the hydrolysis, condensation reactions occurs (Bakal, 2014).

Polymerization: This step is the dispersion of the sediment by solvent. A sol is prepared for the dispersion of the sediment. As a result of the polymerization, the viscosity of the solution increases (Suneel, n.d).

Aging of the gel: Until the gel transforms into a solid mass, expulsion of solvent from gel pores occurs. The affected factors are pH, temperature, reaction time, concentration, aging temperature and aging duration (Suneel, n.d).

Gelation: This is an important step to create gel form without creating any cracks. The drying of the gel is to remove the excess of the solvent (alcohol, water). The gel is shrinking and the solid resultant contains high amount of pore. This solid is called xerogel (Suneel, n.d).

Drying: This is reached by calcinations of the monolith at temperatures up to 800^oC (Suneel, n.d). Drying is irreversible transformation of the gel which is composed of a solid and liquid (Bakal, 2014).

Sintering: After the densification and decomposition of the gels at high temperatures (T>800^{o}C), the sintering process occurs. The remaining organic materials are volatilized. The dense material is obtained after the sintering process (Suneel, n.d).

Sol – gel method includes dip, spray and spin coating techniques. Through these techniques, $K_2La_2Ti_3O_{10}$ films of high photocatalytic activity can be produced (Merabet et al, 2009). In this study, spin coating method is used to produce thin films. Spin coating is a cheap and faster method to produce homogeneous layers and includes 4 main steps. Firstly, an excess amount of the solvent (fluid) is placed on the substrate. Secondly, the rotation is occurred at high speed in order to spread the fluid by centrifugal force. The film thickness can be adjusted by changing the rotation speed, the rotation time, and the concentration of the solution which is used. Thirdly, the fluid is slowly becoming thin. And finally, solvent evaporation occurs and the coating becomes thin (Politi, 2014). Figure 2.8 demonstrates schematically the spin coating technique.

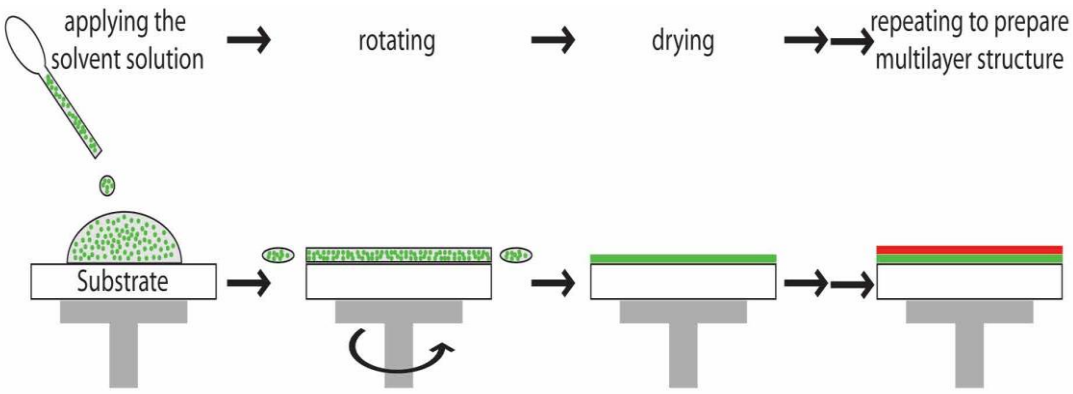

Figure 2. 8 A schematic demonstration of spin coating technique (Anonym, n.d).

CHAPTER THREE
MATERIAL AND METHOD

3.1 The Purpose of the Study

The aim of this study is to produce layered perovskite potassium lanthanum titanate $K_2Ln_2Ti_3O_{10}$ (Ln= La, Nd, Gd, Sm, Dy) by using spin coating to investigate photocatalytic activity. For this reason, K, La and Ti based precursor materials, solvent and chelating agent solutions were prepared. With this aim, pH values, turbidity and rheological characteristics of the prepared solutions were examined before the coating process. Si(100) as silica glass substrates were used for coating. To obtain suitable process regime and to identify the structure of $K_2Ln_2Ti_3O_{10}$ (Ln= La, Nd, Gd, Sm, Dy), Thermogravimetry-Differential Thermal Analyzer (DTA – TG) and Fourier Transform Infrared (FTIR) machines were used. In order to make structural and morphological analysis of thin films, X-Ray Diffraction (XRD) and Scanning Electron Microscopy (SEM) were used respectively. The optical properties were determined by the help of a UV-Vis spectrophotometer.

The photocatalytic degradation processes were realized to degrade phenol, methylene blue and cyanide. Light intensity, pH and initial concentration are important parameters and have direct effect on the reaction rate. In this context, the three parameters are selected and by changing the values, the degradation efficiencies were investigated. Photocatalytic degradation experiments were carried out in a solar box ATLAS SUNTEST CPS+ which is simulating natural radiation (Figure 3.1). The light source of Atlas Suntest Cps+ has a vapor xenon lamp (300 nm $< \lambda <$800 nm) and the power can change between 250 and 765 W/m^2. To determine the photocatalytic effectiveness of phenol, methylene blue and cyanide, specific UV absorbance (SUVA), total organic carbon (TOC) and dissolved organic carbon (DOC) tests were carried out according to the treatment results. To achieve more precise results and to make a comparison, the same experiments were observed for blank solutions.

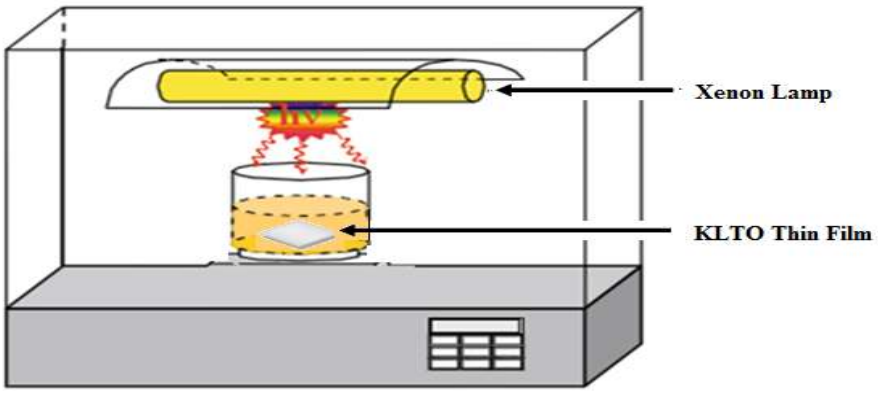

Figure 3.1 A schematic representation of the photoreactor (based on Merabet et al, 2009).

3.2 Materials

Chemical materials which were used to produce solutions, gels, powders and thin films can be seen in Table 3.1. To prepare $K_2Ln_2Ti_3O_{10}$ (Ln= La, Nd, Gd, Sm, Dy) thin films, Si(100) and silica glass were used as substrates. All of the precursor materials were alkoxide materials. Solvent and chelating agent were used to dissolve precursors.

Table 3.1 Precursors, solvent and chelating agent for KLTO based thin film production

Chemical Type	Chemical Name	Chemical Formula	Purity	Molecular Weight (gram)
Precursors	Lanthanum (III) 2,4 pentanedionate hydrate	$C_5H_{21}LaO_{6.}xH_2O$	-	436.24
	Potassium 2,4 pentanedionate hydrate	$C_5H_7KO_{2.}xH_2O$	97 %	138.21
	Titanium (IV) isopropoxide	$C_{12}H_{28}O_4Ti$	95 %	284.23
	Dysprosium (III) 2,4 pentanedionate hydrate	$C_{15}H_{21}DyO_6$	99.9%	459.83
	Neodymium (III) 2,4 pentanedionate	$C_{15}H_{21}NdO_6$	99.9%	441.57
	Samarium (III) acetylacetone hydrate	$C_{15}H_{21}SmO_6$	99.9%	447.69
	Gadolinium (III) acetylacetone hydrate	$C_{15}H_{21}GdO_6$	99.9%	454.57
Solvent	Propionic acid	$C_3H_6O_2$	99 %	74.08
Chelating agent	Glacial acetic acid (GAA)	CH_3COOH	99.9 %	60.05

3.3 Production Process

3.3.1 Substrate Preparation

Si(100) was used as a substrate materials. The crystalline structure of Si(100) was cubic-textured and the surface was polished. To obtain desired size for coating process, Si(100) was cut by using Logitech APD Annular & Peripheral Diamond Saw. Prior to the coating process, silica glass substrates, Si(100) were cleaned 1:1 acetone-water medium with ultrasonic cleaner.

3.3.2 Solution Preparation

In order to obtain effective thin films, homogenous solutions must be prepared. Solution preparation steps to produce thin films were summarized as shown in Figure 3.2. To investigate how the dopant amount changes mechanical, physical and photocatalytic properties in a controlled manner, production at three different dopant concentrations was performed.

At this stage potassium lanthanum titanate solutions and powders were produced to use in the production of thin films. As shown in the block flow diagram, Figure 3.2, to prepare the *Ln* (La, Nd, Gd, Sm, Dy) homogenous solutions, the La, Nd, Gd, Sm and Dy based powder precursors were mixed with solvent (propionic acid), chelating agent (glacial acetic acid) and titanium (IV) isopropoxide till the La, Nd, Gd, Sm and Dy based chemical materials were dissolved. To reduce the surface tension, toluene was added to the Nd solution. After this process, K compound was putted in the beaker, and the mixing process continues as far as K is dissolved. The temperature of sublimation of the potassium is low. That is why, the nimiety of K compound was added according the literature (Wang et al., 2010). The solution was mixed with ultrasonic mixer at 25^{o}C until they became transparent approximately 2 hours. The homogenous solution of potassium lanthanum titanium oxide in stoichiometric ratios was stirring to obtain gel form. At the end of this process, transparent solutions were prepared for powder production and were dried over

magnetic stirrer and xerogels were obtained. The obtained xerogels were subjected to heat treatment.

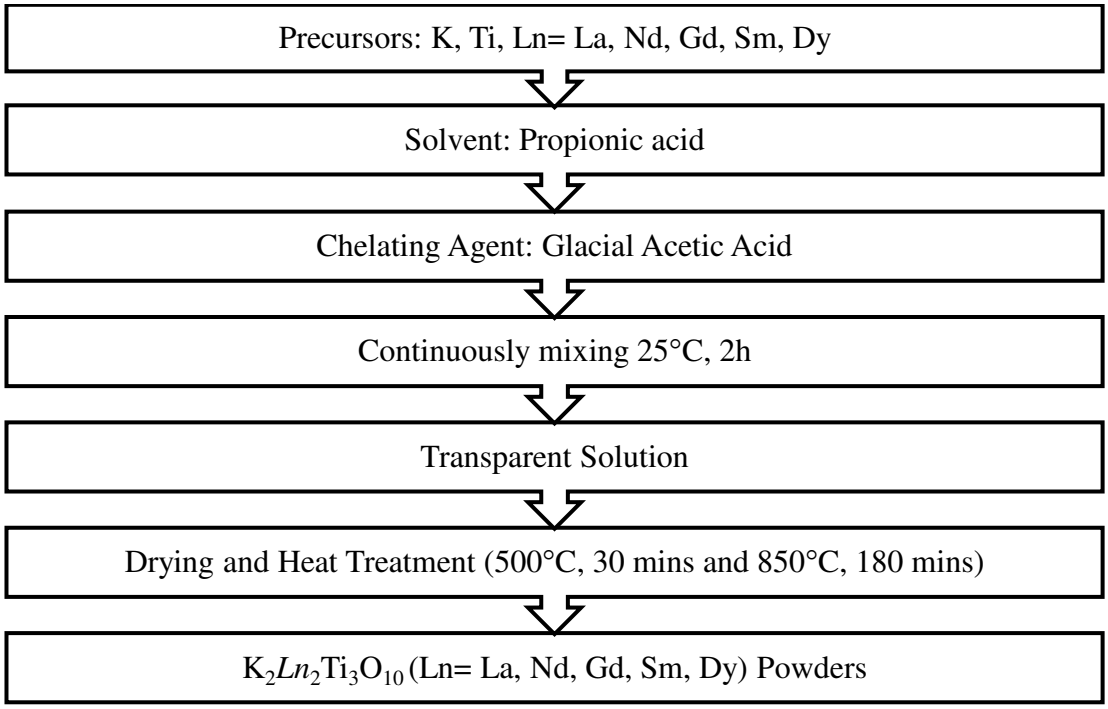

Figure 3.2 Production flow chart for powder.

3.3.3 Preparation of Thin Films

The following step was the coating procedure of the thin films. Before the coating application, substrates were cleaned with acetone bath by ultrasonic cleaner. Spin coating technique were used to obtain uniform thin films. Excess amount of a solution is placed on the substrate. The rotation is occurred at high speed in order to spread the fluid by centrifugal force. The film thickness can be adjusted by changing the rotation speed, the rotation time, and the concentration of the solution which is used. Spin coater machine is used for spin coating. Prior to the coating operation, glass substrates were kept for 15 minutes at room temperature in air by waiting in ultrasonic bath with acetone solution for cleaning purposes. Rotation is continued until the fluid spins off the edges of the substrate and desired thickness is achieved. The thickness of the films depends on the concentration of the solution and solvent. The schematic representation of spin coating is shown in Figure 2.8. Figure 3.3

demonstrates thin film flow chart. After the production of the powders, the powders were mixed by the addition of propionic acid till the powders dispersed and this process was carried out into ultrasonic mixer. General preparation steps for the production of thin films were summarized in Figure 3.4. Stoichiometric ratios used to prepare the thin films of $K_2Ln_2Ti_3O_{10}$ (Ln= La, Nd, Gd, Sm, Dy) are shown in Table 3.2.

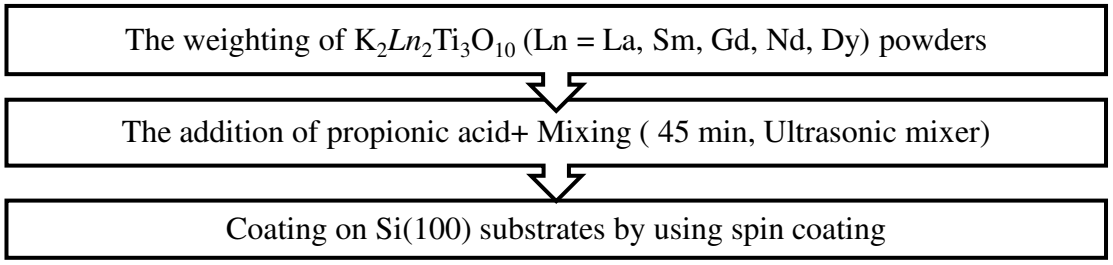

Figure 3.3 Thin film production flow chart.

Table 3.2 Stoichiometric ratios used to prepare the powder samples

Name of the material	**Quantity (g)**	**The quantity of Propionic acid (ml)**
$\mathbf{K_2La_2Ti_3O_{10}}$	0.658	10
$\mathbf{K_2La_{1.9}Sm_{0.1}Ti_3O_{10}}$	0.660	10
$\mathbf{K_2La_{1.5}Sm_{0.5}Ti_3O_{10}}$	0.720	10
$\mathbf{K_2La_{1.1}Sm_{0.9}Ti_3O_{10}}$	0.944	10
$\mathbf{K_2La_{1.9}Dy_{0.1}Ti_3O_{10}}$	0.660	10
$\mathbf{K_2La_{1.5}Dy_{0.5}Ti_3O_{10}}$	0.671	10
$\mathbf{K_2La_{1.1}Dy_{0.9}Ti_3O_{10}}$	0.680	10
$\mathbf{K_2La_{1.9}Gd_{0.1}Ti_3O_{10}}$	0.661	10
$\mathbf{K_2La_{1.5}Gd_{0.5}Ti_3O_{10}}$	0.668	10
$\mathbf{K_2La_{1.1}Gd_{0.9}Ti_3O_{10}}$	0.676	10
$\mathbf{K_2La_{1.9}Nd_{0.1}Ti_3O_{10}}$	0.640	10
$\mathbf{K_2La_{1.5}Nd_{0.5}Ti_3O_{10}}$	0.636	10
$\mathbf{K_2La_{1.1}Nd_{0.9}Ti_3O_{10}}$	0.600	10

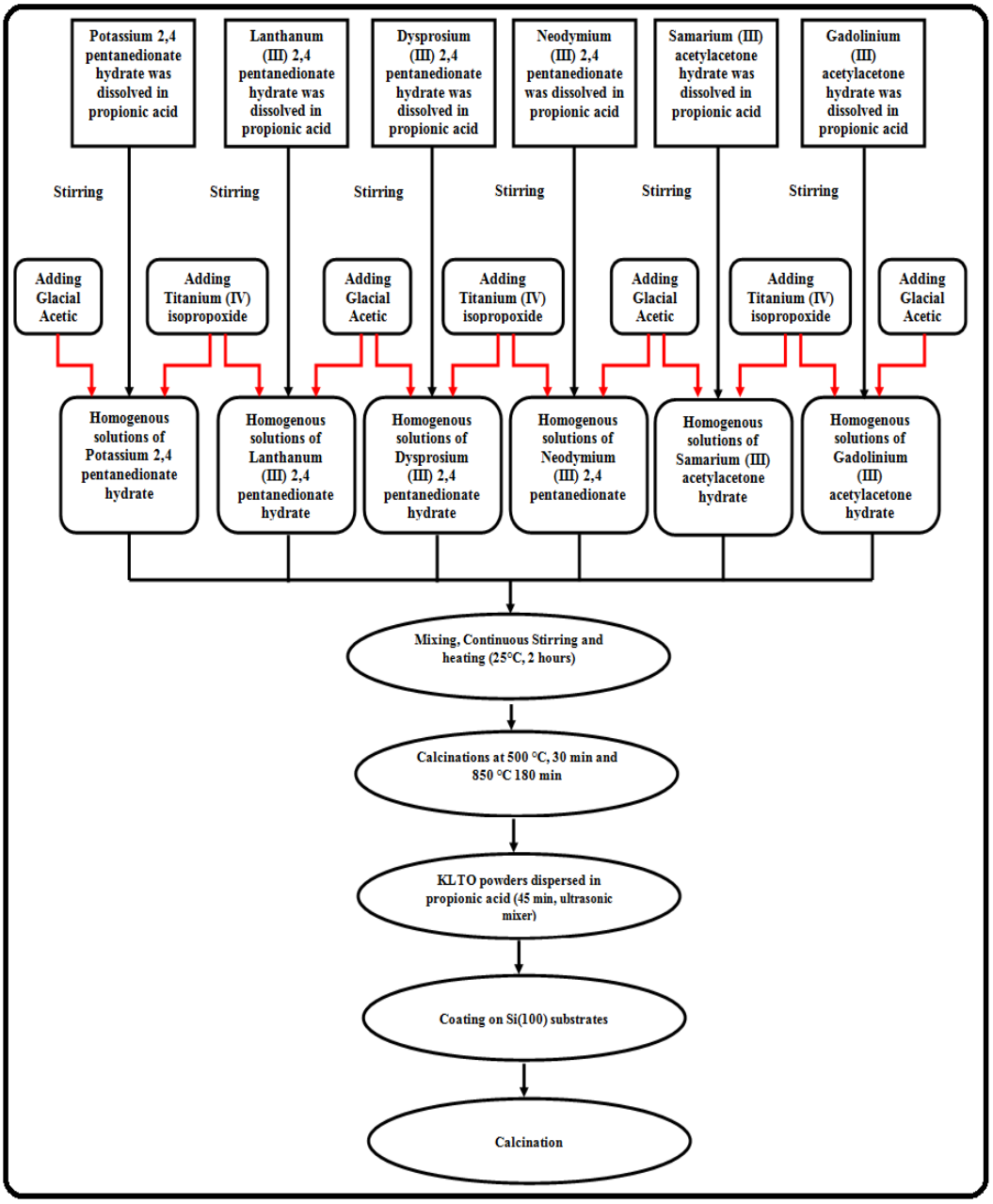

Figure 3.4 The flow chart for production of surface coatings.

In order to increase the harmony between the layers, the coating samples were produced by coating 8 times and XRD analysis was made. To make multilayer coating production, coated Si(100) plates were dried at 300°C for 10 min and at 500°C for 5 min in air after each layer was coated. And heat treatment was applied which can be shown in Figure 3.5. Coating times and speeds were given in Table 3.3. The last step of the spinning vaporized the volatiles and removed the residuals in 10 seconds.

Table 3.3 Spin coating parameters

Step	Time (s)	Rotational Speed (rpm)
1	5	100
2	10	500
3	15	3000
4	10	0

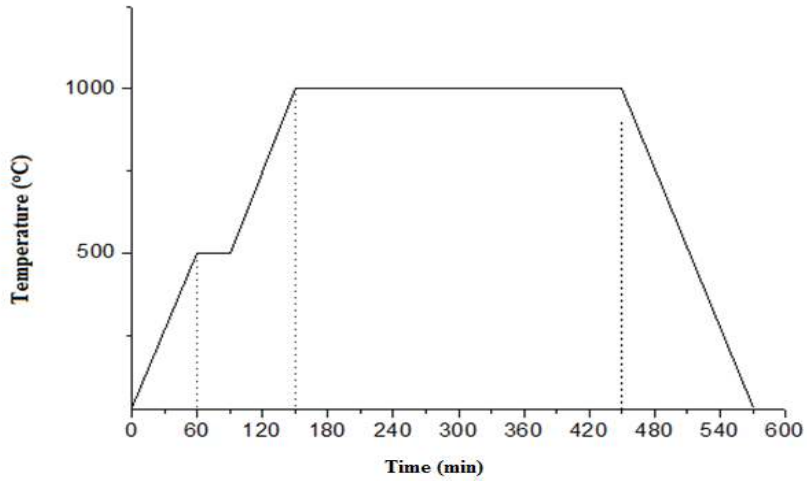

Figure 3.5 Heat treatment regime.

In order to find the ceramic phase, temperature related to this phase was determined. For this reason, thermal behaviors were determined by using DTA/TG equipment. These data were required for the heat treatment of the films. The image of KLTO thin film is given in Figure 3.6.

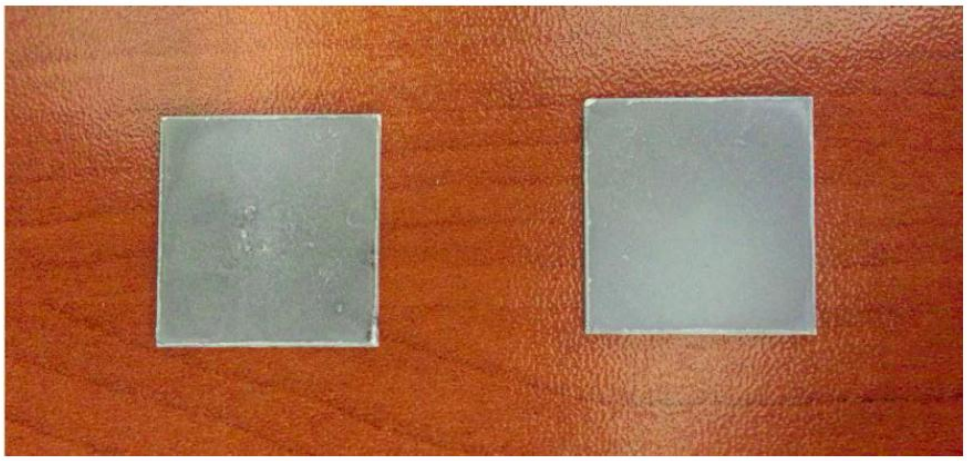

Figure 3.6 KLTO thin films on Si (100) substrate.

3.4 Characterization

The main issue which is focused was the structure of semiconductors and its applications. But now, the characterization and the composition of materials will be explained. To identify if the method is successful when a material is fabricated in the laboratory condition, some techniques are used to investigate the structure. That is why; in this stage, the techniques which are available to characterize KLTO compounds will be explained.

3.4.1 Solution Characterization

The sol-gel process is an advanced process to produce gel, polymeric crystalline or glass phase in wide range from liquid form. The characterization directly affects the ultimate film stoichiometry. The aim is to produce the liquid form carefully. Therefore, to identify solution characteristics which affect thin films, turbidity, pH values, contact angle and rheological properties of the prepared solutions were measured.

3.4.1.1 Turbidity Measurement

Turbidity gives the optical characteristics of suspended particles in an aqueous solution. The unit of turbidity is nephelometric turbidity unit (ntu). The aim of the turbidity test is to understand the solubility of the powder which is added to the solution before the coating process. Turbidity tests were made by standard VELP TB1 Model Turbidity Meter. Test range is between 0 and 1000 ntu. If the turbidity is approached to 0, the powder based precursors are fully dissolved. But if the turbidity is near to 1000 ntu, particles suspends. In order to find transparent solutions, turbidity value should be near to 0 ntu.

3.4.1.2 pH Measurement

The pH values of the prepared solutions are measured by using Mettler Tolede electrode pH meter to understand the solution conditions including basic or acidic characteristics. The pH is an important factor of gelling and gel polymeric structure.

3.4.1.3 Contact Angle Measurement

The contact angle is measured between a solid surface and a liquid surface which is in touch. It depends on cohesion forces (the relative strength of the affinity between the own molecules of liquid) and adhesive forces (the affinity between liquid and solid). This measurement quantifies the wettability of a solid surface via Young equation. If the cohesion forces are bigger than adhesive forces, the angle between solid and liquid increases. So, bigger contact angle means that the affinity between liquid and solid is less and the contrary of this is exist. If contact angle is less than 90^{o}, liquid soaks the cape, if it is bigger than 90^{o}, wetting does not exist. Contact angle is important to make a good coating. Contact angle measurements of the solutions were realized by using Contact Angle Meter - CAM 100.

3.4.1.4 Rheological Measurement

The rheological properties including, viscosity, gel point, shear stress and modulus of elasticity were determined by using CVO 100 Digital Rheometer. Viscosity is the main controller of the film thickness. Because of this, the solutions which will be used in thin films should be in low viscosity, in other words it should be diluted. The viscosity and shear values are important to characterize the gelation behavior. The viscosity values of KLTO solutions were analyzed at 300 Hertz frequency and 25°C at single shear mode.

3.4.2 Process Characterization

To decide optimum temperatures for heat treatment condition, material characterization tests are needed. For this reason, Differential Thermal Analysis

(DTA – TG) and Fourier Transform Infrared Spectroscopy (FTIR) analysis were performed.

3.4.2.1 Differential Thermal Analysis/Thermogravimetry (DTA/TG)

This method is used to determine the suitable process regime and the reaction type of intermediate temperature products. This method gives information about the thermal stability, phase formation, reactions type, and suitable heat treatment. DTA/TG analyses were examined under O_2 flowing for xerogels by using Shimadzu DTG-60H Model DTA-TG device. DTA/TG analysis were examined. Prepared xerogels were examined from 25 to 1200°C at heating rate of 10°C/min in oxygen atmosphere.

3.4.2.2 Fourrier Transform Infrared (FTIR)

In order to determine how the chemical bonds of the fabricated gels change before the transformation from solution to crystalline state (powder) and to determine the organic components of the samples, FTIR analysis is carried out. In varying temperatures (100, 200, 300, 400, 600, 800 and 1000^{o}C) and after 15 minutes in air, FTIR absorption spectra were measured in the ranges of 4000 to 400 cm^{-1} at room temperature (25°C). According to the measurement, %transmittance vs. wavelength and %absorbance vs. wavelength curves was obtained. FTIR spectrum of $K_2Ln_2Ti_2O_{10}$ (Ln=La, Nd, Gm, Sm, Dy) samples were carried out by using Thermo Scientific Nicolet i-S10 device.

3.4.3 Film Characterization

3.4.3.1 X – Ray Diffraction (XRD)

To identify existing phase of the thin films which obtained by using sol – gel method, XRD analyze were performed with using Thermo-Scientific ARL X'tra diffractometer. The measurements were realized with Cu tubes at voltage of 45 kV and current of 44 mA by using CuKα radiation (λ = 0.15405 nm). The ray beams diffracted into three dimensional crystal lattice of the material and as a result, the

diffraction patterns were obtained. The crystal structure was identified by comparing with the standard patterns.

3.4.3.2 Scanning Electron Microscopy (SEM)

To analyze and determine the surface qualities, topographies and surface morphologies of the thin films on Si (100) substrates, JEOL JSM – 6060 Scanning Electron Microscope was used. Accelerated electrons under high voltage were sent on the substrates to obtain images on scanning electron microscopy. Subsequently, the interaction between electrons and substrate atoms was examined according to the micro structure images.

3.4.3.3 X-Ray Photoelectron Spectroscopy (XPS)

X-Ray photoelectron spectroscopy is using to do the elemental analysis, thus the chemical or electronic state of the surface elements, detection of chemical contamination of KLTO based surfaces can be performed. The principal of XPS is to send X rays to the material and to measure kinetic energy of the ejected electrons and the number of ejected electron from surface between 1-10 nm of depth. Surface chemistry of KLTO thin films was determined by Thermo-Scientific K - Alpha XPS.

3.4.3.4 Roughness and Thickness Measurement

Atomic force microscopy (AFM) provides high resolution of three dimensional surfaces by the help of needle which is sharpened to the atomic size. This microscopy provides 3 D display of the surface to determine the roughness and to obtain two and three dimension image. Because of the high surface roughness of the thin films, the surface roughness could not be realized by using AFM. Instead, surface profilometer measured the surface profile of the films to quantify the roughness and thickness. The thickness of the films was determined by using Ambios Technology XP-2 Stylus Profiler.

3.4.3.5 Mechanical Tests

Hardness is a characteristic ability of the material to resist penetration or abrasion by other bodies. Elastic modulus defines as a measure of the material's resistance to being deformed elastically. To determine the mechanical properties of the produced coatings, nanoindentation test was applied. As a result of the test, the hardness of the coatings which change under varying loads, elastic modulus and the penetration depth were determined by using IBIS (Fischer-Cripps Laboratories, Australia) nanoidentation. Before the experiments, contact area A_c and contact depth h_c were calibrated by using fused silica samples. Adhesion strength of the coatings was determined by using scanning scratch tester (IBIS Fischer-Cripps Laboratories, Australia). According to the test results, critical force was defined as adhesion strength.

3.5 Photodegradation Experiments with Synthetic Wastewaters

Phenol (C_6H_5OH), methylene blue ($C_{16}H_{18}ClN_3S.3H_2O$) and cyanide (CN) were selected as the pollutants which must be removed. There is a specific object for the pollutant selection. Each pollutant represents a different chemical component including organic, azo dye and inorganic. Phenol (99%) and cyanide (97%) were available from Merck Millipore and methylene blue (97%) was obtained from Sigma-Aldrich. Initial concentration of each substance was selected as one of the variables which affect the degradation rate and chosen according to the literature. Initial concentration of phenol was selected 10 mg/l at pH of 7. 10^{-5} M of methylene blue was selected for experiments and three different pH conditions including 3 (acidic), 7 (neutral) and 10 (basic) were examined. The pH of the solutions was adjusted by using H_2SO_4 or NaOH. Initial concentration of cyanide was selected 100 mg/l at pH 10. Degradation experiments were examined at 250 W/m^2 and 750 W/m^2.

3.5.1 Experimental Set-up

All experiments were performed in a flatbed Xenon exposure system, Atlas Suntest CPS+ reactor. The main goal is to degrade phenol, methylene blue and

cyanide with maximum degradation rate by selecting optimum pH and light intensity condition. The beakers with a volume of 25 ml which include 2x2 cm photocatalyst were put into the reactor. The light source produces heat and to conduct experiment at controlled temperature and to prevent the evaporation of wastewater, a glass cap was placed above the beakers. ATLAS Suntest CPS+ is equipped with 1 x 1500 W air-cooled Xenon lamps. It involves 560 cm^2 exposure area. Specific informations about the reactor can be shown in Table 3.4 and Figure 3.7 demonstrates the schematic diagram of the reactor. The details about the apparatus are edited from Suntest CPS/CPS+ operating manual.

Table 3.4 Properties of SUNTEST CPS+

SUNTEST Features	**CPS+**	
Air – cooled Xenon lamps	1500 W	
Minimum Guaranteed Lamp Life (at one sun level)	1500 Hours	
Physical Dimension (WxDxH)	78 cm x 35 cm x 35 cm	
Direct Setting and Control of Irradiance in the wavelength range	300 - 800 nm/Lux; or 300-400 nm/340 nm	
Footprint	100 cm x 95 cm	
Floor Weight	29 kg (64 lb)	
Specimen rack capacity	560 cm^2	
Specimen tray size in cm x cm	28 x 20	
SUNSENSIV sensor for controlling irradiance at 300-800nm / Lux	Daylight Filter	Window Glass Filter
	250-765 W/m^2	250-765 W/m^2

Xenon lamps are a specialized type of gas discharge lamp by passing current through a gas under pressure. The current which flows between the lamp's electrodes is an arc and it ignites the gas. At xenon lamp technology, an electric light is produced a light by passing electricity through ionized xenon gas at high pressure by using Xenon gas. A bright light is producing and it imitates natural sunlight. The main difference between the Xenon and other lamp types like mercury lamp is the light spectrum. Xenon lamp emits all wavelengths through the visible zone (400 nm to 700 nm). This zone is approximately corresponding to the natural daylight. On the

other side, mercury-vapor lamp shows strong peaks through the visible zone. Three different mercury lamps exist. Low pressure mercury lamps emit 253 nm to 185 nm. It is UV light source. In medium mercury lamp, the wavelength is between 200 and 600 nm. It is UVA (around 315 nm - 400 nm) or UVC (around 200 nm - 280 nm). The wavelength range of high pressure mercury lamps are 248 to 1014 nm. Xenon lamp is used in this study to imitate natural daylight.

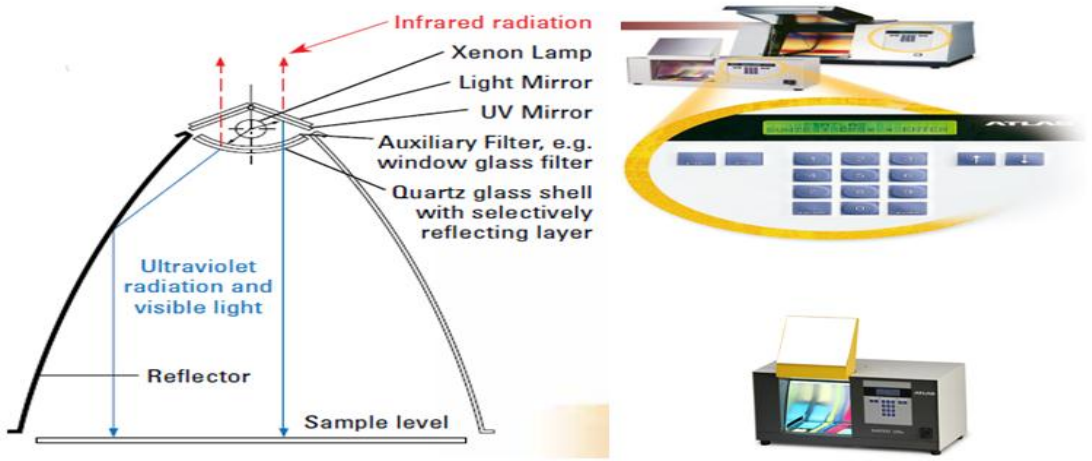

Figure 3.7 ATLAS Suntest CPS+ images (Suntest CPS/CPS+ Operating Manual).

3.5.2 Properties of the Pollutants

3.5.2.1 Properties of Phenol

Phenol is a member of organic compounds characterized by a formula of C_6H_5OH. It is a white crystalline mass which turns red or pink if it is exposed to air or light. In most of the industries and daily life, phenolic compounds have a widespread using area and it is widely distributed as pollutant in waste water bodies. Table 3.5 shows the properties of phenol. This compound causes a huge damage on aquatic life and human health. The treatment of the phenol is very difficult. This study has focused on the photocatalyst with using the photocatalytic principles and the factors which influence the photocatalytic rate and the reaction kinetics. Figure 3.8 demonstrates the structure of phenol.

Theoretically, 8.3 gram of phenol is dissolving in 100 ml of water. If phenol comes into contact with heat, flame or oxidizers, it is combustible. When it is heated, it discharges toxic fumes. Phenols are very toxic and when it is in liquid or vapor form and it has a burning taste and an acrid odor (Baycan, 2005). Phenols are considered as priority pollutants because it is harmful at low concentrations. And in addition, phenols are classified as hazardous pollutants. Owing to the higher toxicity and higher oxygen demand (theoretically, 2.4 kg O_2/kg phenol), US Environmental Protection Agency (EPA) and World Health Organization (WHO) accept phenol in the first pollutant group. The toxic problem is occurring under 1 μg/l concentrations and it changes the taste and creates odor problem in drinkable water (Chen et al., 2009). It is very dangerous owing to the stability; high toxicity and it has a carcinogenic character (Abdalwahab et al., 2009).

Table 3.6 prepared to choose an optimum initial concentration, pH value and duration of experiment among the photocatalytic method studies. pH value of the phenol solution was adjusted to 7, initial concentration of phenol was selected 10 mg/l and 5 hours of degradation time was chosen according to the literature studies.

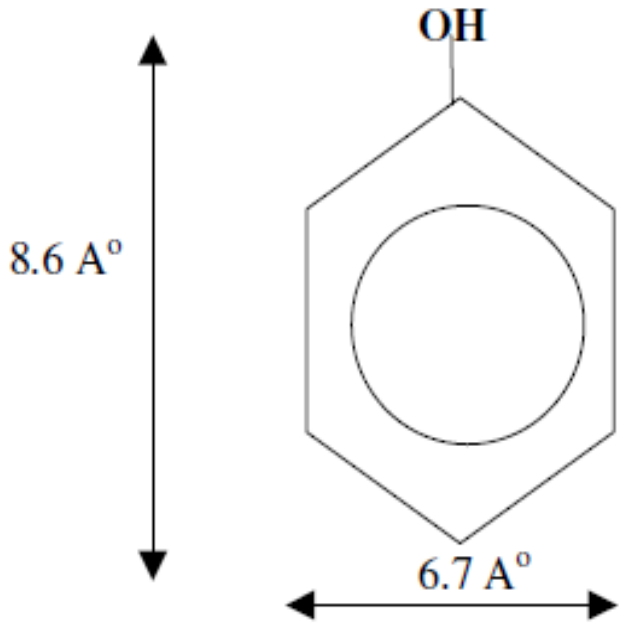

Figure 3.8 Dimensions of phenol (Molva, 2004).

Table 3.5 Properties of Phenol (Merck Millipore)

Properties	**Values**
Chemical formula	C_6H_5OH
Molar mass	94.11 g/mol
Ignition temperature	595 °C
Solubility	84 g/l (20°C)
Melting point	40.8 °C
Density	1.06 g/ cm^3 (20 °C)
Flash point	81 °C
pH	5
Conversion factor	1 ppm=3.85 mg/m^3
Discharge limit of phenols in inland water	1 mg/l (Water pollution control regulation Turkey, 2004)
Accepted concentration for drinking water	0.001 mg/l (WHO,1994)
Sources	Coking, synthetic rubber, plastics, paper, oil refineries, petrochemical, ceramic, steel, conversion process, phenolic resin industries, gasification, coke production, pharmaceuticals, pesticides, fertilizers, construction, automotive, produce synthetic resins, dyes, biocides (Abdelwahab et al., 2009) Phenol is used as indoor products in different areas. It becomes a disinfectant, slime-killing agent , additive in medicines (Metcalf&Eddy, 2003)
Health effect	Phenol irritates the skin, eyes, and mucous membranes in humans after acute (short-term) inhalation or dermal exposures. The symptoms of the long - term exposure are anorexia, progressive weight loss, diarrhea, vertigo, and salivation, a dark coloration of the urine, and blood and liver. According to the animal studies, animals which exposed to phenol by oral way have some findings as the reduction of fetal body weights, growth retardation, and abnormal development in the offspring of animals (U.S. EPA 63FR).

Table 3.6 A summary table for the photocatalytic treatment methods of phenol according to the literature

Initial Concentration	The catalyst/ method used	Efficiency %	Reaction time (hour)	pH	Lamp Type	References
75 ppm	Aqueous zinc oxide suspension using solar energy	47	9	5.61	1000 W Xenon Lamp	Pardeshi, & Patil, (2008)
100 mg/l	TiO_2 + UV	76	12		253.7 nm UV lamp	Guo, Ma, & Li, (2006)
$0.5 * 10^{-4}$ mol/l (4.7 mg/l)	TiO_2	30	3		180W medium pressure mercury lamp	Sobczynski, Duczmal, & Zmudzinski, (2004)
$0.75 * 10^{-4}$ mol/l (7.05 mg/l)		25				
$1 * 10^{-4}$ mol/l (9.4 mg/l)						
$1.5 * 10^{-4}$ mol/l (14 mg/l)						
$2 * 10^{-4}$ mol/l (18 mg/l)						
0.13 mM (12 mg/l)	TiO_2 + UV	90	3		400 W high-pressure mercury lamp	Chiou, Wu, & Juang, (2008)
0.71 mM (66.82 mg/l)		42				
100 mg/L	UV/H_2O_2	97.1	5	7	16 W Mercury Lamp	Çatalkaya, Bali, & Şengül, (2004)
100 mg/l	$UV/H_2O_2 + Fe^{2+}$	100	5		16 W Mercury Lamp	Çatalkaya, Bali, & Şengül, (2004)
200 mg/l	Fenton	57	1		8 W Pressure Mercury Lamp	Babuponnu-sami, & Muthukumar, (2012)
	Electro Fenton	89.5				
	Sono – electro – Fenton	100				
	Foto – electro - Fenton	100				

3.5.2.2 Properties of Methylene Blue

Methylene blue (MB) is a type of thiazine, azo and cationic dye and it has large scale utilization in industries. Methylene blue takes place within heterocyclic aromatic and the chemical formula is as $C_{16}H_{18}ClN_3S$. $3H_2O$ (3,7-bis (dimethylamino)-fenazotionium chloride) (Yao & Wang, 2010). At room temperature, it demonstrates a solid dark green and odorless condition. The chemical structure can be seen in Figure 3.9 (Yao & Wang, 2010). Table 3.7 demonstrates the properties of methylene blue. Table 3.7 shows the properties of methylene blue.

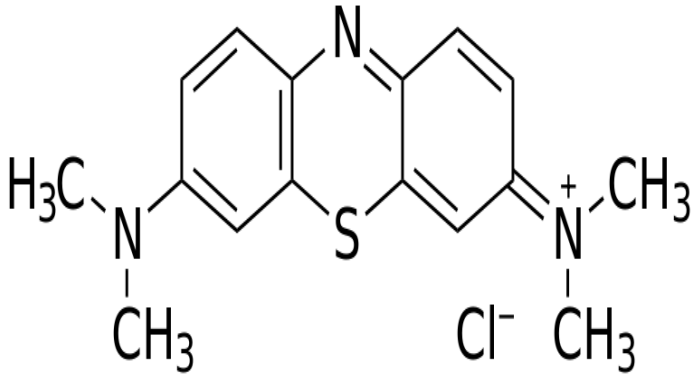

Figure 3.9 The chemical structure of methylene blue (Yao & Wang, 2010).

During the dissolution of methylene blue in water, three absorbances can be seen in the UV - visible beam zone. The absorbance bands are 264 nm, 291 nm and 664 nm, respectively. During the degradation and decolorization experiments of methylene blue 291 nm and 664 nm are mostly using. In this study, 664 nm is chosen to make the analysis in visible radiation (Yao & Wang, 2010).

For the selection of optimum conditions to obtain maximum degradation efficiency, the table below is created. As a result of the Table 3.8, 10^{-5} M initial concentration was examined at pH 3, 7 and 10.

Table 3.7 Properties of methylene blue (Sigma Aldrich)

Properties	**Values**
Chemical formula	$C_{16}H_{18}ClN_3S.\ 3H_2O$
Molar mass	373.90 g/mol
Ignition temperature	No data available
Solubility in water	40 g/l (20°C)
Melting point	190 °C
Density	1.0 g/ cm^3 (20 °C)
Flash point	15 °C
pH	No data available
Conversion factor	1 ppm=15.29 mg/m^3
Discharge limit of methylene blue	As principle, Turkish Standards Institute is forbidden to release the materials which cannot degrade biologically (Su Kirliliği Kontrolü Yönetmeliği - Water pollution control regulation Turkey, 2004)
Sources	The areas of usage are coloring the papers, hair dye, fabric dying and wool dying. The applications of methylene blue are mostly from textile industries. It is commonly used in dyestuff applications and as a redox indicator. For this reason, it is the major pollutant of textile industry wastewaters (Yao & Wang, 2010).
Health effect	Methylene blue is not very toxic, but it can cause some damages. If it is inhaled, the complication of breathing appears in short - term. If it is given orally, some symptoms appear as a combustible sense, a heartbeats increase, going into shock, sickness, vomiting, diarrhea, gastritis, cyanosis, jaundice, and quadriplegia and cell necrosis.

Table 3.8 A summary table for the photocatalytic treatment methods of methylene blue according to the literature

Initial Concentration	The catalyst/ method used	Efficiency %	Reaction time	pH	Lamp Type	References
0.20 g/l (5.3×10^{-4} M)	TiO_2 particle sol at 663 nm	0	0 min	2	UV light (mercury vapor lamp, 253.7 nm) 40 W	Yao and Wang (2010)
		36.1	60 min			
		56	100 min			
		92.3	160 min			
		0	0 min	7		
		12	60 min			
		15.6	100 min			
		19.9	160 min			
		0	0 min	9		
		20	60 min			
		25	100 min			
		30	160 min			
3.12×10^{-5} M	P-25 Degussa TiO_2	100	360 min	6.5	UV-LED (light emitted diodes)	Tayade, Natarajan & Bajaj, (2009)
	Blank	12				
100 mg/l	Photocatalytic reactor	80		9		Rizzo, Koch, Belgiorno, & Anderson, (2006)
	TiO_2 coating (9×6 cm^2) 40 ml at 660 nm	80	5 h		10 W/m^2	Tschirch et al., 2008

3.5.2.3 Properties of Cyanide

The presence of free cyanide including HCN and CN^- and complex cyanide in water bodies affect aquatic life at low concentration and the presence of cyanide is toxic to human body (Osathaphan et al., 2008). Both organic and inorganic forms of cyanide are available. (-1) valence form of carbon and nitrogen (CN) is an important group in inorganic carbon chemistry. Cyanide is weaker than air. The specific weight is 0.687 g/ml. That is why, the half - life of cyanide in the air is very long. But it can

disperse in the air and becomes non toxic. It is using for varying purposes. The little doses have lethal effect. The lethal effect in liquid phase is estimated 1 - 3 mg (Gümüş, 2001).

Different treatment methods such as physical, chemical, adsorption and oxidation are used to treat cyanides; however other treatment methods except oxidation give high concentrated product in which toxic cyanides still exist (Osathaphan et al., 2008). Especially, certain forms of cyanide for example hydrogen cyanide (HCN) are very toxic. That is why, acceptable limits of cyanide in water are very low (Dzombak et al., 2005). Therefore cyanide in wastewater must be in alkali condition. Thus, since excess amount of HCN gas respiration is harmful for human body, pH was adjusted to 10 to avoid the evaluation of HCN gas. The chemical structure can be seen in Figure 3.10. Table 3.9 demonstrates the properties and the health effect of cyanide.

Figure 3.10 The chemical structure of cyanide

Table 3.9 Properties of cyanide (Merck Millipore)

Properties	**Values**
Chemical formula	CN^-
Molar mass	26.007 g/mol
Material used	KCN
Molar mass	65.12 g/mol
Solubility in water	716 g/l (25°C)
Melting point	634 °C
Density	1.52 g/cm^3 (20 °C)
Flash point	Non-flammable
pH	11-12
Conversion factor	1 ppm=1. 06 mg/m^3
Drinking Water Quality Standard EPA	0.2 mg/l
Sources	Cyanide discharge is produced from several industries as gas production, electrolysis coating (NaCN), gold and silver mining (NaCN), metal plating (alkali and metal cyanide), pesticides, oil refinery, coal gasification, pharmaceutical and electroplating processes (Osathaphan et al., 2008).
Health effect	Cyanide is acutely toxic to humans. Liquid or gaseous forms of hydrogen cyanide and alkali salts of cyanide can enter into the body by inhalation, ingestion, and absorption through the eyes and skin. Lower doses can be transformed to thiocyanide (SCN) during the period of 20 minutes and 1 hour by an enzyme in liver and released by urinary tract. But the higher doses have lethal effect. The lethal dose for HCN is 50 mg, for sodium and potassium salts is 200 - 300 mg. If 0.2 - 0.3 mg/l cyanide is inhaled by air, it kills immediately. If 0.13 mg/l is inhaled, the lethal effect reveals after 1 hour. 0.02 - 0.03 mg are harmless (Vij, 2008).

The table below (Table 3.10) shows a comparison of photocatalytic methods and the effectiveness of these processes. The effect of various parameters on cyanide

degradation such as the initial concentration of cyanide in wastewater, pH and the light intensity were examined to select optimum values for variables. As a result of the literature review, initial concentration of KCN solution was selected 250 mg/l and CN^- concentration was automatically 100 mg/l according to the stoichiometry. 26 g/mol of cyanide is included in 65 g/mol KCN solution. To determine 100 mg/l cyanide, 250 mg/l KCN solution was used. 4 hour of reaction time was examined into Atlas Suntest CPS+ reactor.

Table 3.10 A summary table for the photocatalytic treatment methods of cyanide according to the literature

Initial Concentration	**The catalyst/ method used**	**Efficiency %**	**Reaction time**	**pH**	**Lamp Type**	**References**
100 ppm	Degussa P25 TiO_2 photooxidation	96	350 min	11.5	150 W medium pressure mercury lamp	Aguado et al. (2002)
100 mg/l KCN	$AgInS_2$ nanoparticles	35	35 min	10.5	Fluorescent lamp (150 W) 450 nm	Aazam (2013)
	0.5 wt % Pt/$AgInS_2$ nanoparticles	40				
	1.0 wt % Pt/$AgInS_2$ nanoparticles	50				
	1.5 wt % Pt/$AgInS_2$ nanoparticles	80				
	2.0 wt % Pt/$AgInS_2$ nanoparticles	100				
100 mg/l KCN	0.10 wt % Au/CdS nanoparticles	60	40 min	10.5	Fluorescent lamp (150 W) 450 nm	Aazam (2014)
	0.15 wt % Au/CdS nanoparticles	82				
	0.20 wt % Au/CdS nanoparticles	98				
	0.25 wt % Au/CdS nanoparticles	100				

3.5.3 Photocatalytic Tests

Photocatalytic degradation experiments of phenol, methylene blue and cyanide were carried out in a solar box; ATLAS SUNTEST CPS+ which is simulating natural radiation to evaluate the photocatalytic activity of the coatings. The light source was a vapor xenon lamp and the wavelength range of the light is between 300 nm and 800 nm. The light intensity can be adjusted from 250 to 765 W/m^2. The size of KLTO photocatalyst was selected as 2 cm x 2 cm. The volume of solutions for each beaker was arranged as 25 ml. Thin film coating samples were immersed in the phenol, methylene blue and cyanide solutions. To prevent the evaporation of the wastewater, a glass cap was placed above the beaker. The experimental design and setup for phenol, methylene blue and cyanide removal using KLTO/Si samples were shown in Figure 3.11. For the adjustment of phenol, methylene blue and cyanide concentrations in the prepared solutions, required amount of sulphuric acid or sodium hydroxide was added to obtain desired pH values. pH was controlled with a pH meter electrode. Experiments were performed separately for each pollutant. Blank solutions (without photocatalyst) were performed for each set of experiments. Sampling took place 5 hours for phenol degradation, 3 hours for methylene blue degradation and 4 hours for cyanide degradation. To understand the effect of light intensity, 250 and 750 W/m^2 was performed in solar box.

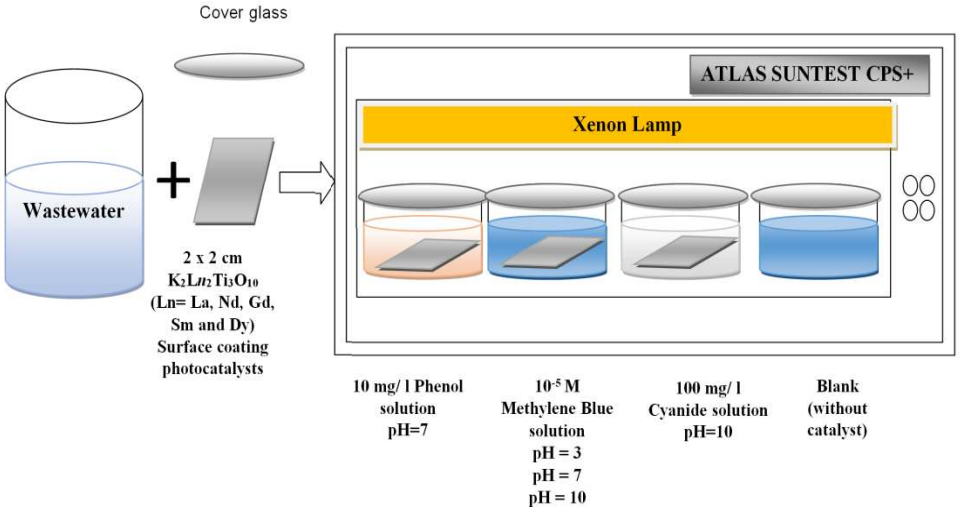

Figure 3.11 Experimental setup.

The samples were analyzed immediately to avoid any reaction. Experimental standard methods can be shown in Appendix. In addition to the degradation efficiencies, Specific Ultraviolet Absorbance (SUVA), Total Organic Carbon (TOC) and Dissolved Organic Carbon (DOC) were analyzed.

Synthetic industrial wastewaters were prepared as follows:

- To create 10 mg/l phenol (Merck Millipore, 99-100.5%) solution, 10 mg of phenol was weighting out with using analytic balance. 10 mg/l phenol was completed with 1 liter of pure water. To provide the homogeny mix, 15 minutes of stirring was observed with using magnetic mixer.
- 10^{-5} M methylene blue (Sigma-Aldrich, 97%) solution was prepared by measuring 0.03199 g of metylene blue powder. The degradation efficiencies of the wastewaters were measured by using Shimadzu UVmini-1240 spectrophotometer. The maximum UV-Vis absorption at wavelength was 664 nm.
- To produce 100 mg/l cyanide initial concentration, 250 mg/l potassium cyanide (Merck Millipore, 97%) solution was prepared by weighting out 250 mg of potassium cyanide. 250 mg potassium cyanide poured over 1 liter of pure water. To provide the homogeny mix, 15 minutes of stirring was performed with using magnetic mixer.

3.5.4 Specific Ultraviolet Absorbance (SUVA) Test

Specific Ultraviolet Absorbance is identified as the UV absorbance of the water sample at a given wavelength to estimate dissolved organic carbon (DOC) concentration. SUVA tests were performed at 254 nm by using Shimadzu UV-mini 1240 spectrophotometer. Tests were realized with the most effective photocatalyst which is $K_2La_{1.5}Sm_{0.5}Ti_3O_{10}$. In addition, blank solutions were tested. The effect of pH on SUVA was investigated. Dissolved Organic Carbon (DOC) and UV Absorbance (UVA) are necessary to determine SUVA (L/mg-m). DOC is a general

description of the organic material dissolved in water. DOC is harmful when it combines with the water bodies. When DOC is high, chlorinated harmful byproducts can be produced. For this reason, DOC concentration of wastewaters is an important parameter to purify completely the wastewater. So, degradation of the pollutants is not sufficient. Also, DOC, TOC and SUVA tests must be carried out.

The formulas to determine SUVA can be shown below. It is calculated by dividing the UV absorbance of the sample ($cm^{-}1$) by the DOC of the sample (mg/l) and multiplying by 100 cm/m. To determine UVA-the calculated UV absorbance of the sample (cm^{-1}), A is equal to the measured absorbance value at 254 nm and d is the length of the quartz cell path (cm) (EPA, 2005). SUVA specifies the amount of removal required depends on the chemical characteristics of the solution. It is a good predictor of chemical characteristics of DOC (Weishaar et al.).

$$SUVA = \frac{UVA}{DOC} * 100\ cm/m \tag{3.1}$$

$$UVA = \frac{A}{d} \tag{3.2}$$

3.5.5 Dissolved Organic Carbon (DOC) Test

Dissolved Organic Carbon (DOC) is the concentration of carbon remaining a water sample after the filtration of all particulate carbon and inorganic carbon. For DOC tests, the most effective photocatalyst $K_2La_{1.5}Sm_{0.5}Ti_3O_{10}$ in each photocatalyst set were sent to the laboratory to do analysis for 100 ml of wastewater. DOC was analyzed to determine SUVA.

3.5.6 Total Organic Carbon (TOC) Test

Total Organic Carbon (TOC) is a measure of the total amount of organic matter which present in water and it is an indicator of water purification. It is the total amount of dissolved and non dissolved organic carbon. For TOC tests, the most

effective photocatalyst $K_2La_{1.5}Sm_{0.5}Ti_3O_{10}$ in each photocatalyst set were sent to the laboratory to do analysis for 100 ml of wastewater.

3.5.7 Reaction Kinetic Method

Kinetic studies were performed according to the degradation results to determine the reaction order for photodegradation. The degradation curves were taken out and zero, first and second order reaction kinetics were tested. Kinetic studies were carried out for methylene blue.

The components of the equations below can be explained as follow:

Co = initial concentration,
C = the concentration after the reaction time,
t = reaction time (h) and
k_0, k_1 and k_2 = rate constants for zero, first and second order kinetics, respectively (Baycan, 2005; Kargı & Pala, 2009). Table 3.11 demonstrates the equation required to determine the reaction kinetics.

Table 3.11 The equations which required for determining the reaction kinetic

	Zero order kinetics	**First order kinetics**	**Second order kinetics**
Reaction rate	$k_0 = -\frac{dC}{dt}$	$k_1 C = -\frac{dC}{dt}$	$k_2 C^2 = -\frac{dC}{dt}$
After integration	$C = C_0 - k_0 t$	$C = C_0 e^{-k_1 t}$	$\frac{1}{C} = \frac{1}{C_0} + k_2 t$
Conversion degree	$x = \frac{k_0}{C_0} t = \frac{C_{0-C}}{C_0}$	$-\ln(1-x) = k_1 t$	$\frac{x}{1-x} = 1 + k_2 C_0 t$

3.5.8 Factorial Experimental Design

Statistical methods develop the understanding and the description of the variability. And also it gives a framework to describe which variables are the most important or which have the greatest impact on the efficiency.

The factorial statistical experimental design determines the effects of the variables on degradation efficiency and to find the combination of variables which creates maximum degradation efficiency. This methodology investigates the relationship between the variables. It is a model to evaluate the relationship of controlled experimental factors with making some hypothesis guesses. This method includes four steps: guessing the hypothesis, designing the experiments, estimating the data from the experimental analysis, and predicting the response. As a result of this study, the adequacy of the model will be checked (Politi, 2014).

In this study, degradation system of methylene blue was investigated and the effects of pH and light intensity were examined on degradation efficiency. pH and light intensity are chosen as independent variables according to the literature reviews. Degradation efficiency was selected as dependent variable for two factor two replicates factorial design method. Each experiment was tested 2 times and 12 different experiments were carried out in detail for methylene blue.

The pH was selected 3, 7 and 10. On the other hand, light intensity was 250 W/m^2 and 750 W/m^2. The computation was observed by using two replicated ANOVA test. The response function of the degradation efficiency (Y) was correlated with using Minitab Package Software V14 computer program.

CHAPTER FOUR
RESULTS AND DISCUSSION

4.1 Solution Properties

4.1.1 Turbidity Values

Prior the coating process, turbidity tests were carried out to characterize suspended particles in liquid which means that the understanding of the solubility of the precursors which are added into the solution is described. Before the measurement of the solution turbidity values, turbidity meter was calibrated between 0 and 1000 ntu by using formazine. After the calibration process, the prepared solutions putted into the glass tube (25 mm diameter and 50 mm length) and the measurement was performed. Turbidity tests were made by standard VELP TB1 Model Turbidity Meter.

If the turbidity value approaches to 0 ntu, it ensures that powder based precursors are completely dissolved. On the other hand, if the turbidity value approaches to 1000 ntu, it means that the particulate precursors are suspended and not dissolved into solution. The aim is to obtain approximately 0 ntu to produce homogenous thin films. The high turbidity value cannot provide the desired electronic, photocatalytic structure.

The solution turbidity values are shown in Table 4.1. To measure more correctly the turbidity, 5 measurements were completed for each solution and the arithmetic mean of the values was calculated. According to the results, the prepared solutions were homogenizes and transparent. The powder based precursors were almost completely dissolved in solutions.

Table 4.1. Turbidity values of K, *Ln*(La, Sm, Dy, Gd, Nd), Ti - based solutions

Solution	Turbidity (ntu) *
$K_2La_2Ti_3O_{10}$	14.32
$K_2La_{1.9}Sm_{0.1}Ti_3O_{10}$	15.72
$K_2La_{1.5}Sm_{0.5}Ti_3O_{10}$	17.28
$K_2La_{1.1}Sm_{0.9}Ti_3O_{10}$	16.24
$K_2La_{1.9}Dy_{0.1}Ti_3O_{10}$	19.2
$K_2La_{1.5}.Dy_{0.5}Ti_3O_{10}$	18.63
$K_2La_{1.1}Dy_{0.9}Ti_3O_{10}$	21.45
$K_2La_{1.9}Gd_{0.1}Ti_3O_{10}$	21.2
$K_2La_{1.5}Gd_{0.5}Ti_3O_{10}$	19.83
$K_2La_{1.1}Gd_{0.9}Ti_3O_{10}$	17.31
$K_2La_{1.9}Nd_{0.1}Ti_3O_{10}$	17.76
$K_2La_{1.5}Nd_{0.5}Ti_3O_{10}$	28.52
$K_2La_{1.1}Nd_{0.9}Ti_3O_{10}$	35.23

* The mean value

4.1.2 pH Values

The pH values of the solutions are an important factor which affects the formation of three dimensional polymeric structure of the gel during the gelation process. Table 4.2 gives data about pH values of K, *Ln*(La, Nd, Gd, Sm, Dy) and Ti - based solutions. To estimate the solutions pH's, 5 measurements was carried out for each solution and their arithmetic mean was calculated. It can be seen from Tables 4.2 that the pH values of K, La, Ti - based solutions exhibit acidic characteristic. This acidic condition is the consequence of the solvent (propionic acid) and chelating agent (glacial acetic acid).

Table 4.2 pH values of K, *Ln*(La, Sm, Dy, Gd, Nd), Ti - based solutions

Solution	pH *
$K_2La_2Ti_3O_{10}$	3.47
$K_2La_{1.9}Sm_{0.1}Ti_3O_{10}$	4.42
$K_2La_{1.5}Sm_{0.5}Ti_3O_{10}$	4.39
$K_2La_{1.1}Sm_{0.9}Ti_3O_{10}$	4.41
$K_2La_{1.9}Dy_{0.1}Ti_3O_{10}$	3.24
$K_2La_{1.5}.Dy_{0.5}Ti_3O_{10}$	3.23
$K_2La_{1.1}Dy_{0.9}Ti_3O_{10}$	3.21
$K_2La_{1.9}Gd_{0.1}Ti_3O_{10}$	3.12
$K_2La_{1.5}Gd_{0.5}Ti_3O_{10}$	3.08
$K_2La_{1.1}Gd_{0.9}Ti_3O_{10}$	3.09
$K_2La_{1.9}Nd_{0.1}Ti_3O_{10}$	3.91
$K_2La_{1.5}Nd_{0.5}Ti_3O_{10}$	3.92
$K_2La_{1.1}Nd_{0.9}Ti_3O_{10}$	3.93

* The mean value

4.1.3 Contact Angle Measurement

Contact angle describes the wettability characteristics of the solutions. Contact angle directly influences the film quality. The contact angle values of K, *Ln* (La, Sm, Dy, Gd, Nd), Ti - based solutions were determined 4° in general. The results are less than 90°. According to the results, good wettability can expected from solutions for disperse into Si (100) substrate.

4.1.4 Rheological Properties

Viscosity is the main factor to control the film thickness. For this reason, solution's viscosities must be low and diluted. Viscosity is measured as time dependent. Viscosity measurement of K, *Ln* (La, Sm, Dy, Gd, Nd), Ti - based solutions were examined under 300 Hz, 25°C and 2500 seconds. The viscosity-time graphs of the solutions can be seen in figure below. A slight decrease at the viscosity of the solutions is a sign of the polymeric structure due to the formation of complex compounds. As can be shown in figures that the prepared solutions have low

viscosity and therefore it is not a problem for thin film production. Figure 4.1 illustrates module - time graphs.

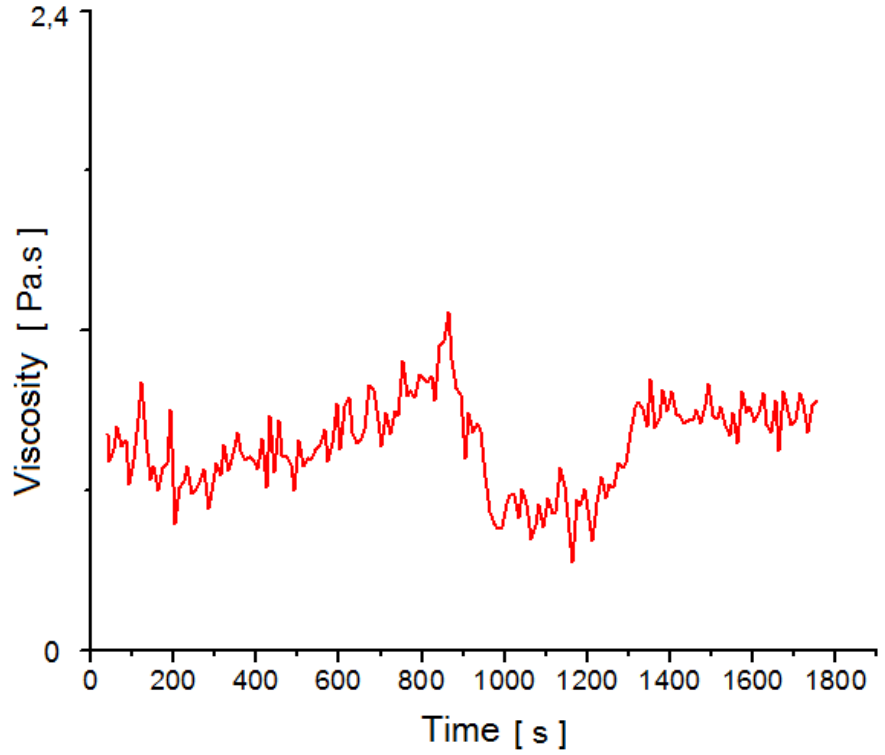

Figure 4.1 Viscosity curve for $K_2La_{1.9}Gd_{0.1}Ti_3O_{10}$.

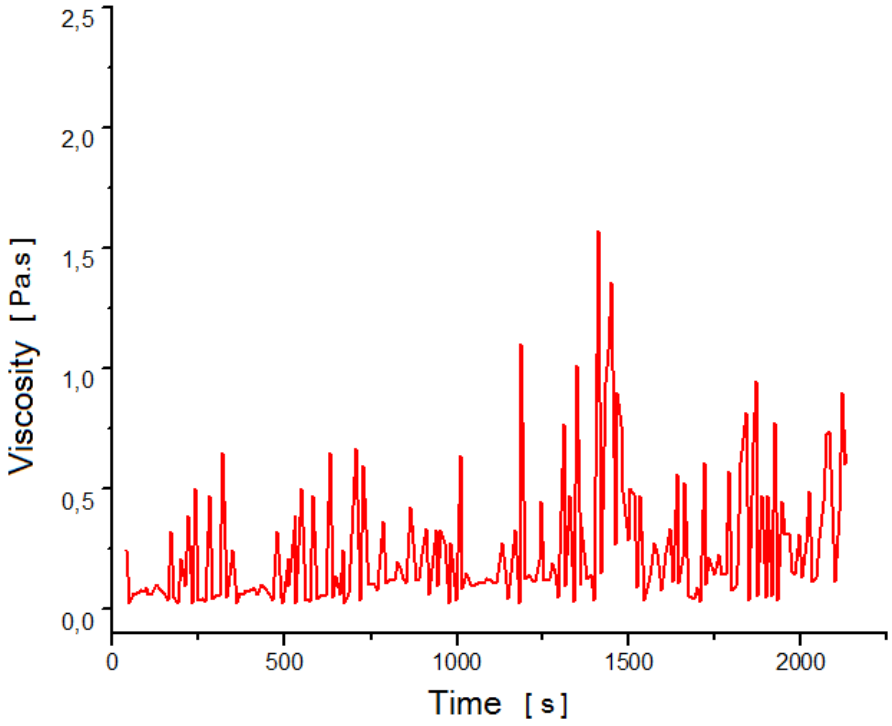

Figure 4.2 Viscosity curve for $K_2La_{1.1}Sm_{0.9}Ti_3O_{10}$.

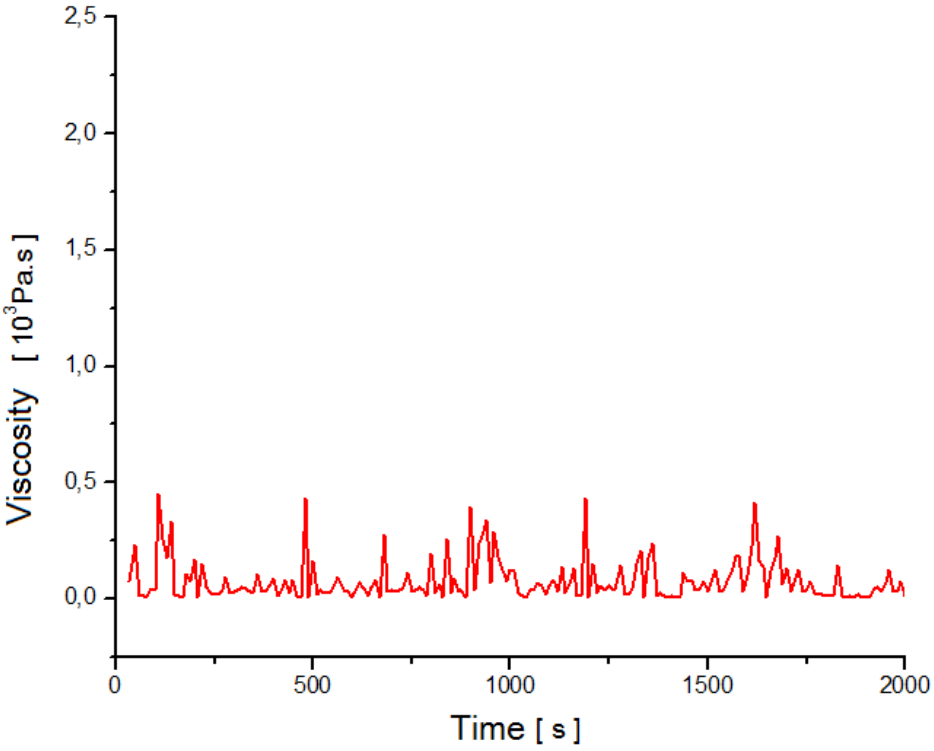

Figure 4.3 Viscosity curve for $K_2La_{1.5}Dy_{0.5}Ti_3O_{10}$.

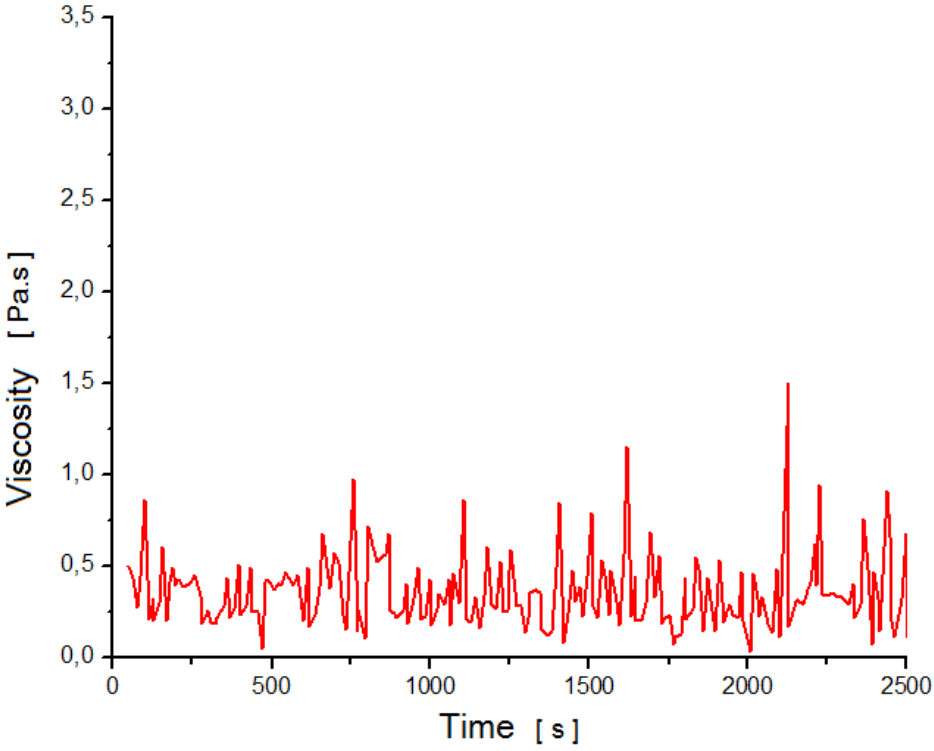

Figure 4.4 Viscosity curve for $K_2La_{1.1}Nd_{0.9}Ti_3O_{10}$.

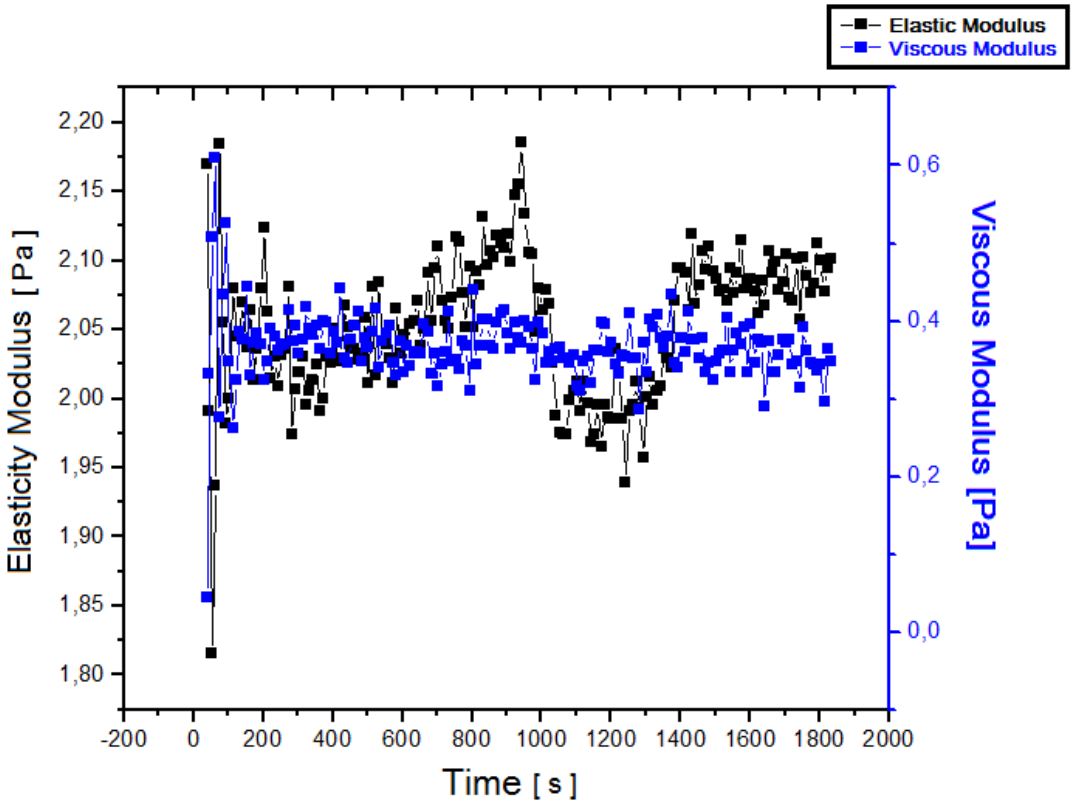

Figure 4.5 Viscosity and elastic curve for $K_2La_{1.9}Gd_{0.1}Ti_3O_{10}$.

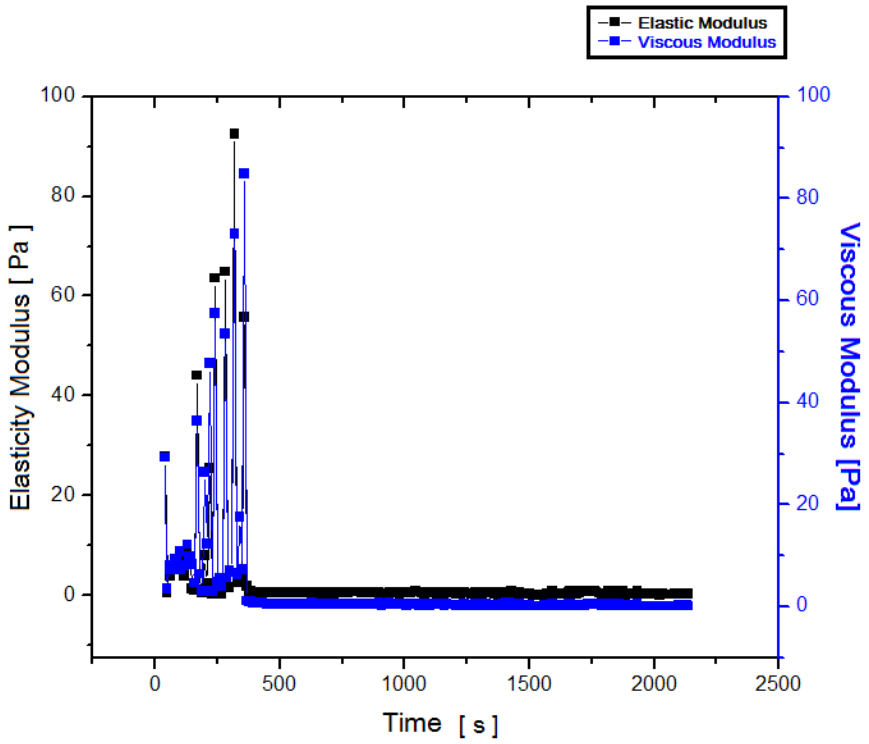

Figure 4.6 Viscosity and elastic curve for $K_2La_{1.1}Sm_{0.9}Ti_3O_{10}$.

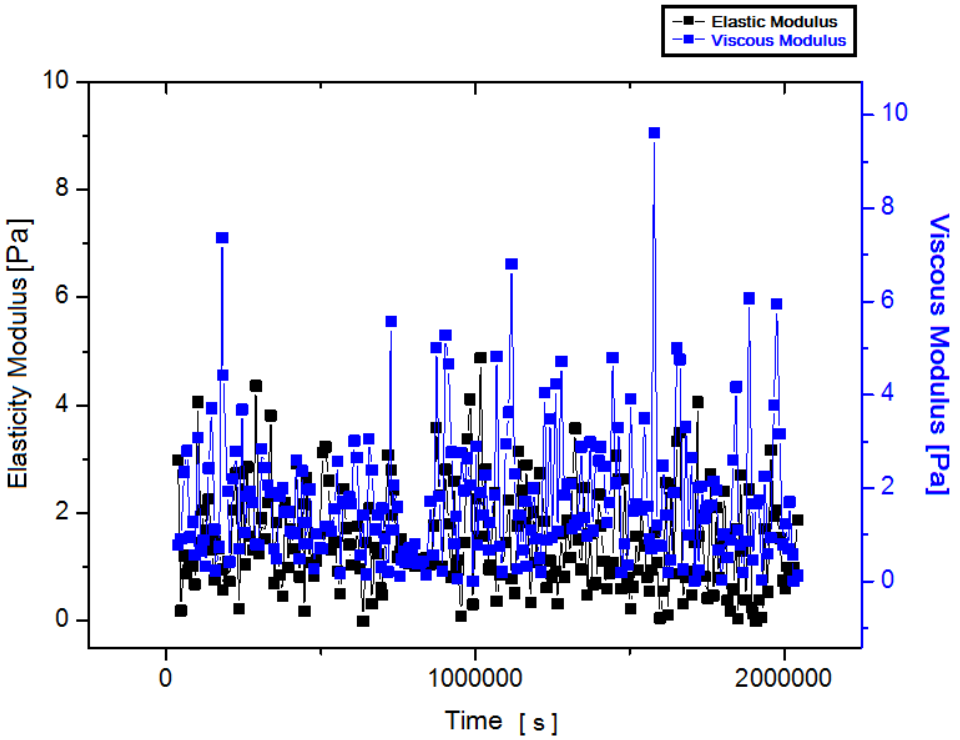

Figure 4.7 Viscosity and elastic curve for $K_2La_{1.1}Dy_{0.9}Ti_3O_{10}$.

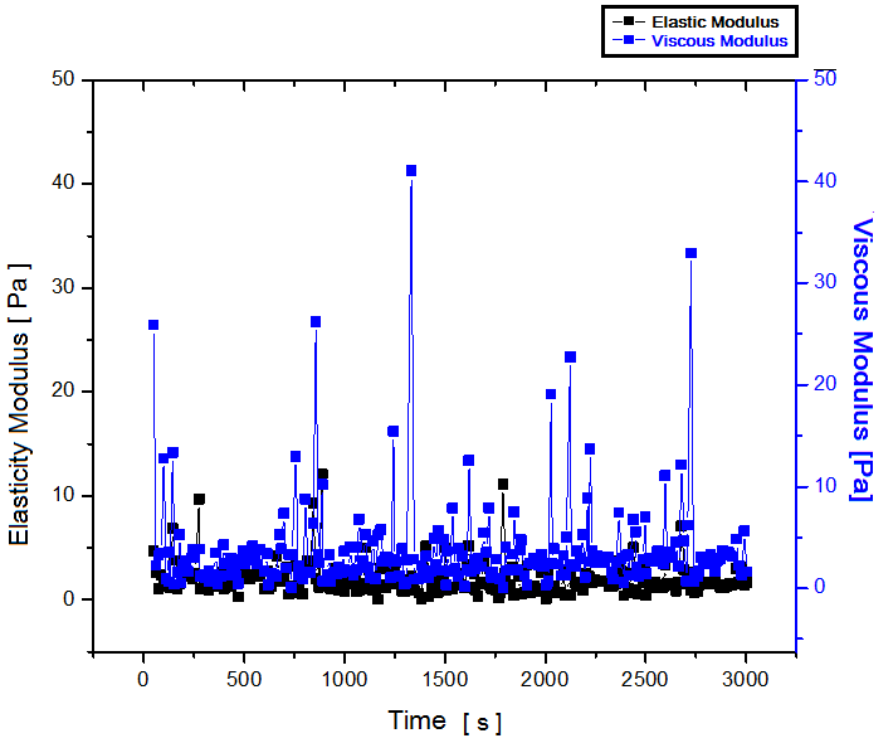

Figure 4.8 Viscosity and elastic curve for $K_2La_{1.1}Nd_{0.9}Ti_3O_{10}$.

4.2 Process Characterization

4.2.1 DTA/TG Analysis

Thin film optimization depends on the reactions which occur during the heat treatment and the beginning and ending temperature of the reactions. For these reasons, differential thermal analysis was analyzed to understand thermal decomposition of K, *Ln* (La, Sm, Dy, Gd, Nd), Ti-based solutions and xerogels during the heat treatment process.

The solutions were dried at 300°C in 30 minutes and xerogels were produced. DTA/TG curve from Figures 4.9 to 4.13 indicates that endothermic and exothermic reactions occur between 25°C and 1200°C. In the first step, the evaporation of volatile organic compounds with the endothermic reactions was occurred. It represents the solvent removal. In second step, the carbon which exists in alcoxide materials, solvent (propionic acid) and chelator (GAA) was burned and created exothermic reaction. Finally, endothermic phase conversion reactions of KLTO phase composed for the formation of ceramic oxides.

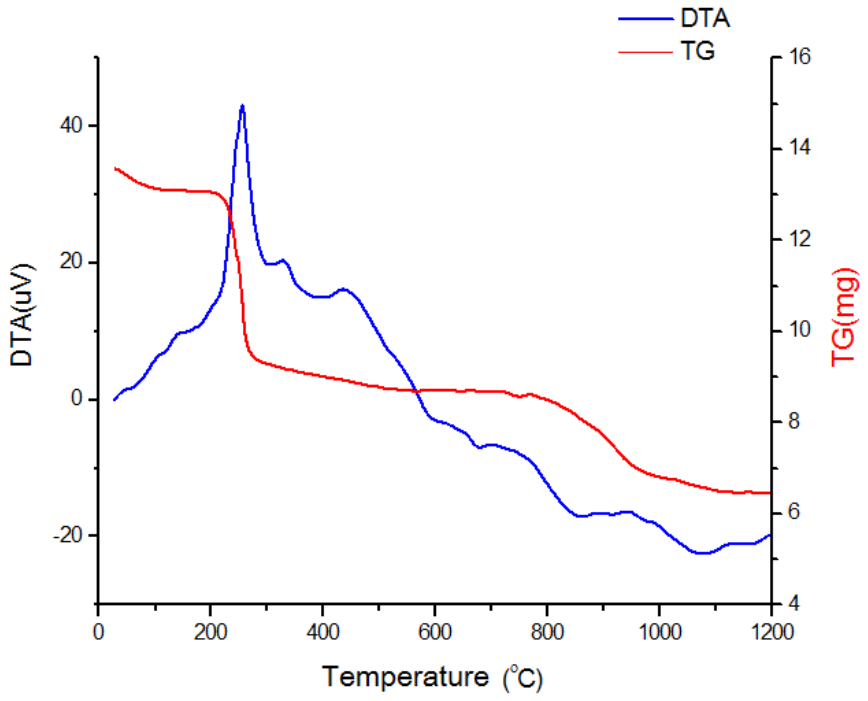

Figure 4.9 DTA/TG curve of $K_2La_2Ti_3O_{10}$ xerogel.

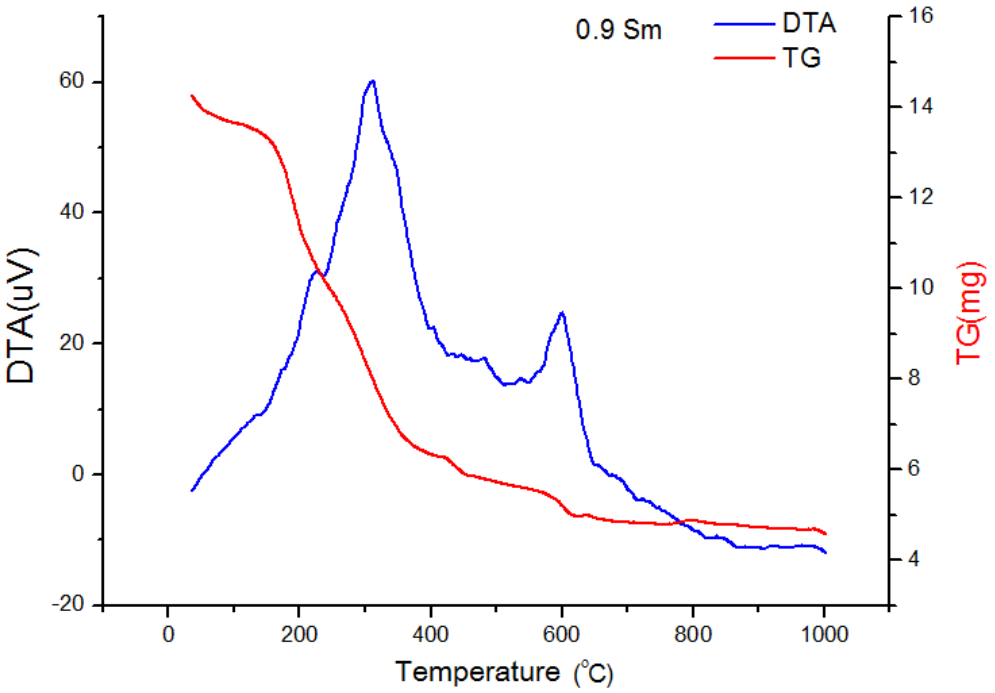

Figure 4.10 DTA/TG curve of $K_2La_{1.1}Sm_{0.9}Ti_3O_{10}$ xerogel.

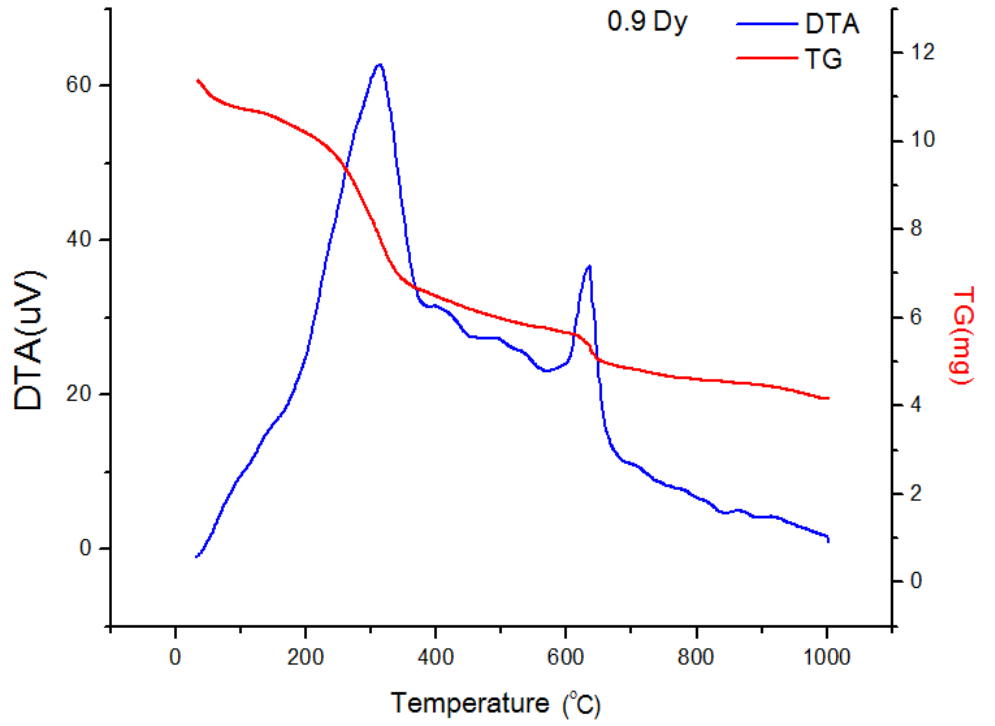

Figure 4.11 DTA/TG curve of $K_2La_{1.1}Dy_{0.9}Ti_3O_{10}$ xerogel.

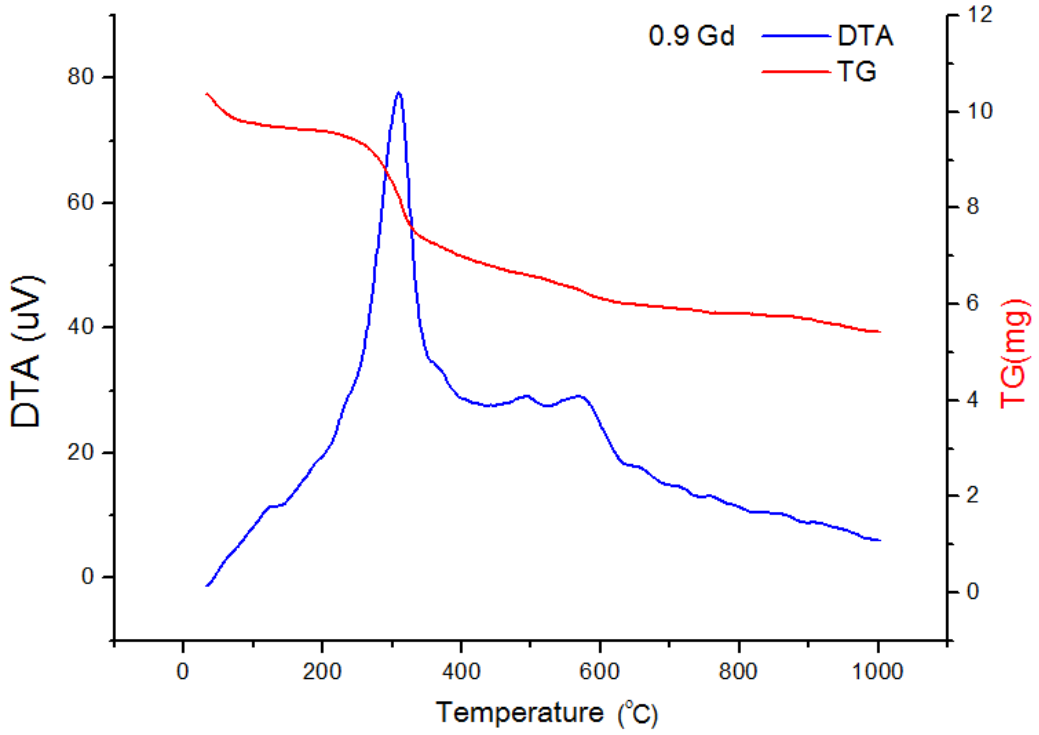

Figure 4.12 DTA/TG curve of $K_2La_{1.1}Gd_{0.9}Ti_3O_{10}$ xerogel.

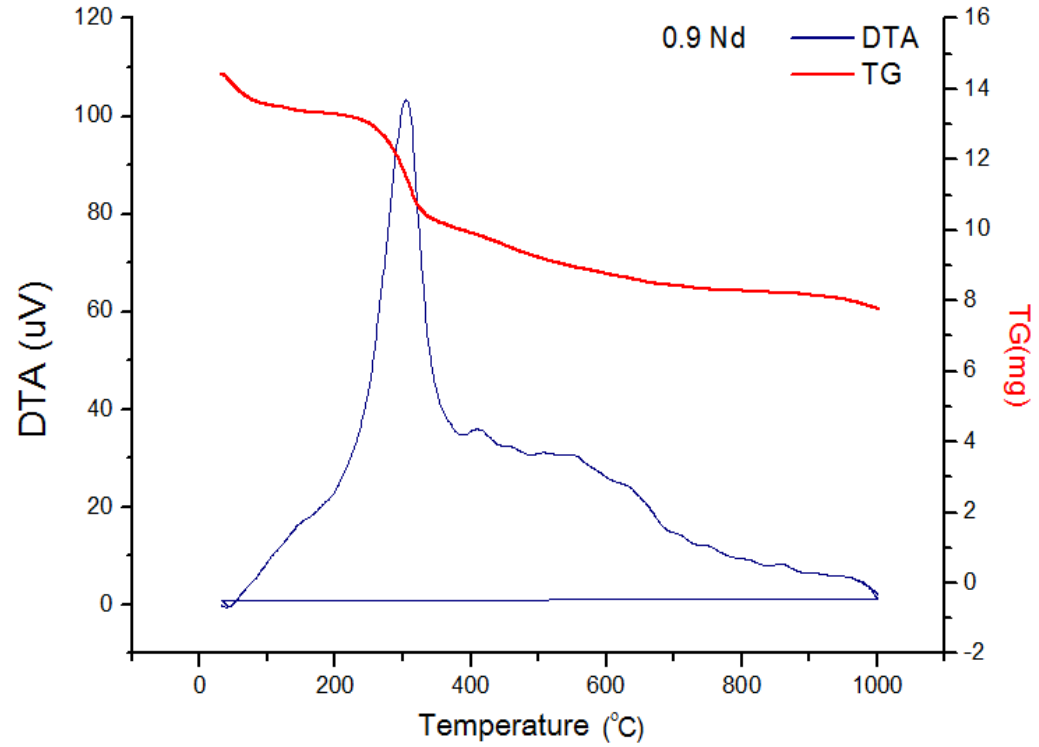

Figure 4.13 DTA/TG curve of $K_2La_{1.1}Nd_{0.9}Ti_3O_{10}$ xerogel.

According to the DTA/TG curve, beginning temperature, ending temperature of the reactions, reaction energy and reaction type were identified. As a result of this analysis, the optimum temperature and detention period were determined between a specific temperature ranges. With respect to these data's thermal treatment phase were given in Table 4.3. The optimum annealing temperature for the phase transformation is determined in 850 °C and 1200 °C. According to the prepared film phase analysis, the optimum conditions were obtained in 1000 °C for 5 hours. This regime was applied for the coatings.

Table 4.3 Thermal treatment analysis phase

Process	**Reaction Temperature Range** (°C)	**Reaction Type**	**Optimum Temperature Value (°C)**	**Foreseen Detention Time**
Drying - Burning organics	27.29 - 500.08	Endothermic Exothermic	500	30 minutes
Phase conversion	850.08 - 1200.07	Exothermic	850/1200	5 hours

4.2.2 FTIR Analysis

FTIR spectra are an important parameter to identify organic groups. The spectrum gives information about the characteristic of bonds between the groups and the decomposition of the organic gels (Bakal, 2014). The absorbance spectrum of the samples was found by drying the solution at different temperatures. Figures between 4.14 and 4.26 give information about the KLTO spectrums at specified temperatures such as 25°C, 100°C, 200°C, 300°C, 400°C, 600°C, 800°C and 1000°C for 15 minutes in air. FTIR data were in accordance with the DTA - TG results. The signals between 400 and 1200 cm^{-1} demonstrated the formation of O-Ti-O characteristics. O-H, C=O and M-OCOO-M bond frequencies are vanished around 800 °C. This situation demonstrated that organic structures and hydroxyls were completely destroyed. The peaks which are appeared by a decrease with increasing temperature band between the ranges of 850 - 900 cm^{-1} are thought to be K, *Ln* (La, Sm, Dy, Gd, Nd), Ti ions related to oxygen bond.

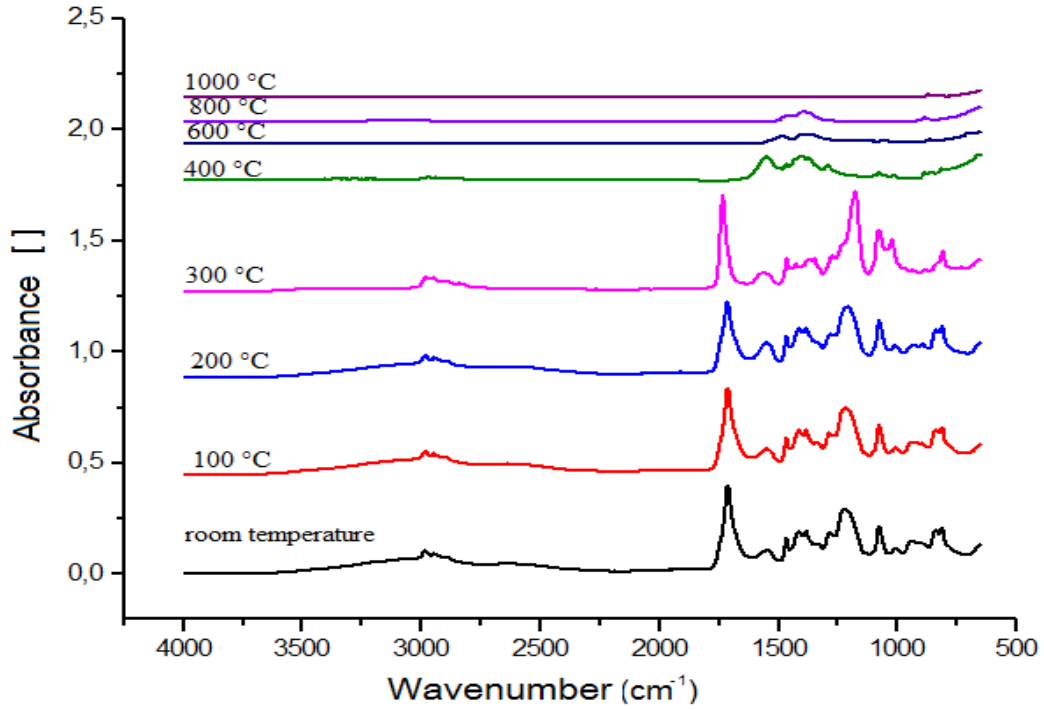

Figure 4.14 FTIR spectra of the $K_2La_2Ti_3O_{10}$ xerogels heat treated at different temperatures.

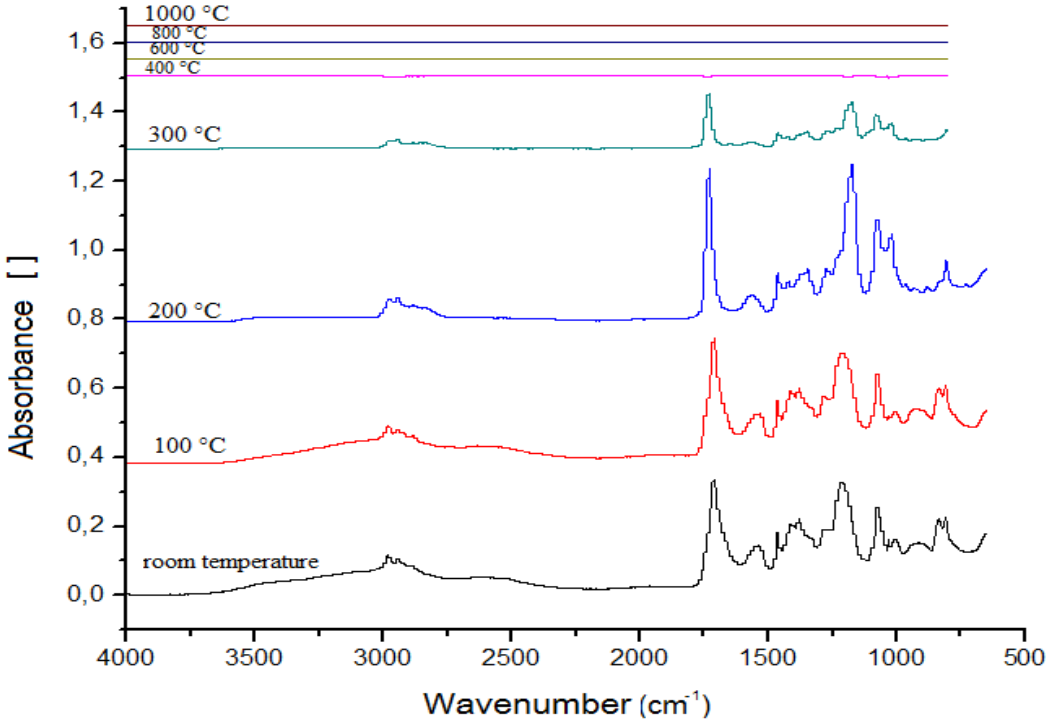

Figure 4.15 FTIR spectra of $K_2La_{1.9}Sm_{0.1}Ti_3O_{10}$ xerogels heat treated at different temperatures.

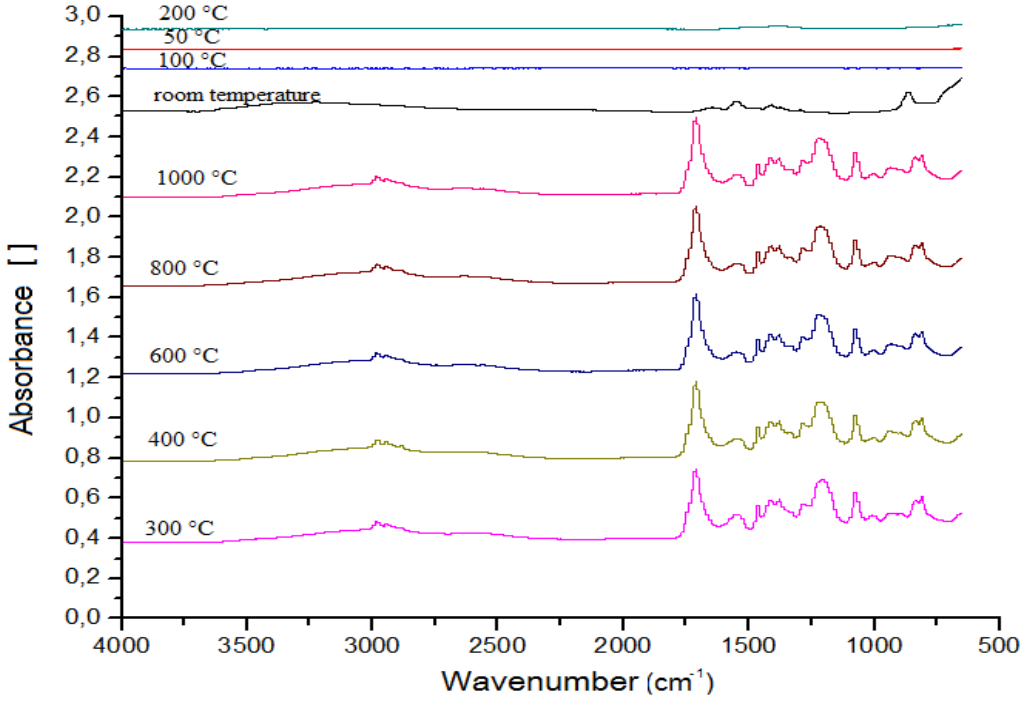

Figure 4.16 FTIR spectra of $K_2La_{1.5}Sm_{0.5}Ti_3O_{10}$ xerogels heat treated at different temperatures.

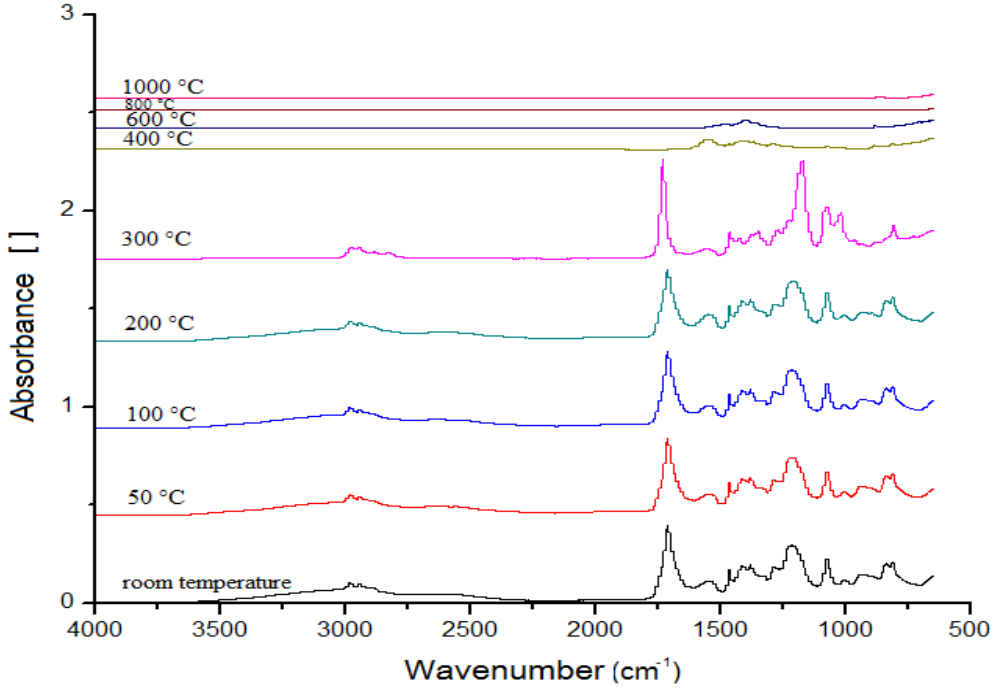

Figure 4.17 FTIR spectra of $K_2La_{1.1}Sm_{0.9}Ti_3O_{10}$ xerogels heat treated at different temperatures.

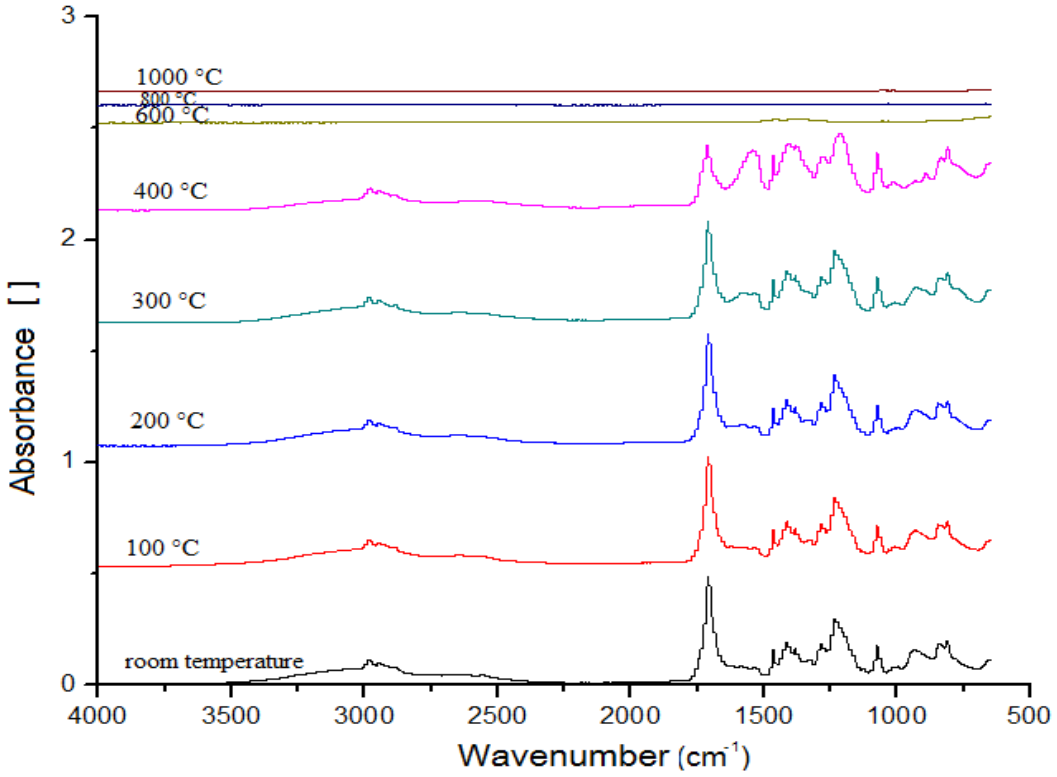

Figure 4.18 FTIR spectra of $K_2La_{1.9}Gd_{0.1}Ti_3O_{10}$ xerogels heat treated at different temperatures.

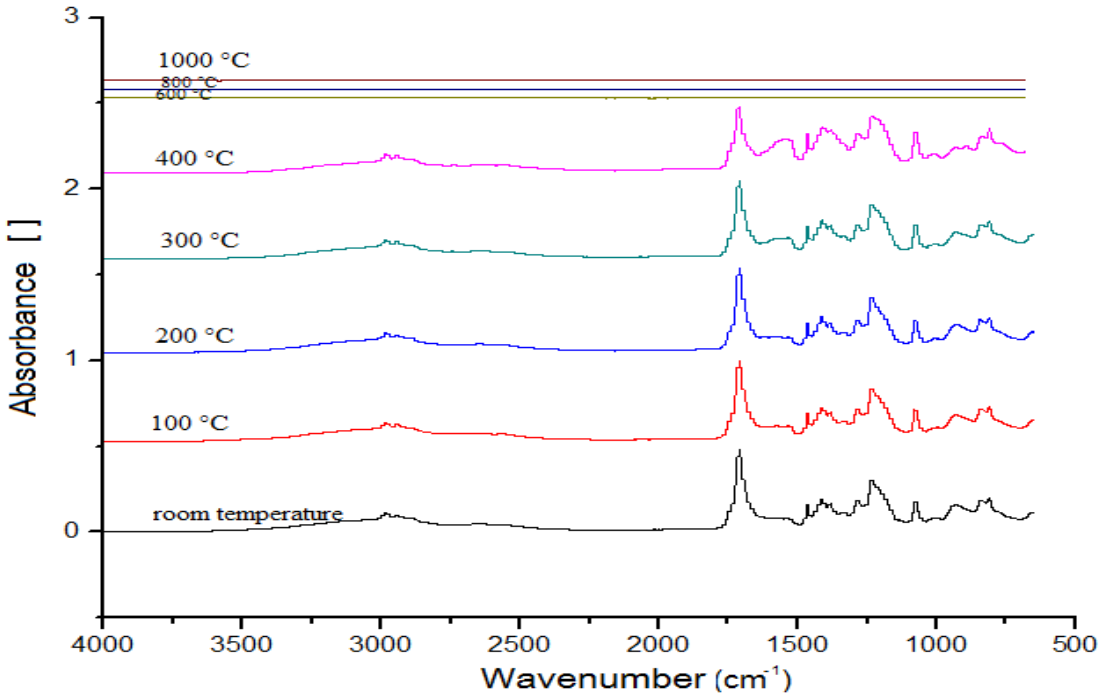

Figure 4.19 FTIR spectra of $K_2La_{1.5}Gd_{0.5}Ti_3O_{10}$ xerogels heat treated at different temperatures.

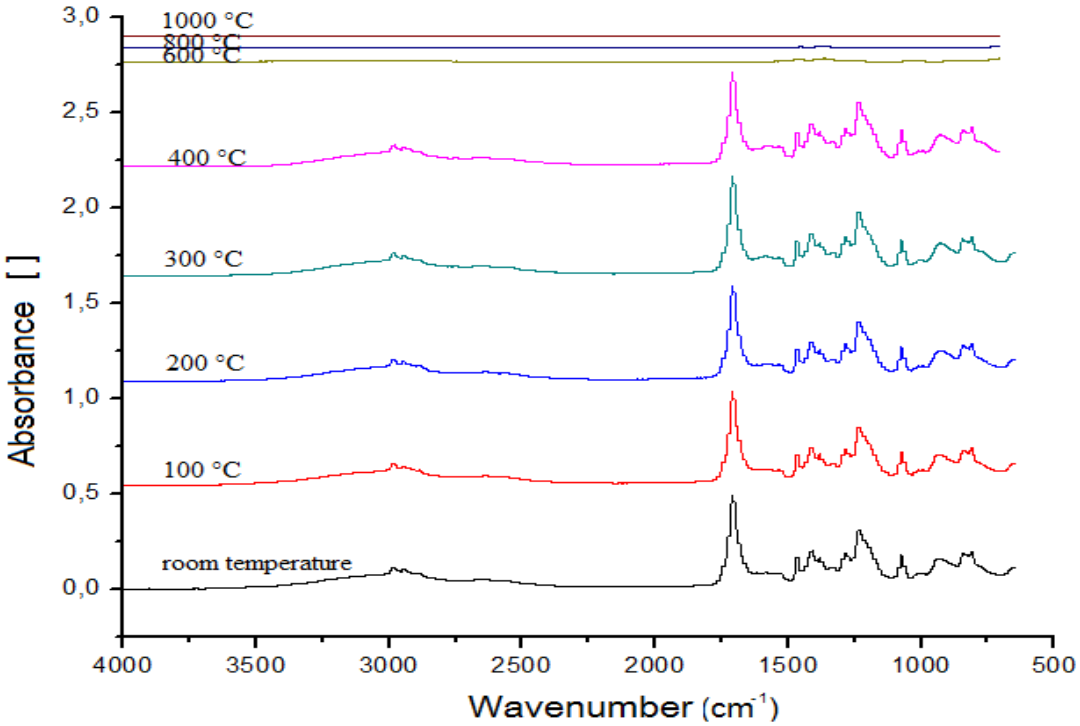

Figure 4.20 FTIR spectra of $K_2La_{1.1}Gd_{0.9}Ti_3O_{10}$ xerogels heat treated at different temperatures.

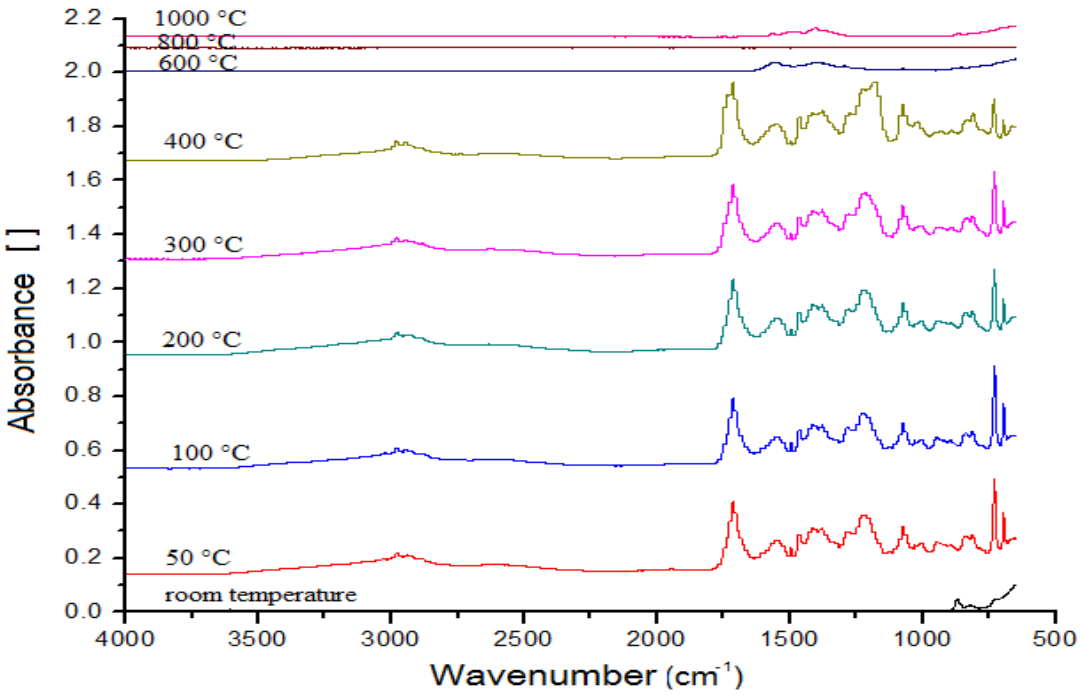

Figure 4.21 FTIR spectra of $K_2La_{1.9}Nd_{0.1}Ti_3O_{10}$ xerogels heat treated at different temperatures.

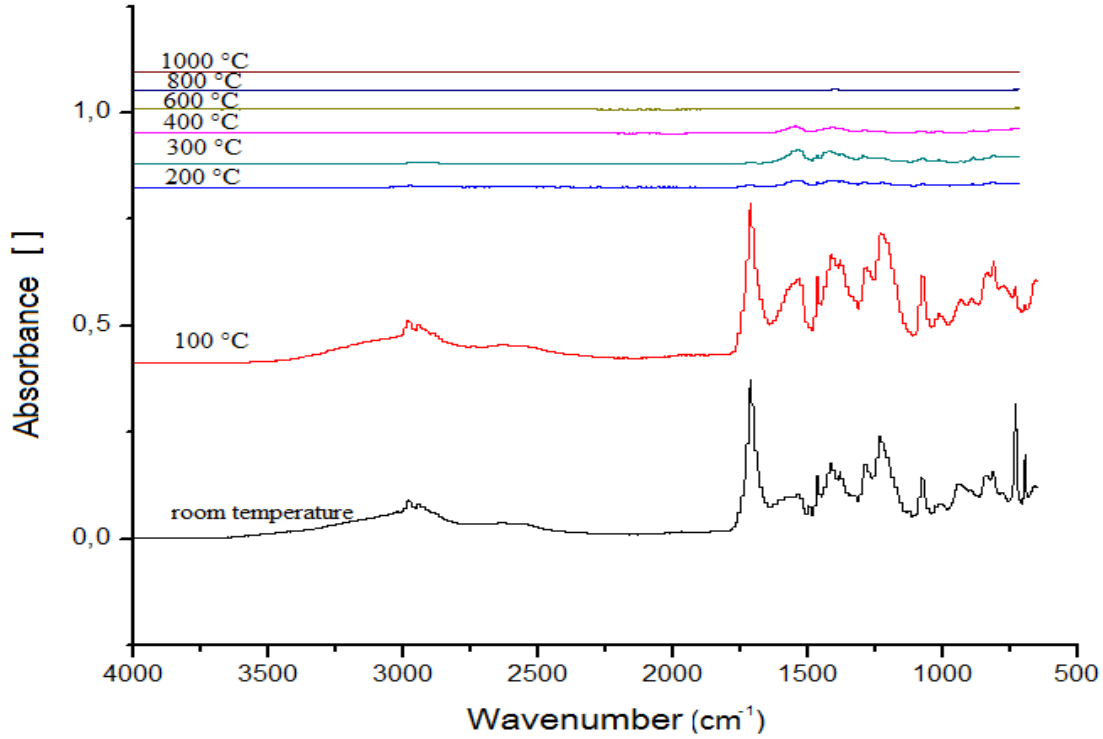

Figure 4.22 FTIR spectra of $K_2La_{1.5}Nd_{0.5}Ti_3O_{10}$ xerogels heat treated at different temperatures.

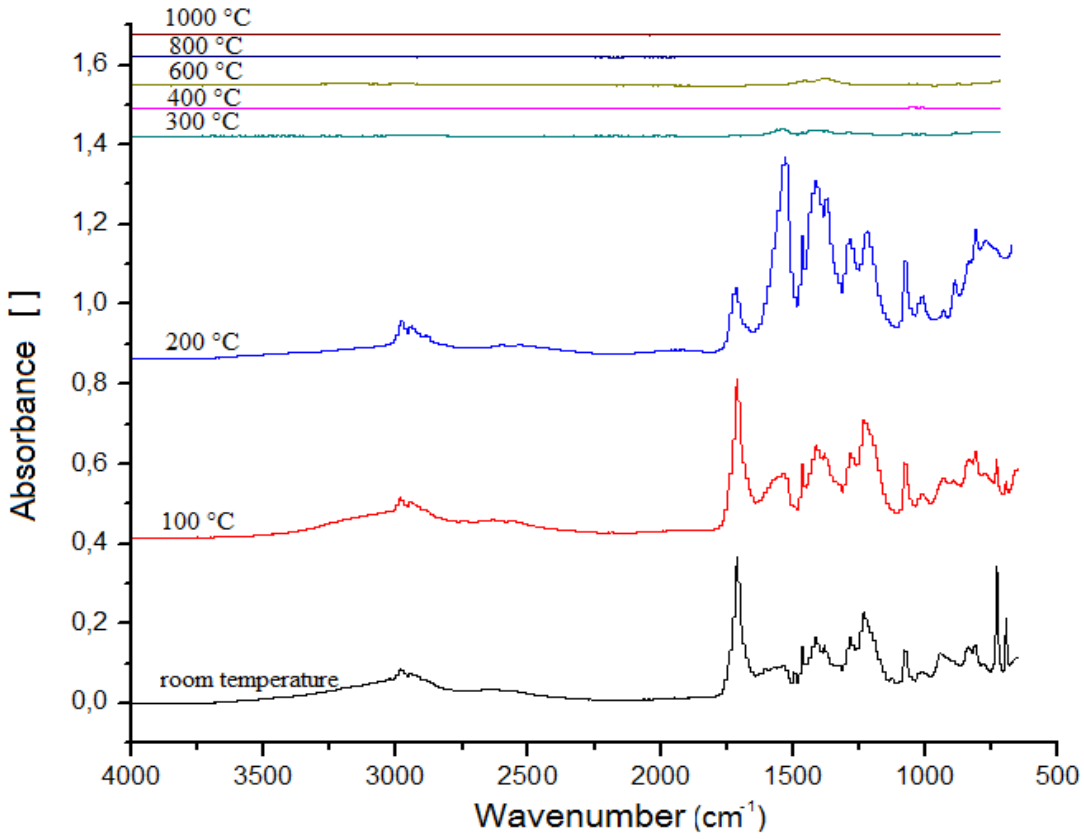

Figure 4.23 FTIR spectra of $K_2La_{1.1}Nd_{0.9}Ti_3O_{10}$ xerogels heat treated at different temperatures.

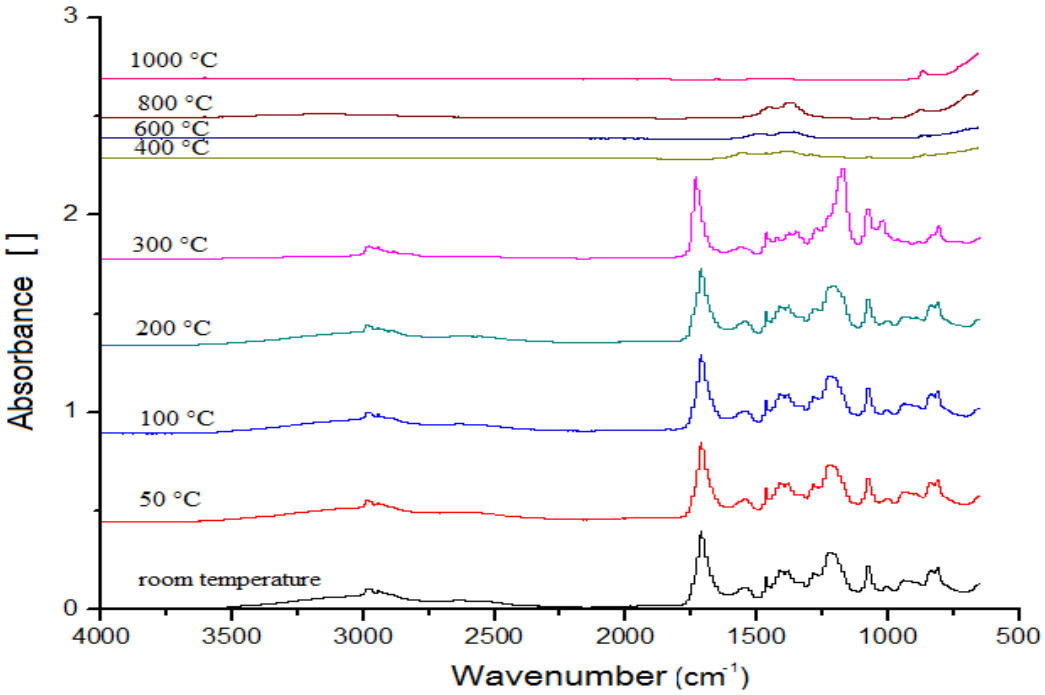

Figure 4.24 FTIR spectra of $K_2La_{1.9}Dy_{0.1}Ti_3O_{10}$ xerogels heat treated at different temperatures.

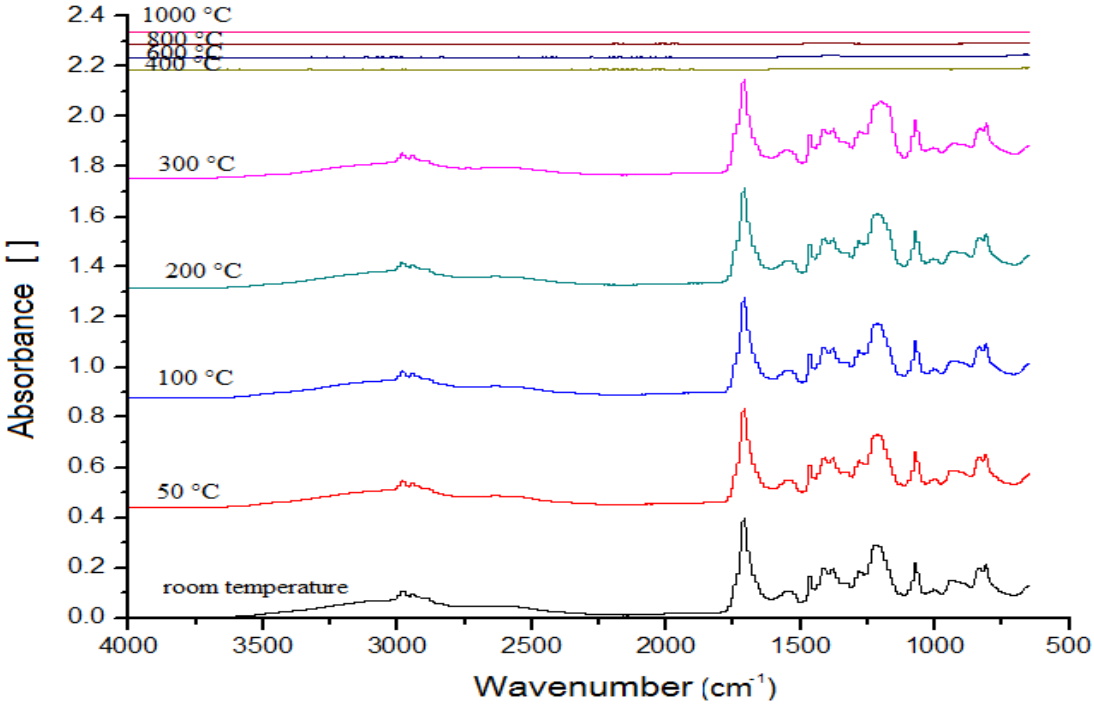

Figure 4.25 FTIR spectra of $K_2La_{1.5}Dy_{0.5}Ti_3O_{10}$ xerogels heat treated at different temperatures.

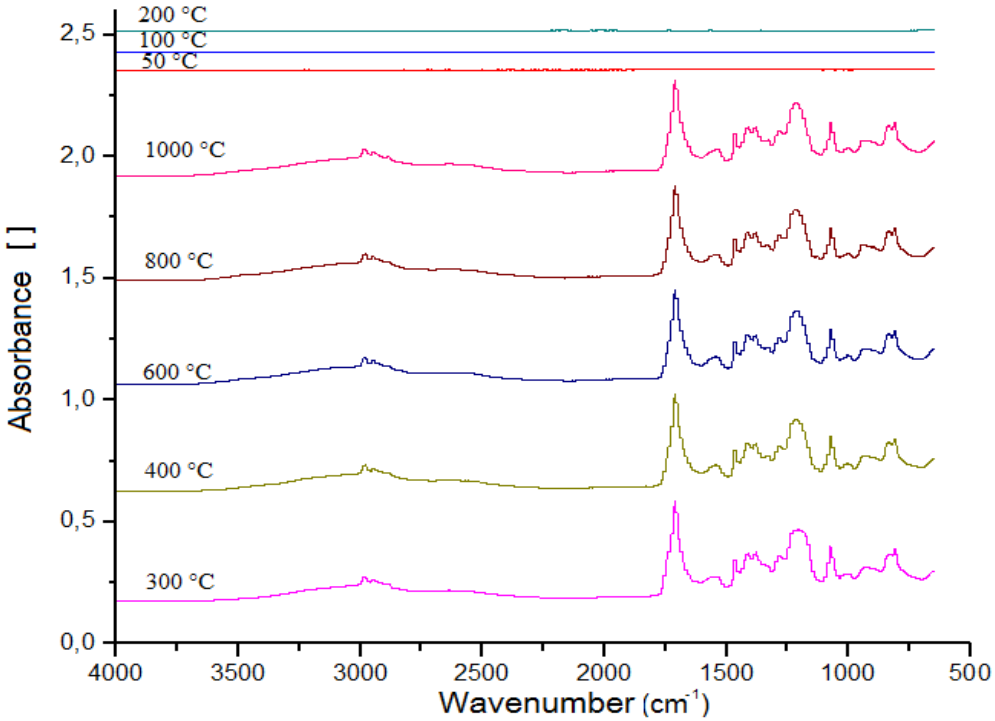

Figure 4.26 FTIR spectra of $K_2La_{1.1}Dy_{0.9}Ti_3O_{10}$ xerogels heat treated at different temperatures.

4.3 Film Characterization

4.3.1 XRD Analysis

According to the XRD results of the thin films, phase analysis can be determined. The figures between 4.27 and 35 show the XRD patterns of the thin films which coated on Si (100) substrate. To obtain XRD results, $K_2Ln_2Ti_3O_{10}$ (Ln=La, Nd, Gd, Sm, Dy) thin films were crystallized into perovskite phase after 1000°C annealing for 300 minutes. Sharp peaks show that the crystalline structure is obtained. XRD patterns showed different angle peaks. Different additives and concentrations are thought to result this situation.

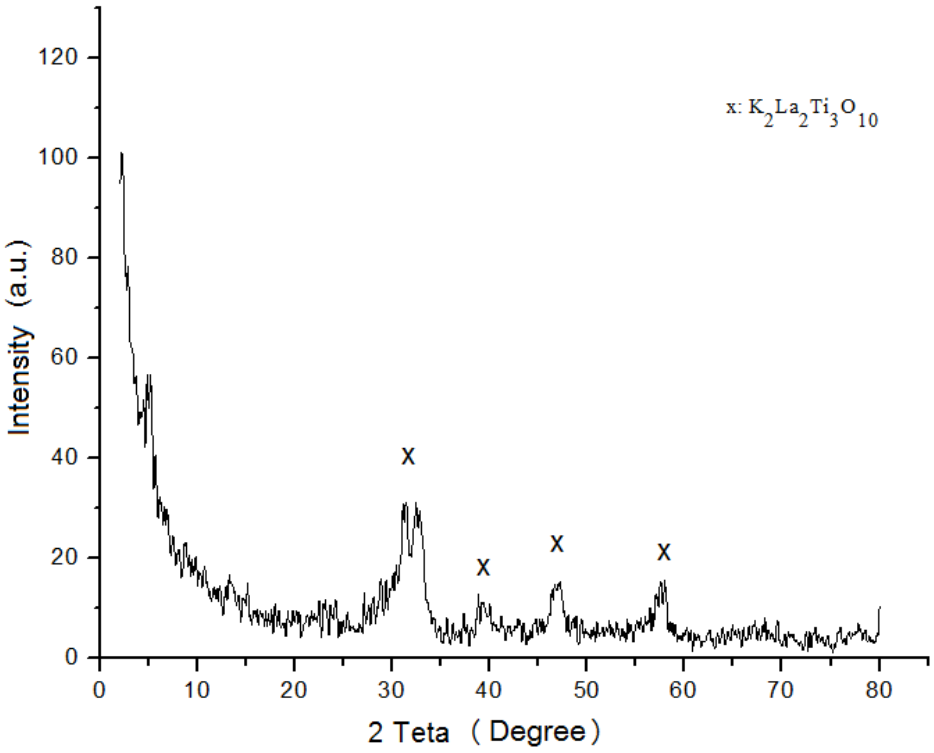

Figure 4.27 XRD pattern of $K_2La_2Ti_3O_{10}$ coated on Si(100) substrates.

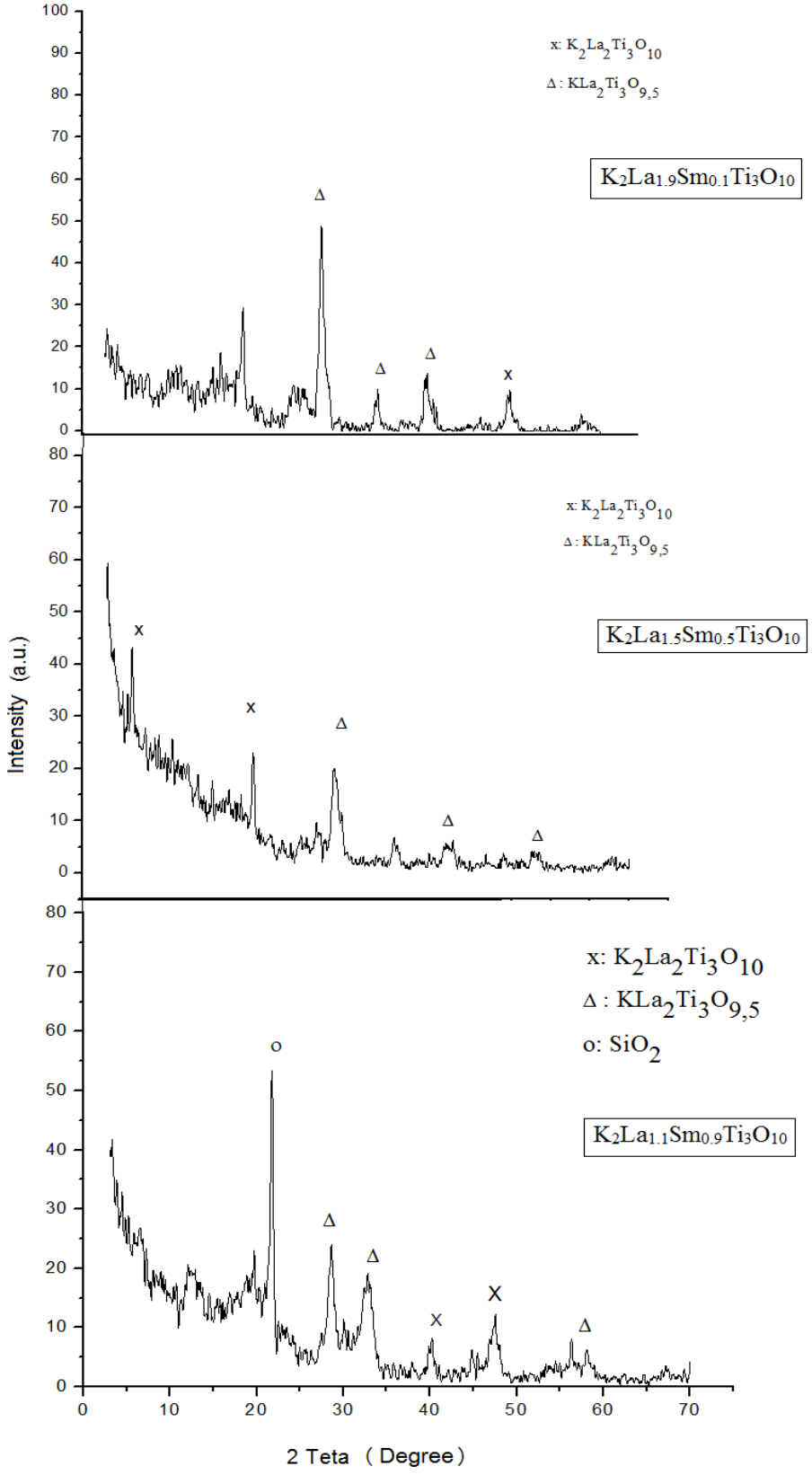

Figure 4.28 XRD pattern of $K_2La_{1.9}Sm_{0.1}Ti_3O_{10}$, $K_2La_{1.9}Sm_{0.5}Ti_3O_{10}$ and $K_2La_{1.9}Sm_{0.9}Ti_3O_{10}$ coated on Si(100) substrates.

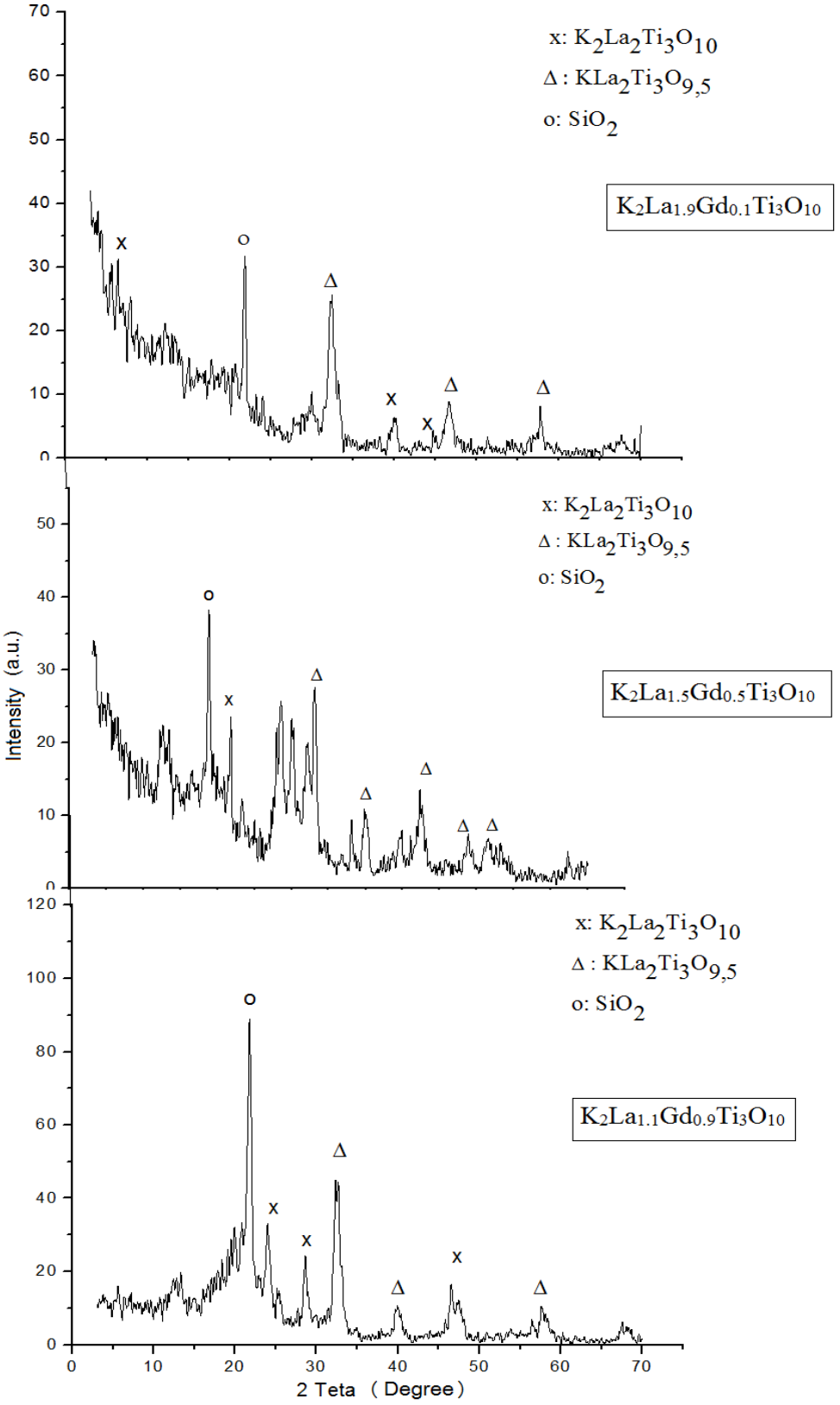

Figure 4.29 XRD pattern of $K_2La_{1.9}Gd_{0.1}Ti_3O_{10}$, $K_2La_{1.5}Gd_{0.5}Ti_3O_{10}$ and $K_2La_{1.1}Gd_{0.9}Ti_3O_{10}$ coated on Si(100) substrates.

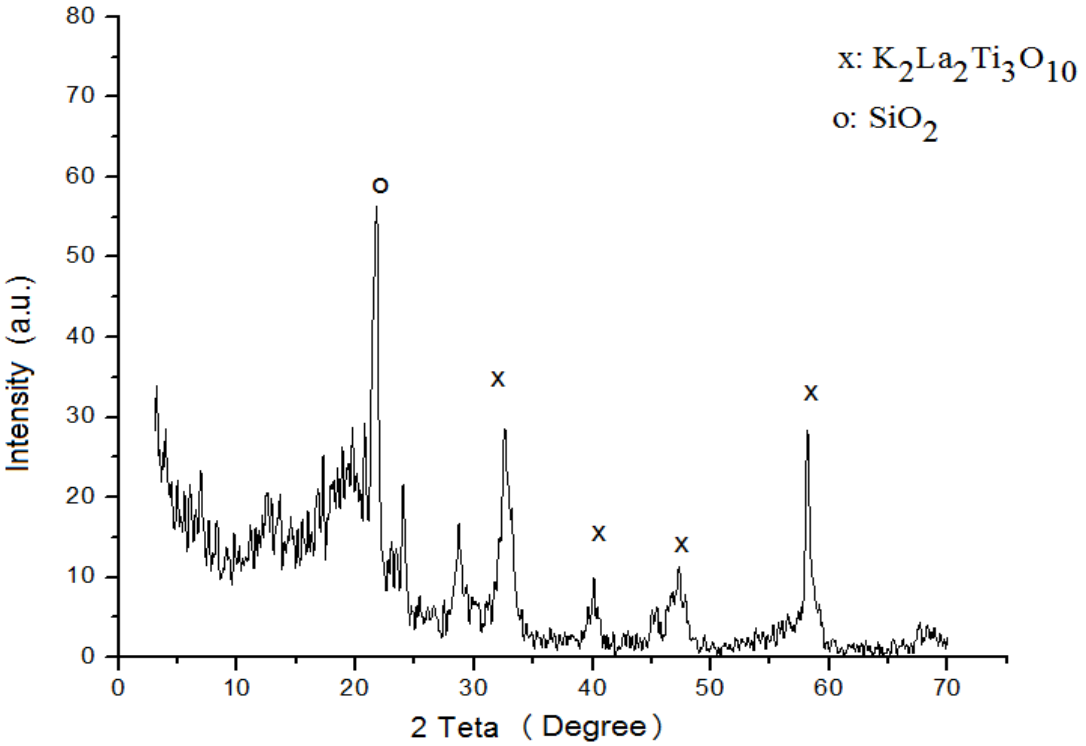

Figure 4.30 XRD pattern of $K_2La_{1.9}Nd_{0.1}Ti_3O_{10}$ coated on Si(100) substrates.

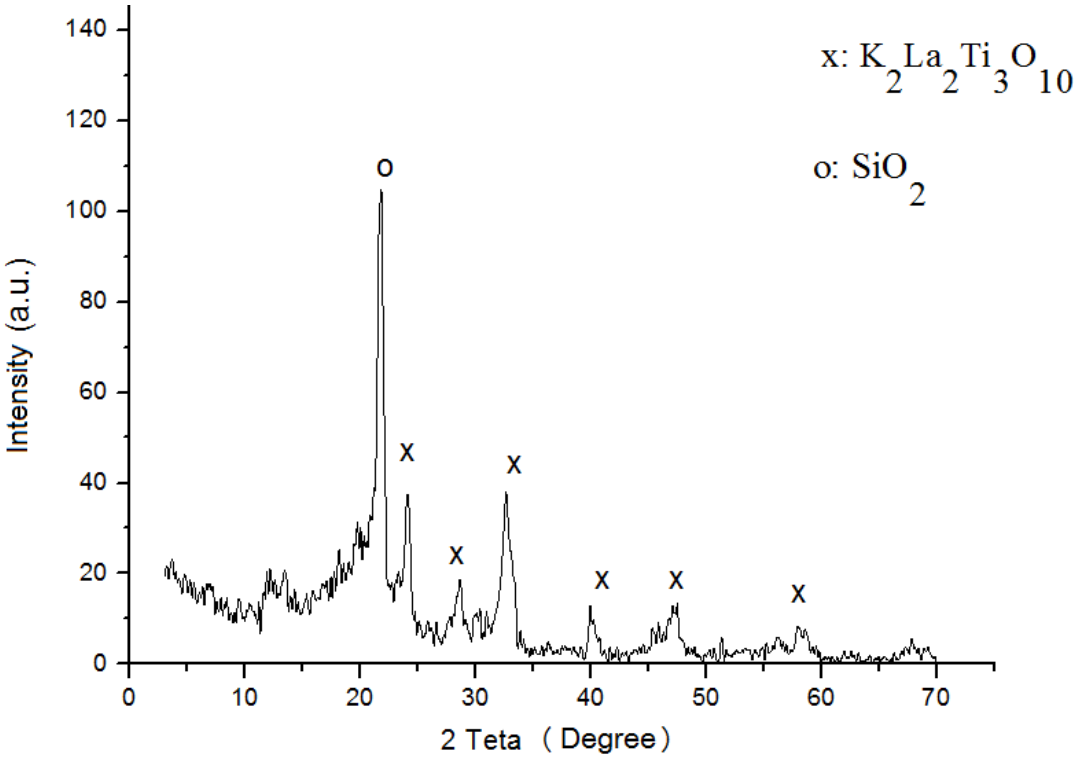

Figure 4.31 XRD pattern of $K_2La_{1.5}Nd_{0.5}Ti_3O_{10}$ coated on Si(100) substrates.

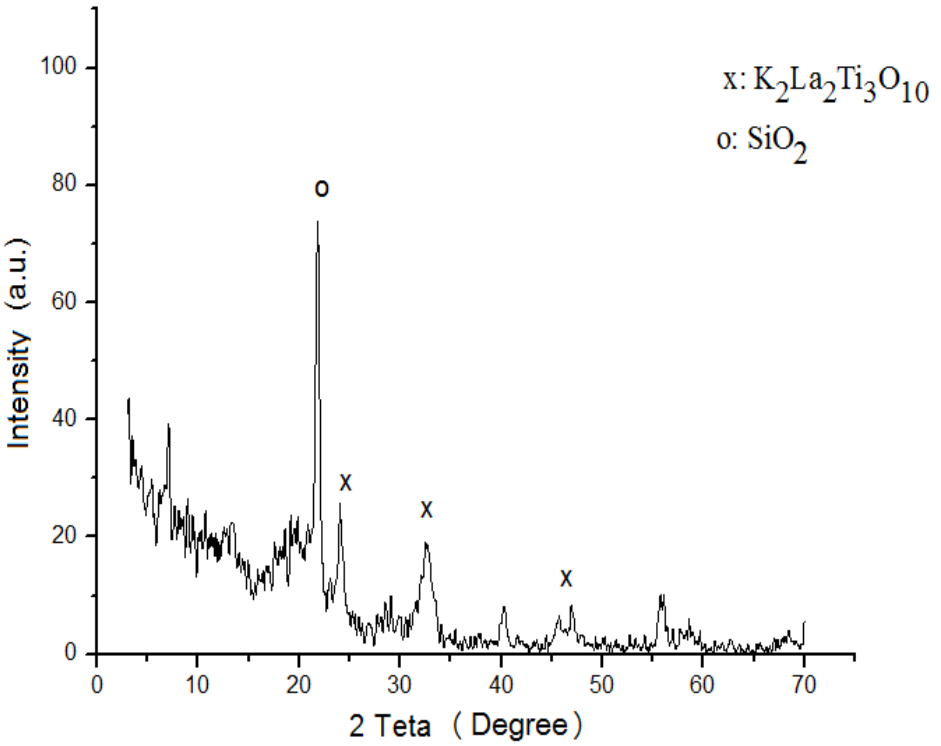

Figure 4.32 XRD pattern of $K_2La_{1.1}Nd_{0.9}Ti_3O_{10}$ coated on Si(100) substrates.

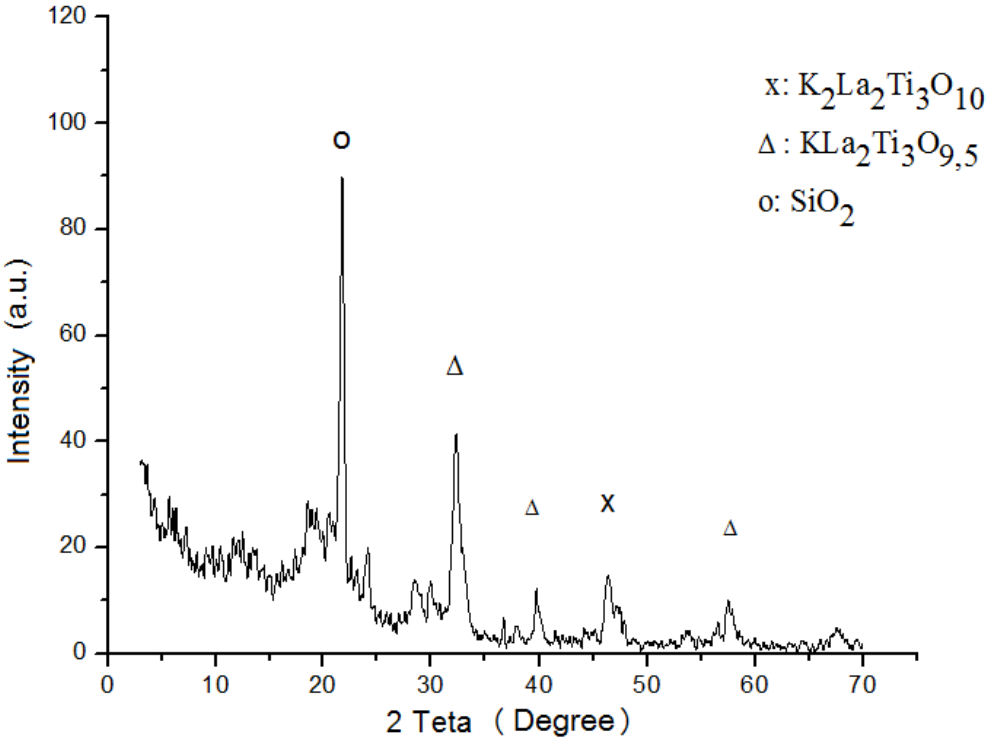

Figure 4.33 XRD pattern of $K_2La_{1.9}Dy_{0.1}Ti_3O_{10}$ coated on Si(100) substrates.

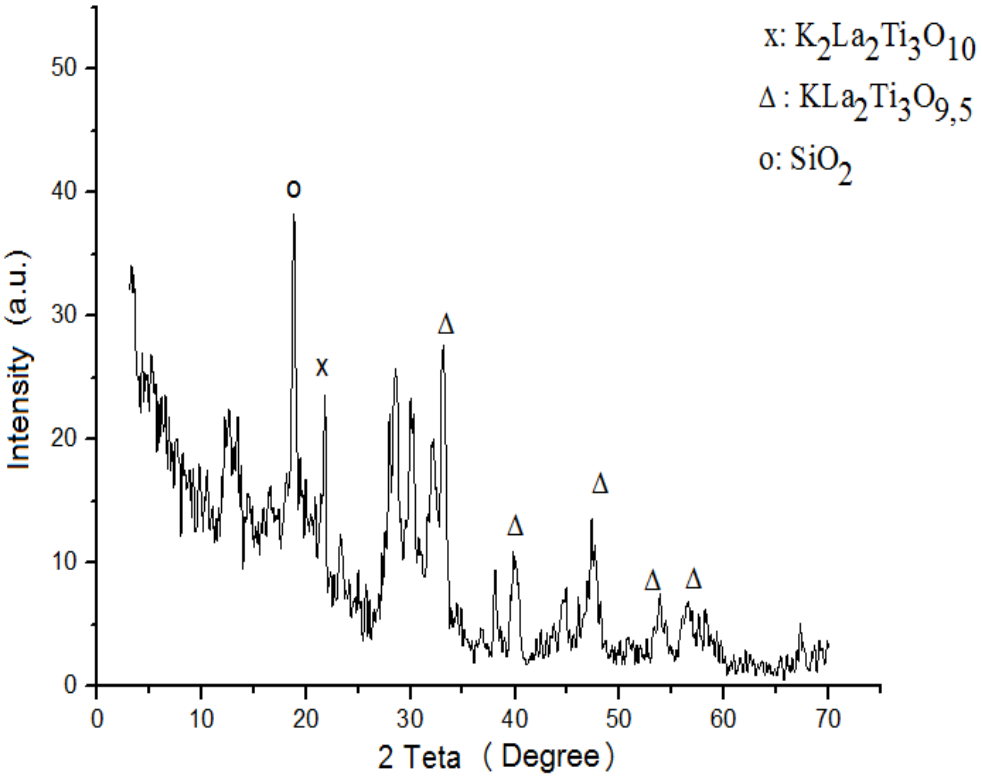

Figure 4.34 XRD pattern of $K_2La_{1.5}Dy_{0.5}Ti_3O_{10}$ coated on Si(100) substrates.

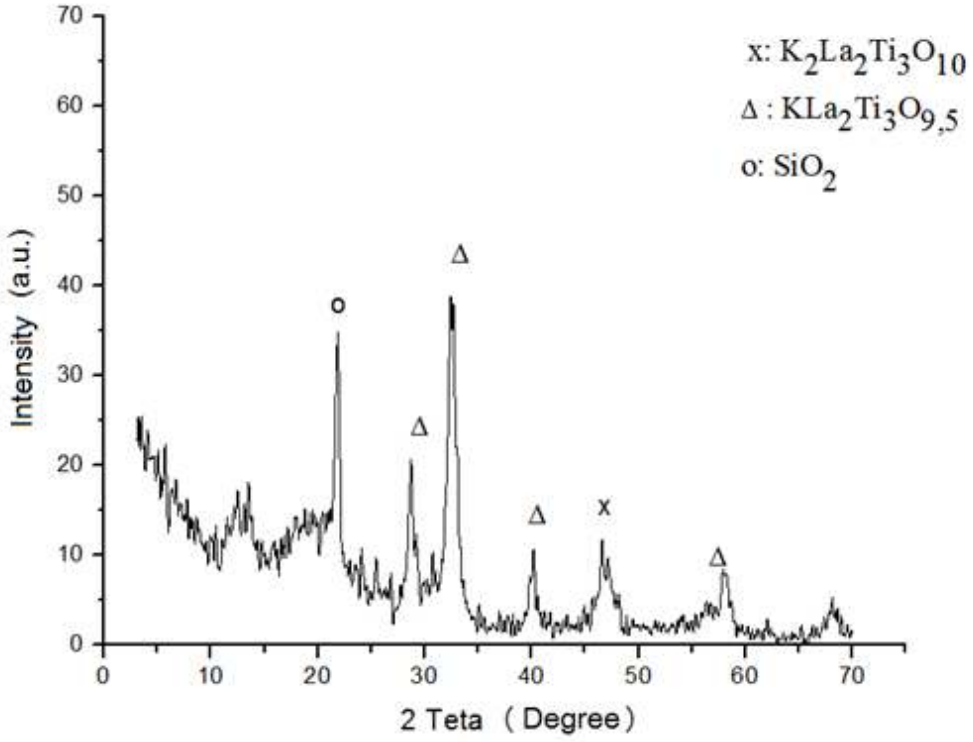

Figure 4.35 XRD pattern of $K_2La_{1.1}Dy_{0.9}Ti_3O_{10}$ coated on Si(100) substrates.

4.3.2 SEM Analysis

Microstructure of the thin films was determined by SEM analysis. Surface morphology is an important parameter which affects the photocatalytic activity. The pH, solution concentration, viscosity, film thickness, heat treatment regime and coating method affect the surface morphology. SEM micrographs of thin films at different magnification can be seen in the following figures. The powders which dispersed with propionic acid were hold to Si (100) substrate. Cracks, channels and coating islands can be seen on the micrographs of thin films. The figures between 4.36 and 4.48 demonstrate SEM micrographs. Surface area is the important parameter for photocatalytical application. It can be seen that when the surface area that acting with pollution is increased, the photocatalytic efficiency is also rised (Bakuy, 2009). For this reason, it can be said that the thin films are morphologically good candidates for photocatalytic applications.

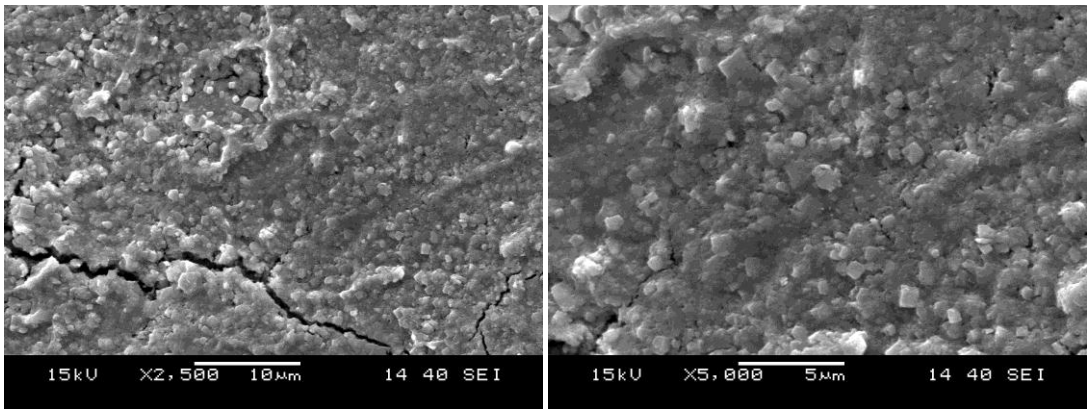

Figure 4.36 SEM micrographs of $K_2La_2Ti_3O_{10}$ thin films at different magnifications.

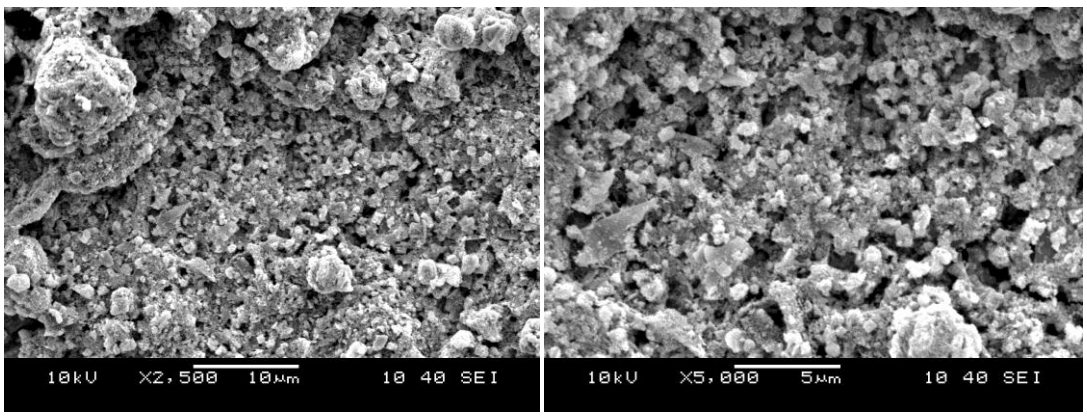

Figure 4.37 SEM micrographs of $K_2La_{1.9}Sm_{0.1}Ti_3O_{10}$ thin films at different magnifications.

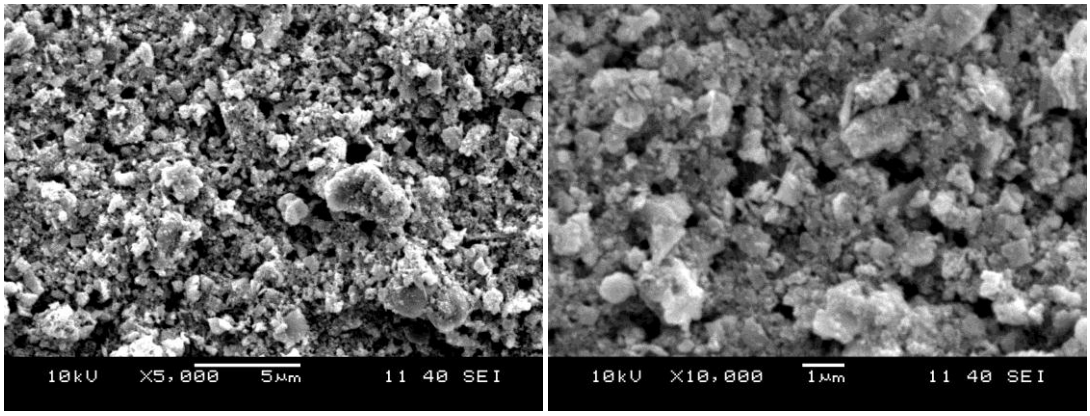

Figure 4.38 SEM micrographs of $K_2La_{1.5}Sm_{0.5}Ti_3O_{10}$ thin films at different magnifications.

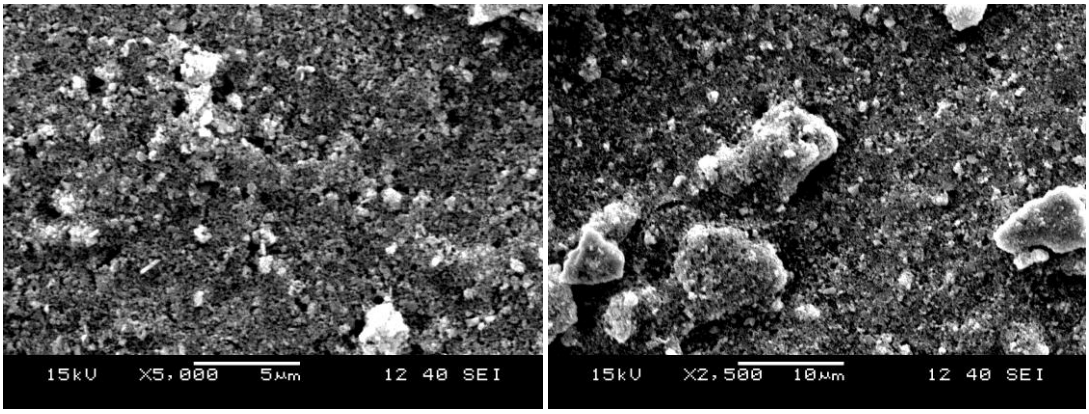

Figure 4.39 SEM micrographs of $K_2La_{1.1}Sm_{0.9}Ti_3O_{10}$ thin films at different magnifications.

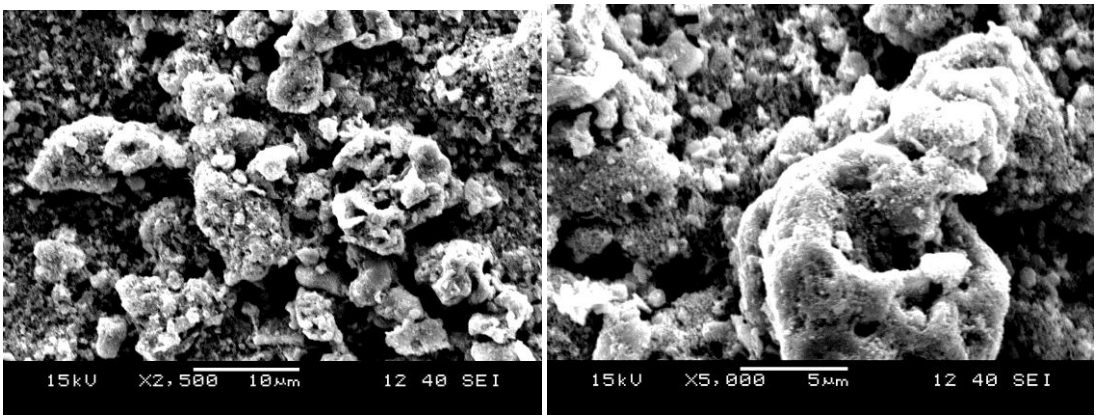

Figure 4.40 SEM micrographs of $K_2La_{1.9}Gd_{0.1}Ti_3O_{10}$ thin films at different magnifications.

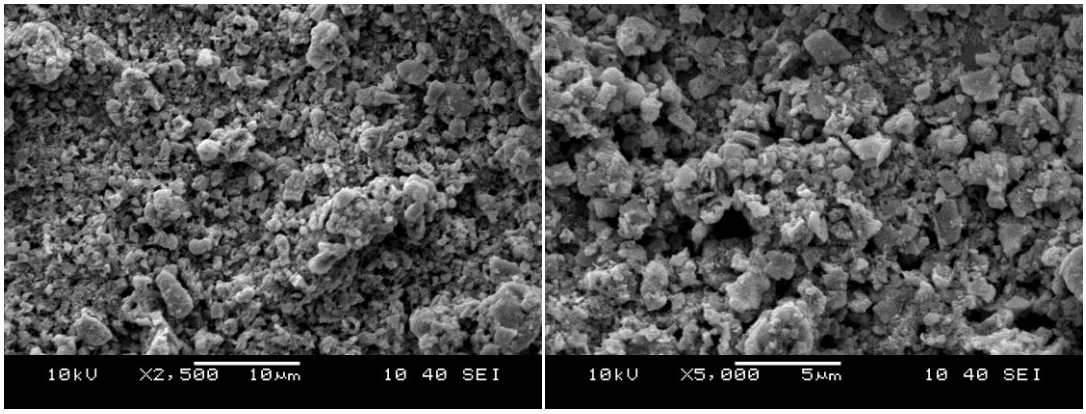

Figure 4.41 SEM micrographs of $K_2La_{1.5}Gd_{0.5}Ti_3O_{10}$ thin films at different magnifications.

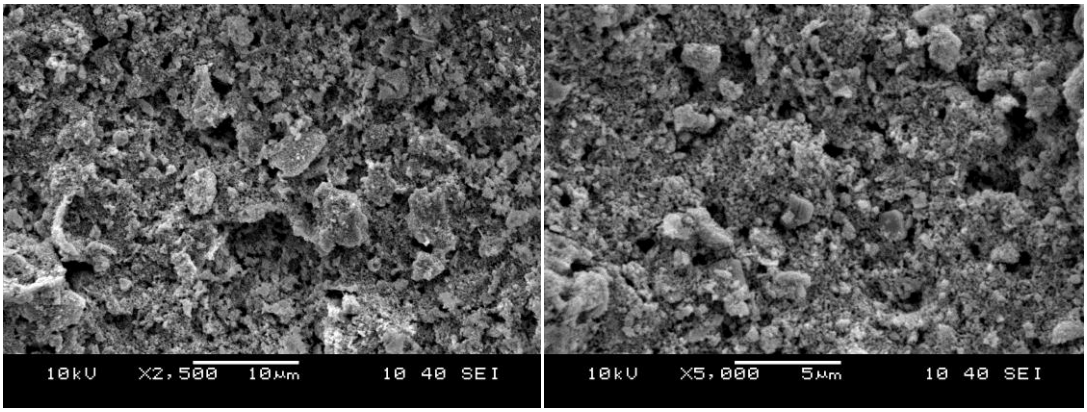

Figure 4.42 SEM micrographs of $K_2La_{1.1}Gd_{0.9}Ti_3O_{10}$ thin films at different magnifications.

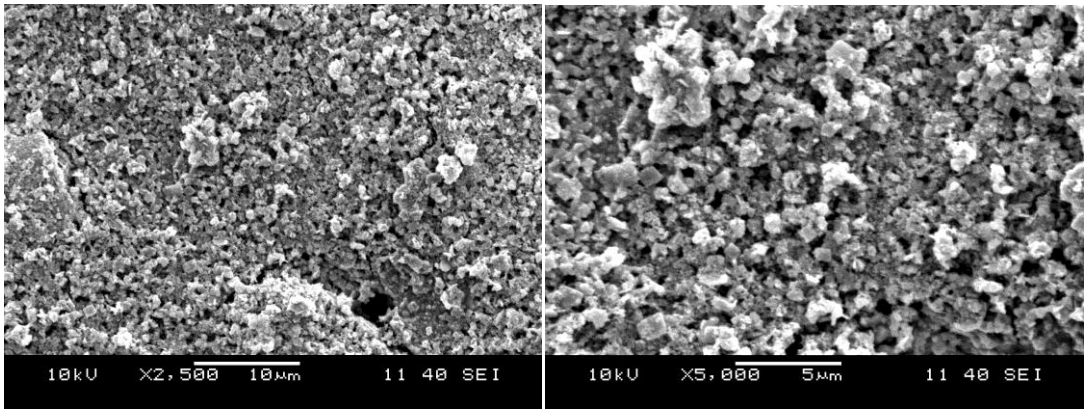

Figure 4.43 SEM micrographs of $K_2La_{1.9}Nd_{0.1}Ti_3O_{10}$ thin films at different magnifications.

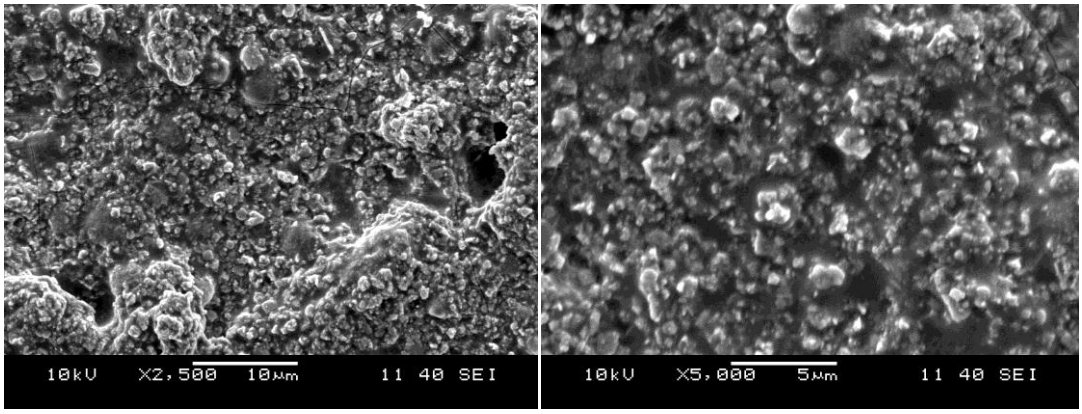

Figure 4.44 SEM micrographs of $K_2La_{1.5}Nd_{0.5}Ti_3O_{10}$ thin films at different magnifications.

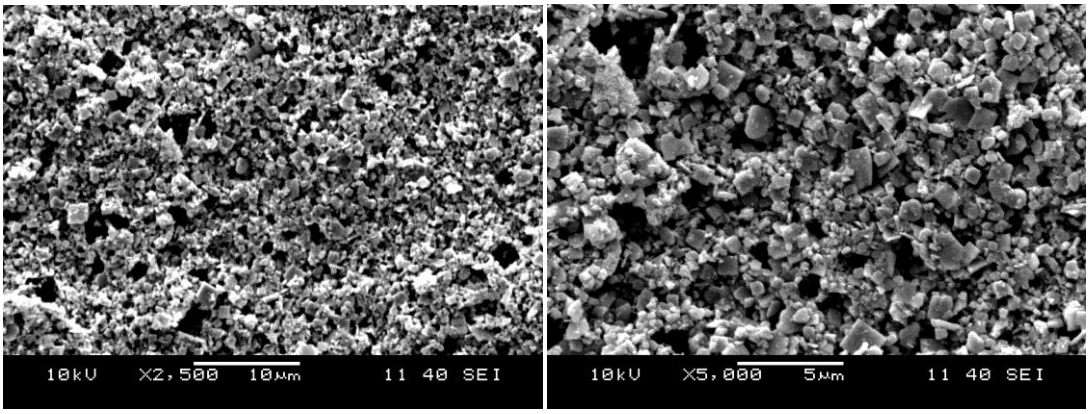

Figure 4.45 SEM micrographs of $K_2La_{1.1}Nd_{0.9}Ti_3O_{10}$ thin films at different magnifications.

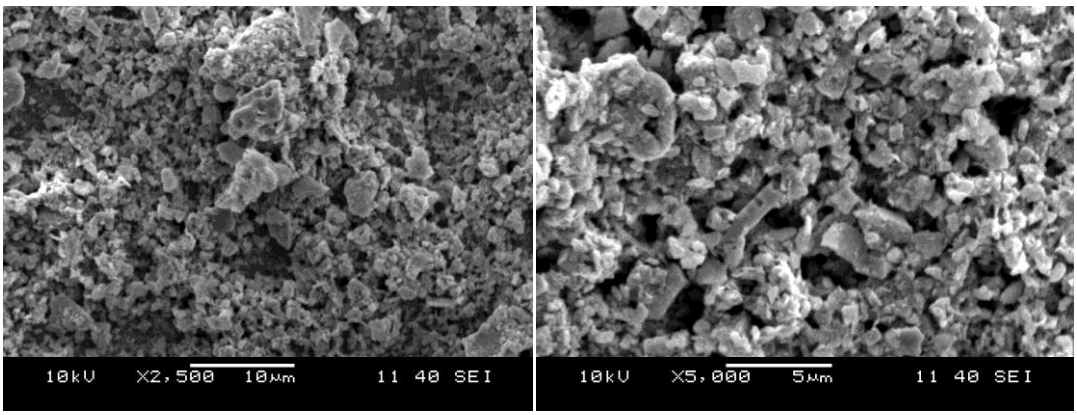

Figure 4.46 SEM micrographs of $K_2La_{1.9}Dy_{0.1}Ti_3O_{10}$ thin films at different magnifications.

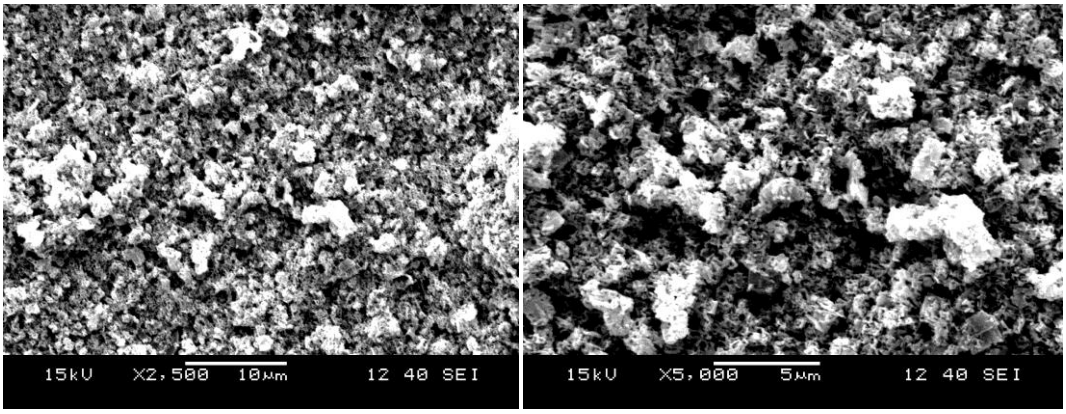

Figure 4.47 SEM micrographs of $K_2La_{1.5}Dy_{0.5}Ti_3O_{10}$ thin films at different magnifications.

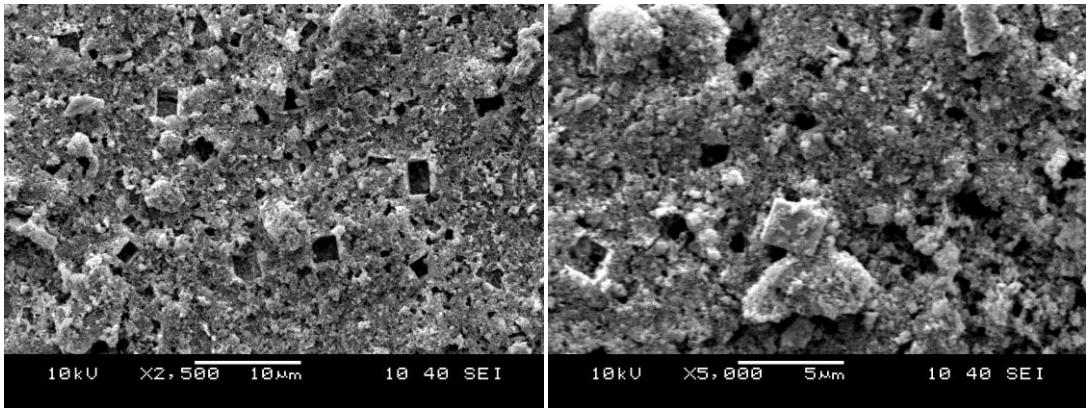

Figure 4.48 SEM micrographs of $K_2La_{1.1}Dy_{0.9}Ti_3O_{10}$ thin films at different magnifications.

4.3.3 XPS Analysis

XPS analysis is method of elemental analysis. XPS measured the chemical or electronic state of surface element and identify chemical uniformity of KLTO based Si (100) coatings. Doped elements could not be seen by 0.1 doped coating. This is considered to be due to the slight amount of doping.

The La 3d core level of the samples and spin–orbit components of Ti 2p peak and the K 2p peak were well described at different binding energy for all the figures between 4.49 and 4.61. The dopant chemicals can be seen as Sm 3d (Figures 4.51 and 4.52), but the Gd dopants cannot be seen (Figure 4.53, 4.54 and 4.55). The Nd 4d (Figures 4.57 and 4.58) and Dy 3d (Figures 4.60 and 4.61) levels can also observe. The peaks demonstrated that the chemicals were occurred into the thin films.

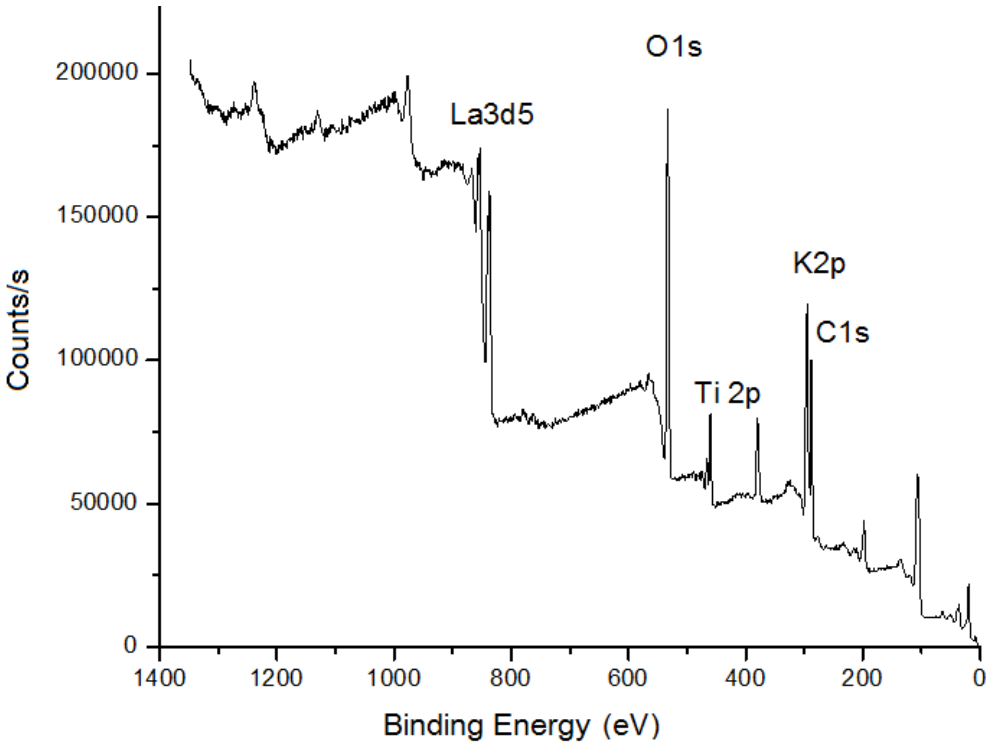

Figure 4.49 XPS spectrum for $K_2La_2Ti_3O_{10}$.

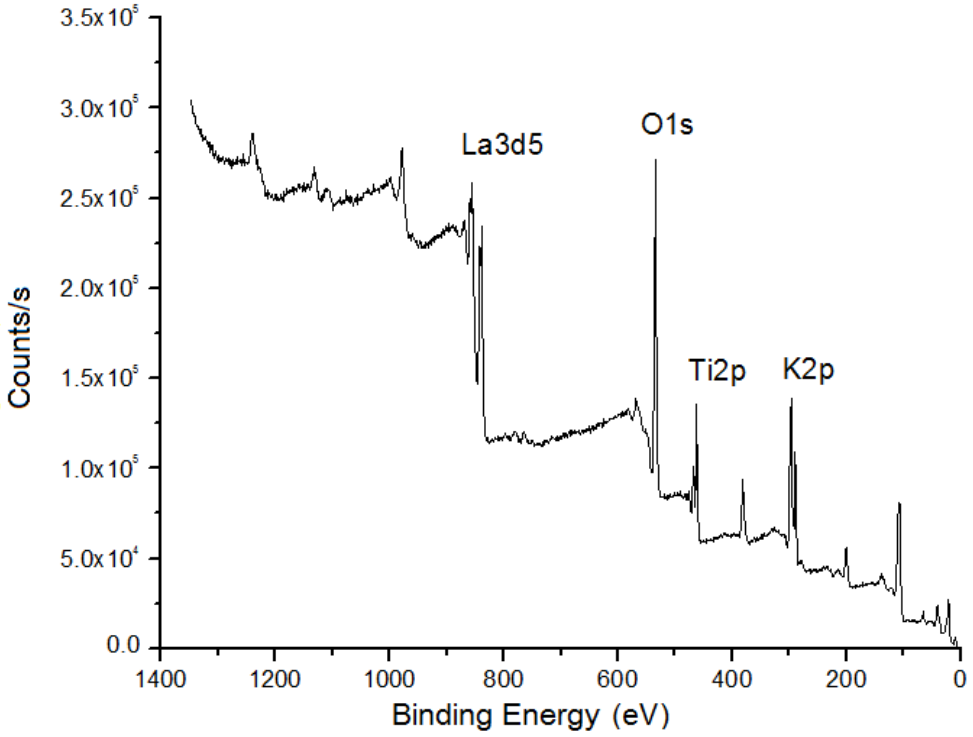

Figure 4.50 XPS spectrum for $K_2La_{1.9}Sm_{0.1}Ti_3O_{10}$.

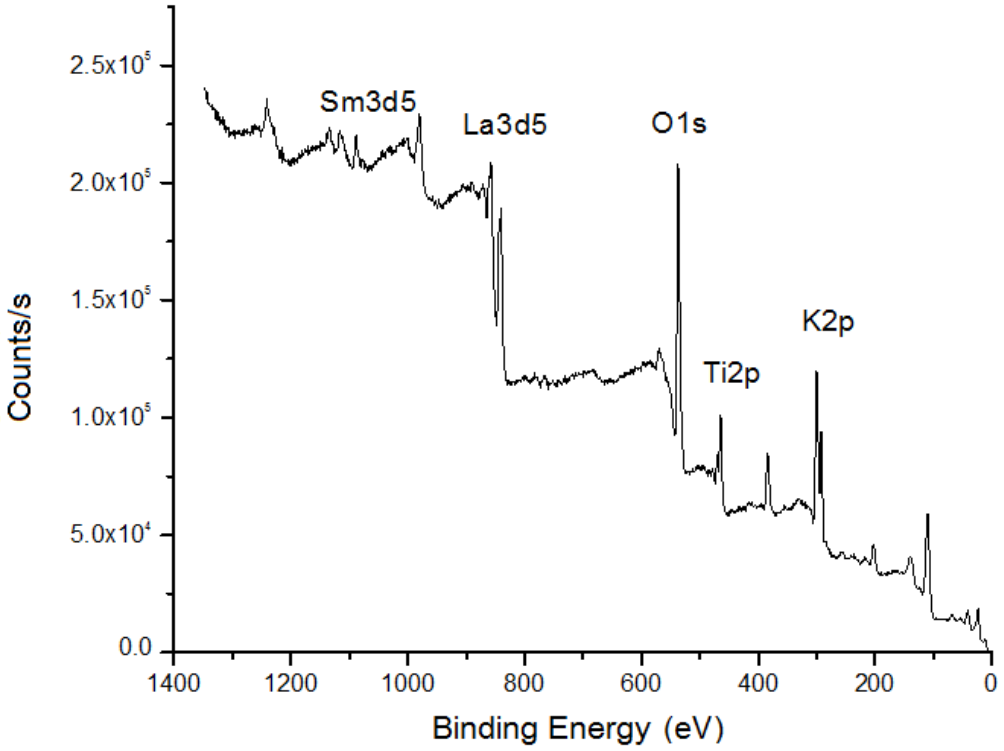

Figure 4.51 XPS spectrum for $K_2La_{1.5}Sm_{0.5}Ti_3O_{10}$.

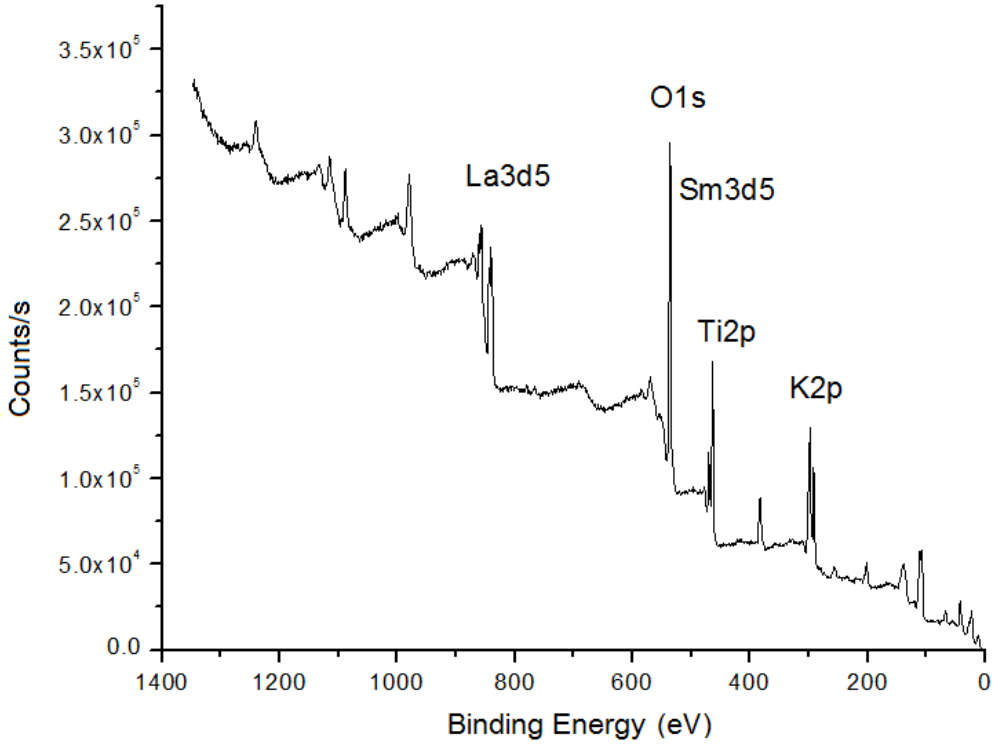

Figure 4.52 XPS spectrum for $K_2La_{1.1}Sm_{0.9}Ti_3O_{10}$.

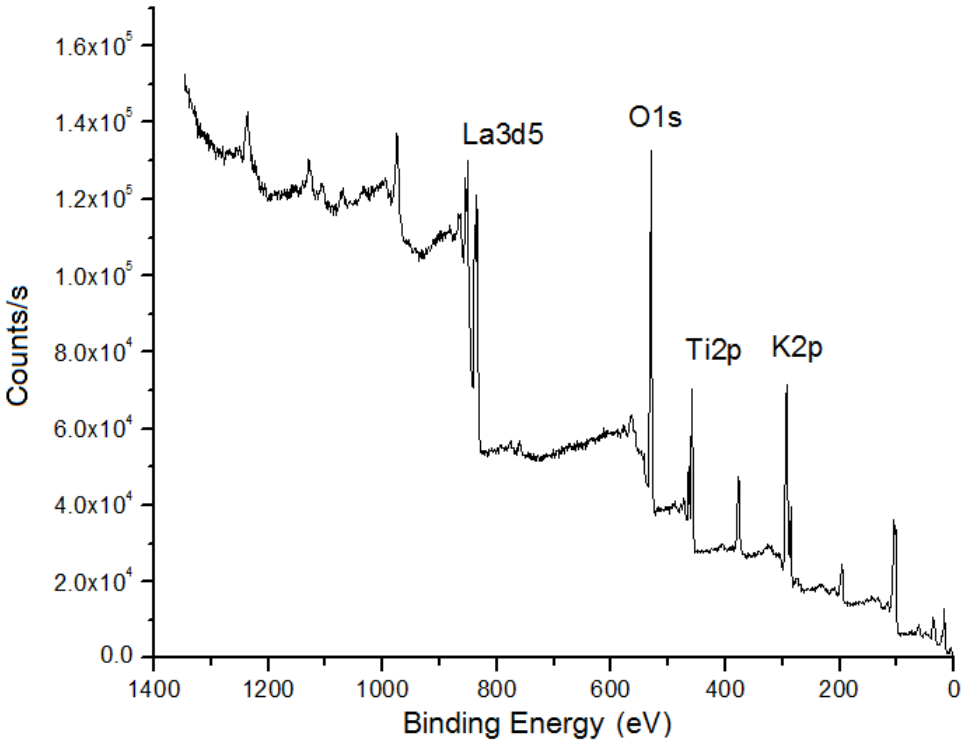

Figure 4.53 XPS spectrum for $K_2La_{1.9}Gd_{0.1}Ti_3O_{10}$.

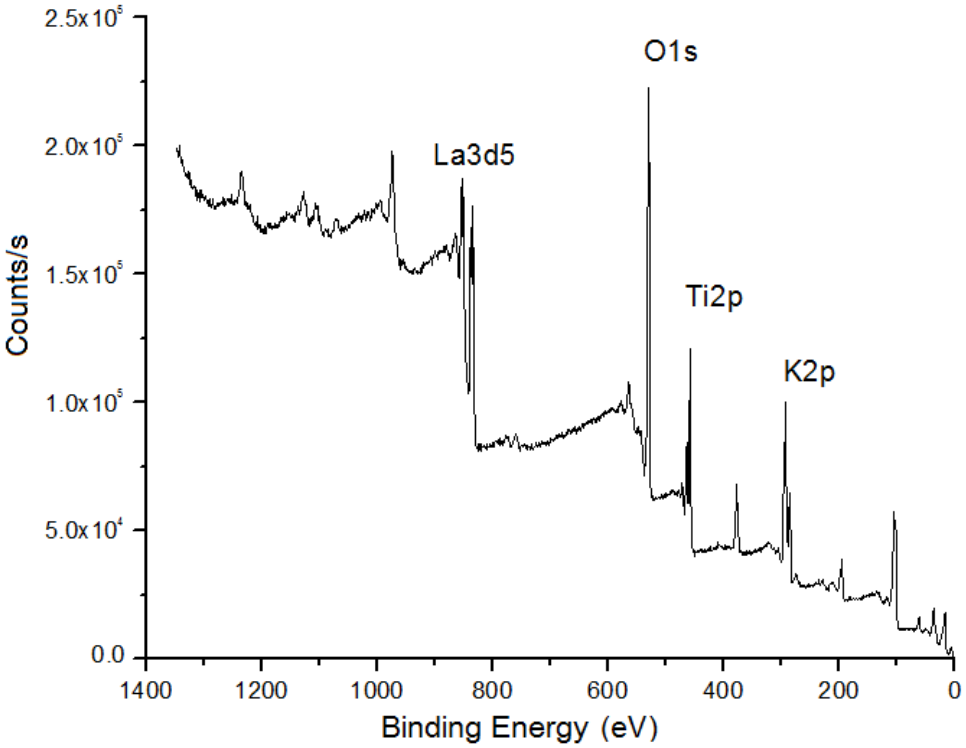

Figure 4.54 XPS spectrum for $K_2La_{1.5}Gd_{0.5}Ti_3O_{10}$.

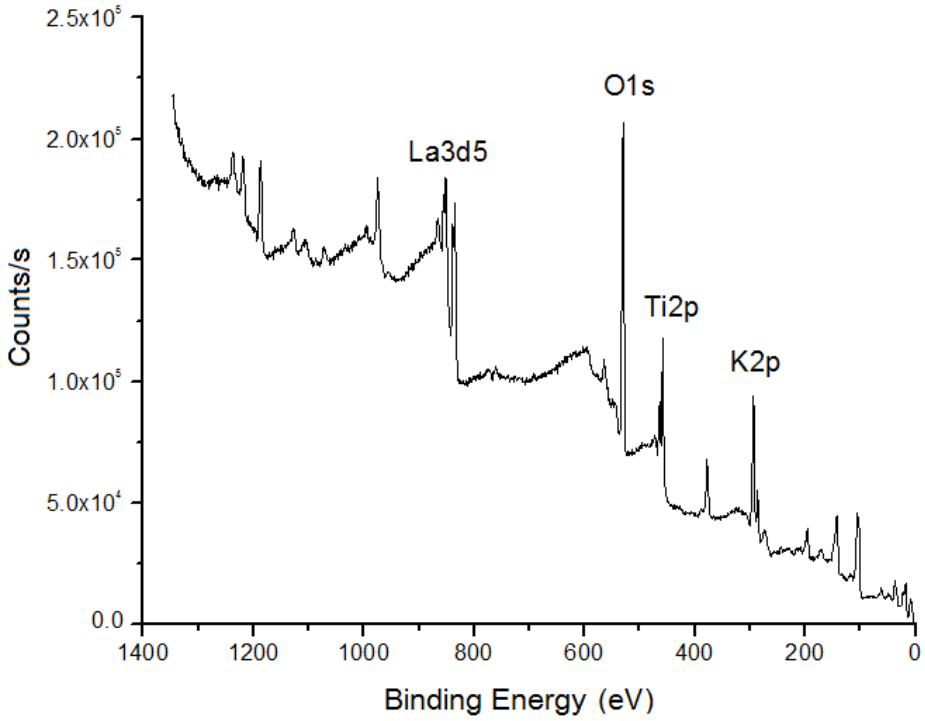

Figure 4.55 XPS spectrum for $K_2La_{1.1}Gd_{0.9}Ti_3O_{10}$.

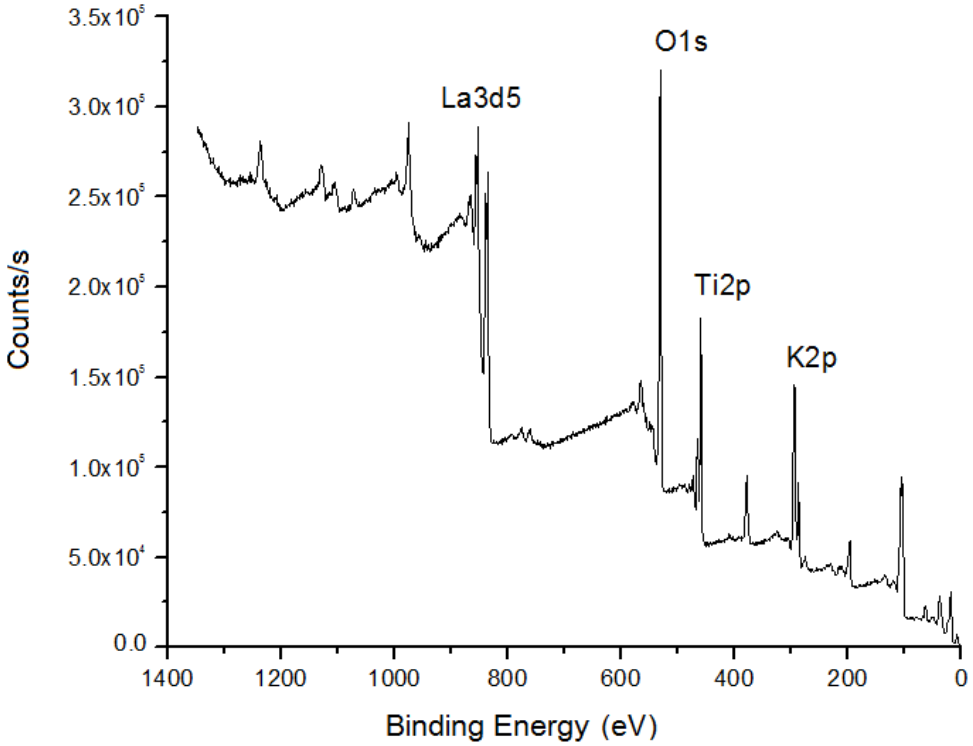

Figure 4.56 XPS spectrum for $K_2La_{1.9}Nd_{0.1}Ti_3O_{10}$.

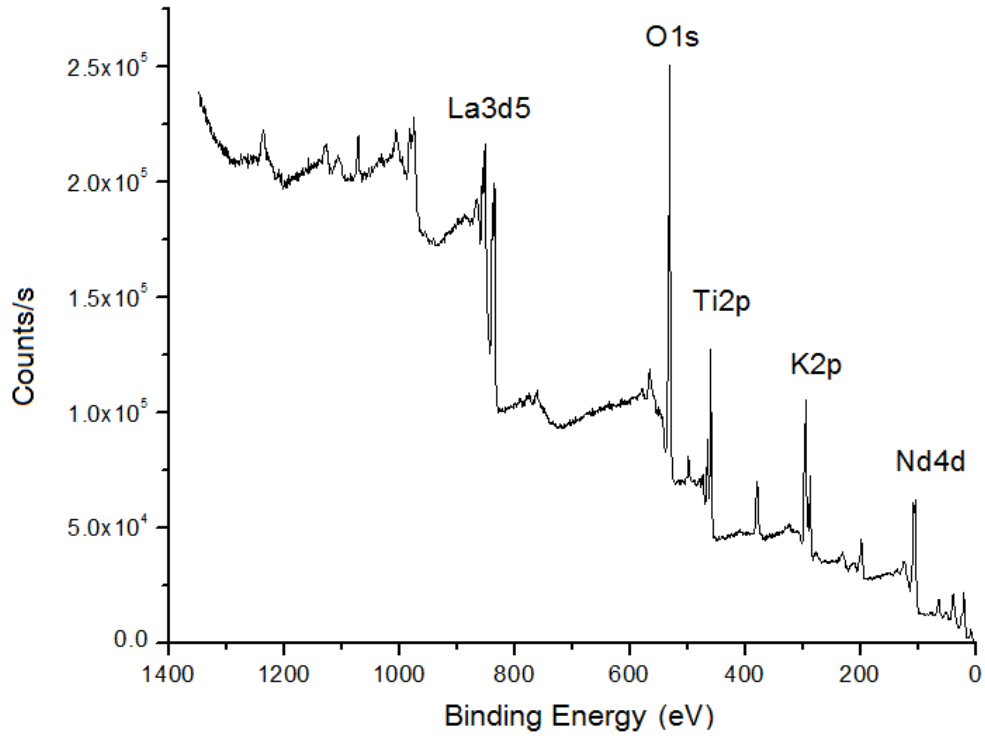

Figure 4.57 XPS spectrum for $K_2La_{1.5}Nd_{0.5}Ti_3O_{10}$.

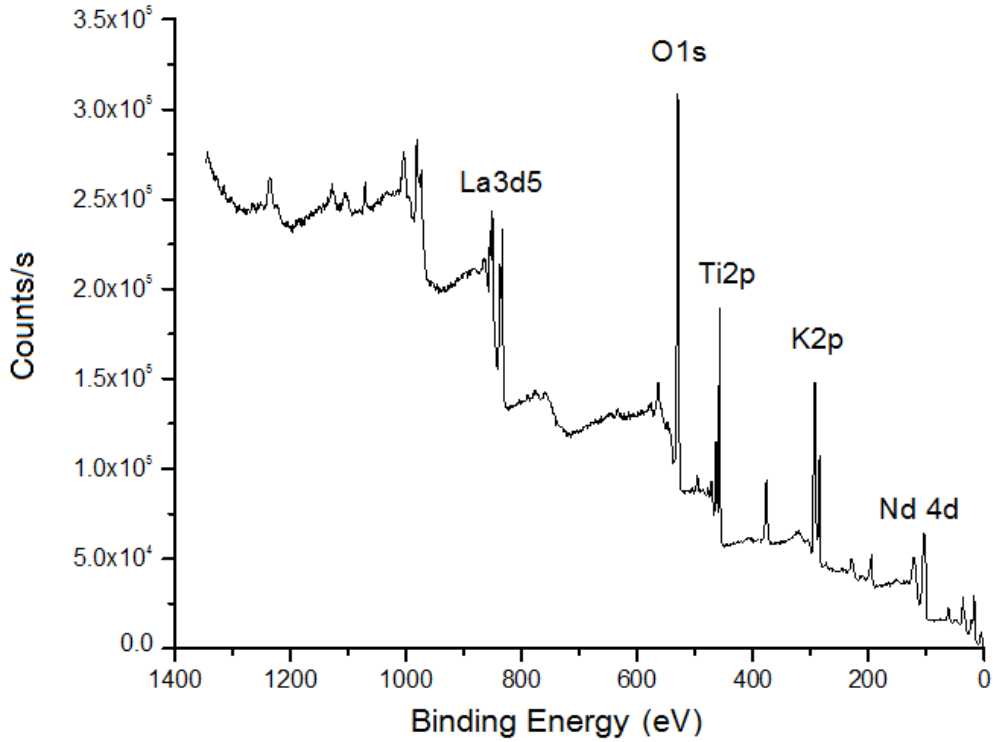

Figure 4.58 XPS spectrum for $K_2La_{1.1}Nd_{0.9}Ti_3O_{10}$.

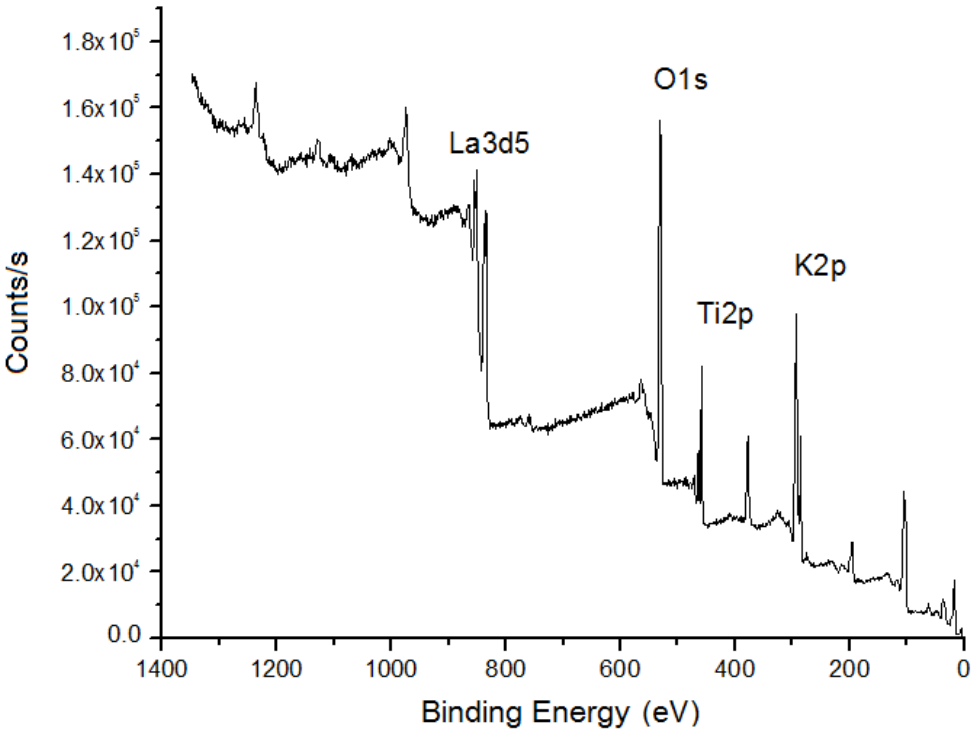

Figure 4.59 XPS spectrum for $K_2La_{1.9}Dy_{0.1}Ti_3O_{10}$.

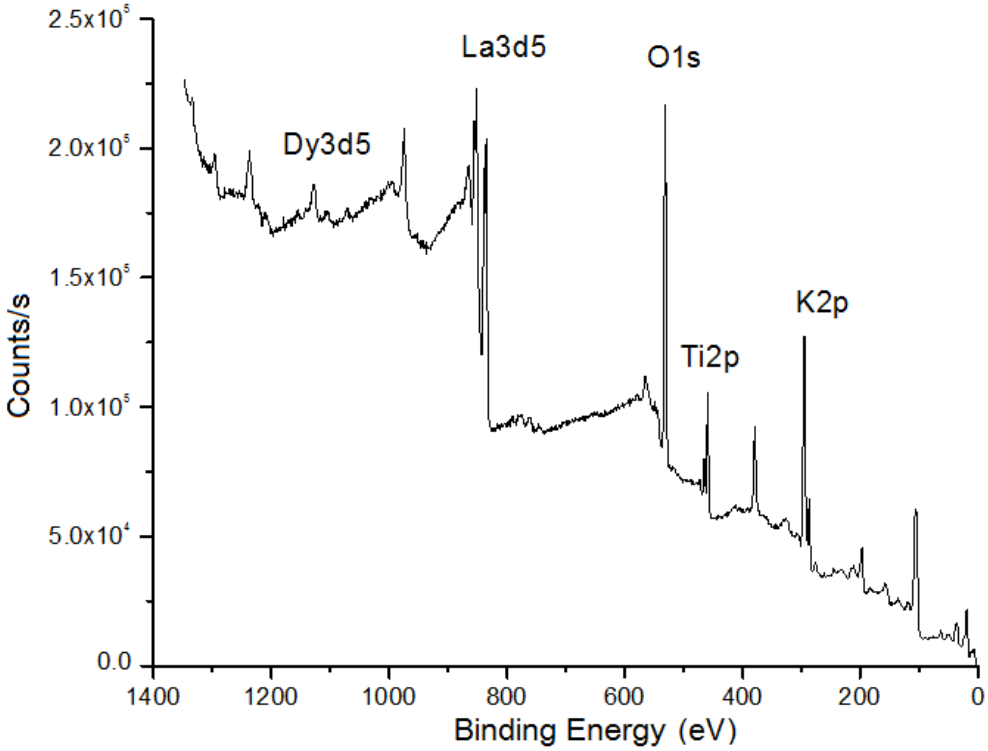

Figure 4.60 XPS spectrum for $K_2La_{1.5}Dy_{0.5}Ti_3O_{10}$.

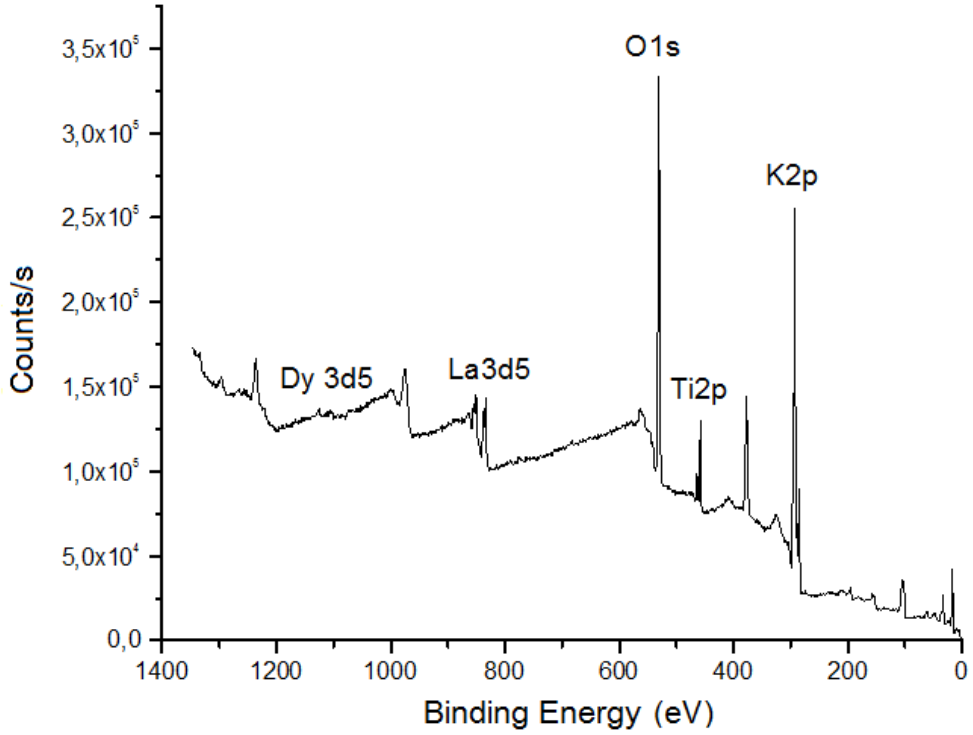

Figure 4.61 XPS spectrum for $K_2La_{1.1}Dy_{0.9}Ti_3O_{10}$.

4.3.4 Surface Roughness

Surface roughness was measured for each sample with different amount of dopant. As can be seen in Table 4.4 that the change of the surface roughness was not depend on dopant amount or type. The reason is due to the variety of the grain size of the powders and that is why, the coating was realized after the dispersion of the powders.

Table 4.4 Surface roughness

Sample	R_a	R_z	Sample	R_a	R_z
Pure	3.73	26.13	0.1 Gd	0.18	1.77
0.1 Sm	1.84	15.77	0.5 Gd	0.25	2.66
0.5 Sm	0.9	8.27	0.9 Gd	1.01	12.26
0.9 Sm	0.29	3.43	0.1 Nd	0.61	6.53
0.1 Dy	0.64	5.98	0.5 Nd	0.884	7.48
0.5 Dy	0.32	3	0.9 Nd	0.49	5.10
0.9 Dy	0.35	4			

4.3.5 Mechanical Tests

Nanoidentaiton tests were applied with five different loads including, 2, 4, 6, 8 and 10 mN. The applied load (P), penetration depth (h_t), hardness (H) and modulus of elasticity (E) can be seen in Table 4.5. Due to the increase of the applied load, it is expected that the penetration depth also will increase. But according to the results of the analysis a fluctuation occurred. Although the increase of the depth which was seen in some places, it was determined that some coatings had a decrease of the depth with the increase of the load. The reason can be the inhomogenity of the coatings. To obtain the best results, coating was carried out separately for each sample. Depending on the results of the nanoidentation of coatings, the highest hardness and modulus of elasticity were determined for $K_2La_{1.5}Nd_{0.5}Ti_3O_{10}$ (0.5Nd). The results can be seen in Table 4.5.

Table 4.5 Mechanical properties of the coatings

Sample	P (mN)	h_t (m)	E (GPa)	H (GPa)	Sample	P (mN)	h_t (m)	E (GPa)	H (GPa)
Pure KLTO	2	1.06	7.98	0.07	**0.1 Gd**	2	0.92	4.54	0.12
	4	1.44	21.76	0.08		4	1.28	1.92	0.01
	6	2.13	15.20	0.05		6	2.12	4.35	0.05
	8	3.55	9.29	0.02		8	1.85	2.45	0.002
	10	254	24.35	0.06		10	5.18	3.01	0.007
0.1 Sm	2	2.68	3.20	0.01	**0.5 Gd**	2	0.83	5.60	0.13
	4	2.39	3.04	0.03		4	3.49	1.84	0.01
	6	3.12	4.41	0.02		6	2.43	4.39	0.04
	8	1.71	7.66	0.12		8	8.24	2.73	0.004
	10	3.90	3.04	0.02		10	7.17	2.92	0.008
0.5 Sm	2	0.46	13.72	0.47	**0.9 Gd**	2	1.88	1.93	0.02
	4	4.44	1.50	0.008		4	1.34	5.39	0.10
	6	3.60	3.16	0.01		6	3.25	3.32	0.0241
	8	3.38	7.11	0.02		8	3.73	2.88	0.0247
	10	2.38	12.6	0.07		10	4.43	335	0.0216
0.9 Sm	2	1.12	2.83	0.07	**0.1 Nd**	2	1.43	4.44	0.04
	4	2.91	1.12	0.02		4	2.34	6.64	0.03
	6	8.17	0.87	0.003		6	3.14	6.29	0.025
	8	6.66	1.33	0.007		8	3.52	8.84	0.026
	10	1.16	6.93	0.43		10	1.96	19.37	0.11
0.1 Dy	2	0.83	11.9	0.12	**0.5 Nd**	2	0.12	84.47	51.39
	4	2.17	8.22	0.035		4	0.27	28.69	9.94
	6	2.85	8.98	0.03		6	0.41	18.48	5.22
	8	2.37	13.12	0.05		8	0.57	12.98	3.06
	10	1.92	18.91	0.11		10	0.72	10.30	2.39
0.5 Dy	2	3.62	5.48	0.04	**0.9 Nd**	2	1.71	4.16	0.029
	4	3.85	5.33	0.01		4	2.76	4.61	0.0219
	6	2.68	2.93	0.03		6	3.42	4.70	0.0213
	8	2.62	4.65	0.054		8	2.81	10.04	0.04
	10	2.14	5.51	0.09		10	4.14	7.50	0.024
0.9 Dy	2	0.48	18.4	0.39	**Si (100)**	2	0.03	3481	434
	4	2.11	8.23	0.03		4	0.06	940	145
	6	1.09	19.9	0.22		6	0.07	1006	162
	8	1.32	27.7	0.1956		8	0.09	758	129
	10	1.47	29.3	0.195		10	0.13	447	65

4.4 Photocatalytic Degradation Experiment Results

The aim is to determine the effect of pH and light intensity on the degradation efficiencies. For different photocatalyst, the beakers were filled till 25 ml and it was placed on the testing apparatus Atlas Suntest CPS+.

To determine effective pH value for the photodegradation of methylene blue, different pH values were carried out: acidic (pH=3), neutral (pH=7) and alkali (pH=10) conditions at 10^{-5} M initial pollutant concentrations. In cyanide studies, pH value was observed at alkali condition due to the toxic effect of cyanide at low pH values. Phenol tests were carried out at pH 7. pH was kept constant by using H_2SO_4 or NaOH depending on the experimental conditions.

The removal efficiencies of phenol, methylene blue and cyanide are given in tables below as a function of light intensity. The degradation experiments were analyzed with 13 different thin films, and a beaker without photocatalyst was analyzed as blank to make a comparison. The testing sets were planned 5 hours reaction time for phenol, 4 hours for cyanide and 3 and 5 hours for methylene blue. Some experiments were given in detail at the tables below.

4.4.1 Photodegradation Results of Phenol

Phenol degradation tests were carried out by using 10 mg/l initial phenol concentration. The pH was adjusted at 3 and different light intensities were observed to determine the effect of light intensity on the photodegradation process. Therefore, experiments were carried out at two different light intensities: 250 W/m^2 and 750 W/m^2. To understand the degradation efficiencies of thin films, a reference experiment (blank which not includes any photocatalyst into the phenol solution) was analyzed. According to the results, a slight degradation efficiency difference was determined between 250 W/m^2 and 750 W/m^2.

The most effective results of 250 W/m^2 were examined at Table 4.6 which gives phenol degradation efficiencies under 10 mg/l initial concentration, and pH at 7 conditions. Figure 4.63 and 4.64 were illustrated graphically based on the variation of the concentration vs. time and efficiency vs. time of phenol. The reaction time of the experiments was selected 5 hours as mention before. Following 5 hours, the best result obtained by using $K_2La_{1.5}Sm_{0.5}Ti_3O_{10}$ where the phenol concentration decreased from 10 mg/l to 2.78 mg/l and 72.2% degradation efficiency was realized.

Table 4.6 Degradation efficiencies of phenol for 10 mg/l, 250 W/m^2 and pH = 7 after 5 hours reaction time

Photocatalyst	Initial Concentration (mg/l)	Effluent Concentration (mg/l)	Degradation Efficiency (%)
$K_2La_2Ti_3O_{10}$	10	3.13	68.7
$K_2La_{1.9}Sm_{0.1}Ti_3O_{10}$	10	3.49	65.1
$K_2La_{1.5}Sm_{0.5}Ti_3O_{10}$	10	2.78	72.2
$K_2La_{1.1}Sm_{0.9}Ti_3O_{10}$	10	4.56	54.4
Blank	10	7.32	26.8

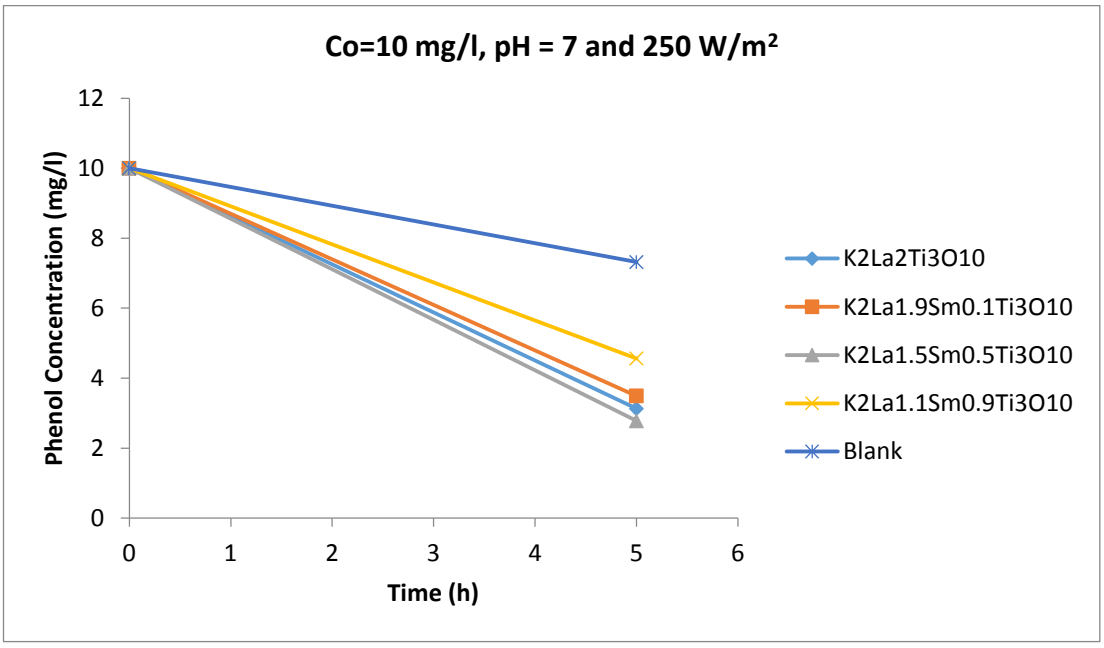

Figure 4.62 Phenol concentration vs. time results (Co=10 mg/l, 250 W/m^2 and pH = 7).

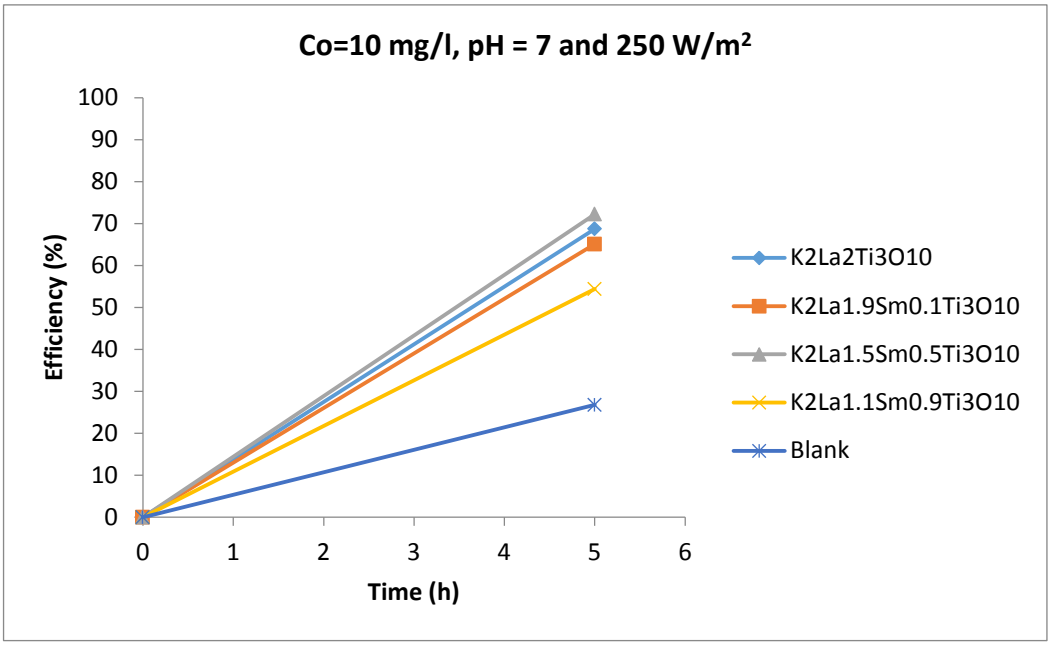

Figure 4.63 Phenol removal efficiencies (%) (Co = 10 mg/l, 250 W/m^2 and pH = 7).

The same conditions realized at this stage but instead of using 250 W/m^2 light intensity, 750 W/m^2 was observed. The experiments took again 5 hours. After the 5 hours reaction time, phenol concentrations were measured. Detailed information can be seen at Table 4.7 and Figure 4.65 and 4.66 demonstrate graphically the decrease of the phenol concentration and degradation efficiency, respectively. As can be seen at the Table 4.8 and the figures below that the best photocatalyst for phenol degradation among the 13 photocatalyst was determined $K_2La_{1.5}Sm_{0.5}Ti_3O_{10}$. 75.3% of degradation efficiency was found according to the results.

Table 4.7 Degradation efficiencies of phenol for 10 mg/l, 750 W/m^2 and pH = 7 after 5 hours reaction time

Photocatalyst	**Initial Concentration (mg/l)**	**Effluent Concentration (mg/l)**	**Degradation Efficiency (%)**
$K_2La_2Ti_3O_{10}$	10	2.98	70.2
$K_2La_{1.9}Sm_{0.1}Ti_3O_{10}$	10	3.19	68.1
$K_2La_{1.5}Sm_{0.5}Ti_3O_{10}$	10	2.47	75.3
$K_2La_{1.1}Sm_{0.9}Ti_3O_{10}$	10	3.68	63.2
Blank	10	6.07	39.3

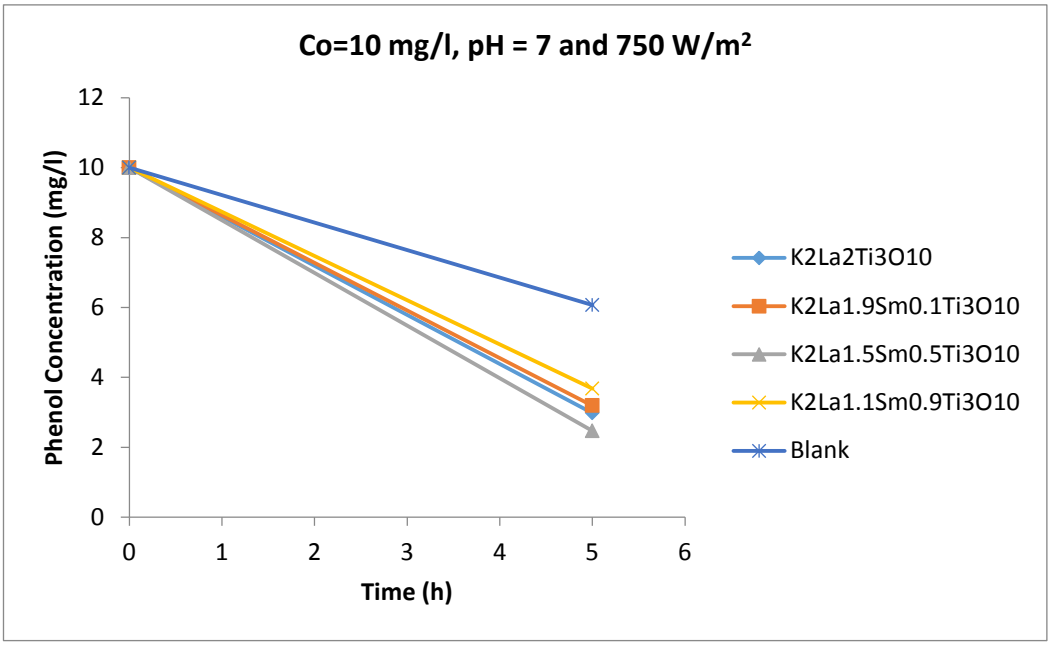

Figure 4.64 Phenol concentration vs. time results (Co=10 mg/l, 750 W/m^2, pH=7).

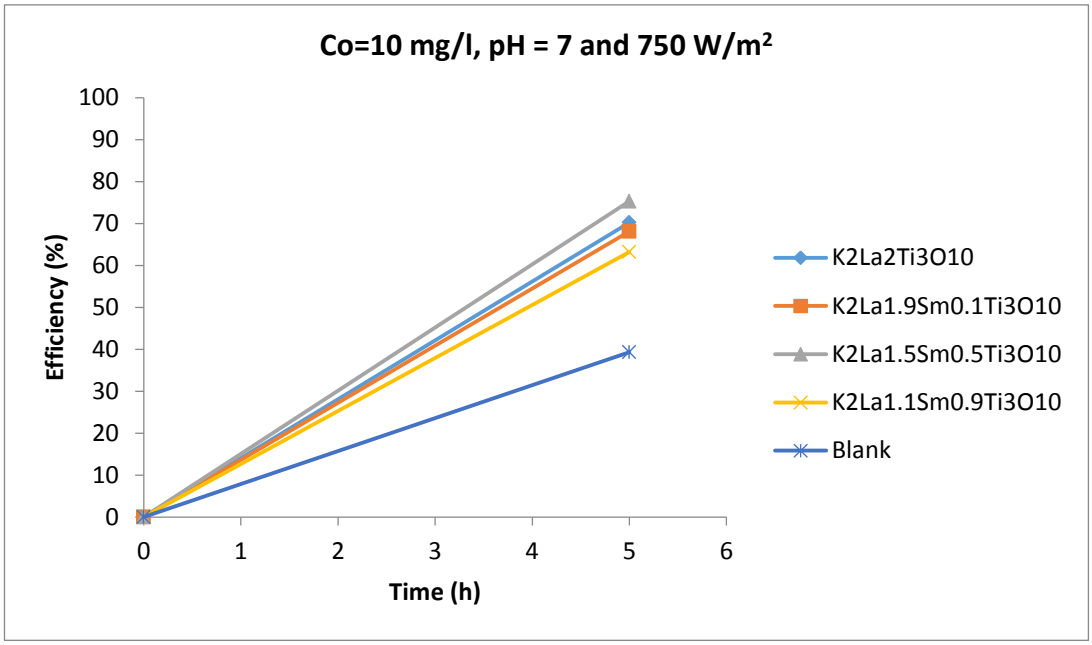

Figure 4.65 Phenol removal efficiencies (%) (Co = 10 mg/l, 750 W/m^2 and pH = 7).

Table 4.8 shows summary information on phenol degradation. According the two different conditions, the most effective photocatalyst were chosen $K_2La_{1.5}Sm_{0.5}Ti_3O_{10}$. The increase of light intensity has small effect on phenol removal. The bold characters illustrate the best effective results on phenol removal.

Table 4.8 Effect of light intensity for phenol removal

Photocatalyst	Effluent Concentration (mg/l)	Degradation Efficiency (%)	Effluent Concentration (mg/l)	Degradation Efficiency (%)
	250 W/m^2		750 W/m^2	
$K_2La_2Ti_3O_{10}$	3.13	68.7	2.98	70.2
$K_2La_{1.9}Sm_{0.1}Ti_3O_{10}$	3.49	65.1	3.19	68.1
$K_2La_{1.5}Sm_{0.5}Ti_3O_{10}$	**2.78**	**72.2**	**2.47**	**75.3**
$K_2La_{1.1}Sm_{0.9}Ti_3O_{10}$	4.56	54.4	3.68	63.2
Blank	7.32	26.8	6.07	39.3

4.4.2 Photodegradation Results of Methylene Blue

The concentration of methylene blue was determined by the absorbance of reaction at 664 nm. The pH was selected 3, 7 and 10 to understand the effect of the pH. The photocatalytic degradation of methylene blue by using thin films can be shown at the tables and figures below. The main responsible characteristics of color are the chromophores and these were broken down during the degradation reactions. A blank was analyzed to examine the efficiency of the photocatalysts. The aim is to achieve the decolorization during the photocatalytic reaction and to obtain optimum conditions and the best photocatalyst.

Firstly, the degradation rate of methylene blue experiment which pH is 3 was given in detail at Table 4.9 and 4.10 for 10^{-5} M initial concentration, and 250 or 750 W/m^2 light intensity, respectively. Figure 4.67, 4.68, 4.69 and 4.70 gave information about the change of the absorbance vs. time and efficiency vs. time of methylene blue.

Table 4.9 Degradation efficiencies of methylene blue for 10^{-5} M, 250 W/m^2 and pH = 3 after 5 hours reaction time

Photocatalyst	Initial Absorbance	Effluent Absorbance	Degradation Efficiency (%)
$K_2La_2Ti_3O_{10}$	0.765	0.451	41
$K_2La_{1.9}Sm_{0.1}Ti_3O_{10}$	0.765	0.344	55
$K_2La_{1.5}Sm_{0.5}Ti_3O_{10}$	0.765	0.107	86
$K_2La_{1.1}Sm_{0.9}Ti_3O_{10}$	0.765	0.214	72
$K_2La_{1.9}Dy_{0.1}Ti_3O_{10}$	0.765	0.428	44
$K_2La_{1.5}.Dy_{0.5}Ti_3O_{10}$	0.765	0.275	64
$K_2La_{1.1}Dy_{0.9}Ti_3O_{10}$	0.765	0.421	45
$K_2La_{1.9}Gd_{0.1}Ti_3O_{10}$	0.765	0.398	48
$K_2La_{1.5}Gd_{0.5}Ti_3O_{10}$	0.765	0.428	44
$K_2La_{1.1}Gd_{0.9}Ti_3O_{10}$	0.765	0.352	54
$K_2La_{1.9}Nd_{0.1}Ti_3O_{10}$	0.765	0.413	46
$K_2La_{1.5}Nd_{0.5}Ti_3O_{10}$	0.765	0.375	51
$K_2La_{1.1}Nd_{0.9}Ti_3O_{10}$	0.765	0.360	53
Blank	0.765	0.612	20

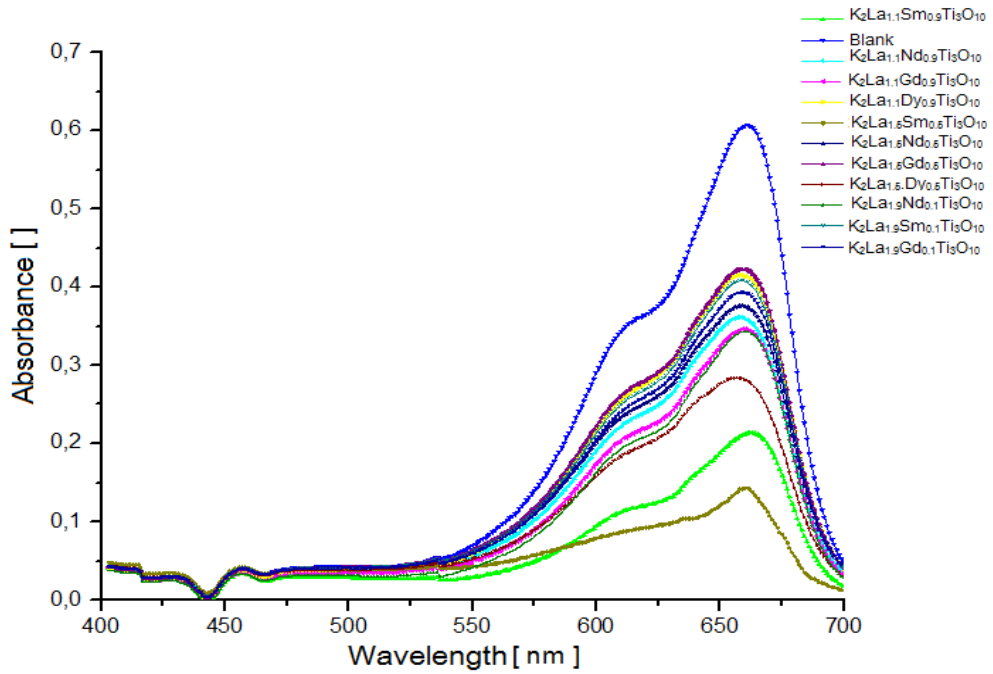

Figure 4.66 Methylene blue degradation absorbance vs. time after 5 hours (Co = 10^{-5} M, 250 W/m^2 and pH = 3).

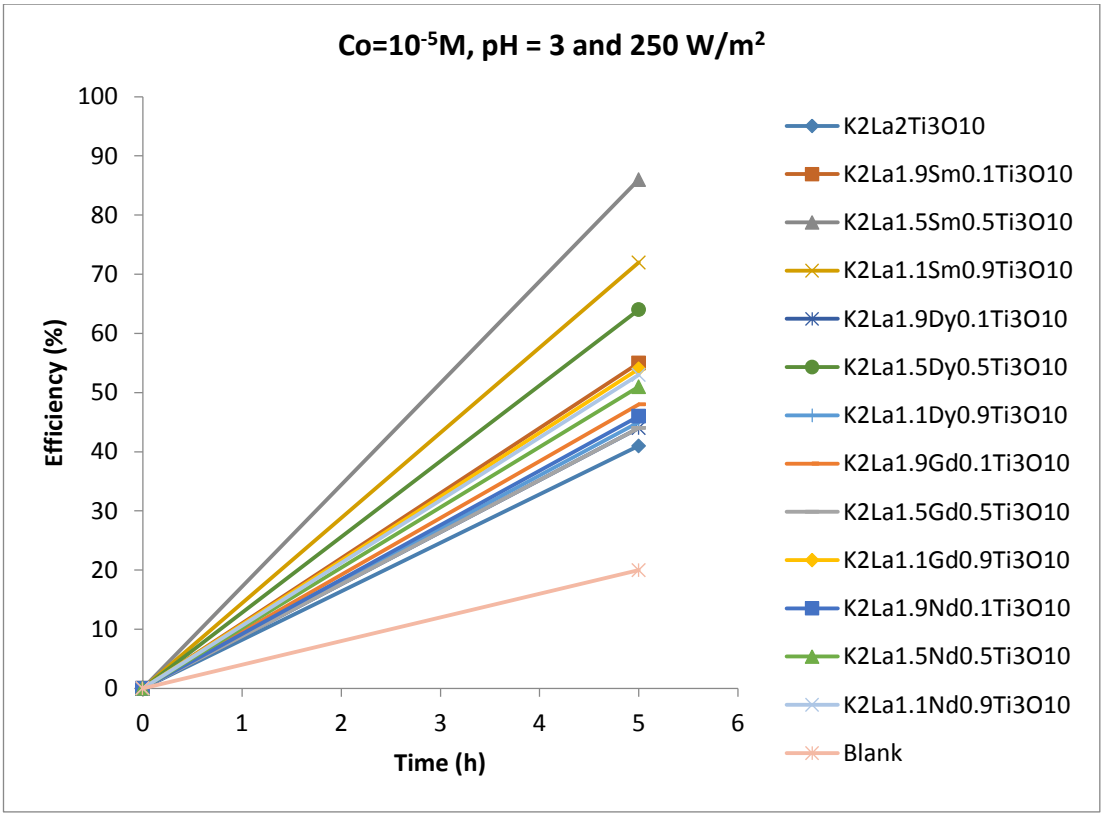

Figure 4.67 Methylene blue removal efficiencies (%) (Co = 10^{-5} M, 250 W/m^2 and pH = 3).

According to the results above, it can be say that the maximum degradation was occurred by using $K_2La_{1.5}Sm_{0.5}Ti_3O_{10}$ photocatalyts which was determined 86% degradation rate under 250 W/m^2 light intensity and after 5 hours reaction time into Atlas Suntest CPS+ at pH 3. At the same conditions, blank demonstrated 20% degradation efficiency.

Now, the light intensity changed and the experiments were analyzed for 750 W/m^2 for the same conditions.

Table 4.10 Degradation efficiencies of methylene blue for 10^{-5} M, 750 W/m^2 and pH = 3 after 5 hours reaction time

Photocatalyst	Initial Absorbance	Effluent Absorbance	Degradation Efficiency (%)
$K_2La_2Ti_3O_{10}$	0.765	0.275	64
$K_2La_{1.9}Sm_{0.1}Ti_3O_{10}$	0.765	0.337	56
$K_2La_{1.5}Sm_{0.5}Ti_3O_{10}$	0.765	0.077	90
$K_2La_{1.1}Sm_{0.9}Ti_3O_{10}$	0.765	0.268	65
$K_2La_{1.9}Dy_{0.1}Ti_3O_{10}$	0.765	0.237	69
$K_2La_{1.5}.Dy_{0.5}Ti_3O_{10}$	0.765	0.237	69
$K_2La_{1.1}Dy_{0.9}Ti_3O_{10}$	0.765	0.314	59
$K_2La_{1.9}Gd_{0.1}Ti_3O_{10}$	0.765	0.245	68
$K_2La_{1.5}Gd_{0.5}Ti_3O_{10}$	0.765	0.291	62
$K_2La_{1.1}Gd_{0.9}Ti_3O_{10}$	0.765	0.329	57
$K_2La_{1.9}Nd_{0.1}Ti_3O_{10}$	0.765	0.291	62
$K_2La_{1.5}Nd_{0.5}Ti_3O_{10}$	0.765	0.230	70
$K_2La_{1.1}Nd_{0.9}Ti_3O_{10}$	0.765	0.314	59
Blank	0.765	0.360	53

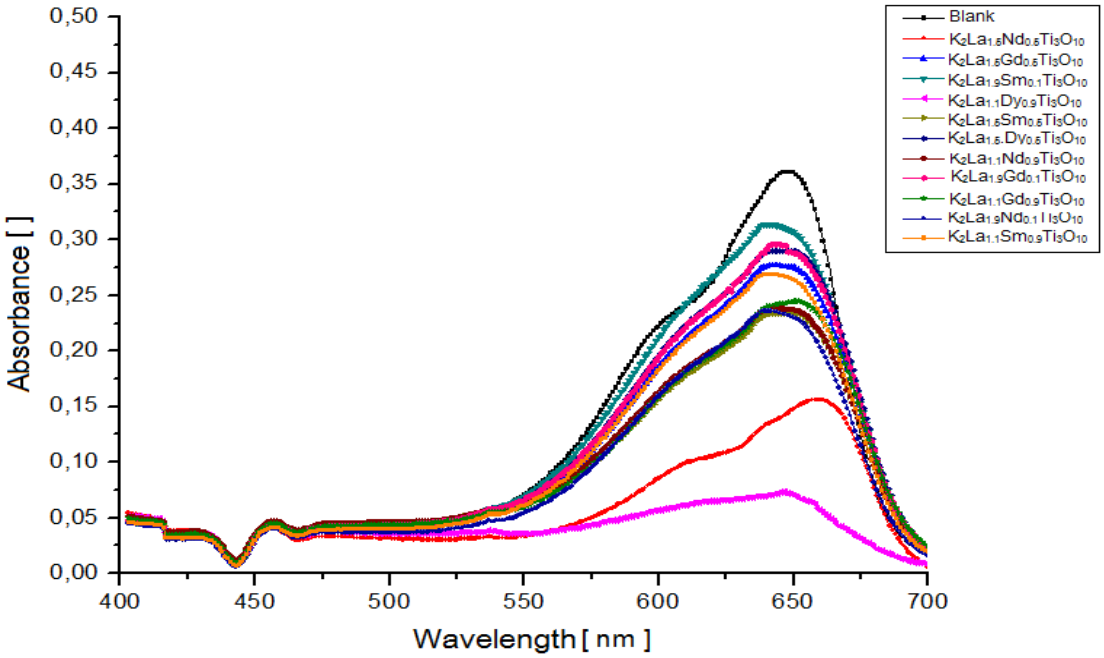

Figure 4.68 Methylene blue degradation absorbance vs. time after 5 hours (Co = 10^{-5} M, 750 W/m^2 and pH = 3).

As a result of the experiments, the best removal was examined by using $K_2La_{1.5}Sm_{0.5}Ti_3O_{10}$ photocatalyts which was determined 90% degradation rate under 750 W/m^2 light intensity and after 5 hours reaction time into Atlas Suntest CPS+ at pH 3. At the same conditions, blank demonstrated 53% degradation efficiency.

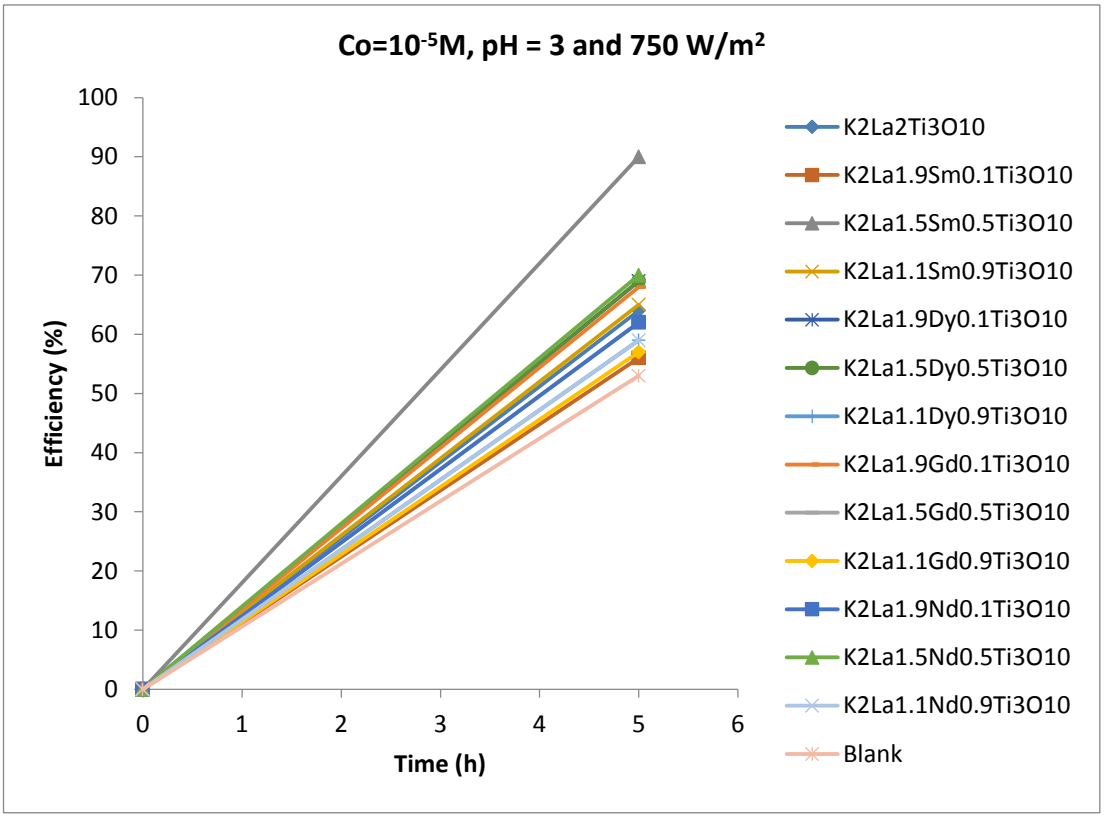

Figure 4.69 Methylene blue removal efficiencies (%) (Co = 10^{-5} M, 750 W/m^2 and pH = 3).

Secondly, the degradation rate of methylene blue experiment at 7 for pH was given in detail at Table 4.11 and 4.12 for 10^{-5} M initial concentration, and 250 or 750 W/m^2 light intensity, respectively. Figure 4.71, 4.72, 4.73 and 4.74 show information about the change of the absorbance vs. time and efficiency vs. time of methylene blue.

Table 4.11 Degradation efficiencies of methylene blue for 10^{-5} M, 750 W/m^2 and pH = 7 after 3 hours reaction time

Photocatalyst	Initial Absorbance	Effluent Absorbance	Degradation Efficiency (%)
$K_2La_2Ti_3O_{10}$	0.765	0.161	79
$K_2La_{1.9}Sm_{0.1}Ti_3O_{10}$	0.765	0.107	86
$K_2La_{1.5}Sm_{0.5}Ti_3O_{10}$	0.765	0.038	95
$K_2La_{1.1}Sm_{0.9}Ti_3O_{10}$	0.765	0.099	87
$K_2La_{1.9}Dy_{0.1}Ti_3O_{10}$	0.765	0.153	80
$K_2La_{1.5}.Dy_{0.5}Ti_3O_{10}$	0.765	0.099	87
$K_2La_{1.1}Dy_{0.9}Ti_3O_{10}$	0.765	0.069	91
$K_2La_{1.9}Gd_{0.1}Ti_3O_{10}$	0.765	0.077	90
$K_2La_{1.5}Gd_{0.5}Ti_3O_{10}$	0.765	0.054	93
$K_2La_{1.1}Gd_{0.9}Ti_3O_{10}$	0.765	0.054	93
$K_2La_{1.9}Nd_{0.1}Ti_3O_{10}$	0.765	0.130	83
$K_2La_{1.5}Nd_{0.5}Ti_3O_{10}$	0.765	0.099	87
$K_2La_{1.1}Nd_{0.9}Ti_3O_{10}$	0.765	0.130	83
Blank	0.765	0.245	68

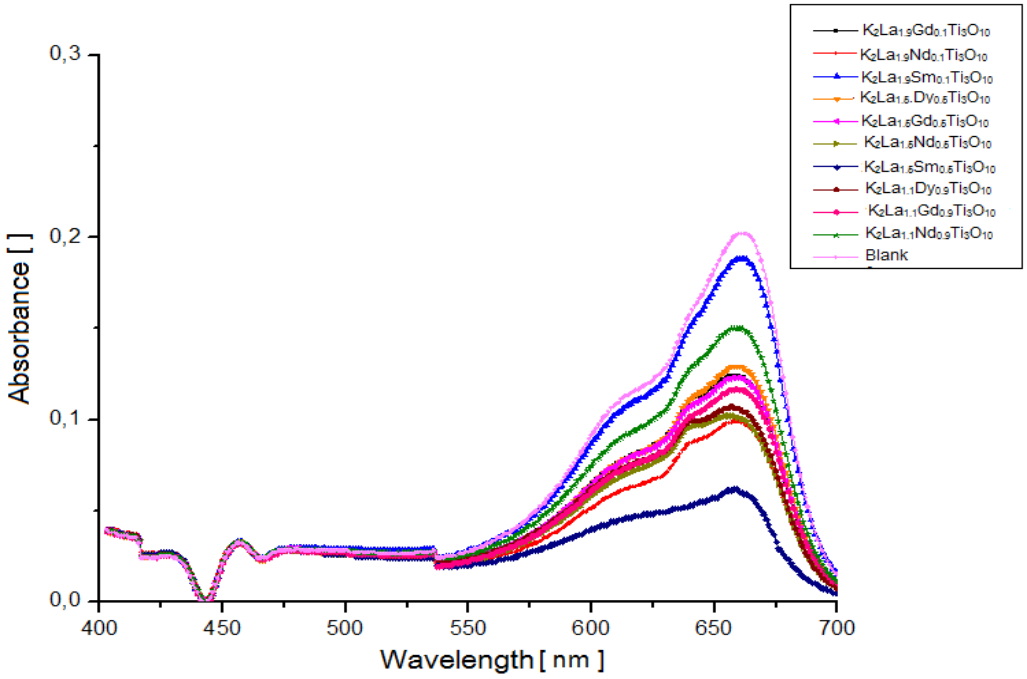

Figure 4.70 Methylene blue degradation absorbance vs. time after 3 hours (Co = 10^{-5} M, 250 W/m^2 and pH = 7).

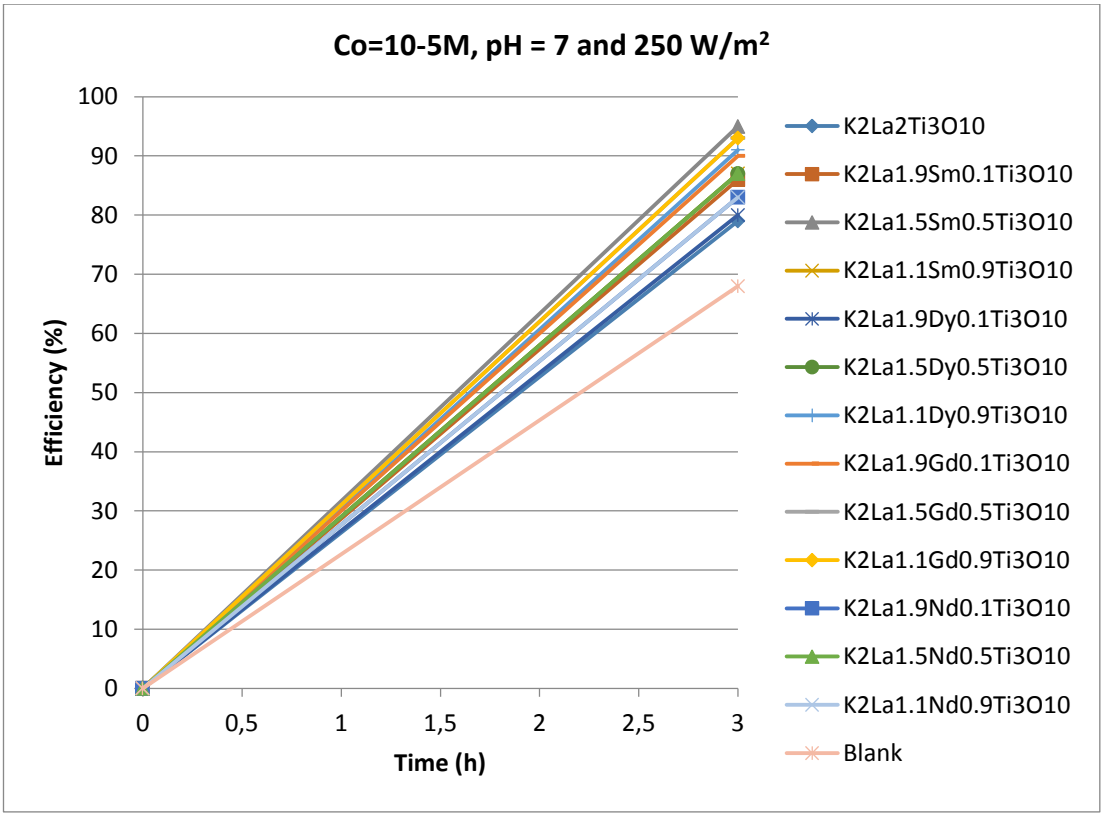

Figure 4.71 Methylene blue removal efficiencies (%) (Co = 10^{-5} M, 250 W/m^2 and pH = 7).

As a result of the removal rates which can be seen at Table 4.11, the best removal was observed by using $K_2La_{1.5}Sm_{0.5}Ti_3O_{10}$ photocatalyts which was determined 95% degradation rate under 250 W/m^2 light intensity and after 3 hours reaction time into Atlas Suntest CPS+ at pH 7. At the same conditions, blank demonstrated 68% degradation efficiency.

Now, the light intensity condition changed and the experiments were carried out for 750 W/m^2.

Table 4.12 Degradation efficiencies of methylene blue for 10^{-5} M, 750 W/m^2 and pH = 7 after 3 hours reaction time

Photocatalyst	Initial Absorbance	Effluent Absorbance	Degradation Efficiency (%)
$K_2La_2Ti_3O_{10}$	0.765	0.145	81
$K_2La_{1.9}Sm_{0.1}Ti_3O_{10}$	0.765	0.115	85
$K_2La_{1.5}Sm_{0.5}Ti_3O_{10}$	0.765	0.023	97
$K_2La_{1.1}Sm_{0.9}Ti_3O_{10}$	0.765	0.099	87
$K_2La_{1.9}Dy_{0.1}Ti_3O_{10}$	0.765	0.153	80
$K_2La_{1.5}.Dy_{0.5}Ti_3O_{10}$	0.765	0.099	87
$K_2La_{1.1}Dy_{0.9}Ti_3O_{10}$	0.765	0.069	91
$K_2La_{1.9}Gd_{0.1}Ti_3O_{10}$	0.765	0.084	89
$K_2La_{1.5}Gd_{0.5}Ti_3O_{10}$	0.765	0.054	93
$K_2La_{1.1}Gd_{0.9}Ti_3O_{10}$	0.765	0.054	93
$K_2La_{1.9}Nd_{0.1}Ti_3O_{10}$	0.765	0.138	82
$K_2La_{1.5}Nd_{0.5}Ti_3O_{10}$	0.765	0.099	87
$K_2La_{1.1}Nd_{0.9}Ti_3O_{10}$	0.765	0.138	82
Blank	0.765	0.222	71

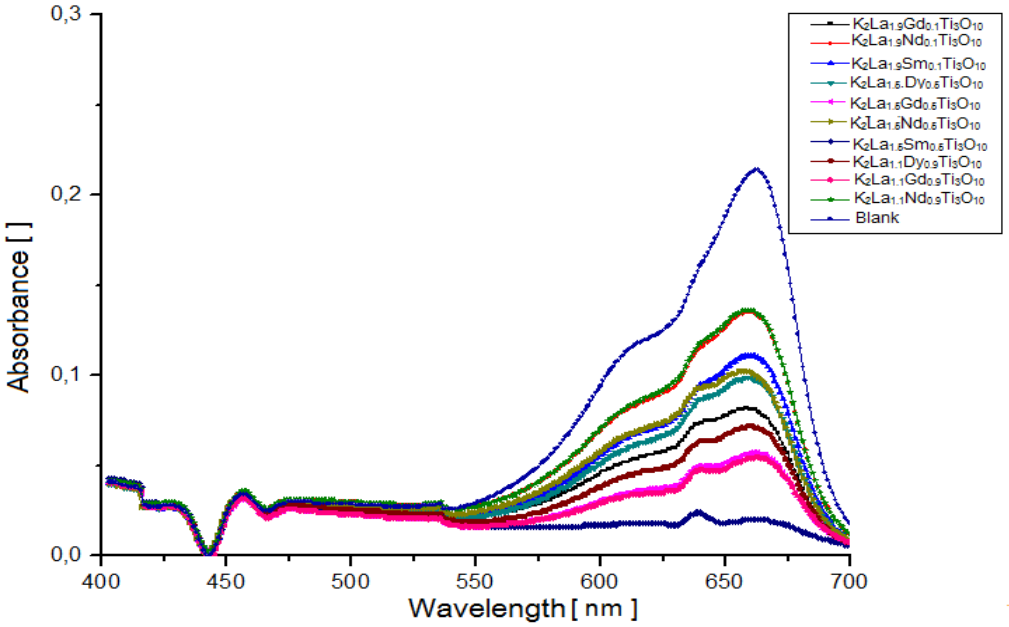

Figure 4.72 Methylene blue degradation absorbance vs. time after 3 hours (Co = 10^{-5} M, 750 W/m^2 and pH = 7).

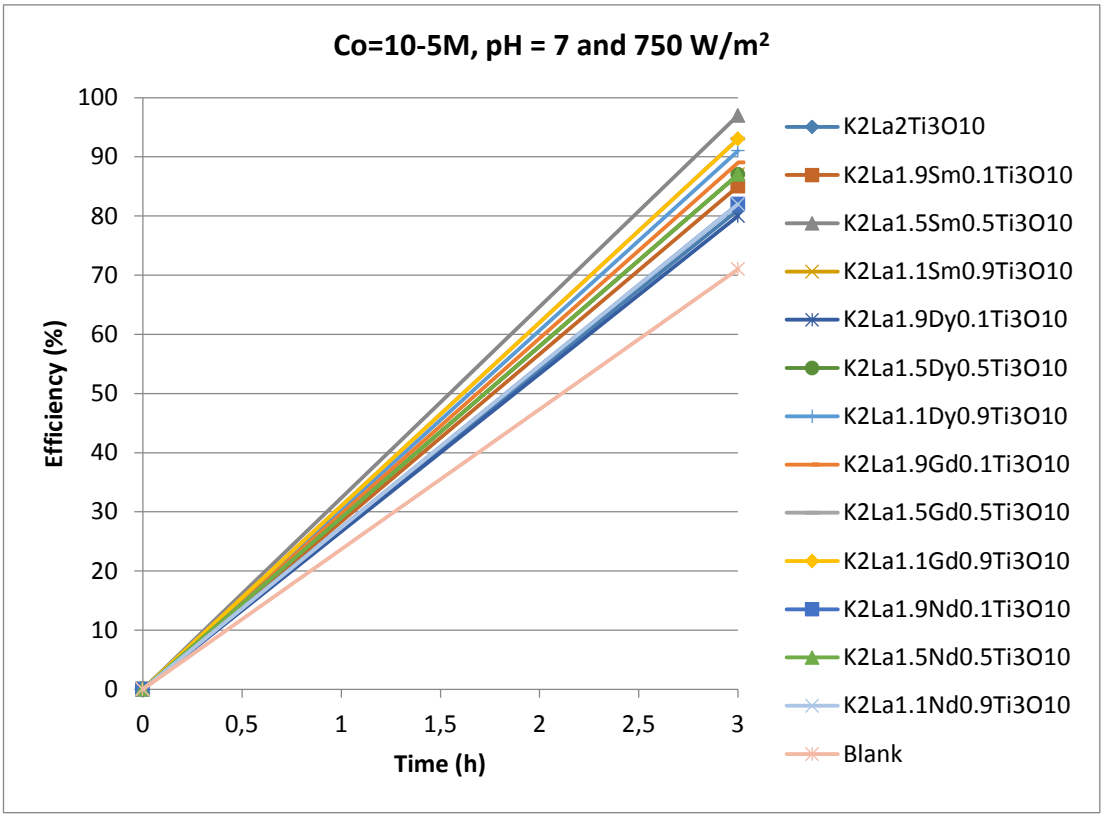

Figure 4.73 Methylene blue removal efficiencies (%) (Co = 10^{-5} M, 750 W/m^2 and pH = 7).

According to the results which are seen in Table 4.12, it can be say that the maximum degradation was determined by using $K_2La_{1.5}Sm_{0.5}Ti_3O_{10}$ photocatalyts which was 97% degradation rate under 750 W/m^2 light intensity and after 3 hours reaction time into Atlas Suntest CPS+ at pH 7. At the same conditions, blank demonstrated 71% degradation efficiency.

Thirdly, the degradation rate of methylene blue experiment at pH 10 was shown in detail at Table 4.13 and 4.14 for 10^{-5} M initial concentration, and 250 or 750 W/m^2 light intensity, respectively. Figure 4.75, 4.76, 4.77, 4.78, 4.79, 4.80, 4.81 and 4.82 show information about the change of the absorbance vs. time and efficiency vs. time of methylene blue. Absorbance values were separately given because the results are very close and were not clear to read.

Table 4.13 Degradation efficiencies of methylene blue for 10^{-5} M, 250 W/m^2 and pH = 10 after 30 minutes reaction time

Photocatalyst	Initial Absorbance	Effluent Absorbance	Degradation Efficiency (%)
$K_2La_2Ti_3O_{10}$	0.765	0.184	76
$K_2La_{1.9}Sm_{0.1}Ti_3O_{10}$	0.765	0.214	72
$K_2La_{1.5}Sm_{0.5}Ti_3O_{10}$	0.765	0.069	91
$K_2La_{1.1}Sm_{0.9}Ti_3O_{10}$	0.765	0.092	88
$K_2La_{1.9}Dy_{0.1}Ti_3O_{10}$	0.765	0.153	80
$K_2La_{1.5}.Dy_{0.5}Ti_3O_{10}$	0.765	0.099	87
$K_2La_{1.1}Dy_{0.9}Ti_3O_{10}$	0.765	0.107	86
$K_2La_{1.9}Gd_{0.1}Ti_3O_{10}$	0.765	0.115	85
$K_2La_{1.5}Gd_{0.5}Ti_3O_{10}$	0.765	0.153	80
$K_2La_{1.1}Gd_{0.9}Ti_3O_{10}$	0.765	0.107	86
$K_2La_{1.9}Nd_{0.1}Ti_3O_{10}$	0.765	0.115	85
$K_2La_{1.5}Nd_{0.5}Ti_3O_{10}$	0.765	0.107	86
$K_2La_{1.1}Nd_{0.9}Ti_3O_{10}$	0.765	0.107	86
Blank	0.765	0.314	59

The maximum degradation was determined by using $K_2La_{1.5}Sm_{0.5}Ti_3O_{10}$ photocatalyts which was 91% degradation rate under 250 W/m^2 light intensity and after 30 minutes reaction time into Atlas Suntest CPS+ at pH 10. At the same conditions, blank demonstrated 59% degradation efficiency.

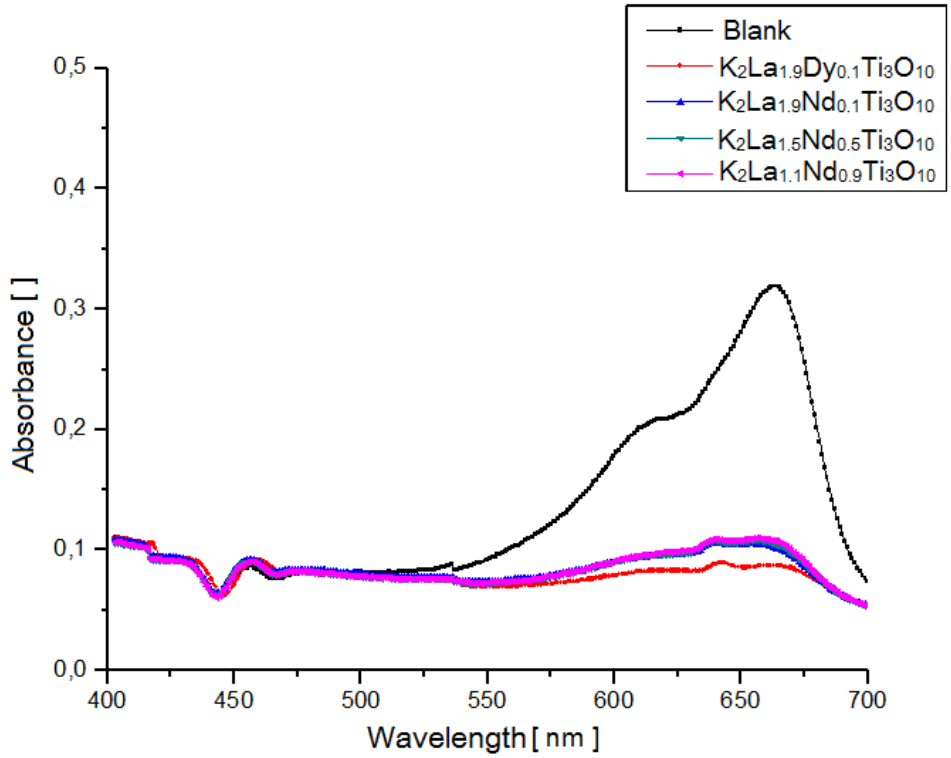

Figure 4.74 Methylene blue degradation absorbance vs. time after 30 minutes (Co = 10^{-5} M, 250 W/m^2 and pH = 10).

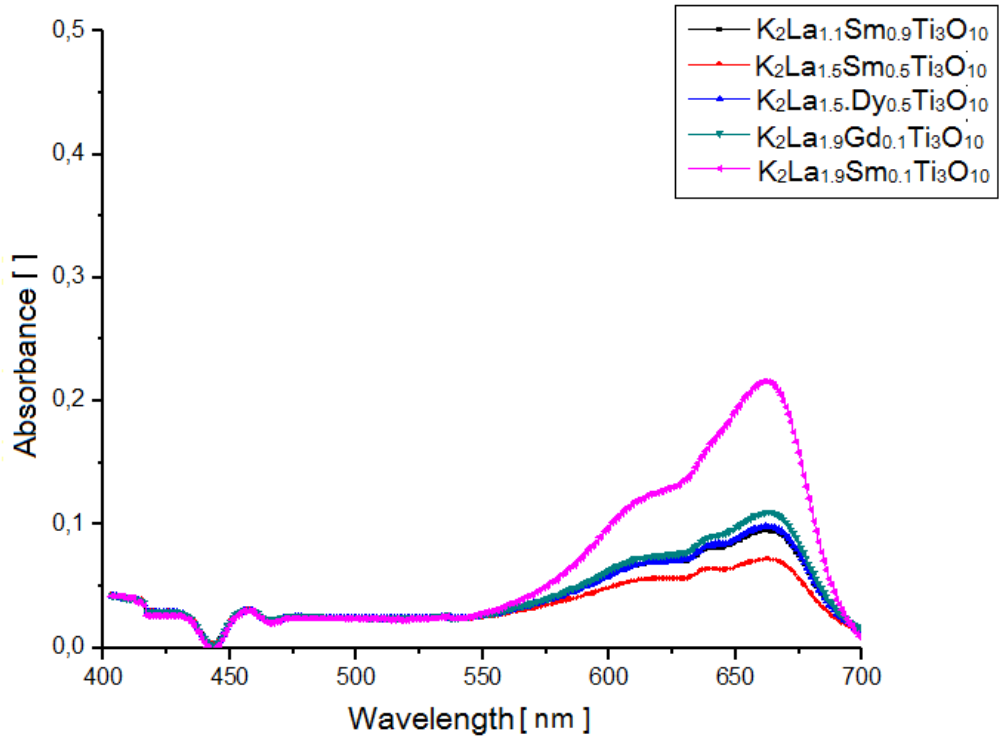

Figure 4.75 Methylene blue degradation absorbance vs. time after 30 minutes (cont.) (Co = 10^{-5} M, 250 W/m^2 and pH = 10).

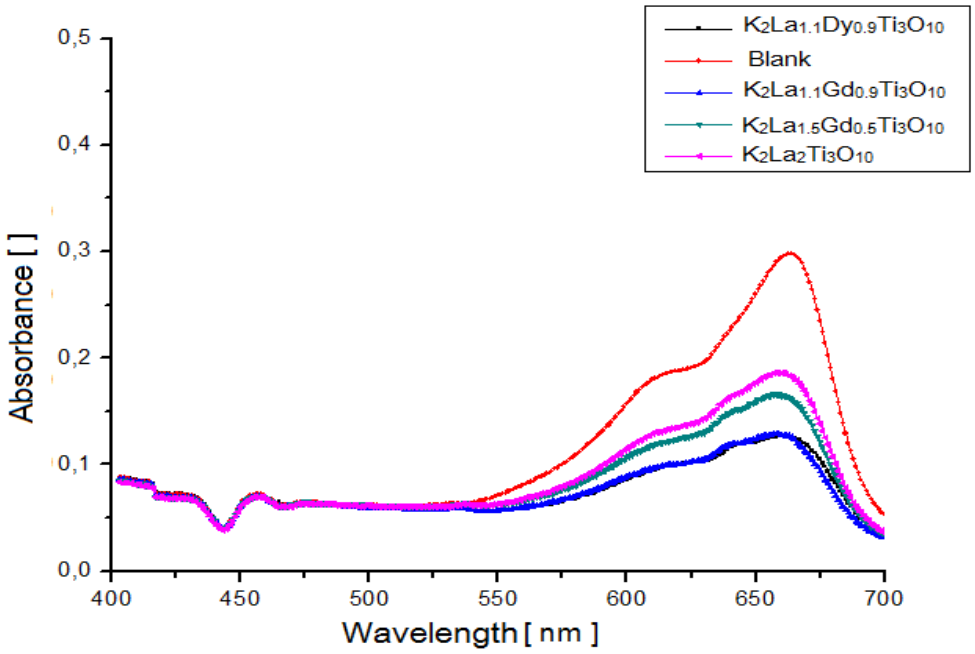

Figure 4.76 Methylene blue degradation absorbance vs. time after 30 minutes (cont.) (Co = 10^{-5} M, 250 W/m^2 and pH = 10).

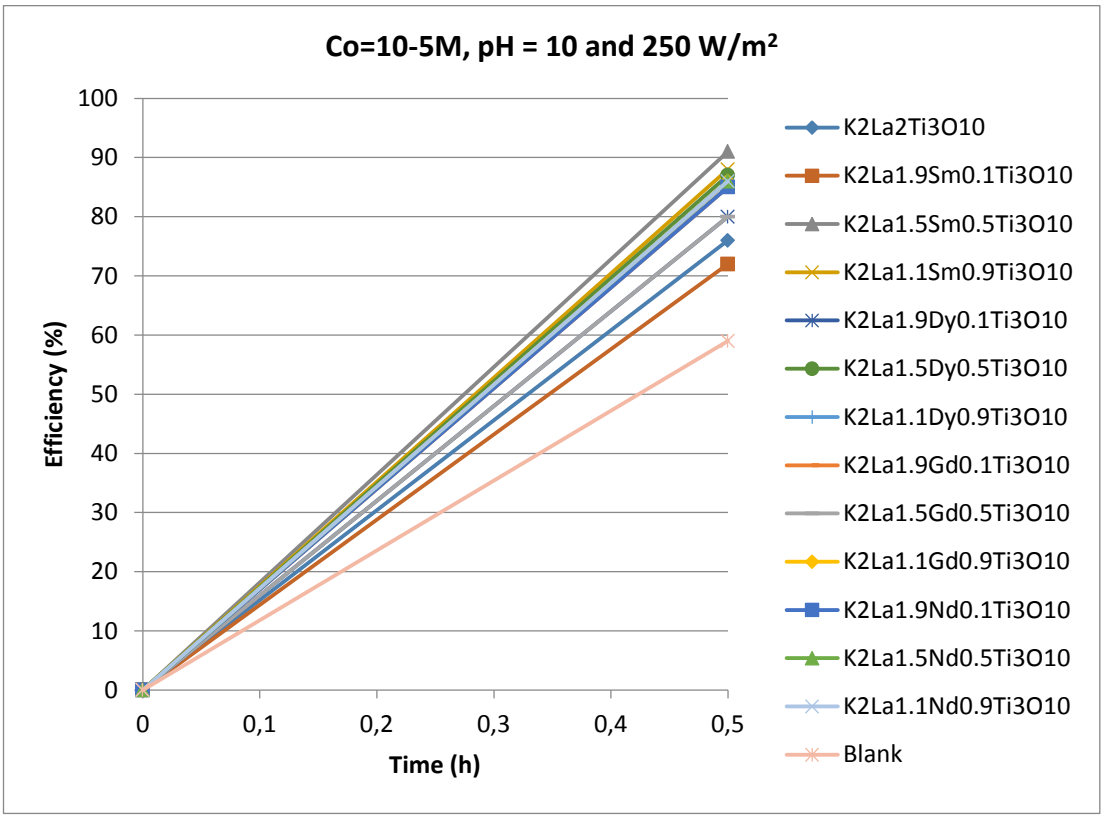

Figure 4.77 Methylene blue removal efficiencies (%) (Co = 10^{-5} M, 250 W/m^2 and pH = 10).

For 750 W/m^2 light intensity, the results can be seen as follows.

Table 4.14 Degradation efficiencies of methylene blue for 10^{-5} M, 750 W/m^2 and pH = 10 after 30 minutes reaction time

Photocatalyst	Initial Absorbance	Effluent Absorbance	Degradation Efficiency (%)
$K_2La_2Ti_3O_{10}$	0.765	0.061	92
$K_2La_{1.9}Sm_{0.1}Ti_3O_{10}$	0.765	0.084	89
$K_2La_{1.5}Sm_{0.5}Ti_3O_{10}$	0.765	0.054	93
$K_2La_{1.1}Sm_{0.9}Ti_3O_{10}$	0.765	0.107	86
$K_2La_{1.9}Dy_{0.1}Ti_3O_{10}$	0.765	0.214	72
$K_2La_{1.5}.Dy_{0.5}Ti_3O_{10}$	0.765	0.184	76
$K_2La_{1.1}Dy_{0.9}Ti_3O_{10}$	0.765	0.023	97
$K_2La_{1.9}Gd_{0.1}Ti_3O_{10}$	0.765	0.138	82
$K_2La_{1.5}Gd_{0.5}Ti_3O_{10}$	0.765	0.015	98
$K_2La_{1.1}Gd_{0.9}Ti_3O_{10}$	0.765	0.015	98
$K_2La_{1.9}Nd_{0.1}Ti_3O_{10}$	0.765	0.122	84
$K_2La_{1.5}Nd_{0.5}Ti_3O_{10}$	0.765	0.061	92
$K_2La_{1.1}Nd_{0.9}Ti_3O_{10}$	0.765	0.099	87
Blank	0.765	0.275	64

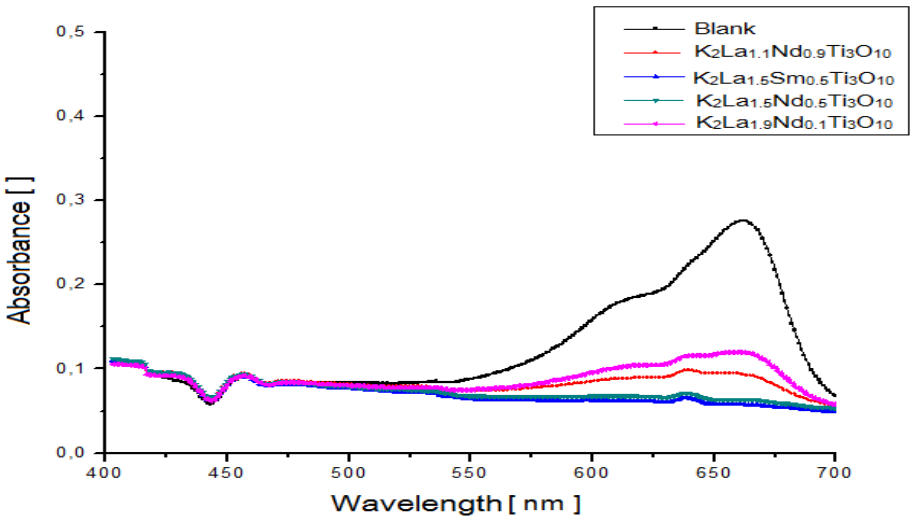

Figure 4.78 Methylene blue degradation absorbance vs. time after 30 minutes (Co = 10^{-5} M, 750 W/m^2 and pH = 10).

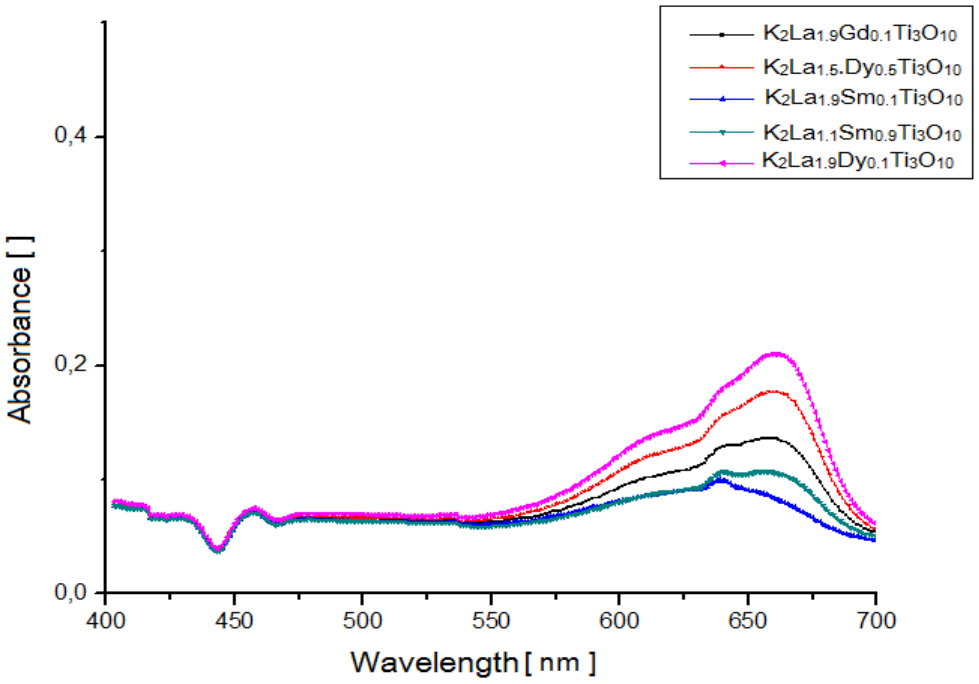

Figure 4.79 Methylene blue degradation absorbance vs. time after 30 minutes (cont.) (Co = 10^{-5} M, 750 W/m^2 and pH = 10).

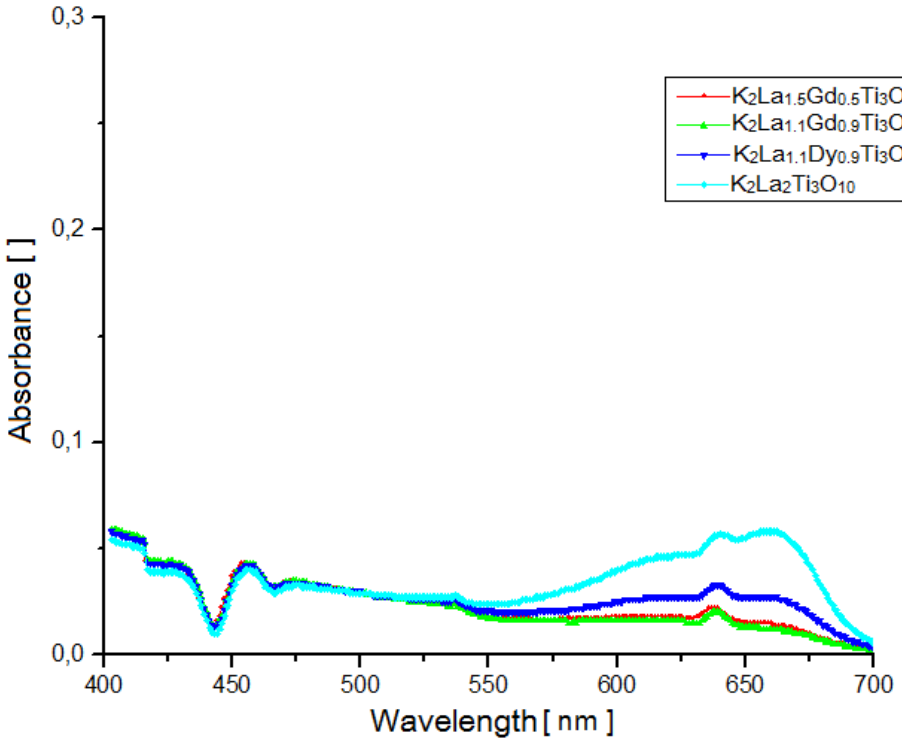

Figure 4.80 Methylene blue degradation absorbance vs. time after 30 minutes (cont.) (Co = 10^{-5} M, 750 W/m^2 and pH = 10).

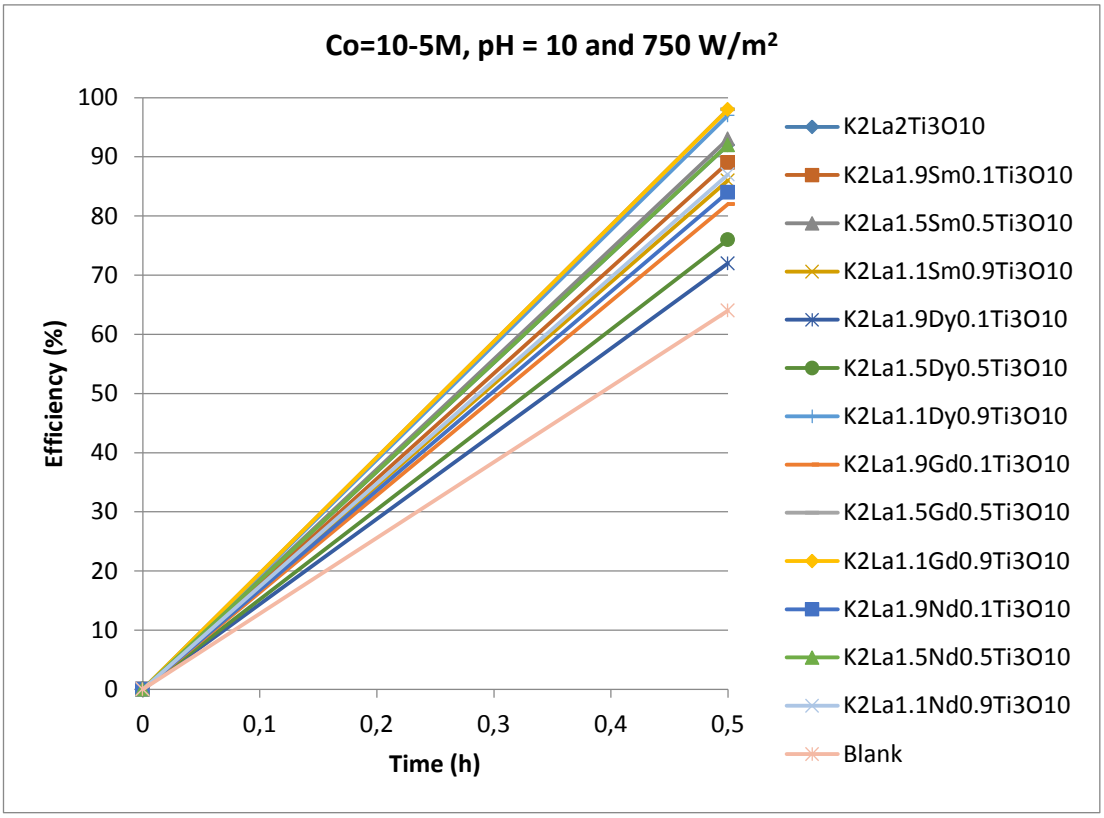

Figure 4.81 Methylene blue removal efficiencies (%) (Co = 10^{-5} M, 250 W/m^2 and pH = 10).

The best effective photocatalysts were determined $K_2La_{1.5}Gd_{0.5}Ti_3O_{10}$ and $K_2La_{1.5}Gd_{0.9}Ti_3O_{10}$ photocatalyts. The degradation rates were the same, 98% under 750 W/m^2 light intensity and after 30 minutes reaction time into Atlas Suntest CPS+ at pH 10. Same conditions were observed for the blank and the degradation rate determined 64% degradation efficiency.

Finally, Table 4.15 shows summary information of methylene blue degradation. According to the different conditions, the best effective photocatalyst were generally chosen $K_2La_{1.5}Sm_{0.5}Ti_3O_{10}$. The bold characters demonstrate the best effective degradation results.

Table 4.15 Effect of pH and light intensity for methylene blue removal

Photocatalyst	Degradation Efficiencies (%)					
	pH = 3 (5 h reaction time)		pH = 7 (3 h reaction time)		pH = 10 (30 min reaction time)	
	250 W/m^2	750 W/m^2	250 W/m^2	750 W/m^2	250 W/m^2	750 W/m^2
$K_2La_2Ti_3O_{10}$	41	64	79	81	76	92
$K_2La_{1.9}Sm_{0.1}Ti_3O_{10}$	55	56	86	85	72	89
$K_2La_{1.5}Sm_{0.5}Ti_3O_{10}$	**86**	**90**	**95**	**97**	**91**	93
$K_2La_{1.1}Sm_{0.9}Ti_3O_{10}$	72	65	87	87	88	86
$K_2La_{1.9}Dy_{0.1}Ti_3O_{10}$	44	69	80	80	80	72
$K_2La_{1.5}.Dy_{0.5}Ti_3O_{10}$	64	69	87	87	87	76
$K_2La_{1.1}Dy_{0.9}Ti_3O_{10}$	45	59	91	91	86	97
$K_2La_{1.9}Gd_{0.1}Ti_3O_{10}$	48	68	90	89	85	82
$K_2La_{1.5}Gd_{0.5}Ti_3O_{10}$	44	62	93	93	80	**98**
$K_2La_{1.1}Gd_{0.9}Ti_3O_{10}$	54	57	93	93	86	**98**
$K_2La_{1.9}Nd_{0.1}Ti_3O_{10}$	46	62	83	82	85	84
$K_2La_{1.5}Nd_{0.5}Ti_3O_{10}$	51	70	87	87	86	92
$K_2La_{1.1}Nd_{0.9}Ti_3O_{10}$	53	59	83	82	86	87
Blank	20	53	68	71	59	64

4.4.3 Photodegradation Results of Cyanide

After the experiments of methylene blue, cyanide degradation tests were carried out by using 100 mg/l initial cyanide concentration on 250 mg/l KCN solution. The pH was adjusted at 10 because the excess amount of cyanide is very toxic and cyanide in wastewater must be in alkali condition. 250 and 750 W/m^2 light intensities were observed to determine the effect of light intensity on the photodegradation process. To understand the degradation efficiencies of thin films, a blank was analyzed. The experiments were carried out into Atlas Suntest CPS+ with 4 hours reaction time.

The effective degradation results of 250 W/m^2 were examined at Table 4.16. Figure 4.83 and 4.84 demonstrated graphics based on the variation of the concentration vs. time and efficiency vs. time of phenol.

Table 4.16 Degradation efficiencies of cyanide for 100 mg/l, 250 W/m^2 and pH = 10 after 4 hours reaction time

Photocatalyst	Initial Concentration (mg/l)	Effluent Concentration (mg/l)	Degradation Efficiency (%)
$K_2La_2Ti_3O_{10}$	100	28.3	71.7
$K_2La_{1.9}Sm_{0.1}Ti_3O_{10}$	100	39.4	60.6
$K_2La_{1.5}Sm_{0.5}Ti_3O_{10}$	100	28.2	72.8
$K_2La_{1.1}Sm_{0.9}Ti_3O_{10}$	100	42.5	57.5
Blank	100	65.8	34.2

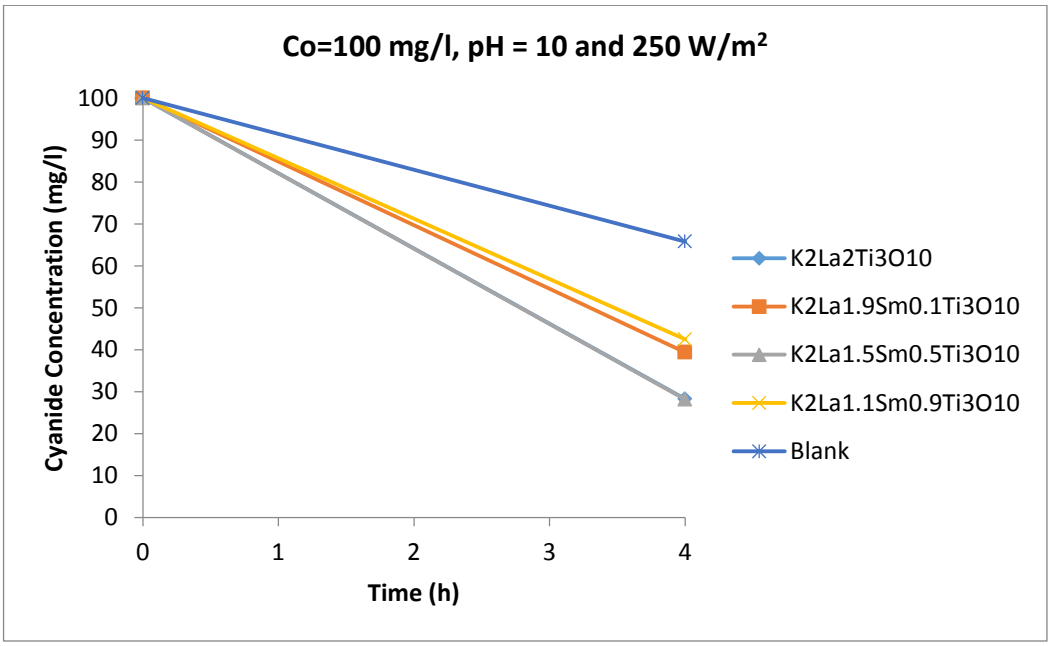

Figure 4.82 Cyanide concentration vs. time results (Co=100 mg/l, 250 W/m^2 and pH = 10).

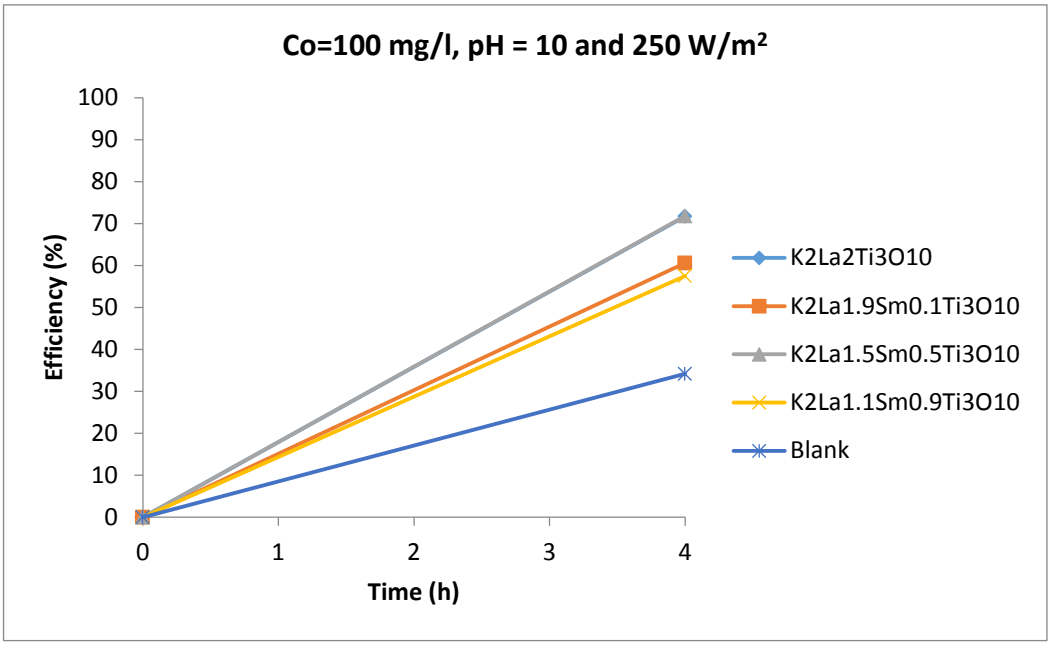

Figure 4.83 Cyanide removal efficiencies (%) (Co = 100 mg/l, 250 W/m^2 and pH = 10).

After 4 hours reaction time, the best result obtained by using $K_2La_{1.5}Sm_{0.5}Ti_3O_{10}$ and 72.7% degradation efficiency was achieved. On the other hand, 34.2% of degradation rate was observed by blank.

Cyanide removal results for 750 W/m^2 were given in Table 4.17. Figure 4.85 and 4.86 gave detail about of the concentration vs. time and efficiency vs. time of phenol.

Table 4.17 Degradation efficiencies of cyanide for 100 mg/l, 750 W/m^2 and pH = 10 after 4 hours reaction time

Photocatalyst	**Initial Concentration (mg/l)**	**Effluent Concentration (mg/l)**	**Degradation Efficiency (%)**
$K_2La_2Ti_3O_{10}$	100	21.3	78.7
$K_2La_{1.9}Sm_{0.1}Ti_3O_{10}$	100	32.9	67.1
$K_2La_{1.5}Sm_{0.5}Ti_3O_{10}$	100	19.8	80.2
$K_2La_{1.1}Sm_{0.9}Ti_3O_{10}$	100	38.1	61.9
Blank	100	59.2	40.8

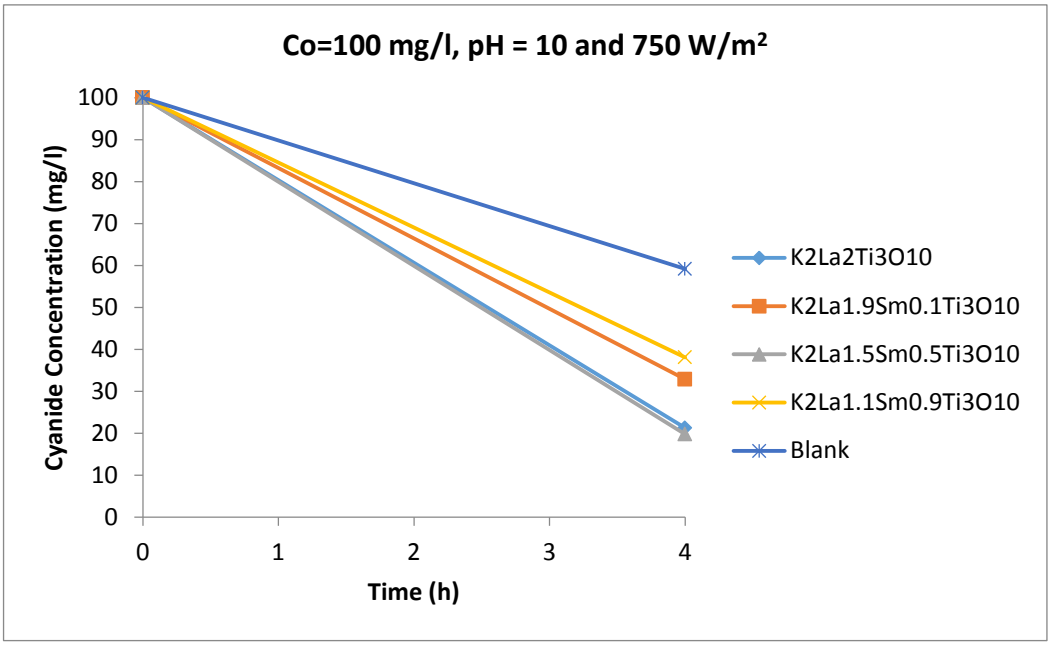

Figure 4.84 Cyanide concentration vs. time results (100 mg/l, 750 W/m^2 and pH = 10).

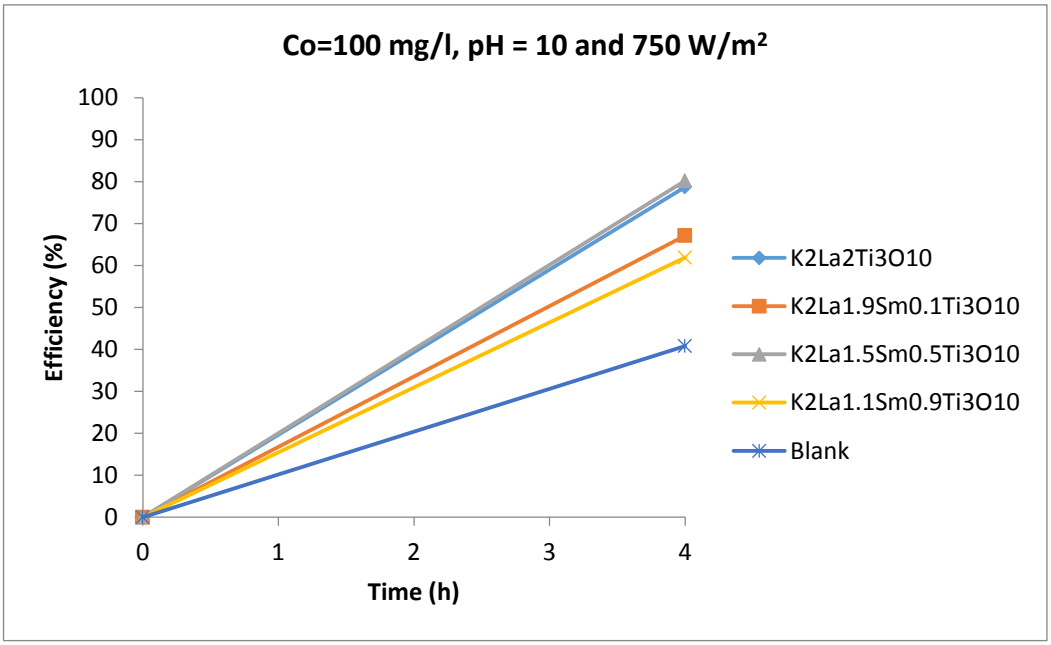

Figure 4.85 Cyanide removal efficiencies (%) (Co = 100 mg/l, 750 W/m^2 and pH = 10).

Cyanide reduction was obtained 80.2% by using $K_2La_{1.5}Sm_{0.5}Ti_3O_{10}$ after 4 hours treatment. On the other hand, 40.8% of degradation rate was observed by blank.

Table 4.18 demonstrates summary information on cyanide degradation. The best effective photocatalyst were chosen $K_2La_{1.5}Sm_{0.5}Ti_3O_{10}$ for the two different light

intensities which are observed. The bold characters illustrate the best effective results on phenol removal.

Table 4.18 Effect of light intensity for cyanide removal

Photocatalyst	Effluent Concentration (mg/l)	Degradation Efficiency (%)	Effluent Concentration (mg/l)	Degradation Efficiency (%)
	250 W/m^2		**750 W/m^2**	
$K_2La_2Ti_3O_{10}$	28.3	71.7	21.3	78.7
$K_2La_{1.9}Sm_{0.1}Ti_3O_{10}$	39.4	60.6	32.9	67.1
$K_2La_{1.5}Sm_{0.5}Ti_3O_{10}$	**28.2**	**72.8**	**19.8**	**80.2**
$K_2La_{1.1}Sm_{0.9}Ti_3O_{10}$	42.5	57.5	38.1	61.9
Blank	65.8	34.2	59.2	40.8

Table 4.19 summaries all conditions and degradation results which were obtained from the photocatalytic oxidation reactions. It can be clearly stated that $K_2La_{1.5}Sm_{0.5}Ti_3O_{10}$ thin film photocatalyst is very effective to remove the pollutants in all circumstances.

Table 4.19 Summary of the degradation efficiencies (%)

Degradation Efficiencies (%)										
Initial Concentration	**10 mg/l Phenol**		**10^{-5} M Methylene Blue**						**100 mg/l Cyanide**	
Photocatalyst	**pH=3 (5 h reaction time)**		**pH = 3 (5 h reaction time)**		**pH = 7 (3 h reaction time)**		**pH = 10 (30 min reaction time)**		**pH=10 (4 h reaction time)**	
	250 W/m²	**750 W/m²**	**250 W/m²**	**750 W/m²**	**250 W/m²**	**750 W/m²**	**250 W/m²**	**750 W/m²**	**250 W/m²**	**750 W/m²**
$K_2La_2Ti_3O_{10}$	68.7	70.2	41	64	79	81	76	92	71.7	78.7
$K_2La_{1.9}Sm_{0.1}Ti_3O_{10}$	65.1	68.1	55	56	86	85	72	89	60.6	67.1
$K_2La_{1.5}Sm_{0.5}Ti_3O_{10}$	72.2	75.3	86	90	95	97	91	93	72.8	80.2
$K_2La_{1.1}Sm_{0.9}Ti_3O_{10}$	54.4	63.2	72	65	87	87	88	86	57.5	61.9
$K_2La_{1.9}Dy_{0.1}Ti_3O_{10}$			44	69	80	80	80	72		
$K_2La_{1.5}.Dy_{0.5}Ti_3O_{10}$			64	69	87	87	87	76		
$K_2La_{1.1}Dy_{0.9}Ti_3O_{10}$			45	59	91	91	86	97		
$K_2La_{1.9}Gd_{0.1}Ti_3O_{10}$			48	68	90	89	85	82		
$K_2La_{1.5}Gd_{0.5}Ti_3O_{10}$			44	62	93	93	80	98		
$K_2La_{1.1}Gd_{0.9}Ti_3O_{10}$			54	57	93	93	86	98		
$K_2La_{1.9}Nd_{0.1}Ti_3O_{10}$			46	62	83	82	85	84		
$K_2La_{1.5}Nd_{0.5}Ti_3O_{10}$			51	70	87	87	86	92		
$K_2La_{1.1}Nd_{0.9}Ti_3O_{10}$			53	59	83	82	86	87		
Blank	26.8	39.3	20	53	68	71	59	64	65.8	40.8

4.4.4 SUVA Results

To determine specific UV absorbance results, Equation 3.1 was used. The experiments were completed by using $K_2La_{1.5}Sm_{0.5}Ti_3O_{10}$ thin film photocatalyst due to their higher photocatalytic degradation effect. The values were read at 254 nm by changing the pH values. Table 4.20 gave the results and Figure 4.87 demonstrates the comparison of the pH effect with UV absorbance.

Table 4.20 The absorbance and SUVA values at 254 nm

Photocatalyst	Absorbance at 254 nm	$SUVA_{254}$	pH
$K_2La_{1.5}Sm_{0.5}Ti_3O_{10}$	0.129	2.29 L/mgM	3
Blank	0.408	5.53 L/mgM	
$K_2La_{1.5}Sm_{0.5}Ti_3O_{10}$	0.13	2.31 L/mgM	7
Blank	0.409	5.54 L/mgM	
$K_2La_{1.5}Sm_{0.5}Ti_3O_{10}$	0.133	2.36 L/mgM	10
Blank	0.408	5.53 L/mgM	

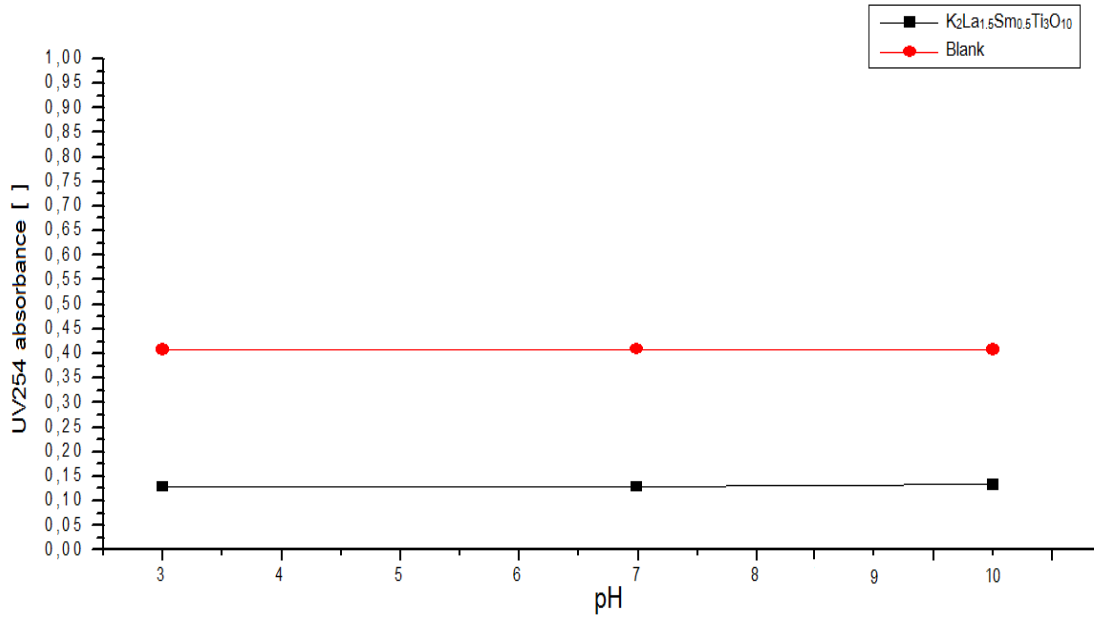

Figure 4.86 The comparison of UV_{254} absorbance and pH.

According to the results, $SUVA_{254}$ value of $K_2La_{1.5}Sm_{0.5}Ti_3O_{10}$ thin film photocatalyst is less than $SUVA_{254}$ value of blank. This demonstrates that thin film has low aromaticity. That is why, the degradation is easier.

4.4.5 DOC Results

To determine specific DOC values, the best effective thin film photocatalyst, $K_2La_{1.5}Sm_{0.5}Ti_3O_{10}$ was examined. The values were obtained for thin film and blank and DOC values were estimated for methylene blue. Table 4.21 gave the results at pH of 7. 23.47% of mineralization was achieved.

Table 4.21 DOC values

Photocatalyst	**DOC (mg/l)**	**DOC Removal Efficiency (%)**
Initial DOC	7.37	23.47
DOC after the degradation by $K_2La_{1.5}Sm_{0.5}Ti_3O_{10}$	5.64	

4.4.6 TOC Results

TOC results for phenol, methylene blue and cyanide were given in Table 4.22, 4.23 and 4.24 as a function of irradiation time. TOC removal efficiencies are higher for the best effective photocatalyst - $K_2La_{1.5}Sm_{0.5}Ti_3O_{10}$. 50.26% of TOC removal of phenol was achieved after 5 hours irradiation at pH of 7. This means that 5 hours treatment is not enough to completely destroyed phenol. TOC removal efficiency for methylene blue was investigated 84.42% after 3 hours irradiation at pH of 7. The photocatalyst was effective to destroyed TOC at 3 hours. 79.89% of TOC removal was realized for cyanide at 4 hours irradiation under alkali condition. It was found that TOC treatment was good enough but must be enhanced. Figure 4.88 demonstrates TOC removal efficiencies for different pollutants.

Table 4.22 TOC values for phenol solution after 5 hours reaction at pH 7

Photocatalyst	TOC (mg/l)	TOC Removal Efficiency (%)
Initial TOC	45.34	
$K_2La_{1.5}Sm_{0.5}Ti_3O_{10}$	22.55	50.26
$K_2La_{1.1}Dy_{0.9}Ti_3O_{10}$	27.27	39.85
$K_2La_{1.9}Gd_{0.1}Ti_3O_{10}$	36.44	19.63
$K_2La_{1.1}Nd_{0.9}Ti_3O_{10}$	26.89	40.69

Table 4.23 TOC values for methylene blue solution after 3 hours reaction at pH 7

Photocatalyst	TOC (mg/l)	TOC Removal Efficiency (%)
Initial TOC	70.55	
$K_2La_{1.5}Sm_{0.5}Ti_3O_{10}$	10.99	84.42
$K_2La_{1.1}Dy_{0.9}Ti_3O_{10}$	34.39	51.25
$K_2La_{1.9}Gd_{0.1}Ti_3O_{10}$	36.97	47.60
$K_2La_{1.1}Nd_{0.9}Ti_3O_{10}$	20.95	70.30

Table 4.24 TOC values for cyanide solution after 4 hours reaction at pH 10

Photocatalyst	TOC (mg/l)	TOC Removal Efficiency (%)
Initial TOC	57.73	
$K_2La_{1.5}Sm_{0.5}Ti_3O_{10}$	11.61	79.89
$K_2La_{1.1}Dy_{0.9}Ti_3O_{10}$	33.03	42.79
$K_2La_{1.9}Gd_{0.1}Ti_3O_{10}$	52.64	8.82
$K_2La_{1.1}Nd_{0.9}Ti_3O_{10}$	41.45	28.20

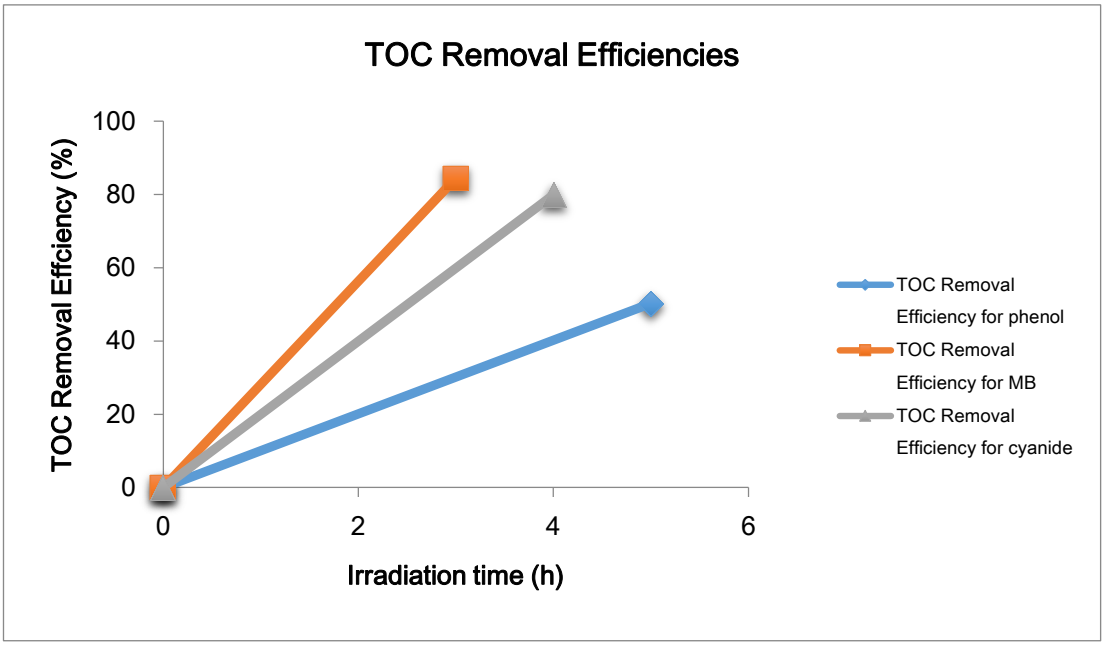

Figure 4.87 TOC removal efficiencies.

4.4.7 Kinetic Studies Results

The determination of the reaction order for photodegradation of methylene blue was performed according to the treatment results. The degradation curves were taken out and zero, first and second order reaction kinetics were tested. k_0,k_1 and k_2 are the rate constants for zero, first and second order kinetics, respectively which can be seen at the tables below.

To determine the reaction kinetics, the experiments were performed with the photocatalyst which showed the highest degradation results. $K_2La_{1.5}Sm_{0.5}Ti_3O_{10}$ was the best effective photocatalyst among the photocatalyst set. Methylene blue experiments were made with three different pH values and the highest degradation rate was determined at pH 7. That is why, at pH for 7, the experiments were repeated for 30, 60, 90, 120, 150, 180, and 210 minutes. As a result of the kinetic studies, second order reaction achieved the highest R^2 (correlation value).

To identify the reaction order, the experiment conditions of the photocatalytic degradation for methylene blue was observed as follows: initial concentration was selected 3.2 mg/l, 750 W/m^2 and pH at 7. Blank also was tested and the reaction

order was determined. Blank studies can be fitted to a zero order reaction law. The results of the methylene blue were shown in Table 4.25 which lists the order rate constants and correlation (R^2) constants. If the correlation constants are higher, the model is proper for the degradation of the methylene blue. The curves for the each reaction orders were given in Figure 4.89. 4.90, 4.91 and 4.92.

As a result of the Methylene blue kinetic studies, it was found that all correlations for each kinetic order were greater than 95%. This demonstrates a good statistical fit and second order kinetic model can be a good model kinetic for methylene blue degradation during the treatment process. As can be seen in Table 4.25, the maximum reaction rate constant, k, was observed for first order reaction.

Table 4.25 The reaction orders for methylene blue (Co=3.2 mg/l, 750 W/m^2, pH = 7)

	0^{th} order		**1^{st} order**		**2^{nd} order**	
	k_0 (mg/l.min)	**R^2**	**k_1 (min^{-1})**	**R^2**	**k_2 ($Lmg^{-1}min^{-1}$)**	**R^2**
$K_2La_{1.5}Sm_{0.5}Ti_3O_{10}$	0.0025	0.9873	**0.0009**	**0.9914**	0.0003	0.9912
Blank	0.0105	0.9545				

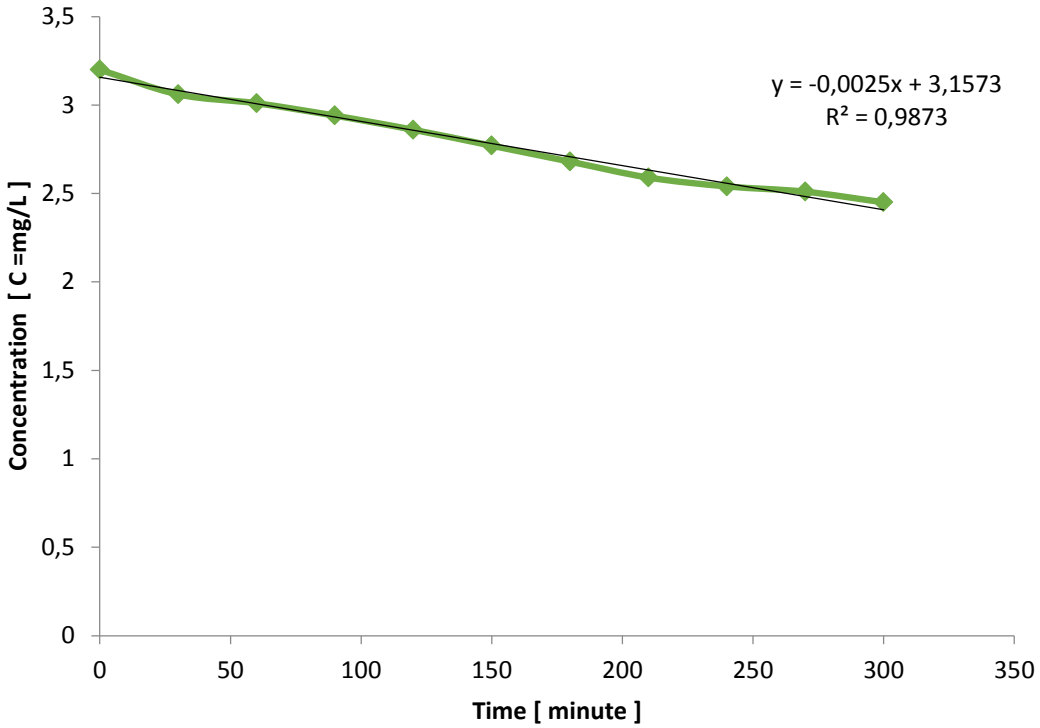

Figure 4.88 Concentration vs. time for zero order degradation of methylene blue by $K_2La_{1.5}Sm_{0.5}Ti_3O_{10}$.

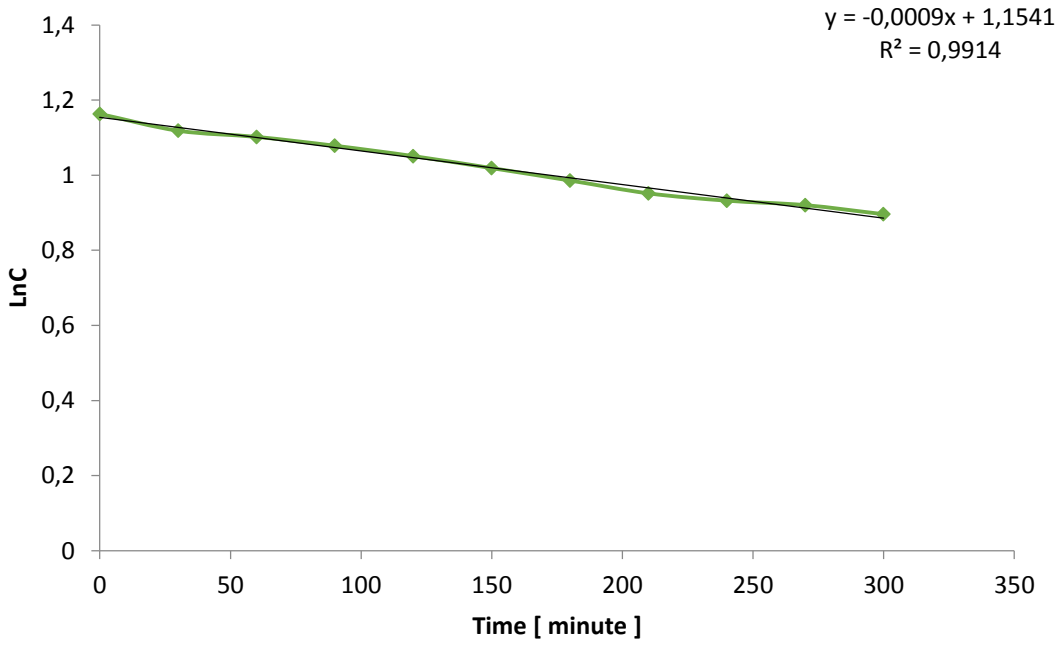

Figure 4.89 Concentration vs. time for first order degradation of methylene blue by $K_2La_{1.5}Sm_{0.5}Ti_3O_{10}$.

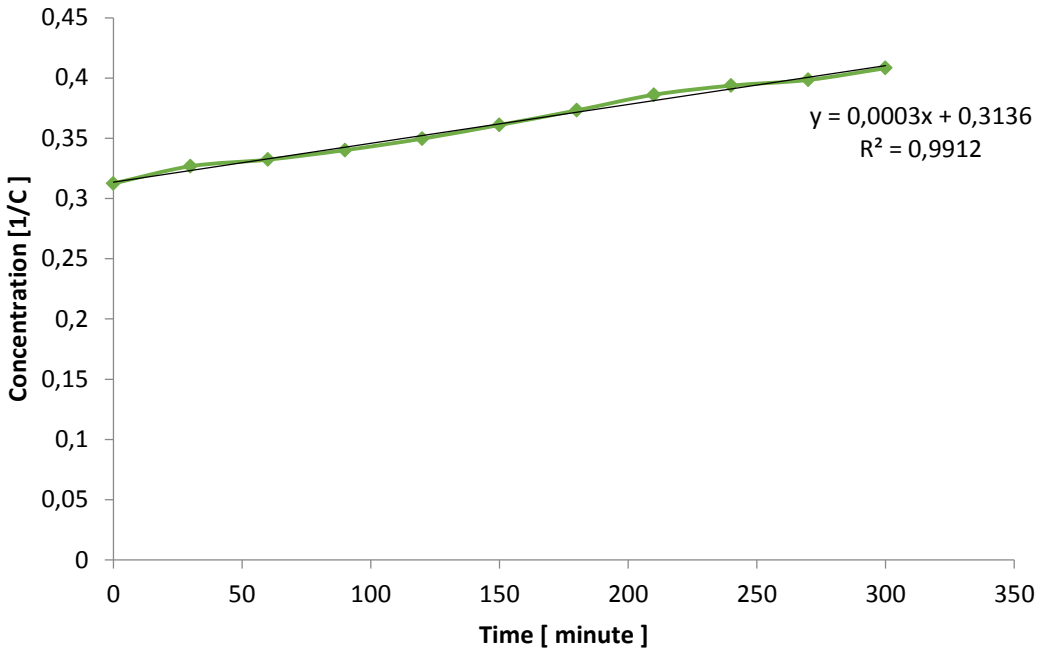

Figure 4.90 Concentration vs. time for second order degradation of methylene blue by $K_2La_{1.5}Sm_{0.5}Ti_3O_{10}$.

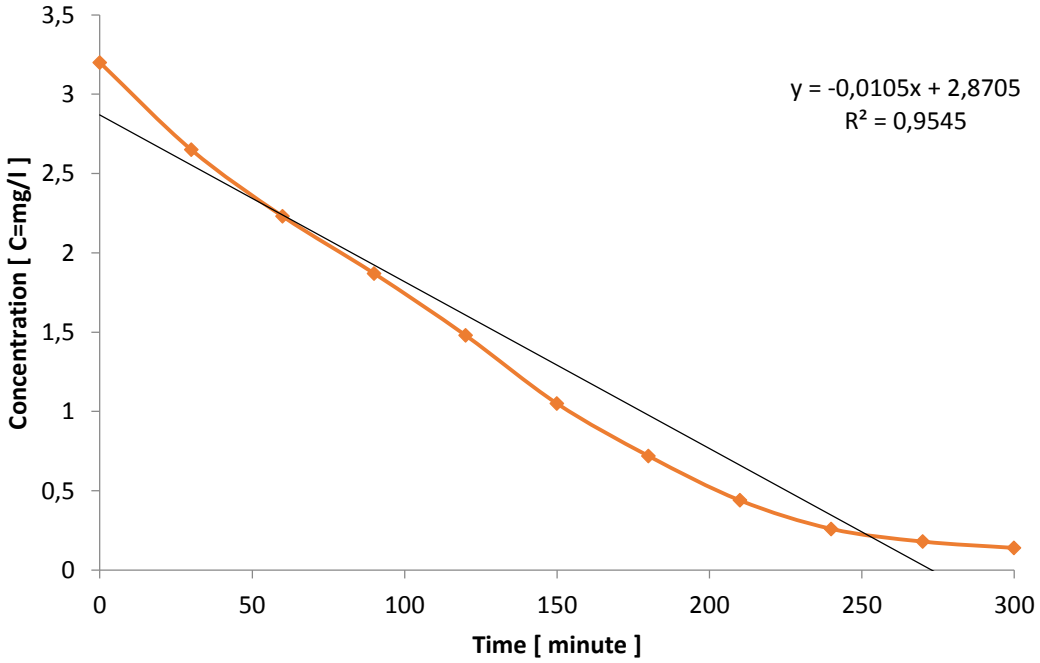

Figure 4.91 Concentration vs. time for zero order degradation of blank methylene blue (without photocatalyst).

4.4.8 Factorial Experimental Design Results

Analysis of Variance (ANOVA) statistical experimental design was set up to determine the effects of the variables on degradation efficiency of the pollutants and to find the best effective combination which results maximum efficiency. The significant variables were selected pH and light intensity. Experimental design was employed for methylene blue as two factors two replicated factorial design. 6 different experimental conditions were performed for 2 times.

This optimization process is based on two hypothesis test with a margin of error. After the performance of the statistically designed experiments, the decision is making for zero or alternative hypothesis. Zero hypothesis (null hypothesis) (H_o) explains that there is not a relation or difference between the mean and distribution. On the other hand, alternative hypothesis (H_1) stands up that there is a relation or difference between the mean and distribution. If the hypothesis is accepted, the degradation efficiency does not depend on the variables which are selected. The design was made by using Minitab Statistical Software V14. The results represent 95% confidence intervals which means the significance level is selected as α=5% (0.05). This means that the findings have 95% chance of being true and have a 5% of chance for not being true. Degradation efficiencies were considered as dependent variables and represented as Y which is the observation data. The acceptance or rejection of the hypothesis can be found with p value and F value which is determined by F tables. Acceptance or rejection criteria can be seen at Table 4.26. Every experiment is repeated 2 times. The independent variables can be shown in Table 4.27. The response is the degradation efficiency (%). If Ho's are true, the variances are equal to other variances. ANOVA test is applied for the $K_2La_{1.5}Sm_{0.5}Ti_3O_{10}$ surface coating.

Table 4.28 demonstrated the response (degradation efficiencies of methylene blue) and the experiment conditions. The experiments were carried out for 3 hours reaction time. To make sure about the degradation efficiency, the experiments were performed 2 times for the conditions below. The software outputs are shown in the Table 4.29 and the graphs can be seen at Figure 4.93, 4.94 and 4.95.

Table 4.26 Acceptance and rejection criteria of H_0 for Anova test

Acceptance Criteria		**Rejection Criteria**	
If p value > 0.05 (α)	Cannot reject Null Hypothesis (Means are the same).	If p value < 0.05 (α)	Reject Null Hypothesis (Means are different).
If $F_{determined} < F_{table}$		If $F_{determined} > F_{table}$	

Table 4.27 Independent variables for methylene blue experimental design

Level	**pH**	**Irradiance Ranges (W/m^2)**
Min	3	250
		750
Center	7	250
		750
Max	10	250
		750

Table 4.28 Two factors two replicates factorial design for methylene blue

Number	**pH**	**Light intensity (W/m^2)**	**Y (%)**
1	3	250	86
2	3	250	87
3	7	250	95
4	7	250	91
5	10	250	91
6	10	250	90
7	3	750	90
8	3	750	95
9	7	750	97
10	7	750	98
11	10	750	93
12	10	750	94

Table 4.29 General linear model: Response versus pH; Light Intensity (Minitab output)

Factor	Type	Levels	Values
pH	fixed	3	3; 7; 10
Light Intensity	fixed	2	250; 750

Analysis of Variance for Response, using Adjusted SS for Tests

Source of variation	DF	Seq SS	Adj SS	Adj MS	F	F(α=0,05)
pH	2	60,667	60,667	30,333	8,27	> 5,14 H_{01} = reject
Light Intensity	1	56,333	56,333	56,333	15,36	> 5,99 H_{02} = reject
pH*Light Intensity	2	4,667	4,667	2,333	0,64	< 5,14 H_{03} = accept
Error	6	22,000	22,000	3,667		
Total	11	143,667				

Source	P	
pH	0,019 < 0,05	means are different.
Light intensity	0,008 < 0,05	means are different.
pH*Light Intensity	0,562 > 0,05	means are same.

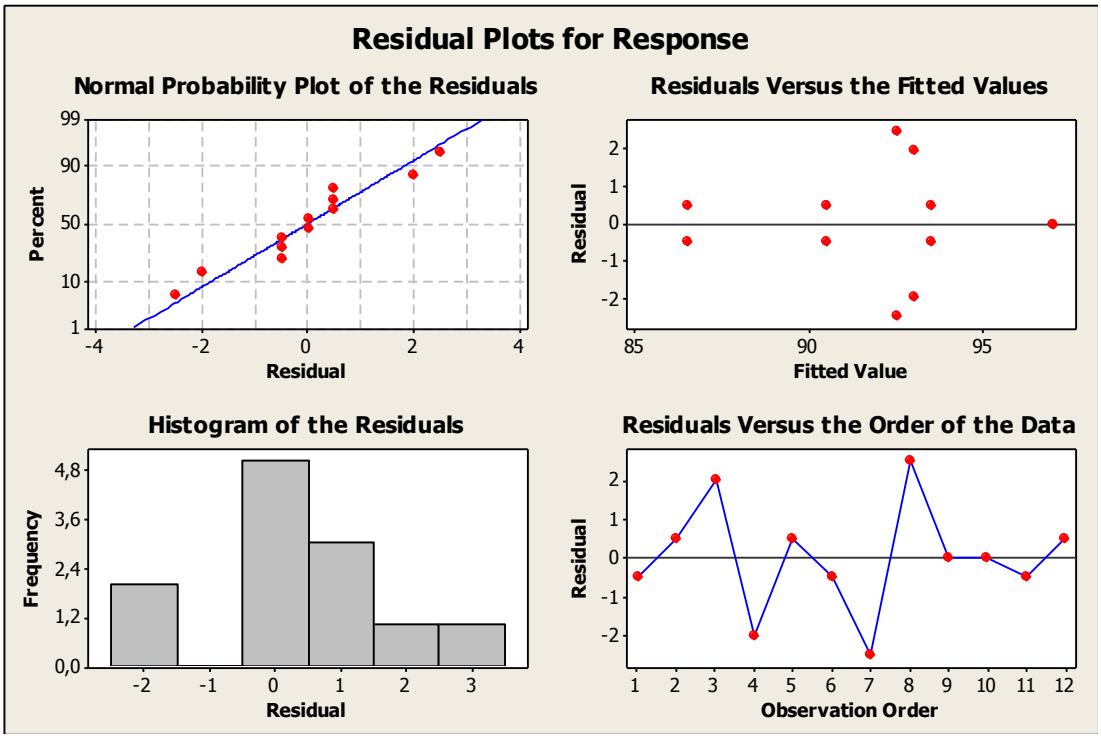

Figure 4.92 Residual plots for results.

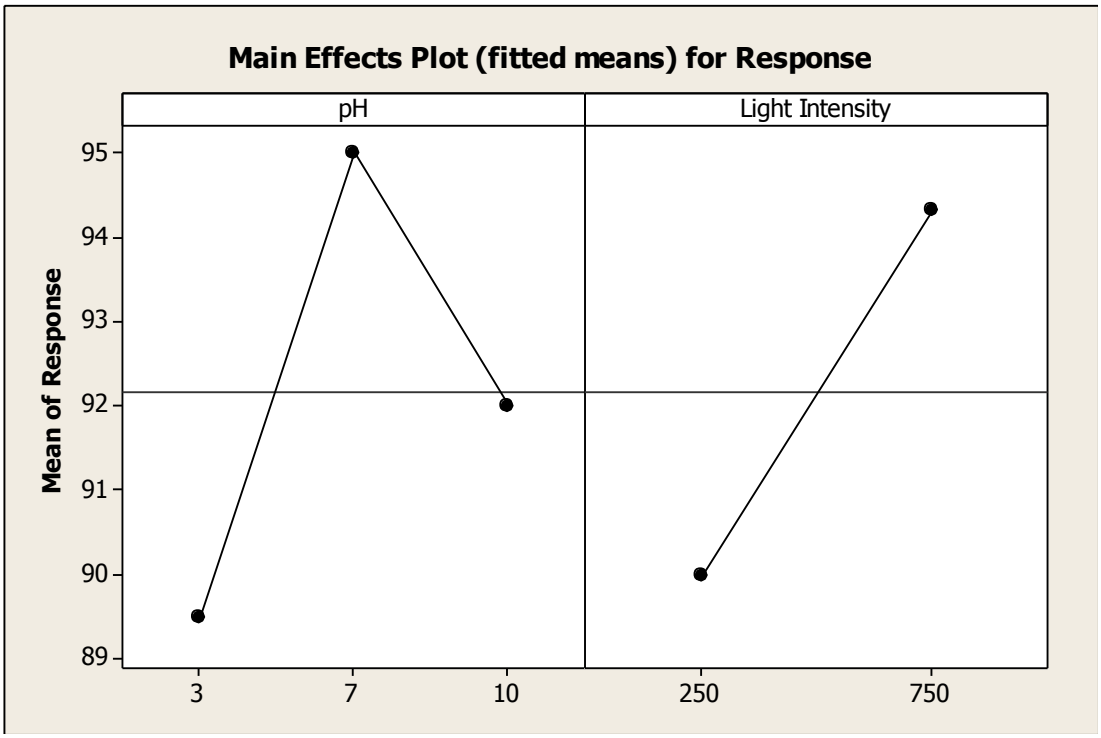

Figure 4.93 Main effects plot (fitted means) for results.

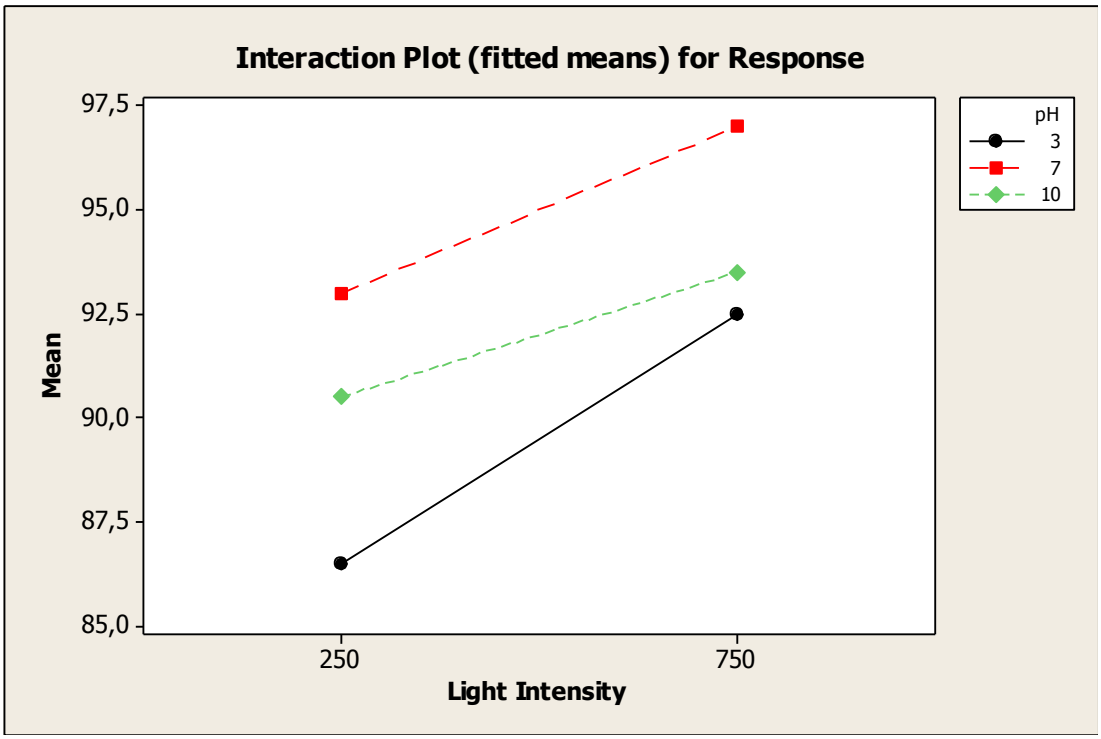

Figure 4.94 Interaction plot (fitted means) for results.

According to the results of the methylene blue performance tests, two hypotheses are rejected and one hypothesis was accepted. The hypotheses were as follows:

H_{01} = pH has no effect on removal. (Null hypothesis)

H_{11} = pH has an effect on removal. (Alternative hypothesis)

H_{02} = Light intensity has no effect on removal. (Null hypothesis)

H_{12} = Light intensity has an effect on removal. (Alternative hypothesis)

H_{03} = pH and light intensity have no effect on removal. (Null hypothesis)

H_{13} = pH and light intensity effect the performance of degradation. (Alternative hypothesis)

It can be said that pH significantly effects the removal efficiency. Different pH values (3-7-10) are applied. So, it effect by oneself. Light intensity is a significant factor also on removal. So, it effect by oneself. The calculated F values were bigger than F_{table} values and the calculated P values were smaller than 0.05. The hypotheses were rejected. On the other hand, the interaction of pH and light intensity hypothesis was accepted. That is why; pH and light intensity is not effected each other, and the interaction has not an influence together on degradation performance.

Residuals are used in ANOVA test to check how well the model fits to the data. According to the Figure 4.93 normal probability plot, the data points fall at least approximately on a straight line. As a result, the data follows a normal distribution. Residuals versus fits plot were created. Plot of residuals can be seen on y axis and fitted values which are the Y values (estimated responses) on the x axis. The plot suggests a bounce randomly around 0 lines. This demonstrates that the assumption is reasonable. The shape of the histogram of the residuals supports the conclusion of normal probability which is linear. The residuals in time order can be seen at Residuals versus the order the data plot. The number of experiments for each data point can be seen on the x axis. Experiments 3,4,7 and 8 provide superior residuals. Figure 4.94 shows that pH is optimum at pH 7. The degradation efficiency is increased from pH = 3 to 7 and decreased from 7 to 10. On the other hand, the increase of light intensity from 250 to 750 W/m^2, enhance the degradation process. Figure 4.95 demonstrates that the lines do not overlap. This indicates that there is no interaction between pH and light intensity which was already calculated with F test.

Table 4.30 A briefly comparison of the variables and their effects by surface coating

Effects	Metyhlene Blue	
pH	3-7-10	Effective
Light intensity	250-750 W/m^2	Effective
pH x Light intensity	Not effective	

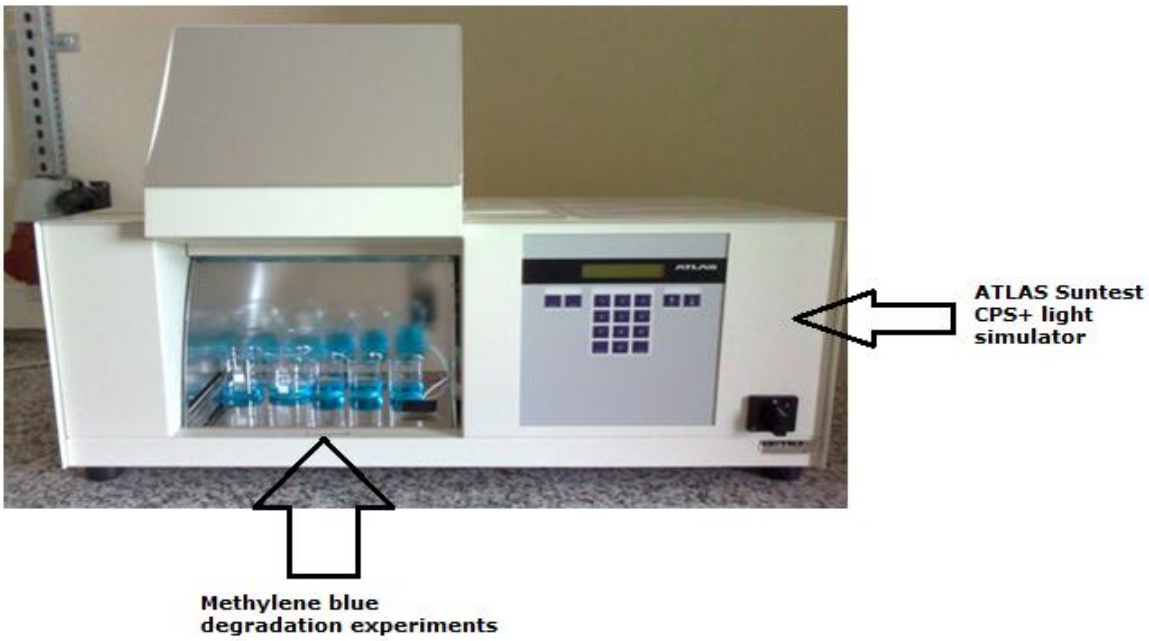

Figure 4.95 Photos from experimental studies.

CHAPTER FIVE
CONCLUSION AND RECOMMENDATIONS

5.1 General Results

The main objective of this study is to investigate the photocatalytic degradation of the persistent pollutants in wastewater with using the new generation photocatalytic materials ($K_2Ln_2Ti_3O_{10}$ (Ln=La, Nd, Gd, Sm, Dy)). For this reason, to understand the effect of pH and light intensity on the degradation, synthetic wastewaters were prepared and phenol, methylene blue and cyanide were used as pollutants. The treatment of these chemicals by photocatalytic oxidation was developed by newly generated photocatalysts. Metal alkoxides, propionic acid and glacial acetic acid were used to prepare the solutions and the coating of the prepared solutions was performed on Si (100) substrates. In addition, the reaction orders and the effects of pH and light intensity on degradation efficiency are characterized.

As a result of the literature researches, the perovskite-type oxides, $K_2Ln_2Ti_3O_{10}$ was generally produced by solid state reaction, polymerization complex method and sol-gel method. In addition, it has not been developed any study about $K_2Ln_2Ti_3O_{10}$thin film which is coated on Si(100) substrate. For this reason, this study is focused on to produce $K_2Ln_2Ti_3O_{10}$ (*Ln* = La, Nd, Gd, Sm, Dy) thin films by sol-gel method because of some advantages such as better mixing of the starting materials and excellent chemical homogeneity in the final product. In addition, the molecular level mixing aids the structure evolution lowering the crystallization temperature and the sol-gel layer can be deposited desired thickness in one step because this thickness depends only on precursor's concentration.

According to the findings; very high photocatalytic activity for $K_2La_{1.5}Sm_{0.5}Ti_3O_{10}$ was achieved. The conclusions of the experimental results from are given below.

1. The turbidity values, pH values, contact angle and rheological properties were measured to understand the effectiveness of the K, *Ln*, Ti based initial solution properties of the catalyst which were prepared. Turbidity values of the solutions pointed that the powder based precursors was dissolved into the solution. It can be seen that the turbidity was increased by the addition of the dopant into $K_2La_2Ti_3O_{10}$. So the solutions were homogeny and adequately transparent. The pH measurement of the solutions showed acidic condition. The wetting capacity was measured by contact angles measurement. Contact angle values of the KLTO solutions were determined approximately 4° and this value is lower than 90°. This demonstrated that the solutions can wet the Si (100) substrates. The slight decrease of the solution viscosity demonstrated is depending on the formation of the complex compounds and it is the indicative of the polymeric network distribution. The prepared solutions have low viscosity values and it is an advantage for thin film generation.

2. The thermal analysis of the xerogels was examined by DTA-TG analysis. Firstly, the endothermic peaks demonstrated the solvent removal. Secondly, the combustion of the organic groups occurred. Finally, the formation of ceramic oxides was observed at the temperatures between 850 and 1200°C. To optimize the characterization and to determine the removal of organic compounds in the structure, FTIR analysis was carried out. Chen et al. (2005) observed that the signal between the ranges of 400 - 1200 cm^{-1} shows the characteristic formation of O-Ti-O. According to this observation, the signals between 400 and 1200 cm^{-1} were carried out and were represented the formation of O-Ti-O characteristics for KLTO based films. As a result of FTIR, O-H, C=O and M-OCOO-M bond frequencies are vanished around 800 °C. This situation demonstrated that organic structures and hydroxyls were completely destroyed. The peaks which are appeared by a decrease with increasing temperature band between the ranges of 850 - 900 cm^{-1} are thought to be K, *Ln*(La, Sm, Dy, Gd, Nd), Ti ions related to oxygen bond. FTIR results were regularly conformed to DTA-TG results.

3. XRD analysis was performed to determine the phase composition of the samples. According to Yang et al. (2007), the sharp and intense diffraction peaks with different angle in the XRD patterns showed that the KLTO was well crystallized. Based on Cui et al. (2013) studies, the peaks had low intensity and when the diffraction peaks compared to the literature, it can be seen that the crystalline structure of KLTO was obtained. As a result of the XRD results, powders and thin films were synthesized successfully. Chemical state of surface elements was measured by elemental analysis - XPS. XPS measured the chemical state of surface elements and identified the chemical uniformity of KLTO based on Si (100) coatings. As a result of the elemental analysis, the dopant elements were determined as sharp peaks. This demonstrated that XPS and XRD were consentaneously. Only 0.1 doped elements could not observe because it is very small amount. The La 3d core level of samples and spin-orbit components of Ti 2p peaks and the K 2p peaks were well described for all of the photocatalysts similar to Cui et al. (2013). The dopant chemicals as Sm 3d, Nd 4d and Dy 3d were observed. But the Gd dopant cannot be determined according to the XPS analysis. To identify the surface morphologies of thin films, SEM analysis was used. Surface area is an important parameter for photocatalytical application. It can be seen that when the surface area that acting with pollution is increased, the photocatalytic efficiency also rises (Bakuy, 2009). For this reason, it can be said that the thin films are morphologically good candidates for photocatalytic applications and the surface morphologies are suitable according to the literature findings. The mechanical properties and the hardness of thin films were determined by nanoidentation. The highest hardness and elasticity modulus was determined for $K_2La_{1.5}Nd_{0.5}Ti_3O_{10}$.

4. $K_2Ln_2Ti_3O_{10}$ was produced with using sol-gel method and spin coating method. The dimensions of the surface coating photocatalysts were 2x2 cm. The evaporation of the wastewater into the solar simulator was a problem. That is why; a glass cap was putted above the beaker to prevent the

evaporation. For every experimental procedure, the beakers were filled till 25 ml and it was placed into ATLAS Suntest CPS+.

5. The photodegradation of phenol, methylene blue and cyanide was performed by using thin films under solar simulator. The pollutants were selected as organic (phenol and methylene blue as azo dye) and inorganic (cyanide).

6. The experiments were performed with 13 different KLTO thin films ($K_2La_2Ti_3O_{10}$, $K_2La_{1.9}Sm_{0.1}Ti_3O_{10}$, $K_2La_{1.5}Sm_{0.5}Ti_3O_{10}$, $K_2La_{1.1}Sm_{0.9}Ti_3O_{10}$, $K_2La_{1.9}Dy_{0.1}Ti_3O_{10}$, $K_2La_{1.5}.Dy_{0.5}Ti_3O_{10}$, $K_2La_{1.1}Dy_{0.9}Ti_3O_{10}$, $K_2La_{1.9}Gd_{0.1}Ti_3O_{10}$, $K_2La_{1.5}Gd_{0.5}Ti_3O_{10}$, $K_2La_{1.1}Gd_{0.9}Ti_3O_{10}$, $K_2La_{1.9}Nd_{0.1}Ti_3O_{10}$, $K_2La_{1.5}Nd_{0.5}Ti_3O_{10}$ and $K_2La_{1.1}Nd_{0.9}Ti_3O_{10}$) and without photocatalyst (blank). Blank was examined to make a comparison on degradation efficiencies and to understand the effectiveness of the films.

7. Reaction times for phenol, methylene blue and cyanide were considered according to the literature studies.

8. During the treatment of phenol, two different conditions were examined at pH for 7. The initial concentration of phenol solution was selected 10 mg/l and light intensity was independent variable and selected 250 and 750 W/m^2. The maximum degradation rates for two conditions were observed with $K_2La_{1.5}Sm_{0.5}Ti_3O_{10}$ thin film photocatalyst. 72.2% degradation efficiency with $K_2La_{1.5}Sm_{0.5}Ti_3O_{10}$ photocatalyst and 26.8% without photocatalyst (blank) was obtained for 250 W/m^2 after five hours treatment into solar simulator. Under 750 W/m^2 light intensity, the maximum degradation efficiency was obtained 75.3% with $K_2La_{1.5}Sm_{0.5}Ti_3O_{10}$ photocatalyst and 39.3% without photocatalys (blank). According to the results, it can be said that the increase of the light intensity has a slight effect on phenol degradation by photocatalytic oxidation. And the degradation results with using photocatalyst are higher than blank. It can be pointed that the natural sunlight and the photocatalysts are effective to degrade phenolic compounds.

According to the literature study, degradation of phenol is very difficult. Pardeshi & Patil (2008) were obtained 47% of degradation efficiency of phenol by using aqueous zinc oxide as photocatalyst at pH for 5.61 with using Xenon lamp and 75 ppm initial phenol concentration after 9 hours reaction time. According to the results of Guo, Ma & Li (2006), the degradation efficiencies of phenol was obtained 16% and 76% in the presence of TiO_2 and was also obtained 40% and 81.6% in the absence of TiO_2 for 3 and 12 hours, respectively..

9. For the treatment studies of methylene blue by using surface coating catalyst, 6 different conditions were examined. The independent variables were selected pH (3-7-10), light intensity (250-750 W/m^2) and reaction time. According to the degradation results with 13 different photocatalysts and blank, it can be clearly seen that $K_2La_{1.5}Sm_{0.5}Ti_3O_{10}$ was the best effective photocatalyst except one condition. The experiments were carried out by using 10^{-5} M methylene blue initial concentration. The maximum degradation rate of methylene blue was observed 98% by using $K_2La_{1.5}Gd_{0.5}Ti_3O_{10}$ and $K_2La_{1.1}Gd_{0.9}Ti_3O_{10}$ at pH 10 and 750 W/m^2 light intensity after 30 minutes treatment process by using ATLAS Suntest CPS+. At the same condition, the blank demonstrated 71% of degradation efficiency. The other best results for the other conditions can be explained as follows: 86% at pH for 3, 250 W/m^2 light intensity for 5 hours reaction by using $K_2La_{1.5}Sm_{0.5}Ti_3O_{10}$ and 20% was achieved by blank. 90% was observed at pH 3, 750 W/m^2 light intensity for 5 hours reaction by using $K_2La_{1.5}Sm_{0.5}Ti_3O_{10}$ and 53% was obtained by blank. 95% was obtained at pH 7, 250 W/m^2 light intensity for 3 hours reaction by using $K_2La_{1.5}Sm_{0.5}Ti_3O_{10}$ and 68% was obtained by blank. 97% was examined at pH 7, 750 W/m^2 light intensity for 3 hours reaction by using $K_2La_{1.5}Sm_{0.5}Ti_3O_{10}$ and 71% was observed by blank. And finally, 91% was obtained at pH 10, 250 W/m^2 light intensity for 30 minutes reaction by using $K_2La_{1.5}Sm_{0.5}Ti_3O_{10}$ and 59% was obtained by blank. As a result of the studies, it can be said that the increase of the light intensity and pH rise the degradation efficiency of methylene blue. Rizzo et al. (2011) were prepared

TiO_2 nanofilm by using sol-gel method. At pH 9, the degradation efficiency was obtained 80% after 10 minutes into photocatalytic reactor under UV lamp (335 nm) radiation. Tayade et al. (2009) were used light emitting diodes in aqueous solution by using 1.2 g/l P-25 Degussa TiO_2. The decomposition of methylene blue was carried out in UV-LED photocatalytic reactor at pH of 8.84. After 6 hours, 100% of degradation was achieved in contrast to blank which was achieved 12% of degradation efficiency. Yao et al. (2009) obtained 92.3% of decolorization of 0.2 g/l methylene blue aqueous solutions after 160 minutes by using TiO_2 sol under UV light.

10. With the experiments of cyanide, two different conditions were tested. Light intensity was selected independent variable and the experimental analysis was performed at pH 10 with 100 mg/l cyanide solution for 4 hours reaction time into solar box. The degradation efficiencies were determined 71.8% with using $K_2La_{1.5}Sm_{0.5}Ti_3O_{10}$ surface coating catalyst and 34.2% without using photocatalyst (blank) at 250 W/m^2. On the other hand, 80.2% was measured with using $K_2La_{1.5}Sm_{0.5}Ti_3O_{10}$ surface coating catalyst and 40.8% without using photocatalyst (blank) at 750 W/m^2. Aazam (2013) was obtained 35%, 40%, 50%, 80% and 100% degradation efficiencies by increasing the weight % of the $Pt/AgLnS_2$ nanoparticles in 35 minutes at pH 10.5. Same experiments were completed in 2014 by Aazam that 60%, 82%, 98% and 100% were obtained by increasing the %weight of Au/CdS nanoparticles.

11. As a result of the SUVA test of methylene blue, it can be said that SUVA value of the $K_2La_{1.5}Sm_{0.5}Ti_3O_{10}$ photocatalyst was significantly lower than blank sample. The low value indicates that the aromacity of the sample is low. That is why; the degradation process is much easier. The aromacity of blank was high so the degradation is more difficult.

12. Throughout the TOC studied, the maximum TOC removal efficiencies were obtained by $K_2La_{1.5}Sm_{0.5}Ti_3O_{10}$ which is the best surface coating photocatalyst among the 13 photocatalyst. TOC removal efficiency for

phenol was observed 50.3% after 5 hours irradiation. As can be seen, TOC removal of phenol at 5 hours is not sufficient. 84.4% of TOC removal achieved for methylene blue after 3 hours irradiation. And cyanide TOC removal efficiency was reached to 79.9% after 4 hours irradiation.

13. According to the methylene blue results, the reaction kinetics was investigated. Reaction kinetics was examined at pH 7 and 750 W/m^2. It is the best degradation result which was carried out by using $K_2La_{1.5}Sm_{0.5}Ti_3O_{10}$ photocatalyst and blank was also analyzed as a reference to make a comparison. The performances of the catalysts were evaluated by comparison of the samples which exposure only light intensity. The maximum order reaction rate constant, k, was observed for first order and the degradation curve is fitted to first reaction order.

14. Statistical design was set up for methylene blue. The experiments were carried out 2 times to make ANOVA analysis. The results were tested with ANOVA test for different independent variables including pH and light intensity. According to the ANOVA test results, pH and light intensity have an effect on the degradation efficiency by oneself. But the interaction of pH and light intensity are not a significant effect on degradation.

15. The advantage of the KLTO surface coating demonstrated short reaction times in contrast to the experiments which only exposed by light intensity (blank) and it does not require an additional operation as separation or filtration. It does not produce waste and it is more environmental friendly.

5.2 Recommendations

The main advantage of thin film photocatalysts is to be more eco - friendly than particulate catalysts because of the difficulty of separation of particulate from water. The particulate catalysts have many difficulties and foremost among these, the separation of the particles from wastewater plays an important role. For this reason, this study is realized. The new generated KLTO film production and the transfer of

photocatalytic thin films to the industrial applications should be investigated and examined.

Further studies must be enhanced the photocatalyst and designed a photocatalytic reactor for industrial field. Researches should focus on to optimize all independent variables to achieve the maximum degradation rates for all kind of pollutants.

REFERENCES

Aazam, E. S. (2013). Photocatalytic oxidation of cyanide under visible light by Pt doped $AgInS_2$ nanoparticles. *Journal of Industrial and Engineering Chemistry, 20* (6), 4008-4013.

Aazam, E. S. (2014). Environmental remediation of cyanide solutions by photocatalytic oxidation using Au/CdS nanoparticles. *Journal of Industrial and Engineering Chemistry, 20*, 2870–2875.

Abdelwahab, O., Amin, N.K., & El-Astoukhy, E-S.Z. (2009). Electrochemical removal of phenol from oil refinery wastewater. *Journal of Hazardous Materials, 163* (2-3), 711-716.

Aguado, J., Grieken, R., Lopez, M. J., & Marugan, J. (2002). Removal of cyanides in wastewater by supported TiO_2 – based photocatalysts. *Catalysis Today, 75*, 95-102.

Akten, D. (2007). *Application of Box–Wilson experimental design method for the solar photocatalytic degradation of textile dyestuff.* Master Thesis, Dokuz Eylül University, İzmir.

Babuponnusami, A., & Muthukumar, K. (2012). Advanced oxidation of phenol: A comparison between Fenton, electro-Fenton, sono-electro-Fenton and photo-electro-Fenton processes. *Chemical Engineering Journal, 183*, 1-9.

Bahnemann, D. (2004). *Photocatalytic water treatment: Solar energy applications. Solar Energy, 77* (5), 445–459.

Bakal, F. (2014). *Production, characterization and industrial applications of new generation photocatalytic materials.* Master Thesis, Dokuz Eylül University, İzmir.

Bakuy, Ş. (2009). *Kirli su temizleme uygulamaları için cam altlıklar üzerine Ru-TiO_2 ince film üretimi ve fotokatalitik özelliklerinin incelenmesi*. Dissertation Thesis Dokuz Eylül University, Izmir.

Banerjee, S., Gopal, J., Muraleedharan, P., Tyagi, A. K., & Raj, B. (2006). Physics and chemistry of photocatalytic titanium dioxide: Visualization of bactericidal activity using atomic force microscopy. *Current Science, 90*, 1378-1383.

Barakat, M.A., Schaeffer, H., Hayes, G., & Ismat-Shah, S. (2005). Photocatalytic degradation of 2-chlorophenol by Co-doped TiO_2 nanoparticles. *Applied Catalysis B:Environmental, 57* (1), 23-30.

Basics notions about solids. (n.d.). Retrieved October 10, 2013, from http://www.porous-35.com/electrochemistry-semiconductors-3.html.

Baycan, N., (2005). *Advanced oxidative treatment of chlorinated hydrocarbons*. Doctoral Dissertation, Dokuz Eylül University, İzmir.

Bayramoglu, G., Gursel, I., Tunali, Y., & Arica, M. Y. (2009). Biosorption of phenol and 2-chlorophenol by Funalia trogii pellets. *Bioresource Technology, 100* (10), 2685-2691.

Beydoun, D., Amal, R., Low, G., & McEvoy, S. (1999). Role of nanoparticles in photocatalysis. *Journal of Nanoparticle Research, 1* (4), 439-458.

Bozkaya, Y. (2006). N*anoteknoloji ve uygulamaları*. Anadolu Üniversitesi İleri Teknolojiler Araştırma Birimi.

Callister, W.D. Jr. (2008).*Materials science and engineering an introduction* (7th ed.). New York: John Wiley & Sons, Inc.

Chambers, L. (n.d.). *Electromagnetic spectrum diagram.* Retrieved January 5, 2015, from http://mynasadata.larc.nasa.gov/science-processes/electromagnetic-diagram/.

Chen, W., Dong, X., Chen, Z., Chen, S., & Lin, W. (2009). Effect of Fe^{3+} doping on photocatalytic activity of $K_2La_2Ti_3O_{10}$ for water decomposition to hydrogen under visible light. *Acta Physico -Chimica Sin*ica, *25* (6), 1107-1110.

Chin, P. (2008). *Kinetics of photocatalytic degradation using titanium dioxide*. Doctoral dissertation, North Carolina State University, Raleigh, North Carolina.

Chiou, C-H., Wu, C-Y., & Juang, R-S. (2008). Photocatalytic degradation of phenol and *m*-nitrophenol using irradiated TiO_2 in aqueous solutions. *Separation and Purification Technology, 62* (3), 559-564.

Chong, M. N., Jin, B., Chow, C. W., & Saint, C. (2010). Recent developments in photocatalytic water treatment technology: a review. *Water Research, 44*(10), 2997-3027.

Cui, W., Liu, L., Feng, L., Xu, C., Li, Z., Lü, S., & Qiu, F. (2006). Preparation of $Pt/K_2La_2Ti_3O_{10}$ and its photo-catalytic activity for hydrogen evolution from methanol water solution. *Science in China Series B, 49* (2), 162-168.

Curcó, D., Giménez, J., Addardak, A., Cervera-March, S., & Esplugas, S. (2002). Effects of radiation absorption and catalyst concentration on the photocatalytic degradation of pollutants. *Catalysis Today, 76*, 177–188.

Çakıroğlu, E. (2011). *Titanyumdioksit esaslı (TiO_2) Fotokatalizör Kullanılarak Toksik Madde İçerikli Atıksuların Detoksifikasyonu*. Master Thesis, Dokuz Eylul University, Izmir.

Çatalkaya, E.Ç., Bali, U., & Şengül F. (2004). Fenolün fotokimyasal yöntemlerle parçalanması ve mineralizasyonu. *Su Kirlenmesi Kontrolü Dergisi, 14* (3), 31-41.

Dimitriev, Y., Ivanova, Y., & Iordanova, R. (2008). History of sol-gel science and technology. *Journal of the University of Chemical Technology and Metallurgy, 43*(2), 181-192.

Dzombak, D. A., Ghosh, R. S., & Wong-Chong, G. M. (2005). *Cyanide in water and soil: chemistry, risk, and management*. Boca Raton: Taylor and Francis/CRC Press.

Environmental Protection Agency/ U.S. EPA (1998). *Hazardous waste management system; identification and listing of hazardous waste; solvents; final rule.* Federal Register 63 FR 64371- 402.

Environmental Protection Agency/U.S. EPA (2013). *Phenol*. Retrieved June 25, 2014, from http://www.epa.gov/airtoxics/hlthef/phenol.html.

EPA. (2005). *Determination of total organic carbon and specific UV absorbance at 254 nm in source water and drinking water (Vol. METHOD 415.3).* National exposure research laboratory office of research and development U.S. Environmental Protection Agency.

Evcin, A. (2006). *Kaplama teknikleri ders notları*. Retrieved November 21, 2013 from http://www.kimmuh.com/evcin/coating/coating8.pdf.

Evcin, A. (nd). *Sol-jel prosesleri ders notları*. Afyon Kocatepe University Materials Science and Engineering Department.

Evcin, A.(n.d.). *İleri sol jel prosesleri*. Retrieved November 20, 2013, from http://www.kimmuh.com/evcin/sol-gel/solgel5.pdf.

Gümüş, G. (2001). *Siyanür tayini için yeni bir spektrofotometrik yöntem*. Doctoral Dissertation, İstanbul Technical University, İstanbul.

Güneşin elektromanyetik spektrumu. (n.d.). Retrieved January, 2014, from http://www.meteor.gov.tr/FILES/arastirma/ozonuv/gunesspectrumu.pdf.

Guo, Z., Ma, R., & Li, G., (2006). Degradation of phenol by nanomaterial TiO_2 in wastewater. *Chemical Engineering Journal, 119* (1), 55-59.

Hoffman, R.V., (2004). *Organic chemistry* (2nd ed.). New Jersey: John Wiley & Sons Press.

Huang, Y., Wei, Y., Cheng, S., Fan, L., Li, Y., Lin, J., et al. (2010). Photocatalytic property of nitrogen-doped layered perovskitee $K_2La_2Ti_3O_{10}$. *Solar Energy Materials & Solar Cells*, 94, 761–766.

Huang, Y., Wu, J., Wei, Y., Lin, J., & Huang, M. (2008). Hydrothermal synthesis of $K_2La_2Ti_3O_{10}$ and photocatalytic splitting of water. *Journal of Alloys and Compounds, 456* (1-2), 364-367.

Ikeda, S., Hara, M., Kondo, J.N., Domen, K., Takahashi, H., Okuba, T., et al. (1997). Preparation of a high active photocatalyst $K_2La_2Ti_3O_{10}$ by polymerized complex method and its photocatalytic activity of water splitting. *Journals of Materials Research, 13* (4), 852-855.

International Cyanide Management Institute (n.d.). *Environmental and health effects.* Retrieved July 4, 2014, from http://www.cyanidecode.org/cyanide-facts/environmental-health-effects.

Kaili, L., Jiayong, P., Yiwei, C., & Rongming, C. (2009). Study the adsorption of phenol from aqueous solution on hydroxyapatite nanopowders. *Journal of Hazardous Materials, 161* (1), 231-240.

Kaneko, M., & Okura, I. (Eds.). (2002). *Photocatalysis: Science and technology* (2nd ed.). New York: Springer.

Kargı, F., & Pala A. (2009). *Kimyasal prosesler ders notları*. Dokuz Eylül University Environmental Engineering Department.

Khakpash, N., Simchi, A., & Jafari, T. (2012). Adsorption and solar light activity of transition- metal doped TiO_2 nanoparticles as semiconductor photocatalyst. *Journal of Material Science: Materials in Electronics, 23* (3), 659-667.

Kiriloy, M., Koumanova, B., Spasoy, L., & Petrov, L. (2006). Effects of Ag And Pd modifications of TiO_2 on the photocatalytic degradation of p- chlorophenol in aqueous solution, *Journal of the University of Chemical Technology and Metallurgy, 41* (3), 343-348.

Kodama, F., & Suzuki, J., (2007). How Japanese Companies have used scientific advances to restructure their business: The receiver-active national system of innovation. *World Development, 35* (6), 976-990.

Krishna, V., Noguchi, N., Koopman, B., & Moudgil, B., (2006). Enhancement of titanium dioxide photocatalysis by water-soluble fullerenes. *Journal of Colloid and Interface Science, 304*, 166-171.

Kusvuran, E., Samil, A., Atanur, O. M., & Erbatur, O. (2005). Photocatalytic degradation kinetics of di- and tri-substituted phenolic compounds in aqueous solution by TiO_2/ UV. *Applied Catalysis B: Environmental, 58* (3-4), 211,216.

Larsen, D. (n.d.). *Chem-Wiki: The dynamic chemistry e-textbook,* Retrieved October 10, 2013, from http://chemwiki.ucdavis.edu/Physical_Chemistry/Quantum_Mech anics/Electro nic_Structure/Intrinsic_Semiconductors.

Liu, L., Cui, W., Liang, Y., & Qiu, F. (2010). Efficiently photocatalytic hydrogen evolution over Ce-doped $K_2La_2Ti_3O_{10}$ under visible light irradiation. *Acta Chimica Sinica, 68* (3), 211-216.

Madigan, J. (2011). *What wavelength goes with a color?* Retrieved 15, 2013 from http://science-edu.larc.nasa.gov/EDDOCS/Wavelengths_for_Colors.html.

Merabet, S., Robert, D, Weber J.V., Bouhelassa, M., & Benkhanouche, S., (2009). Photocatalytic degradation of indole in UV/TiO_2: Optimization and modelling using the response surface methodology (RSM). *Environmental Chemistry Letters, 7* (1), 45-49.

Metal oxide photocatalysis. (n.d.). Retrieved March 18, 2013, from http://photochemistry.wordpress.com/2009/09/30/metal-oxide-photocatalysis/.

Metcalf & Eddy. (2003). *Wastewater engineering: Treatment and reuse* (4th ed.). New-York: McGraw Hill Education.

Molva, M. (2004). *Removal of phenol from industrial wastewaters using lignitic coals*. Master Thesis, Izmir Institute of Technology, Izmir.

Montgomery, C., & Runger, G.C. (2010). *Applied statistics and probability for engineers*, (3rd ed.). Arizona: John Wiley&Sons, Inc.

Nakata, K., & Fujishima, A. (2012). TiO2 photocatalysis: Design and applications. *Journal of Photochemistry and Photobiology C: Photochemistry Reviews, 13*(3), 169-189.

Nano-Zone FAQ. (n.d.). Retrieved October 5, 2013, from http://www.nano-zone.net/faq.php.

Nimetoğlu, Z. (2011). *Yeni nesil fotokatalitik filmlerin üretilmesi ve atıksulardaki organik kirleticilerin temizlenmesinde kullanılması*. Dissertation Thesis Dokuz Eylül University, Izmir.

Ohtani, B. (2010). Photocatalysis A to Z—what we know and what we do not know in a scientific sense. *Journal of Photochemistry and Photobiology C: Photochemistry Reviews, 11,* 157-178.

Osathaphan, K., Chucherdwatanasak, B., Rachdawong, P., & Sharma, V. K. (2008). Effect of ethylenediaminetetraacetate on the oxidation of cyanide in an electrochemical process. *Journal of Environmental Science and Health Part A, 43*, 295-299.

Pala, A. (2010). *Veri Değerlendirme ders notları*. Dokuz Eylül University Environmental Engineering Department.

Pala, A., Çelik, E., Kurşun, G., & Bakal, F. (2013). *Tübitak araştırma projesi final raporu*.

Pardeshi, S.K., & Patil, A.B. (2008). A simple route for photocatalytic degradation of phenol in aqueous zinc oxide suspension using solar energy. *Solar Energy, 82* (8), 700-705.

Photocatalysis. (n.d.). Retrieved 10 March, 2012 from http://dev.nsta.org/evwebs/1952/photocatalysis.htm.

Pierre, A. C. (1998). Introduction to sol-gel processing: Kluwer Academic USA.

Politi, R. R. (2014). *Nanotechnologic methods for water treatment.* Master Thesis, Dokuz Eylül University, İzmir.

Qamar, M., Muneer, M., & Bahnemann, D. (2006). Heterogeneous photocatalysis degradation of two selected pesticide derivatives, triclopyr and daminozide in

aqueous suspensions of titanium dioxide. *Journal of Environmental Management, 80*, 99-106.

Qui, X., Alvarez, P.J.J., Li, Q. (2012). Applications of nanotechnolgy in water and wastewater treatment. *Water Research, 47 (12)*, 3931-3946.

Rizzo, L., Koch, J., Belgiorno, V., & Anderson, M.A. (2007). Removal of methylene blue in a photocatalytic reactor using polymethylmethacrylate supported TiO_2 nanofilm. *Desalination, 211* (1-3), 1-9.

Sayılkan, F., (2007). *Nano-TiO_2 fotokatalizör sentezi ve fotokatalitik aktivitesinin belirlenmesi*. Doctoral Dissertation, İnönü University, Malatya.

Schimidti, H., & Mennig, M. (2000). *Wet coating technologies for glass*. Retrieved March 21, 2012, from http://www.solgel.com/articles/Nov00/mennig.htm.

Semiconductor technology from A to Z (2014). Retrieved January 21, 2015 from http://www.halbleiter.org/en/fundamentals/conductors/

Shapley, P. (2012). *Intrinsic semiconductors.* Retrieved March 15, 2014, from http://butane.chem.uiuc.edu/pshapley/GenChem2/C4/1.html.

Sobczy´nski, A., Duczmal, L., & Zmudzi´nski, W., (2004). Phenol destruction by photocatalysis on TiO_2: An attempt to solve the reaction mechanism. *Journal of Molecular Catalysis A: Chemical*, *213*, 225-230.

Sol gel technology, (n.d.). Retrieved March 20, 2012, from http://sariyusriati.wordpress.com/2008/10/21/sol-gel-technology/.

Sowa, P., Rutkowska-Talipska, J., Sulkowska, U., Rutkowski, K., & Rutkowski, R. (2012). Electromagnetic radiation in modern medicine: Physical and biophysical properties. *Polish Annals of Medicine, 19*(2), 139-142.

Spin coating. (n.d.). Retrieved April 20, 2013 from http://www.solarnenergy.com/kor/pr_service/analyst_show.php?sub_cat=&bbsId=4953&tbl=column.

Su Kirliliği Kontrolü Yönetmeliği (2004). *T.C. Resmi Gazete, 25687*, 31 Aralık 2014.

Subramanian, V., Pangarkar, V. G., & Beenackers, A. A. C. M. (2000). Photocatalytic degradation of para-hydroxybenzoic acid: Relationship between substrate adsorption and photocatalytic degradation. *Clean Products and Processes, 2*, 149–156.

Suneel, S.D. (n.d.). Synthesis and processing of nano powders-bottom-up approach. In *Nanotechnology.* Retrieved March 21, 2012, from http://gitam.edu/eresource/nano/NANOTECHNOLOGY/bottamup%20app.htm.

Suntest CPS/CPS+Operating manual. (n.d.). Retrieved from http://www.atlasmtt.net/ist/data/ger/manuals/UM_suntest_cps_plus.pdf.

Şam, E.D., Ürgen, M., & Tepehan, F.Z. (2007). TiO_2 fotokatalistleri. *İtüdergisi/d, 6* (5-6), 81-92.

Takata, T., Shinohara, K., Tanaka, A., Hara, M., Kondo, J. N., & Domen, K. (1997). A highly active photocatalyst for overall water splitting with a hydrated layered perovskitee structure. *Journal of Photochemistry and Photobiology A: Chemistry, 106* (1-3), 45-49.

Tayade, R. J., Natarajan, T. S., & Bajaj, H. C. (2009). Photocatalytic degradation of methylene blue dye using ultraviolet light emitting diodes. *Industrial & Engineering Chemistry Research, 48*, 10262–10267.

Tek, S. (2008). *Photocatalytic Nanocomposites For Increased Optical Activity.* Master Thesis, Bilkent University, Ankara.

Theurich, J., Lindner, M., & Bahnemann, D. W. (1996). Photocatalytic degradation of 4-chlorophenol in aerated aqueous titanium dioxide suspensions: a kinetic and mechanistic study. *Langmuir, 12*, 6368-6376.

Tiginyanu, I., Langa, S., Foell, H., & Ursachi, V. (2009). *Porous III-V semiconductors*. Retrieved February 26, 2013, from http://www.porous-35.com/electrochemistry-semiconductors-3.html.

Tschirch, J., Dillert, R., Bahnemann, D., Proft, B., Biedermann, A., & Goer, B. (2008). Photodegradation of methylene blue in water, a standard method to determine the activity of photocatalytic coatings. *Research on Chemical Intermediates, 34* (4), 381–392.

Türk Standartları Enstitüsü. (2005). *Phenol Index*.TS 6227 ISO 6439.

Vij, K. (2008). *Textbook of forensic medicine and toxicology: Principles and practice* (4th ed.). New Delhi: Elsevier.

Wade, L.G Jr. (2014). *Phenol.* Retrieved November 9, 2014, from http://www.britannica.com/EBchecked/topic/455507/phenol.

Wang, B., Li, C., Hirabayashi, D., & K. Suzuki, (2010). Hydrogen evolution by photocatalytic decomposition of water under ultraviolet–visible irradiation over $K_2La_2Ti_3$-x MxO_{10}^+ α perovskite. *International Journal of Hydrogen Energy,35*, 3306-3312.

Weishaar, J. L., Aiken, G. R., Bergamaschi, B. A., Fram, M. S., Fujıı, R., & Mopper, K. (2009). Evaluation of specific ultraviolet absorbance as an indicator of the chemical composition and reactivity of dissolved organic carbon. *Environemental Science and Technology, 37*, 4702-4708.

Wenguan, C., Li, L., Liangrong, F., Zijian, L., Shaojie, L., & Fali, Q. (2006). Preparation of Pt/$K_2La_2Ti_3O_{10}$ and its photo-catalytic activity for hydrogen evolution from methanol water solution. *Science in China Series B, 49* (2), 162-168.

What is photocatalyst? (n.d.). Retrieved March 08, 2012 from http://www.abolinco.com/downloads/downloads/What_is_Photocatalyst.pdf.

What is PVD coating? (n.d.). Retrieved April 02, 2013, from htttp://www.richterprecision.com/faq.html.

White, D.M., Pilon, T. A., & Woolard, C.(2000). Biological treatment of cyanide containing wastewater. *Water Research, 34* (7), 2105-2109.

Yahui, Y., Qiyuan, C., & Jie, L. (2006). Photocatalytic activity of $K_2La_2Ti_3O_{10}$ doped with boron for hydrogen production from water splitting. *Chinese Journal of Catalysts,30*, 147-153.

Yang, Y,. Qiu, G., Chen, Q., Feng, Q., & Yin, Z., (2007). Influence of calcination atmosphere on photocatalytic reactivity of $K_2La_2Ti_30_{10}$ for water splitting. *Transactions of Nonferrous Metals Society of China, 17* (4), 836-840.

Yang, Y., Chen, Q., Yin, Z., & Li, Z. (2009). Study on the photocatalytic activity of $K_2La_2Ti_3O_{10}$ doped with zinc (Zn). *Applied Surface Science*, 255, 8419–8424.

Yang, Y., Chen, Q., Yin, Z., &Li, Y., (2009). Study on the photocatalytic activity of $K_2La_2Ti_3O_{10}$ doped with vanadium (V). *Journal of Alloys and Compounds*, *488*,364-369.

Yang, Y., Qui, G., Chen, Q., Feng, Q., & Yin, Z. (2007). Influence of calcination atmosphere on photocatalytic reactivity of $K_2La_2Ti_3O_{10}$ for water splitting.*Transactions of Nonferrous Metals Society of China, 17 (4)*, 836-840.

Yao, J., & Wang, C. (2010). Decolorization of methylene blue with TiO_2 sol via UV irradiation photocatalytic degradation. *International Journal of Photoenergy, 2010*, 6-12.

Yaşar, S. B., & Özcan, M. (2004). Metilen mavisinin çözücü ekstraksiyonu ile sulu çözeltilerden geri kazanımı. *Balıkesir Üniversitesi Fen Bilimleri Enstitüsü Dergisi*, *6* (2), 51 - 58.

Yeddou, A.R., Chergui, S., Chergui, A., Halet, F., Hamza, A.,Nadjemi, B., et al. (2011). Removal of cyanide in aqueous solution by oxidation with hydrogen

peroxide in presence of copper-impregnated activated carbon. *Minerals Engineering, 24* (8), 788-793.

Yu, J., Zhao, X., & Zhao, Q. (2000). Effect of surface structure on photocatalytic activity of TiO2 thin films prepared by sol-gel method. *Thin Solid Films, 379* 7-14.

Yuelin, W., Yunfang, H., Haiting, C., & Jihuai, W. (2008). Effect of tantalum substitution for titanium in layered perovskitee type $K_2La_2Ti_3O_{10}$ photocatalytic property. *Chinese Journal of Materials Research, 1*, 20-24.

Zhang, D. (2012). Heterogeneous photocatalytic removal and reaction kinetics of Rhodamine-B dye with Au loaded TiO2 nanohybrid catalysts. *Polish Journal of Chemical Technology, 14*(2), 42-48.

Zhaohui, L., Po-Hsiang, C., Wei-Teh, J., Jiin-Shuh, J., & Hanlie, H. (2011). Mechanism of methylene blue removal from water by swelling clays. *The Chemical Engineering Journal, 168*, 1193-1200.

APPENDICES

Appendix - A PHENOL AND CYANIDE STANDARDS

PHENOL INDEX (TS 6227 ISO 6439:2005) DIRECT COLORIMETRIC METHOD

Phenol solution is prepared according to standard (HACH), Lot: A0034, Exp: Feb–13. This method provides to measure colorimetrically phenolic compounds (containing affixes such as carboxyl, halogen, hydroxyl, metoxy, sulphonic acid) which react with 4 - aminoanthipyrine as forming colorific compounds and to find the phenol index.

Phenolic compounds are distilled to separate the impurities and the protective materials. The evaporation of the phenolic compounds should be slow. When the pH is 10±0.2 with the presence of the potassium hexacyanoferrate (III), the colorific antipyrine dye is produced by the reaction between phenolic compounds and 4 - aminoantipyrine. The absorbance of colored specimen is measured by the help of spectrophotometer at 510 nm. Phenol index is found as mg phenol (C_6H_5OH)/l. This method is suitable for the samples whose phenol index is bigger than 0.1 mg/l. The minimum determinable phenol amount is equivalent to 0.01 mg when 50 mm cell and 100 ml sample is used. Distillation apparatus, pH meter and spectrophotometer are using for this method.

Reagents:

- Aminoantipyrine solution ($C_{11}H_{13}N_3O$),
- Ammonium chloride solution (NH_4CL),
- Ammonia solution (NH_3 d = 0,90 g/ml),
- Potassium sodium tartrade (Potassium sodium 2,3 - dihyroxybutanedioade (buffer solution)) ($NaKC_4H_4O_6$),
- Copper (II) sulfate pentahydrate solution ($CuSO_4.5H_2O$),
- Hydrochloric acid,

- Methyl orange indicator,
- Phenol stock solution (1 g/l C_6H_5OH),
- Standard phenol solution (0.01 g/l),
- Standard phenol solution (0.001 g/l),
- Concentrated phosphoric acid (d=1.70 g/ml),
- Phosphoric acid solution,
- Potassium hexacyanoferrite (III) (Potassium ferricyanide) solution ($K_3Fe(CN)_6$),
- Sodium sulfate (Na_2SO_4, dehydrated, granular),
- Some special reagents; sulphiric acid solution, sodium chloride, sodium hydroxide solution, chloroform ($CHCl_3$).

Samples should be collected in glass bottles. Phenolic compounds in water are exposed to chemical and biochemical oxidation. That is why, if the samples do not analyze within 4 hours, some protective measures should be taken. For example, pH is arranged nearly 4 with addition of phosphoric acid, to prevent the biochemical oxidation, copper (II) sulfate can be added. The samples are kept cool (5 - 10^0C) and should be analyze within 24 hours.

100 ml phenol solution is transferred to volumetric flask. To regulate the pH value between 1 and 2, phosphoric acid solution is added (2 - 3 drops). Glass beads are putted in the volumetric flask to provide homogeny boiling. The flask is placed in the distillation apparatus. When 75 ml solution is collected in the beaker, the heater is closed. After the cooling, 25 ml purified water is added into the flask and the heater is reopened until 100 ml distillate is collected. To make the comparison with spectrophotometer, the same process is done but instead of the sample, the purified water is used.

5 ml buffer solution or 5 ml NH_4Cl solution is added to 100 ml distillate and to adjust the pH between 9 and 10, ammonia solution put in. 2 ml 4 - aminoantipyrin is mixed and blended. After that, 2 ml potassium ferricyanide ($K_3Fe(CN)_6$) solution is added and stirred. The higher absorbance is read at 510 nm. The absorbance readings

are done 15 minutes later. Water is using for the reference cell. According to the calibration graph, the phenol content of the sample is estimated.

Waters can include some aliasing distortions such as the bacteria that can degrade the phenol, oxidizing or reducing agents and strong alkali properties of the samples. Biological degradation can prevent with the addition of copper (II) sulfate. The acidic conditions with respect to phosphoric acid can reveal the copper (II) and avoid the chemical changes in strong alkali conditions. Some protective methods are used to avoid the aliasing distortions.

$$\text{Phenol Index, mg/l} = \frac{m}{V_0} \times 1000$$

m = The equivalent phenol amount from calibration graph (mg)

V_0 = Test sample volume of distilled (ml)

Reference: TS 6227 ISO 6439/March 2005

THE DETERMINATION OF TOTAL CYANIDE STANDARD METHOD 4500 C/E:2005

TOTAL CYANIDE STANDARD METHOD 4500 - CN^- C

HCN can be released by distillation and air cleaning from acidic sample. HCN gas is collected through NaOH solution. The cyanide concentration can be determined by titrimetric and colorimetric procedures. Boiling flask, inlet tube, water-cooled condenser, gas absorber, gas dispersion tube, heating element are used as apparatus.

Reagents:

- NaOH solution,
- $MgCl_2$ reagent (optional): $MgCl_2.6H_2O$,
- H_2SO_4 1+1,
- $PbCO_3$,
- Sulphamic acid (NH_2SO_3H).

STANDARD METHOD 4500-CN^- E. COLORIMETRIC METHOD

CN^- within the alkali distillate from preliminary preparation step transformed to CNCl with chloramines - T reaction but without hydrolyze to CNO^- under pH<8 condition. After the completion of the reaction, CNCl constitutes to a red - blue color form by the addition of pyridine - barbituric acid reagent. CN^- concentration is determined at 578 nm by using a spectrophotometer. This method is applied to samples whose concentrations are bigger than 1 mg/l. Interferences were removed or minimized with distillation.

Reagents:

- Chlorine - amine - T solution,
- Cyanide stock solution,
- Standard silver nitrate solution ($AgNO_3$),
- Standard cyanide solution,
- Pyridine - barbituric acid reagent,
- Astatine buffer ($NaC_2H_3O_2.3H_2O$),
- NaOH dilute solution.

A tube which contains 0.1 N NaOH is putted to the end of the portion of the distillation apparatus. Glass bead is added to CN^- flask to provide the homogeny. The heater is fixed to 100^0C for 1 hour. The perimeters are flushed with some reagent. The tube which is at the end of the apparatus contains CN^- and this CN^- is transformed to NaOH solution and diluted. A far amount of absorption solution is putted to 50 ml volumetric flask with pipette. 1 ml acetate buffer and 2 ml chlorine - amine - T solution is added and mixed. 2 minutes is allowed to precipitate. 5 ml pyridine - barbituric acid reagent is putted and completed with distilled water and waited 8 minutes. The absorbance is estimated at 578 nm. The same process is done for reference. Instead of using sample, 40 ml diluted water is putted.

THE DETERMINATION OF METHYLENE BLUE (LABORATORY METHOD)

Methylene blue is determined in certain wavelength by measuring the color as absorbance with using a spectrophotometer. The solubility of methylene blue at room

temperature is 4 g/l, and in methanol the solubility is 15 g/l. Practically, 10-5 M of methylene blue is preferable. The experiments are examined at 664 nm. This wavelength is a part of visible spectrum.